UNIVERSITEIT VAN PRETORIA
UNIVERSITY OF PRETORIA
YUNIBESITHI YA PRETORIA

SINTERING AND SLAGGING OF MINERAL MATTER IN SOUTH AFRICAN COALS DURING THE COAL GASIFICATION PROCESS

By

Ratale Henry Matjie

Submitted in partial fulfillment of the requirements for the degree

Philosophiae Doctor (Metallurgy)

in the

Faculty of Engineering, Built Environment and Information Technology

University of Pretoria

May 2008

ABSTRACT

SINTERING AND SLAGGING OF MINERAL MATTER IN SOUTH AFRICAN COALS DURING THE COAL GASIFICATION PROCESS

By Ratale Henry Matjie

Supervisor: Professor P. Chris Pistorius
Department of Materials Science and Metallurgical Engineering,

Philosophiae Doctor (Metallurgy)

Key words:
Coal analysis, Petrology, Mineral matter, Macerals, Coal ash analysis, Lurgi gasification, Glass analysis, Coal sintering and slagging, Pyrometallurgy, Density separation, Screening, Pyrolysis, Sequential leaching, Low temperature ashing, Particle morphology, X-ray diffraction, Electron microprobe, Computer controlled scanning electron microscopy, Quantitative evaluation of materials by scanning electron microscopy, Scanning electron microscope with a light element energy dispersive spectrometer, FactSage modeling.

Coals, from mines in the Highveld coalfield, as well as gasification ash samples were characterised, in order to understand the mineralogical and chemical properties of the individual components in the gasification feedstocks.

X-ray diffraction of low temperature oxygen-plasma ash indicates that the coals contain significant proportions of kaolinite, quartz and a fluxing elements-bearing mineral (dolomite), plus minor concentrations of illite and other fluxing elements-bearing minerals namely calcite, pyrite and siderite.

Of the feed coal, the -75+53 mm size fraction has a high pyrite, and to a lesser extent a high calcite and dolomite content. However, the small proportion of iron-bearing phases (from the reaction between kaolinite and pyrite) in samples taken from the gasifier implies that pyrite contributes minimally to sintering or slagging in this case.

Calcite is mainly present in the >1.8 g/cm^3 density fraction of the feed coal, whereas dolomite is mainly present in the 1.5-1.8 g/cm^3 density fraction, as inclusions or fine cleats in the coal matrix.

Electron microprobe analyses of coals from the six different South African mines confirmed that some Ca, Mg, Al, Si, Na, K, Ti and Fe are present in the organic matrix in the coal samples tested in this study, but the amounts of these are small compared with the fluxing elements in minerals.

XRD and microprobe analyses indicate that the ash clinker samples taken from the gasifiers contain a number of crystalline high temperature phases, including anorthite, mullite, cristobalite, quartz and diopside. FactSage confirmed that anorthite and mullite are equilibrium phases at elevated temperatures in the ash clinkers and heated rock fragments. Limited reaction takes place between the included coal minerals and the extraneous rock fragments.

CONTENTS …..PAGE

Table of Contents……..……..(iv)

Abstract……..(ii)

List of Tables…….....(x)

List of Figures…….……(xiv)

List of Abbreviations…...…….....(xviii)

Acknowledgements…….....(xxii)

CHAPTER ONE: INTRODUCTION

1.1 Background and statement of the problem……1

1.2 Scope and objectives of study…….5

1.2.1 Physical factors: Ash Fusion Temperature (AFT), Particles Size Distribution (PSD)…….....…...5
1.2.2 Chemical factors……..……...5

1.3 List of hypotheses that were tested in this study…….....6

CHAPTER TWO: BACKGROUND INFORMATION AND LITERATURE REVIEW

2.1 Selected South African low-rank bituminous coals as a feedstock for the gasification process…….....8

2.2 Nature of mineral matter in coal……9

2.3 Organic matter in coal……..18

2.4 Volatilisation of organic sulphur and organically-bound cations……20

2.5 Determination of mineral matter (non-minerals and minerals) in coals……..22

2.5.1 Determination of the concentration of mineral matter in coals by oxidation of the organic matter in coals…….....……23
2.5.2 Mineral matter determination by chemical analysis…….....24
2.5.3 Determination of the non-mineral inorganics in low-rank coals using a chemical fractionation technique…….……25
2.5.4 Proximate analysis of coal…….....…….....28
2.5.5 Ash analysis…….....…….....31
2.5.6 Determination of minerals in coal and coal ash by X-ray diffraction (XRD) analysis.....32
2.5.7 Determination of the glass content and glass composition in coal ash using X-ray diffraction techniques…….....……34
2.5.8 Mineral matter qualification and quantification by scanning electron microscope (SEM)…….....36

Table of contents (continued)

2.5.9 Chemical composition of mineral matter and organic matter by electron microprobe (EMP) techniques……37

2.6 Ash Fusion Temperature analysis of coal……38

2.7 Organic matter identification……39

2.7.1 Ultimate analysis……39
2.7.2 Maceral analysis using electron microscope techniques……39

2.8 Mineral reactions at elevated temperatures……40

2.8.1 Excluded mineral mechanisms……41
2.8.2 Included mineral mechanisms……50

2.9 Sintering studies of coal ash……51

2.10 Formation of glass phases in coal ash……54

2.11 Crystallisation of the dissolved inorganic elements from the ash-derived melt……55

2.12 FactSage modeling……56

CHAPTER THREE: EXPERIMENTAL PROCEDURES

3.1 Introduction……57

3.2 Mineralogical analysis across the screened coal fractions ……58

3.3 Density separation of Sasol coals……59

3.3.1 Density separation on the feed coal to the coal-conversion process……59
3.3.2 Density separation on coal from the individual mines……62

3.4 Pyrolysis of coal samples from Highveld coal mines ……63

3.5 Coal and ash sampling methodology - gasifier……65

3.5.1 Sampling methodology of composite turn-out samples, coarse coal and ash particles taken from the coal-conversion process facility……66
3.5.2 Sampling methodology of dig-out samples and coarse coal and ash particles taken from the coal-conversion process facility ……71

3.6 Methods and instrumentation……72

3.6.1 Chemical fractionation method……72
3.6.2 Proximate analysis……73
3.6.3 Ultimate analysis……73
3.6.4 Ash analysis by XRF……74
3.6.5 Elemental analysis by ICP-AES……74
3.6.6 Electron microprobe analysis……75

Table of contents (continued)

3.6.7 Determination of mineral matter in the coal by low temperature asher……..…...77
3.6.8 XRD analysis ……..……..…77
3.6.9 High-temperature X-ray diffraction (HT-XRD).....……...……..78
3.6.10 Determination of clay mineral in the coal ……..……...78
3.6.11 Computer controlled scanning electron microscope (CCSEM) (van Alphen, 2005)….....…..79
3.6.12 QEMSCAN analysis…….....…….....81
3.6.13 Petrographic analysis…….....……..…..82
3.6.14 Ash Fusion Temperature analysis…….....……..……..83
3.6.15 Particle size distribution…….....……83
3.6.16 FactSage Modeling.....83

CHAPTER FOUR: RESULTS AND DISCUSSIONS - COAL ANALYSES

4.1 Chemical analyses of coals from six different Highveld coal mines and feed coal to the coal conversion process.....85

4.1.1 Proximate analysis…….....……85
4.1.2 Ultimate analysis…….....……85
4.1.3 XRF analysis..…….....……...86

4.2 Petrographic analysis of coals from different Highveld coal mines ……..…..87

4.3 Mineralogical analyses of LTA of coals from the different mines and feed coal…….....88

4.3.1 Mineralogy of LTA residues.....……...88
4.3.2 Coal Quality Predictor model results for six coals and their density fractions from the different Highveld coal mines.....……..91
4.3.3 Mineral matter in feed coal and their transformation at elevated temperatures …….....….95
4.3.4 CCSEM and SEM-EDS analyses of coals.….....……96
4.3.5 QEMSCAN analysis of feed coal.....……...100

4.4 Elemental composition of individual coal macerals by electron microprobe…….....103

4.5 Chemical fractionation method …….....107

4.5.1 Proximate analysis of feed coal before and after sequential leaching…….....……107
4.5.2 Ultimate analysis of feed coal before and after leaching…….....……..108
4.5.3 The normalised XRF and ICP-OES analyses for HTA samples produced from the coal samples 1 and 2 before and after the sequential leaching...…….....…..109
4.5.4 Mineralogical analysis of unleached and leached coal particles…....……112
4.5.5 Water leaching…….....115
4.5.6 Ammonium acetate leaching …….....115
4.5.7 Hydrochloric acid leaching …….....115
4.5.8 Physical analysis: Ash Fusion Temperatures (AFT)…….....116

4.6 Distribution of inorganic elements in the minerals and macerals…….....…….118

Table of contents (continued)

CHAPTER FIVE: RESULTS AND DISCUSSION - COAL SIZE AND DENSITY FRACTIONS ANALYSIS

5.1 Characterisation of coal size fractions of feed coal by chemical analyses.....120

5.1.1 Ultimate analysis of coal size fractions.....120
5.1.2 Proximate analysis of coal size fractions.....120

5.2 Mineralogical analysis of coal size fractions.....122

5.2.1 CCSEM analysis of coal size fractions.....122

5.3 Characterisation of density coal fractions by analytical techniques.....131

5.3.1 Petrographic results for float (<1.5g/cm^3), middling (1.5–1.8g/cm^3) and sink (>1.8g/cm^3) fractions.....132
5.3.2 Chemical analysis of density fractions.....133
5.3.3 Mineralogical analyses of float, middling and sink fractions from feed coal.....134

CHAPTER SIX: RESULTS AND DISCUSSION - COAL PYROLYSIS

6.1 Chemical and mineralogical analyses of char samples.....138

6.1.1 XRF analysis of char samples.....138
6.1.2 Mineralogical analysis of corresponding char samples.....139

6.2 Pyrolysis results of the volatilised inorganic species.....140

6.3 Calculated equilibrium volatilisation of cations in inorganic compounds from coal.....143

CHAPTER SEVEN: RESULTS AND DISCUSSION - GASIFICATION ASH ANALYSIS

7.1 Chemical and mineralogical analyses of ash samples taken from the gasifier sampling methodology.....146

7.1.1 Chemical analysis of corresponding ash samples.....146
7.1.2 Chemical composition of bulk gasification ash, heated stone and clinker samples from the turn-out test.....148

7.2 Mineralogy of bulk gasification ash and clinker samples from the turn-out test.....151

7.2.1 Interpretation of glass composition from XRD and chemical data.....152
7.2.2 XRD analysis of the homogenised selected dig-out samples.....155
7.2.3 XRD analysis of the homogenised turn-out samples.....156
7.2.4 QEMSCAN images of the clinker samples.....157
7.2.5 CCSEM of coarse ash and clinker mineralogy.....158

Table of contents (continued)

7.2.6 Phase proportions in coarse ash and clinker fragments……..……..160
7.2.7 CCSEM analysis of hand-picked coal and clinker particles……..……161
7.2.8 CCSEM analysis of the hand-picked heated rock fragments…….....164
7.2.9 Transformation of carbonate and pyrite at high temperatures…….....166
7.2.10 Characterisation of the homogenised turn-out samples taken from the gasifier..……..168
7.2.11 SEM-EDS analysis of the hand-picked clinkers and heated rock fragments from the selected dig-out samples…….....170
7.2.12 Determination of glass and mineral compositions in the gasification ash particles by electron microprobe analysis…….....173

CHAPTER EIGHT: RESULTS AND DISCUSSION - FACTSAGE MODEL

8.1 FactSage Model.....……...180

8.1.1 FactSage results for the feed coal.....180
8.1.2 Predicted equilibrium phases in the float and sink fractions of the feed coal.....……182
8.1.3 Predicted equilibrium phases in the hand-picked dig-out samples.....…….....…...183

CHAPTER NINE: CONCLUSIONS AND RECOMMENDATIONS.....…187

BIBLIOGRAPHY…….……197

APPENDICES

Table A1 Ultimate analyses (dry ash-free basis, %) of Highveld coal samples before and after sequential leaching with water, ammonium acetate and hydrochloric acid…….209

Table A2 Inorganic oxide percentages from ICP-OES analysis of LTA samples of Highveld coal sample 1 (wt %)…….....……209

Table A3 Inorganic oxide percentages from ICP-OES analysis of LTA samples of Highveld coal sample 2 (wt %)…….....……210

Table B1 Mass percentages of phases in ash and clinker (determined by CCSEM)……...211

Table C1 Proportions of high temperature transformation products of coal minerals formed at elevated temperatures and pressures during coal gasification (wt %)……..212

Table C2 Proportions of coal minerals in the turn-out samples and feed coal determined by XRD (wt %)…….....213

Table C3 Mass-% phase proportions determined by CCSEM…….214

Table D1 XRD analysis of the dig-out samples taken from the different zones of the gasifier...216

Table F1 Predicted mass of equilibrium phases in sink fraction calculated at 1000 ^{o}C by FactSage model……...222

Table of contents (continued)

Table F2 Predicted mass of equilibrium phases in the float fraction calculated at 1100 °C by FactSage model……223

Table F3 Predicted mass of equilibrium phases in the heated rock fragment at 1100 °C by FactSage model……224

Table G1 Showing in and out temperatures of the various phases during HT-XRD runs of LTA samples of feed coal, sink and float fractions……...226

Table H1 Calculated concentrations of organic and inorganic elements obtained from all macerals in the coal sample from different Highveld collieries when using electron microprobe and optical microscope analyses…….……227

Table H2 Calculated concentrations of inorganic elements present in the minerals in coal samples from different Highveld collieries (CCSEM analysis)……..….228

Figure C1 Top image of clinker sample 4, showing siltstone fragment lower left with pink quartz …...and green clay (kaolinite) in a glassy matrix determined by QEMSCAN …...Bottom image of clinker sample 8T ……215

Figure E1 Typical X-ray spectrum of kaolinite in coal sample taken from the dig-out test…….217

Figure E2 Typical X-ray spectrum of potassium feldspar in rock fragments taken from coal …...sample 1 during the dig-out test……...218

Figure E3 Typical X-ray spectrum of calcite cleats taken from coal sample 1 during the dig-out ……...test……219

Figure E4 Typical X-ray spectrum of dolomite cleats taken from coal sample 1 during the dig-out ……...test……220

Figure E5 Typical X-ray spectrum of pyrite cleats taken from coal sample 1 during the dig-out ……test……..221

Figure G2 High temperature XRD Scan of minerals in the LTA of fine float coal fraction during ……...thermal treatment…….225

Figure G3 High temperature XRD Scan of minerals in the LTA of fine sink coal fraction during ……..thermal treatment……..226

LIST OF TABLES

Table **.....Page**

2.1 Silicate, clay, interstratified clay, carbonate and sulphate minerals found in coal and LTA samples (compiled from various sources) (slightly modified after Ward and French, 2004).....11

2.1 (a) Sulphate minerals found in coal and LTA samples (compiled from various sources) (slightly modified after Ward and French, 2004)….....12

2.1 (b) Others, sulphide, phosphate minerals found in coals and LTA samples (compiled from various sources) (slightly modified after Ward and French, 2004).....13

2.2 Percentage clay distribution of selected South African Collieries (after Gaigher, 1980)……..15

2.3 Trace element partition classification after Clarke and Sloss (1992)..……..22

2.4 Formulae for calculating mineral matter percentages from other analytical data.....25

2.5 Proportion of selected elements in Mae Moh coals released by different leaching steps (Ward, 1991).....27

2.6 Proportion of selected elements in Mae Moh coals released by different leaching steps after pyrite oxidation (Ward, 1991)…….....27

2.7 Principal minerals identified in high temperature phases associated with coal utilisation (compiled from various sources) (slightly modified after Ward and French, 2004)….....47

2.7 (a) Principal minerals identified in high temperature phases associated with coal utilisation (compiled from various sources) (slightly modified after Ward and French, 2004)……...48

2.8 Decomposition and melting temperatures of selected minerals coal and combustion ash products (Goblirsch, et al., 1984)…….....……...48

2.8 (continued) Decomposition and melting temperatures of selected minerals coal and combustion ash products (Goblirsch et al.,1984)….....49

3.1 Mass (g) and mass-% distribution for the density fractions of Sasol Coal Supplier (SCS) blend…….....……...60

List of Tables (continued)

Table **.....Page**

3.2 Table showing sample number, zones of the gasifier and approximate temperature of the sample…….....……67

3.3 Table showing sample number, zones of the gasifier and approximate temperature of the samples taken from the gasifier during the dig-out tests.....71

3.4 Assumed coal chemistry for equilibrium calculations……...84

4.1 Proximate analyses (air dried basis) of the coals tested…….85

4.2 Normalised ultimate analyses of the coals tested (dry, ash-free basis)…..…...86

4.3 Inorganic oxide percentages (wt %) from normalised XRF analysis of whole-coal samples…….…..87

4.4 Petrographic analysis of coal samples from the different mines (vol. %, mineral free)…..…87

4.5 Mineralogical analyses of LTA from coal samples from the different mines (wt %).....89

4.6 Mineralogy of <2 micron fraction by oriented aggregate XRD…….....91

4.7 Inferred ash chemistry (SO_3-free) based on Siroquant results……...91

4.8 Proportions of minerals in coal composite from Highveld coal mines determined by CQP (mass %)…….....……..93

4.9 Proportions of minerals in float fraction of coals from Highveld coal mines determined by CQP (mass %)…….....……..94

4.10 Proportions of minerals in sink fraction of coals from Highveld coal mines determined by CQP (mass%)……....…….....……94

4.11 Mineralogy of LTA isolated from feed coal and float-sink fractions (wt %)…....95

4.12 Mineral abundance in coal (mass %)…….....98

4.13 Elemental composition of macerals in coal samples from the different mines by electron microprobe analysis…….....…….....……..106

4.14 Proximate analyses (air-dried basis, %) of Highveld coal samples before and after sequential leaching with water, ammonium acetate and hydrochloric acid…….108

List of Tables (continued)

Table **.....Page**

4.15 Normalised ultimate analyses (dry ash-free basis, %) of Highveld coal samples before and after sequential leaching with water, ammonium acetate and hydrochloric acid…109

4.16 Inorganic oxide percentages from normalised XRF and ICP-OES analyses of HTA samples of Highveld coal sample 1 before and after leaching (wt %)……..111

4.17 Inorganic oxide percentages from normalised ICP-OES and XRF analysis of HTA samples of Highveld coal sample 2 (wt %)……...112

4.18 Mineralogical analysis data for coal LTA samples (wt% of LTA)…….114

4.19 Concentration of elements detected in the leachate of coal samples that were subjected to sequential leaching with water, ammonium acetate and hydrochloric acid (ppm)……116

4.20 AFT's (°C) of the feed coal and residual coal particles after sequential leaching with water, ammonium acetate and hydrochloric acid……...117

5.1 The ultimate analysis of coal size fractions feed coal (dry, ash-free basis) (wt%)……..120

5.2 The proximate analysis of coal size fractions……..121

5.3 Inorganic oxide percentages (wt %) from XRF analysis of coal size fractions.....121

5.4 Mineral proportions for the individual size fractions (mass-%)……...…124

5.5 Percent mineral distribution across size fractions (wt%)…….....……125

5.6 Area-% proportions of the major particle types ……..126

5.7 Percent particle type distribution across size fractions…….....127

5.8 Average liberation characteristics of individual minerals……...131

5.9 Maceral group analysis on coal samples (%vol)……..132

5.10 Particle type analysis (Microlithotype group analysis) on coal samples (%vol)…....132

5.11 Ultimate analysis of density coal fractions (dry, ash-free basis)…….133

5.12 Proximate analysis of feed coal and density coal fractions…….133

List of Tables (continued)

Table **.....Page**

5.13 XRF analysis of the feed coal and density coal fractions (wt%)……134

5.14 Proportions of minerals in the float and sink fractions determined by CCSEM (mass percentage)…….....136

6.1 XRF analyses of char samples obtained from the pyrolysis experiments…….....138

6.2 Mineralogical composition of the corresponding char of coals mentioned in Table 4.5 ……140

6.3 Predicted equilibrium compositions when 1.2kg coal with the composition as given in paragraph 3.4 equilibrates with 2.52 mol N_2, at 600°C…….....……142

6.4 Amounts of halogens (Cl and F) in the 1200 g of coals and in 969 g of corresponding char from mine 1 and in 974 g of char from mine 3 before and after pyrolysis…….....……142

7.1 Normalised XRF analysis of ash clinker and coarse ash samples and loss on ignition (L.O.I.) (wt%)…….....……....147

7.2 Chemical composition of coal LTA inferred from XRD, and of coal gasification ash, clinker and heated rock samples determined by XRF analysis (wt%)…….....…...150

7.3 Mineralogy of coal gasification ash, clinker and heated rock samples by XRD and Siroquant (wt %)…….....152

7.4 Inferred composition of mineral and glass fractions for gasification ash and clinker samples (wt%)…….....…….....154

7.5 Inferred composition of mineral and glass fractions for heated stone samples (wt%)....155

7.6 Composition of main mineral fragments and glass matrix in coal gasification ash samples (wt %), as determined by electron microprobe analysis…….....……...175

7.7 Composition of other coal gasification ash components (wt %) as determined by electron microprobe…….....……179

8.1 Area analysis of the selected spots fragments of samples taken from the gasifier during the dig-out test (wt%)…….....……...184

LIST OF FIGURES

Figure **.....Page**

1.1 Sasol-Lurgi Fixed Bed Dry Bottom (FBDB) gasifier…….....2

2.1 Locations of Sasol coal mines (South Africa)…….....9

2.2 Block diagram showing transformations of organically-bound inorganic elements, cations, included minerals as well as rock fragments during coal gasification at elevated temperatures….....…….....….10

2.3 Schematic of ash formation mechanisms during pulverised coal combustion (Buhre et al., 2005)…….....……...18

2.4 Schematic diagram of low temperature asher…….....23

2.5 Selective leaching scheme used for analysis of Mae Moh coal samples (Ward, 1991)…26

2.6 Estimation of glass composition for fly ash bulk chemistry and quantitative XRD data (Ward and French, 2004)……...……....……..35

3.1 Hypotheses tested and experimental procedures used in this study…….……..58

3.2 Mass-% size distribution (mass-% retained)……...59

3.3 Optical images of float coal particles hand-picked from the float fractions (<1.5g/cm^3 to <1.8g/cm^3). The average width of the images is 6.7mm…….....61

3.4 Optical images of rock fragments or stone taken from the sink fractions (> 1.8g/cm^3). The average width of the samples shown in the images is 6.7mm……....……62

3.5 Photograph showing the high temperature autoclave for pyrolysing coal…….64

3.6 Schematic showing the experimental setup for the pyrolysis tests with four water scrubbers……65

3.7 Schematic showing the Sasol-Lurgi fixed bed dry bottom (FBDB) gasifier…….67

3.8 Photographs of ash clinkers, heated rock fragments, partially burned carbon and coal particles selected from the turn-out samples, based on their size and colour……69

3.9 Photographs of the polished sections of the selected clinkers, coal, partially burned carbon and heated rock fragment particles from the turn-out samples……..……70

3.10 Textures of clinker materials (optical images)……..……..70

List of Figures (continued)

Figure **...Page**

3.11 Processed back-scattered electron image of pulverised coal with the regular grid of analytical points superimposed (black dots)…….....…….....79

3.12 Typical X-ray spectrum of coal…….80

3.13 Identification of minerals in coal particles by QEMSCAN (Butcher, 2006; Intellection).....82

4.1 X-ray diffractograms of LTA's from samples from mines 3 (top), 1 and 5 (bottom)…...90

4.2 X-ray diffractograms of LTA's from samples from mines 2 (top), 4 and 6 (bottom)…...90

4.3 Scanning electron micrographs (back-scattered electron images) highlighting mineral attributes and deportment characteristics in the gasifier feedstock…….....97

4.4 The BSE images of feed coal show carbonate cleats (calcite with white colour and dolomite with light grey) between two carbon particles, the bottom image shows included kaolinite associated with dolomite/calcite, kaolinite is also associated with dolomite/calcite/pyrites (white dots)…….....…...99

4.5 Back scattered electron images of dig-out coal stone (from feed coal): Quartz grains (mid grey), kaolinite (dark grey), potassium feldspar (light grey) and pyrite grains (white)…….....100

4.6 Grains of minerals in feed coal sample (32T)…….....…….102

4.7 Mineral associations of feed coal (sample 32T)…….....……102

4.8 X-ray diffractograms of LTA from sample 1 feed (top) to water, ammonium acetate and HCl leaching (bottom)……..... ……...113

4.9 X-ray diffractograms of LTA's from sample 2 feed (top) to water, ammonium acetate and HCl leaching (bottom)…….....…….....114

4.10 Relation between deformation temperature and proportion of CaO, MgO and Fe_2O_3 in coal ashes after each leaching process…….....…….118

5.1 Back-scattered electron images of the eight size fractions……..123

5.2 Overall particle liberation characteristics…….……...…129

5.3 Percent mineral distribution across the different liberation group…….…….....130

5.4 Back-scattered electron image of the three density fractions……..135

List of Figures (continued)

Figure **…Page**

5.5 Mass- % distribution of minerals in the density fractions……...137

6.1 Amounts of elements volatilised during pyrolysis at various temperatures of various Highveld coal sources…….....…….....……145

7.1 Ultimate and proximate analyses of ash particles……147

7.2 Correlation of MgO (left), SrO and BaO (right) with CaO in ash samples studied……148

7.3 Hand picked clinker fragments……158

7.4 Detail of rock fragment (left image) and grey elongated anorthite crystals and Ca- and Fe-bearing glass matrix (light grey)…….....160

7.5 Randomly orientated anorthite laths (an) and mullite (mu) needles in Sasol gasification ash. Image on left is from sample 8 and on the right from sample 1T……162

7.6 Left hand image (sample 1T) consists of prominent dark anorthite laths and white hercynitein two toned glass……..163

7.7 Different rock fragments with varying proportions of kaolinite (k), quartz (q), muscovite/illite (m) and microcline (mi)……..165

7.8 Detailed view of rock fragment in sample 1T……165

7.9 Fine dark mullite needles in light grey glass matrix……166

7.10 Large calcite (Ca) and pyrite rich extraneous cleat fragment……...167

7.11 Large extraneous “Fe-oxide/Fe-S-oxide/pyrrhotite” particle attached to rock fragment and anorthite rich glass fragment in the coarse ash…….....…167

7.12 Proportions of glass, quartz and metakaolinite in the turn-out samples……..…169

7.13 Proportions of silicates and metal oxides in the turn-out samples……...169

7.14 Back scattered images of dig-out clinkers 6D and 7D……..172

7.15 First BSE image of the heated stone 6.7D shows devolatilised kaolinite; and the second image (right) of heated stone 6.11D shows heated carbonaceous shale attached to anorthite and mullite crystals in the heated stone……...…….173

7.16 Electron microprobe images of slag samples (back-scattered electron mode) in clinker 2……...176

List of Figures (continued)

Figure **....Page**

7.17 Correlation between key oxide percentages in aluminosilicate glass as determined by electron microprobe analysis (Table 7.7) and inferred percentages of same oxides in glass fraction interpreted from bulk composition and XRD analysis (Tables 7.4 and 7.5)…….....…177

8.1 Predicted mass percentages of phases in ash (composition 56.0% SiO_2, 26.1% Al_2O_3, 9.1% CaO, 3.4% FeO, 3.0% MgO, 1.1% TiO_2, 0.9% K_2O and 0.4% Na_2O)……..181

8.2 Predicted mass percentages of phases in the ash of the float fraction (<1.5g/cm^3)…….182

8.3 Predicted mass percentages of phases in the ash of the sink fraction (>1.8g/cm^3)……..183

8.4 BSE image of sample 7.4D showing reacted coal ash, containing anorthite crystals in glass; the region at the bottom left is a heated rock fragment (not included in the area analysis)……...184

8.5 Predicted mass percentages of phases in the heated stone 6.7D…….……185

8.6 Predicted mass percentages of phases in the heated stone 7.4D…….……186

LIST OF ABBREVIATIONS

AAL	Ammonium Acetate Leaching
AAS	Atomic Absorption Spectroscopy
AFT	Ash Fusion Temperature
ASTM	American Society for Testing and Materials
AXRD	Ambient X-ray Diffraction
B/A	Base/Acid ratio
BSE	Backscattered Electron
CHF	Chemical Fractionation
CCSEM	Computer Controlled Scanning Electron Microscopy
CMT	Coal and Mineral Technologies
CSIRO	Commonwealth Scientific and Industrial Research Organisation
CQP	Coal Quality Predictor
daf	Dry Ash Free
DC	Dust Collector
DME	Department of Mineral and Energy
DTF	Drop Tube Furnace
EMP	Electron MicroProbe
FBDB	Sasol-Lurgi Fixed Bed Dry Bottom
FC	Fixed Carbon
FT	Fluid Temperature

GL	Gas Liquor
HClL	Hydrochloric Acid Leaching
HLC2	Highveld Leached Coal Two
HLC1	Highveld Leached Coal One
HT	Hemispherical Temperature
HTA	High Temperature Ash
HT-XRD	High Temperature X-ray Diffraction
HUC	Highveld Unleached Coals
IC	Ion Chromatography
ICP	Inductively Coupled Plasma
ICP-AES	Inductively Coupled Plasma Atomic Emission Spectroscopy
ICP-MS	Inductively Coupled Plasma Mass Spectrometry
IDT	Initial Deformation Temperature
IM	Inherent Moisture
KMC	King-Maries-Crossley
LTA	Low Temperature Ash
MM	Mineral Matter
OES	Optical Emission Spectroscopy
PM_1	Particulate Matter less than 1 µm
PSD	Particle Size Distribution

QEM*SEM	Quantitative Evaluation of Materials by Scanning Electron
ROM	Run of Mine
SABS	South African Bureau of Standards
SAMB	South African Low-grade Medium Rank C Bituminous
SCS	Sasol Coal Supplier
SEM-EDS	Scanning Electron Microscope with a light element Energy Dispersive Spectrometer
ST	Softening Temperature (spherical),
Tot	Total
TS	Total Sulphur
TSI	Technology Service International
UC1	Unleached coal 1
UC2	Unleached coal 2
UJ	University of Johannesburg
PC	Personal Computer
WDS	Wavelength Dispersive Spectrometer
WL	Water leaching
XAFS	X-ray Absorption Fine Structure Spectroscopy
XRF	X-ray Fluorescence Spectroscopy
η	Apparent Viscosity
γ	Surface Tension

ACKNOWLEDGEMENTS

An in-depth study like this is impossible by an individual. The author would like to express his sincere gratitude to the following organisations and individuals for their financial support, interest and detailed discussions:

First and foremost, my supervisor, Professor of Material Science and Metallurgical Engineering, Chris Pistorius for his interest and inspiration towards this project and sound advice in preparing this thesis. To colleagues, Dr Johannes van Heerden and Dr John Bunt, for encouragement and support during the compilation of this thesis.

To the Higher Degrees Committee at the University of Pretoria for the approval and registration of the research project.

The entire management of Sasol Technology Research and Development for financial and moral support and also granting permission to do the research work in Sasol Technology Research and Development laboratories.

Professor Colin Ward and Dr Z Li of the University of New South Wales and Dr David French of CSIRO Energy Technology, Barry Searle and Irene Wainwright, of UNSW, are all thanked for assistance with different aspects of the analysis programme. Management of the University of New South Wales in Australia, for granting permission to use their facilities as a part-time student for three months.

Assistance provided by the personnel of Sasol Technology's Syngas and Coal Technologies group and Sasol Synfuels gasification group is also gratefully acknowledged. The work was made possible through their support.

The assistance of Bafana Hlatshwayo and Monica Raghoo in calculations of equilibrium phases in coal ash using the FactSage model, as well as preparation of other figures and tables of the results, is warmly appreciated.

The author would also like to thank Dr Chris van Alphen, Mr Al Cropp and Dr Alan Butcher for CCSEM and QEMSCAN results for coal and ash samples, analysed in this study. Finally, I would like to express my sincere thanks to my wife Jane Lehlalotse Matladi and our children for their patience during the duration of the study.

CHAPTER 1
INTRODUCTION

1.1 Background and statement of the problem

The feed to the Sasol-Lurgi Fixed Bed Dry Bottom (FBDB) gasification process principally consists of coarse coal (>6mm) and extraneous rock fragments ("stone") including siltstone, mudstone, carbonaceous shale and sandstone. These stones, termed roof and floor, are sometimes mined with coal. This low rank bituminous coal is gasified to produce synthesis gas (also referred to as syngas, a mixture of carbon monoxide and hydrogen). Coal ash is a by-product of the gasification process. Coal consists of different types of inorganic constituents (minerals and organically-associated inorganic elements) and organic matter (macerals). The behaviour of the inorganic constituents and organic matter, as well as the operating conditions during gasification of the coal, is important in initiating and controlling clinker formation (Matjie et al., 2006). When the temperature in the combustion zone exceeds the melting point of the ash-forming minerals, the minerals will melt / flow and agglomerate. Due to the counter-current mode of operation, hot ash exchanges heat with the cold incoming agent (steam and oxygen or air), while higher in the gasifier hot raw gas exchanges heat with cold incoming coal. These results in the ash and raw gas leaving the gasifier at relatively low temperatures compared to other types of gasifiers, improving the thermal efficiency and lowering the steam consumption. A schematic representation of a Sasol-Lurgi Fixed Bed Dry Bottom (FBDB) gasifier is shown in Figure 1.1

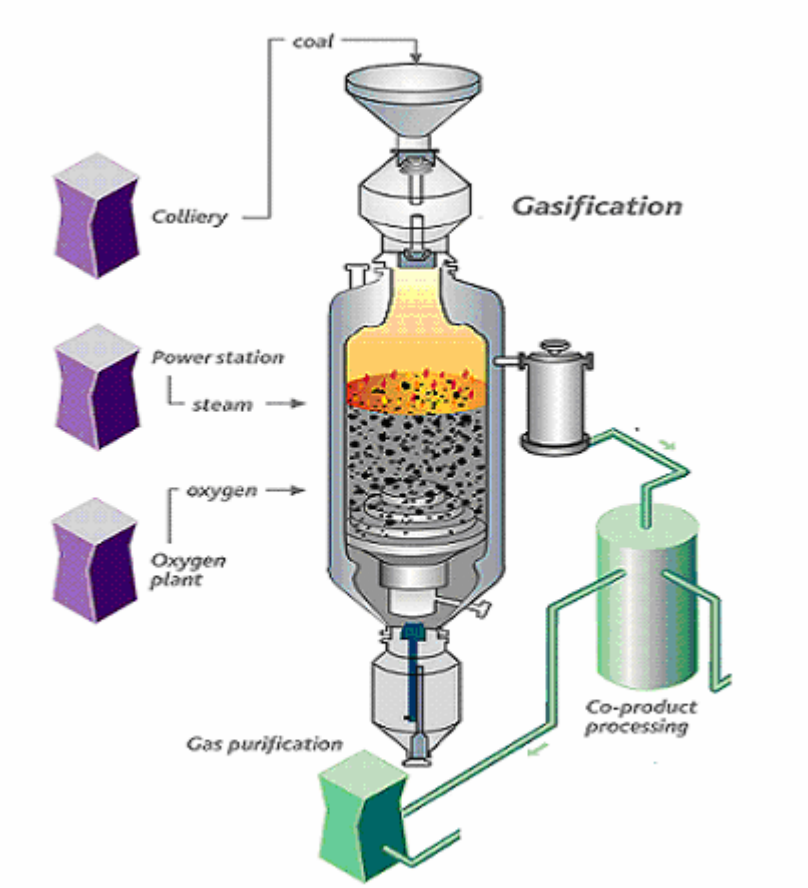


Figure 1.1: Sasol-Lurgi Fixed Bed Dry Bottom (FBDB) gasifier.

In the gasification process, fluxing elements-bearing minerals or non-mineral inorganic elements interact with aluminium silicate present in the coal to lower the melting points of the aluminium silicate and subsequently form the melt (Matjie et al., 2006). Some of the extraneous rock fragments, as well as partially burnt coal, attach themselves to the melt to form a clinker. In most cases, clinker is formed when fluxing elements such as Ca, Fe^{2+} and Mg reduce the ash fusion temperature of aluminium silicates (clays) to form a melt. In some other instances, rock fragments as well as trace amounts of unburnt carbon are encapsulated by the melt (Matjie et al., 2006). In addition, the included minerals that are finely dispersed within the carbon matrix, as well as the organically-bound cations may partially volatilise from the coal gasification process and condense at low temperatures to form a deposit or precipitate. The resultant fouling by the inorganic species and corrosion at the gasification and phenosolvan plants during treatment of gas liquor (quenched water produced during the cooling of syngas) continues to cause significant operational problems (Matjie and Engelbrecht, 2007).

Currently, clinker formation can result in the blockage of gasifiers and also contributes to the loss of carbon (approximately 4 to 6% fixed carbon) which has a negative impact on process efficiencies. Furthermore, the influence of both chemical and physical factors on the sintering (a bonding of particles that may arise from their partial melting during heating) and slagging (melting of the entire mineral matter particle) of coal mineral matter, to control the clinker formation and physical properties of a sintered deposit during gasification, is not properly understood.

Indications of possible behaviour of the inorganic coal constituents are provided by observations relevant to boiler conditions. According to Benson (1987), Jung and Schobert (1991), Ward and French (2004), van Alphen (2005) and Gupta (2005), during the combustion of the pulverised coal particles at elevated temperature, the inorganic constituents are liberated upon burn-out of organic matter to form gas, liquid and solid phases. In most cases, the inorganic constituents subsequently interact with each other to produce fly ash particles, with varying elemental compositions, morphological features (size and shape) and physical characteristics (viscosity and density) (Attalla et al., 2004 and van Alphen, 2005).

At high temperatures, fly ash particles with low melting points adhere to internal boiler surfaces and also form sintered deposits. Molten deposits formed on the internal walls of large furnace cavities are termed a slag.

The inorganic constituents are distributed within the coal matrix in several forms, including: coal-bound (included minerals), coal free (extraneous minerals) and organically-associated inorganic elements. According to Given (1984), low rank coals contain high quantities of the organically-associated cations. The rank of the typical Sasol coals, in terms of vitrinite reflectance, is 0.61 RoV%. Low-rank subbituminous and lignitic coals contain high levels of oxygen that can act as bonding sites for various cations; approximately 25% of oxygen is associated as carboxylic acid groups. Benson and Holm (1985) indicated that carboxylic acid groups can act as ion exchange sites for cations such as sodium, calcium, magnesium, potassium, strontium and barium. Higher-ranked coals do not contain high levels of the organically-associated inorganic elements, because of the lower levels of oxygen.

Extensive research was also conducted on the inorganic matter present in the coal in order to study the sintering temperature and mechanisms of ash deposits in boilers (Raask, 1985; Conn and Austin, 1984; Cumming et al., 1986; Tangsathitkulchai, 1986 and Benson, 1987). During

their studies, an ash pellet was prepared and heated slowly, while simultaneously measuring the electrical resistance across the heated pellet. The sinter point that was observed by these researchers is termed the sintering temperature of the fly ash particles and it is expected to be equal to or greater than the electrical sinter point. Cumming et al. (1986) stated that the electrical sinter point is always below the deformation temperature of the ash, determined in the A.S.T.M. ash fusion test. The sintering of the ash is an important part of the overall process of ash deposition on heat transfer surfaces in boilers.

Slagging of fly ash particles in boilers has also been studied extensively. Minerals on the surface of the coal enhance the slagging propensity of the coal particles during pulverised coal combustion. Slagging can cause several problems which reduce the ability to raise steam, lead to increased corrosion and slag dropping into the bottom of the furnace, leading to hopper blockage in boiler operation. For pulverised coal combustion the sintered deposits were found to be rich in anorthite (Unsworth et al., 1987). Most of the researchers argued that anorthite ($CaAl_2Si_2O_8$) is formed by solid-state reactions and not by crystallisation from a homogeneous melt (slag).

It has similarly been proposed that the included minerals, organically-associated inorganic elements, fluxing elements-bearing minerals (pyrite, dolomite, calcite and siderite), fluxing elements (sodium, calcium, iron and magnesium) and sodium- and potassium-bearing aluminium silicates present in Sasol coals as well as operating conditions are most likely responsible for the clinker formation in the gasifiers (Matjie et al., 2006). During coarse coal gasification, the mineral matter present in the coal feedstock could interact to form melt. On cooling, the molten solution could encapsulate the surrounding “stone”, uncombusted char and large extraneous Fe-oxide/Fe-S-oxide and Ca-oxide/CaMg-oxide particles to form clinkers (Matjie et al., 2006). Management of clinkers in the gasifier, by using the optimal sintering parameters in order to enhance carbon efficiency is important to Sasol.

A comprehensive understanding of chemical and physical processes involved in the formation of clinkers in the gasifiers would include: mode of occurrence of the inorganic constituents in the coal, effect of particle size distribution of coal on the clinker formation, reactions of the organically-bound cations with each other or with coal minerals, effect of the mineralogical composition on the clinker formation, effect of stone (extraneous rock fragments) content on the clinker formation, effects of temperature and pressure on the clinker formation, effects of reducing and oxidising atmospheres on the clinker formation and impact of steam on the

crystallisation from the slag. Understanding of the individual high temperature mineral transformations or mineral interactions during the gasification of the coarse coal particles at elevated temperatures and pressures is not well developed.

1.2 Scope and objectives of study

The primary objective of this study is to determine which mineral matter is primarily responsible for the sintering behaviour of coal ash, and also to test the hypotheses mentioned below in paragraph 1.3. The secondary objective of this study is to optimise or investigate the existing operating parameters for gasification that are possibly responsible for a clinker formation in the gasifiers. An in-depth characterisation study of composite samples of coals taken from various Sasol sources situated in Mpumalanga province in South Africa, their coal blends (Sasol coal feedstock for gasification process) as well as the gasification ash are also included in this study.

1.2.1 Physical factors: Ash Fusion Temperature (AFT), Particle Size Distribution (PSD)

The AFT of the bulk coal blend entering the gasifier, float and sink fractions of coals from the different mines and the coal size fractions, was determined under reducing or oxidising conditions. The AFT of coal samples and that of the samples retrieved from a commercial gasifier were compared.

1.2.2 Chemical factors:

- Mineralogical composition and attributes (included in the carbon-rich particles or extraneous minerals).

Indications are that the mineralogical composition and attributes play a significant role in controlling slagging and clinker formation in the gasifier. Composite samples of the coarse coal and the gasification ash were taken from a commercial gasifier on the Sasol Synfuels Secunda for an in-depth characterisation study.

- Volatilisation of organically-bound cations and sulphur

The hypotheses that describe the possible mechanisms of volatilisation of the organically-bound cations and organic sulphur present in coal, including the interaction of these cations

with each other or with aluminium silicates at elevated temperatures, are given in paragraph 1.3 of this section.

- Mineral reactions at elevated temperatures

When clays such as kaolinite, illite, muscovite and montmorillonite that are originally present in coal are heated at an elevated temperature of around 450°C, they start to lose water of crystallisation during decomposition (Grim, 1962; Bryers, 1986; Unsworth et al., 1987b; Ward and French, 2004 and van Alphen, 2005). In the case of kaolinite, its structure is partially re-arranged to form meta-kaolinite (kaolinite with no water of crystallisation) and it has a lower melting point in comparison with the coal kaolinite. At this elevated temperature cations (sodium, potassium, calcium, iron, magnesium) arising from the metallic salts of carboxylic acids can react with the reactive meta-kaolinite and result in the reduction of the melting point of the aluminium silicates (Tangsathitkulchai, 1986; Benson, 1987).

In this study, a low temperature ashing (LTA), a high temperature X-ray diffraction (HT-XRD) and ambient X-ray diffraction (XRD) were used to better understand the transformation of clays present in coals at elevated temperatures.

The thermodynamic package FactSage was used to predict the equilibrium phases in the lower part of the gasifier, where the temperature decreases from the peak in the coal combustion region towards the grate.

The information obtained from this study could be used to blend coals from various Sasol coal sources, according to their chemical and physical properties in order to control the proportion of the molten glass phases formed in the gasifier and assist in reducing the incidents of slagging and severe clinkering of mineral matter during the gasification process.

1.3 List of hypotheses that were tested in this study

The hypotheses are listed below with a brief discussion:

- Specific minerals, mineral associations as well as the organically-bound inorganic elements are thought to be primarily responsible for slagging and sintering.
  The mineralogical and elemental compositions and AFT of the coal feed, and coal size fractions, were used for this study.

- The Ca-Fe-Mg-K-Ti aluminosilicate glass present in the gasification ash is thought to be produced directly from the included minerals.

- The extraneous rock fragments may attach to the molten material to form clinkers.

In order to test the above-mentioned hypotheses, chemical fractionation (CHF), QEM*SEM or QEMSCAN (quantitative evaluation of materials by scanning electron microscopy), and electron microprobe (EMP) techniques were utilised to determine the concentrations of both organically-bound inorganic elements and minerals that are less than 20 micron in size, present in the coals. In this study the HT-XRD, XRD and X-ray fluorescence (XRF) were also used. A laboratory autoclave, simulating the pyrolysis of coarse coal in the gasification plant, was utilised to qualify and quantify volatilisation of inorganic constituents from the organometallic species present in the coal.

CHAPTER 2

BACKGROUND INFORMATION AND LITERATURE REVIEW

Three constituents of coal are thought to play important roles in slagging and clinker formation. These are listed below, before continuing with a review of the coal types studied and possible high-temperature reactions of and interactions between the constituents.

- **Included minerals in the coal**

Included minerals occur within the coarse carbon-rich (coal) particles. These minerals (approximately 55% of the inorganic material in the coal) could react with aluminium silicates (mainly kaolinite transformation products) in the pyrolysis and gasification zones to form melts.

- **Organically-bound species**

Attalla et al., (2004) indicated clearly that the organically-associated inorganic elements in coal have a significant effect on ash formation mechanisms during coal combustion. Quann and Sarofim (1986) established that organically-associated Ca and Mg interacted with free aluminium silicates (clays) in lignite coals at elevated temperatures to form a melt that resulted in agglomerate formation. Matjie et al., (2007) found that Sasol feed coal contains less than 0.2% organically-bound inorganic elements (Ca, Mg, Al, Si, Na, K, Ti and Fe). These are thus a minor constituent, but are expected to contribute strongly to volatilisation of compounds of the listed elements.

- **Rock fragments**

Sasol feed coal to the gasification contains approximately 15-20% extraneous rock fragments particles. These rock fragments could attach to the molten solution to form heterogeneous clinkers.

2.1 Selected South African low-rank bituminous coals as a feedstock for the gasification process

The South African low-grade, medium rank C bituminous coals (as considered in this study) are mined from six different collieries situated in the Mpumalanga Province in South Africa.

Coarse coal particles (> 6 mm coal fraction) from the various coal sources are transported to the preparation plant, where they are blended according to their availability to form a mixture that is suitable for the gasification process. The feed coal to gasification typically has a 25 - 28% ash yield. The locations of the mines that supply the coals are shown in Figure 2.1. The shaded areas represent mines that belong to Sasol; producing coals that contain slightly different proportions of carbon-rich particles, included mineral particles and rock fragments (extraneous minerals) for use in gasification and combustion processes.

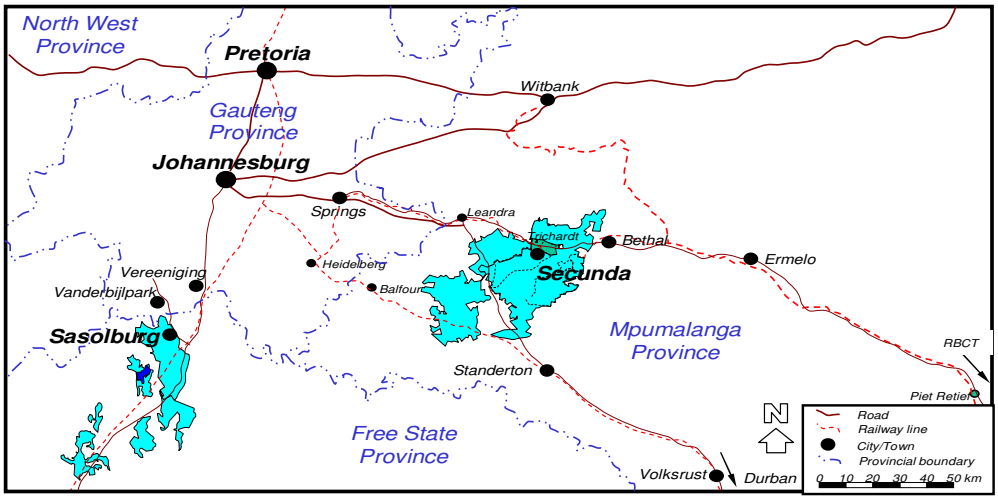


Figure 2.1: Locations of Sasol coal mines (South Africa).

2.2 Nature of mineral matter in coal

Coal contains three fundamentally different types of inorganic constituents, namely:

- Dissolved salts and other inorganic substances in the coal pore water;
- Inorganic elements incorporated within the organic compounds of the macerals;
- Discrete inorganic particles (crystalline or non-crystalline) representing the mineral components (Ward, 1984; Benson, 1987; Ward and French, 2004).

According to Ward and French (2004) the first two types of mineral matter in the list are best described as non-mineral inorganics, substantially contained in the macerals of brown coals, lignite, and subbituminous materials. Low rank coals contain high levels of organically-associated cations (Given, 1984). Such low-rank subbituminous and lignitic coals contain high levels of oxygen that can act as bonding sites for various cations; approximately 25% of the oxygen is associated as carboxylic acid groups. The proportion of organically-associated

inorganic elements is much smaller than the discrete inorganic particles (minerals) in both lower-rank and higher-rank coals (Benson, 1987; Given, 1984).

Coals from the different mines contain different classes of minerals depending on their origin:

- Extraneous minerals may be in the form of ultra-fine material on the surface of coal or rock fragment (siltstone or sand stone), originating from contamination of the mined product by roof or floor strata. These minerals can be easily separated from the carbon-rich fraction of coal by physical methods, including density separation or flotation (van Alphen, 2005; Ward, 1984).
- Included (inherent) minerals are associated with macerals. These types of minerals are encapsulated in the coal matrix (Ward and French, 2004; van Alphen, 2005).

The transformation of mineral matter in coal at elevated temperatures during coal gasification is illustrated in Figure 2.2.

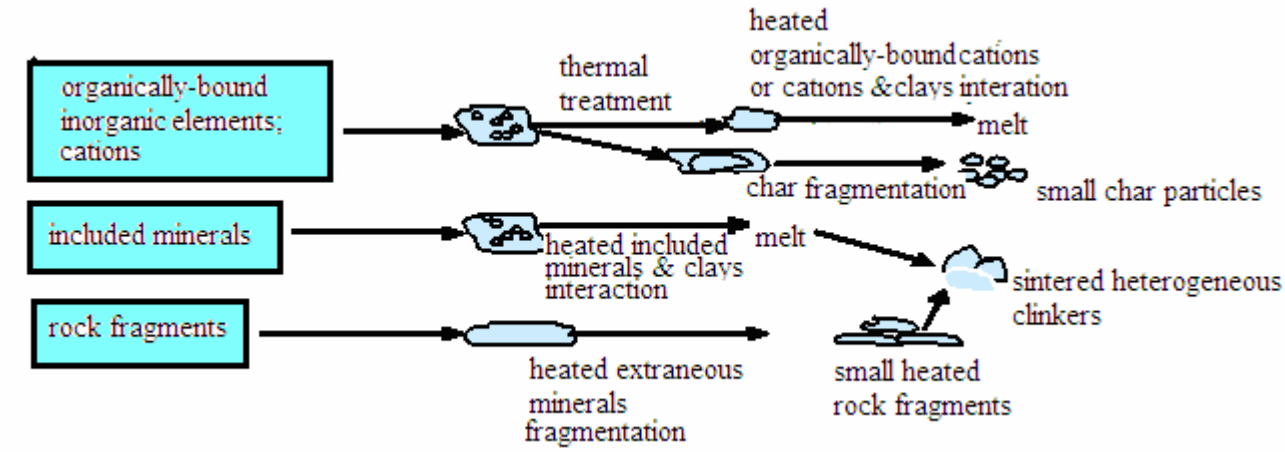


Figure 2.2: Block diagram showing transformation of organically-bound inorganic elements, cations, included minerals as well as rock fragments during coal gasification at elevated temperatures.

A list of minerals found in coals from the different coal mines, as well as in low temperature ash (LTA), was compiled by Ward and French (2004) and is summarised in Tables 2.1, 2.1a and 2.1b.

Table 2. 1: Silicate, clay, interstratified clay, carbonate and sulphate minerals found in coal and LTA samples (compiled from various sources and slightly modified after Ward and French, 2004)

Silicates	
Quartz	SiO_2
Chalcedony	SiO_2
Clay Minerals	
Kaolinite	$Al_2Si_2O_5(OH)_4$
Illite	$K_{1.5}Al_4(Si_{6.5}Al_{1.5})O_{20}(OH)_4$
Smectite	$Na_{0.33}(Al_{1.67}Mg_{0.33})Si_4O_{10}(OH)_2$
Chlorite	$(MgFeAl)_6(AlSi)_4O_{10}(OH)_8$
Muscovite	$K_2O.3Al_2O_3.6SiO_2.2H_2O$
Montmorillonite	$(1\text{-}x)Al_2O_3.x(MgO, Na_2O).4SiO_2.H_2O$
Interstratified Clay Minerals	
Feldspar	$KAlSi_3O_8$
	$NaAlSi_3O_8$
	$CaAl_2Si_2O_8$
Tourmaline	$Na(MgFeMn)_3Al_6B_3Si_6O_{27}(OH)_4$
Analcime	$NaAlSiO_6.H_2O$
Clinoptilolite	$(NaK)_6(SiAl)_{36}O_{72}.20H_2O$
Carbonates	
Calcite	$CaCO_3$
Aragonite	$CaCO_3$
Dolomite	$CaMg(CO_3)_2$
Ankerite	$(Fe, Ca, Mg)CO_3$
Siderite	$FeCO_3$
Dawsonite	$NaAlCO_3(OH)_2$
Strontianite	$SrCO_3$
Witherite	$BaCO_3$
Alstonite	$BaCa(CO_3)_2$

Table 2.1 (a): Sulphate minerals found in coal and LTA samples (compiled from various sources) and slightly modified after Ward and French, 2004)

Mineral	**Composition**
Coquimbite	$Fe_2(SO_4)_3.9H_2O$
Rozenite	$FeSO_4.4H_2O$
Szomolnokite	$FeSO_4.H_2O$
Natrojarosite	$NaFe_3(SO_4)_2(OH)_6$
Thenardite	Na_2SO_4
Glauberite	$Na_2Ca(SO_4)_2$
Hexahydrite	$MgSO_4.6H_2O$
Tschermigite	$NH_4Al(SO4)2.12H2O$
Gypsum	$CaSO_4.2H_2O$
Bassanite	$CaSO4.1/2H_2O$
Anhydrite	$CaSO_4$
Heulandite	$CaAl_2Si_7O_{18}.6H_2O$
Barite	$BaSO_4$
Jarosite	$KFe_3(SO_4)_2(OH)_2$
Alunite	$KAl_3(SO_4)_2(OH)_6$

Table 2.1 (b): Others, sulphide, phosphate minerals found in coals and LTA samples (compiled from various sources and slightly modified after Ward and French, 2004)

Mineral	Composition
Others	
Anatase	TiO_2
Rutile	TiO_2
Boehmite	Al.O.OH
Goethite	$Fe(OH)_3$
Crocoite	$PbCrO_4$
Chromite	$(Fe, Mg)Cr_2O_4$
Clausthalite	PbSe
Zircon	$ZrSiO_4$
Magnetite	Fe_3O_4
Hematite	Fe_2O_3
Limonite	$Fe_2O_3.H_2O$
Sulphides	
Pyrite	FeS_2
Marcasite	FeS_2
Pyrrhotite	$Fe_{(1-x)}S$
Sphalerite	ZnS
Galena	PbS
Stibnite	SbS
Millerite	NiS
Chalcopyrite	CuFeS
Phosphates	
Apatite	$Ca_5F(PO_4)_3$
Crandallite	$CaAl_3(PO_4)_2(OH)_5.H_2O$
Gorceixite	$BaAl_3(PO_4)_2(OH)_5.H_2O$
Goyazite	$SrAl_3(PO_4)_2(OH)_5.H_2O$
Monazite	$(Ce, La, Th, Nd)PO_4$
Xenotime	$(Y, Er)PO_4$

The list was slightly modified to show minerals commonly found in the coals in this study. Clay minerals (kaolinite, illites or muscovite and smectite) and quartz were the dominant included minerals.

van Alphen (2005) indicated that kaolinite is a common mineral deposited in the cavities in fusinite, dispersed through vitrinite as included sub-micron spherical particles and sub-spherical grains filling the microstructures within the coal. Kaolinite can also occur as an epigenetic cleated mineral intersecting the coal seam.

Illites ($K_{1.5-1.0}Al_4[Si_{6.5-7.0}Al_{1.5-1.0}O_{20}](OH)_4$) are characterised by high silica content and low potassium content, physically having clay size (<2µm) particles (Velde, 1985; Chamely, 1989; Deer et al., 1992). Illites contain potassium ions without hydration shells that are more stable in the interlayer sites than the hydrated sodium ions of smectites. When illites are exposed to heat, the grain size of the <2µm fraction increases and subsequently results in a decrease in the proportion of interlayered expandable material. van Alphen (2005) reported that illite is mainly found along bedding planes, rarely dispersing in the coal, or is deposited in the cavities in fusinite.

The principal smectite clays (montmorillonite, beidellite, and nontronite) are di-octahedral 2:1 layered silicates and saponite, hectorite and sanconite are tri-octahedral. Smectite minerals have multi-structural layers with significantly higher loading capacity of cations in comparison with kaolinite and illite clays. They also have marked cation exchange properties that can enable their multi-layer structures to absorb more water or organic molecules and result in expanded structures (Velde, 1985; Chamely, 1989; Deer et al., 1992).

Gaigher (1980) found that South African coals contained major clay minerals (kaolinite and illite), silicate oxide (quartz) and minor carbonate minerals (calcite, dolomite and siderite) as in Table 2.2. Gaigher (1980) stated that there was a strong association between clay minerals and inertinite, but a negative association between clay minerals and vitrinite.

Table 2.2: Percentage clay distribution of selected South African Collieries (after Gaigher, 1980)

Colliery	**Seam**	**Coalfield**	**Kaolinite %**	**Illite %**	**Expandable clays %**
Eikeboom	2	Witbank	87.90	3.60	8.50
Springbok	2	Springbok Flats	63.30	35.80	0.90
New Clydesdal	2	Witbank	64.20	29.10	6.10
Albion	2	Witbank	55.40	43.60	1.00
Delmas	2	Witbank	88.50	0.70	10.80
S.Witbank	4	Witbank	90.60	5.10	4.30
Anglo Power (Kriel)	4	Highveld	92.50	2.70	4.80
Blesbok	5	Witbank	52.40	22.40	25.20
Springbok	5	Springbok Flats	55.40	14.70	29.90
Greenside	5	Witbank	76.60	9.70	13.70
Navigation	5	Witbank	65.00	15.30	19.70

Quartz derived from igneous, sedimentary and metamorphoric rocks is found as an accessory mineral and as a secondary mineral in veins and metasometic deposits (Glikson and Mastalerz, 2000; van Alphen, 2005). Quartz can occur as fine or coarse particles dispersed within the coal matrix. According to Glikson and Mastalerz (2000) and van Alphen (2005), wind and water can transport sub-micron grained quartz particles that could be derived from the conversion of smectite-dominated clays into illite or could be an intrinsic component of the plant material, introducing them into the peat forming swamps. Quartz present in bituminous coals may be detrital in origin, but the majority of quartz occurs from diagenetic transformation (Glikson and Mastalerz, 2000; van Alphen, 2005; Ward, 2002).

Ward (2002) suggests that coals that contain a significantly higher proportion of quartz occur beneath intra-seam claystone bands apparently of pyroclastic origin. During hydrothermal alteration of the volcanic glass, feldspars and other minerals in the pyroclastic sediment, the infilling quartz which represents silica is released. This silica will re-precipitate in the pores of the peat, just below the introduced pyroclastic substance arising after the hydrothermal alteration process.

The percolation of salty ground water, containing carbonate anions and Ca and Mg cations, through existing coal seams precipitates carbonates (dolomite and calcite) in stress fractures and cleats in the coal seam. This is another source of metals that deposit as carbonate minerals is the organic matter (Glikson and Mastalerz, 2000; Ward, 2002; van Alphen, 2005). The precipitation or deposition of carbonate minerals in the coal is normally late-syngenetic or more commonly epigenetic and precipitated carbonates can occur, filling the cell cavities of fusinite (Diessel, 1992; Glikson and Mastalerz, 2000; van Alphen, 2005).

Pyrite (FeS_2) can occur in various forms. Diessel (1992); Glikson and Mastalerz (2000); and van Alphen (2005) noted that raspberry-shaped pyrite framboids containing spherically sub-micron crystals of pyrite (0.1-2µm in size) were bonded in some cases by interstitial kaolinite. The pyrite framboids that commonly occur as clusters and are disseminated throughout the coal seam can reach sizes of 200µm. Pyrite also occurs as lenticular masses, euhedral crystals, and cell infillings, as veins and on cleat surfaces (Ward, 1984, 2002). Rao and Gluskoter (1973) and van Alphen (2005) stated that the colloidal deposition of inorganic species or the activity of micro-organisms (bacterial) could be the source for the formation of pyrite framboids, trace amounts of sphalerite, marcasite and galena. Sub-micron or super-micron grained pyrite particles (in the range of 0.1-100µm) can also be dispersed within the vitrinite and inertinite macerals present in coals. Like precipitated carbonates, precipitated pyrite can fill the cell cavities of fusinite, or appears in fractures, cleats and cracks in the carbon matrix (Rao and Gluskoter, 1973; van Alphen 2005). Stach (1982) stated that a high proportion of pyrite in coal can be attributed to marine influences and also biological reduction of sulphate during deposition of the seam.

The parent of siderite is an acidic fresh water environment that is rich in iron ions, but contains trace amounts of sulphate (Ward et al., 1999a). When carbon dioxide is bubbled through acidic fresh water, siderite will start to precipitate from this water. Siderite is commonly found in coals from Australia, while pyrite is present in South African coals (Ward et al., 1999a). In most cases, siderite is present in the mineral matter of coals which have a low proportion of syngenetic pyrite, such as the Sydney-Bowen Basin seams in eastern Australia (Ward et al., 1999a). Siderite is apparently formed by chemical precipitation during early diagenesis and commonly occurs as spheroidal nodules (Ward, 1984; van Alphen, 2005).

Like syngenetic precipitates of pyrite, kaolinite, quartz and carbonate minerals, trace apatite present in coal is formed by syngenetic precipitation as cell and pore infillings in the original peat bed. Apatite melts at a temperature of greater than 1230°C (Deer et al., 1992). This mineral could lower the melting temperature of aluminium silicates and contribute to clinker formation during the coal gasification.

Attalla et al. (2004) indicated clearly that the mode of occurrence of mineral matter (included minerals, excluded minerals and organically-associated inorganic elements) in coal has a significant effect on ash formation mechanisms during coal combustion. The included minerals can experience conditions which are different (oxidation and reduction) in comparison with the excluded minerals or organically-bound cations. Being associated with carbon, the included minerals can interact with each other at elevated temperatures under more reducing conditions and result in artifact compounds (new aluminium silicate minerals).

Buhre et al. (2005) found that the ash formed from the coalescence of the included mineral is significantly affected by size, type and distribution of the included mineral. During the combustion of the pulverised coal at elevated temperatures, the flame of the burning char particles caused the included minerals to turn viscous and coalesce, due to melting of the inorganic matter (Buhre et al., 2005).

As can be seen in Figure 2.3, the excluded mineral fragmentation produced mainly sub-micron to super-micron-sized ash particles, while the last formation mechanism for included minerals in this figure contributes mainly to micron sized ash particles (Quann and Sarofim, 1982). The amount, size and type of excluded minerals determine the extent of excluded mineral fragmentation. The main fragmenting mineral types in Australian black coals are calcite and pyrite (Yan et al., 2001).

Although extensive fragmentation of these minerals has been noted, the bulk of the newly-formed ash particles are generally super-micron in size (Yan et al., 2001; Ten Brink, 1994). The schematic of ash formation mechanisms during pulverised coal combustion is given in Figure 2.3 on the following page.

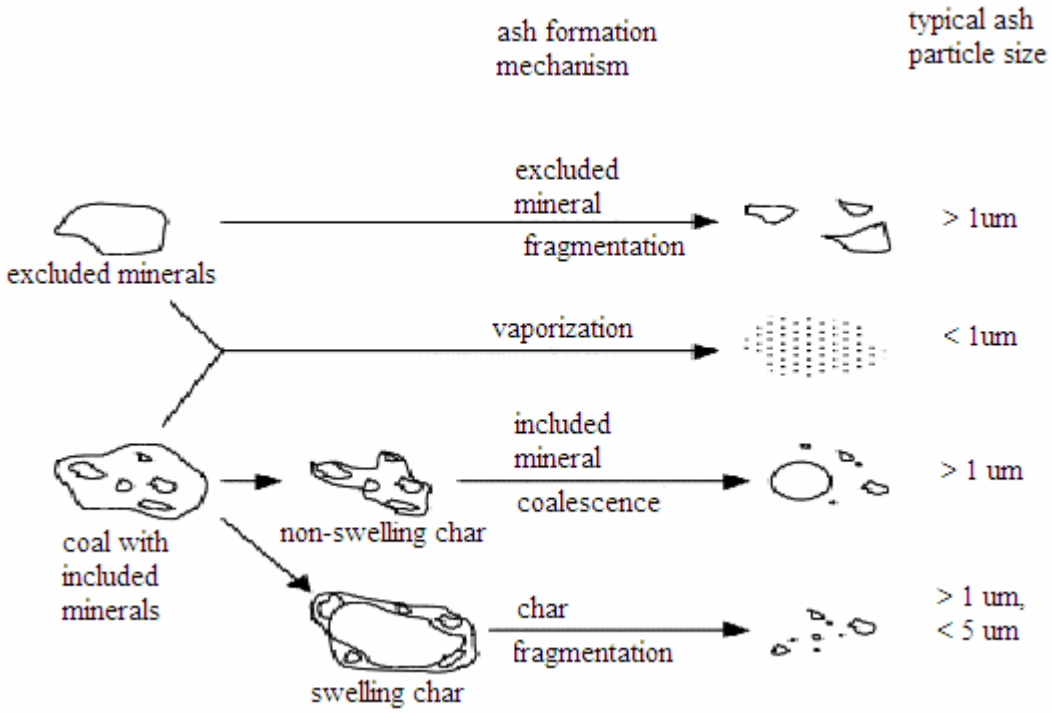


Figure 2.3: Schematic of ash formation mechanisms during pulverised coal combustion (Buhre et al., 2005).

The researchers also found that alkalis, sulphur and phosphorus present in the coal readily vaporise during combustion of coal at elevated temperatures. The extent of vaporisation of the refractory oxides from the included minerals has also been suggested to depend on the size distribution of included minerals containing refractory oxides (Quann and Sarofim, 1982; Eddings et al., 2000; Lee et al., 1990).

2.3 Organic matter in coal

As stated previously, coal is mainly made up of organic matter (macerals). The main objective of this study is to determine which minerals or inorganic constituents are responsible for the sintering of mineral matter at elevated temperatures during coal gasification. Because of this focus, the chemical and physical properties of macerals as well as their behaviour during coal combustion at elevated temperatures are not discussed in detail in this study; only a brief overview follows:

Spackman (1958) defined macerals as organic substances that are contained in coal and have a distinct set of physical and chemical properties.

Macerals are organic components of coal that are closely analogous to the role of minerals in rocks. Macerals and minerals both have reasonably specific physical and chemical properties, and their relative proportions then determine the characteristics of the rock. Spackman (1958), Crelling and Dutcher (1980), Ward (1984) and Gurba (1998) mentioned that coal macerals are divided into three groups:

- Vitrinite group
- Liptinite group
- Inertinite group

Vitrinite group:

Vitrinite is derived from the cell wall material or woody tissue of plants and is the most abundant group that makes up 50-90% of most North American coals (Grelling and Dutcher, 1980). The South African low-rank bituminous coals contain 14-90% vitrinite (Pinheiro et al., 1998-1999). These macerals have reflectance between that of liptinite and inertinite.

Liptinite group:

Liptinite is derived from the waxy and resinous parts of plants such as spores, cuticles and wood resins. These macerals make up about 5-15% of most North American coals. Some of the South African coals contain 2-8% liptinite (Pinheiro et al., 1998-1999). These macerals disappear from coal at a reflectance of 1.35-1.40. They are characterised by significantly higher hydrogen concentration and a high proportion of volatile matter.

Inertinite group:

Inertinite is derived from plant material that has been strongly altered and degraded in the peat stage of coal formation. North American coals contain inertinite macerals in the range of 5-40% and have highest reflectance. The South African low-rank bituminous coals contain 3-28% reactive inertinite and 20-57% inert inertinite (Pinheiro et al., 1998-1999). In the polished section they appear white and opaque and are characterised by significantly higher carbon content and lower hydrogen content in comparison with other macerals in coals of the same rank (Chandra and Taylor, 1982; Ward, 1984).

According to Chandra and Taylor (1982), minerals and macerals present in coals are not significantly transformed at temperatures less than 300°C. However, vitrinite and liptinite macerals could start to deform because of high local stresses during the intrusion process.

They clearly indicated that both vitrinite and liptinite macerals undergo significant petrographic changes at different temperatures (in the range of 300-500°C); in most coals evaluated in their studies the petrographic structure is lost at about 400-500°C. At 500°C structures of liptinite macerals decompose completely and can no longer be recognised. However inertinite does not undergo decomposition during thermal metamorphism below 300°C; its structure starts to change minimally even above 300°C (Chandra and Taylor, 1982).

Gurba (1998) found that liptinite macerals contained a significantly higher proportion of organic sulphur in comparison with the remaining macerals (vitrinite and inertinite). The order for organic sulphur is liptinite > vitrinite > inertinite. No trends were found between the coal rank and organic sulphur determined by electron microprobe. Electron microprobe analysis for samples of coals collected from Sydney-Gunnedah Basins in Australia indicated that Si and Al, which are associated within the organic fraction in coals, are present in macerals (Gurba, 1998).

2.4 Volatilisation of organic sulphur and organically-bound cations

According to Reid (1981), Given (1984), Benson and Holm (1985) and Benson (1987), organic sulphur present in the coal decomposes at high temperatures to first form sulphur dioxide, possibly followed by the formation of sulphur trioxide at a temperature lower than 500°C, under oxidation conditions. Alkali and alkaline earth species present in the fly ash particles formed during combustion of the coal, can preferably interact with the sulphur oxides at approximately 560°C, to form alkali or alkaline earth sulphate (Reid, 1981; Benson, 1987).

Sodium or potassium present in either metallic salts of carboxylic acids, or dissolved in the pore waters, may volatilise in the form of oxides or halides during gasification and combustion. According to Raask (1986), sodium and potassium can react with sulphur from the organic suphur compounds present in the coal under the reducing conditions to form sodium sulphide and potassium sulphide. Hydrogen sulphide can also be formed under reducing conditions. Subsequent to the oxidation of the formed sulphides, sodium sulphate can react with meta-kaolin and coal ash at elevated temperatures to form liquid (Raask, 1986).

Raask (1985) indicated that the temperature and residence time of the ash particle in the flame affect the distribution of volatile sodium between silicate components of the ash and sulphate. Transformed sodium or potassium reduces the viscosity of the molten silicates, resulting in an enhanced rate of sintering.

Wibberley and Wall (1982) found that volatile sodium from the coal reacted directly with silicon-bearing minerals as well as organic sulphur at elevated temperatures, to form sodium silicate and sodium sulphate respectively. In their studies, quartz (pure silica) and silicon-containing minerals in the coal were separately added into a vertical tube furnace and heated to a temperature greater than 1200°C. The results revealed that the formation of sodium sulphate and sodium silicate is sensitive to temperature. Sodium silicate is found to be relatively more stable than sulphates at temperatures from 1200°C to 1600°C. Sodium sulphate is more stable below approximately 1100°C (Wibberley and Wall, 1982).

Attalla et al. (2004) found that trace elements present in the coal volatilise differently during combustion or gasification processes, depending on their modes of occurrence. The trace elements can be classified into three groups as shown in Table 2.3.

From Table 2.3 it is clear that some elements occur in more than one group. The authors suggest that differences in mode of occurrence, operating process conditions (including partial pressure of oxygen, temperature and differing pollution control devices) are most likely responsible for the overlapping of elements between groups. Those elements (As, Cd, Co, Mo, Pb, Se, W and Zn) that have a strong affinity for sulphur (chalcophile), are claimed to be the most readily vaporised as hydrides, halides or metal carbonyls during combustion (Quann et al., 1990). The trace elements listed in Group 1 in Table 2.3 support this (Quann et al., 1990). Those elements (Be, Co, Cr, Cs, Ga, Hf, Li, Rb, Ti, V and Zr) that have a strong affinity for oxygen (lithophile), are expected to coalesce with the aluminosilicate melt (Quann et al., 1990).

Table 2.3: Trace element partition classification after Clarke and Sloss (1992)

Group 3:
Highly volatile, at least partially enriched in the gas phase, depleted in the condensed phases: Hg, Rn, Br, Cl, F, B, Se, I
Group 2:
Volatile, which are enriched in the fly ash, depleted in bottom ash:
B, Se, I, As, Cd, Ga, Ge, Pb, Sb, Sn, Te, Tl, Zn, Ba, Be, Bi, Co, Cr, Cs, Cu, Mo, Ni, Sr, Ta, U, V, W
Group 1:
Low volatility, being evenly distributed between bottom ash and fly ash:
Ba, Be, Bi, Co, Cr, Cs, Cu, Mo, Ni, Sr, Ta, U, V, W, Eu, Hf, La, Mn, Rb, Sc, Sm, Th, Zr

Neville et al. (1981) found that the majority of Mg, Na and Ca that are organically-associated with the organic fraction in the low rank coal was vaporised at 1527°C and produced a sub-micron fume totaling 1.9-9.6wt% of the ash.

Srinivasachar et al. (1990a, b) suggested that refractory metal oxides (including silica) react with carbon at an elevated temperature of 1727°C to form volatile sub-oxides. The sub-micron fraction of the included minerals, being well dispersed within the coal matrix, is most likely the source of those sub-oxides. The results from the experiments with mixtures of finely ground silica and excess carbon in a graphite crucible heated in argon, indicated that substantial volatilisation of silica occurred above 1230°C. It was estimated that for a typical pulverised coal-fired boiler, approximately 1 wt% of the total silica is volatilised in the flame (Srinivasachar et al., 1990a, b). Unlike included minerals under reducing conditions, the excluded minerals experience oxidising conditions at elevated temperatures of greater than 1200-1400°C, fuse and limit the extent of volatilisation of excluded minerals severely.

2.5 Determination of mineral matter (non-minerals and minerals) in coals

As mentioned previously in section 2.1, coal contains both mineral matter and organic matter that play a significant role during mineral transformation at elevated temperatures during coal combustion. A number of different analytical techniques have been utilised to determine concentrations of mineral matter, as well as modes of occurrences of the inorganic species present in coals (Gluskoter, 1965; Miller et al., 1979; Ward, 1986, 1999, 2002; Ward and

French, 2004; Kiss and King, 1977; Miller and Given, 1978; Kiss, 1982; Benson and Holm, 1985). In this thesis techniques that are available for qualification and the quantification of mineral matter in coals are briefly discussed.

2.5.1 Determination of the concentration of mineral matter in coals by oxidation of the organic matter in coals

A number of authors (Gluskoter, 1965; Miller et al., 1979; Ward, 1986, 1999, 2002; Ward and French, 2004; Foscolos et al., 1989) used low-temperature oxygen-plasma ashing (LTA) to oxidise organic matter present in coals at low temperature, without altering the coal minerals. In low-temperature oxygen-plasma ashing, the activated oxygen produced from a radio-frequency oscillator is passed over the pulverised coal particles to selectively oxidise all organic matter at temperatures in the range of 120-150°C, without decomposing the inorganic minerals. They found that the colour of the ash produced at low temperature is grey, indicating that the oxidation process is complete. This technique gave reliable results of the concentration of mineral matter present in higher-rank coals (Frazer and Belcher, 1973; Standards Australia, 2000). A schematic representation of LTA apparatus is given in Figure 2.4.

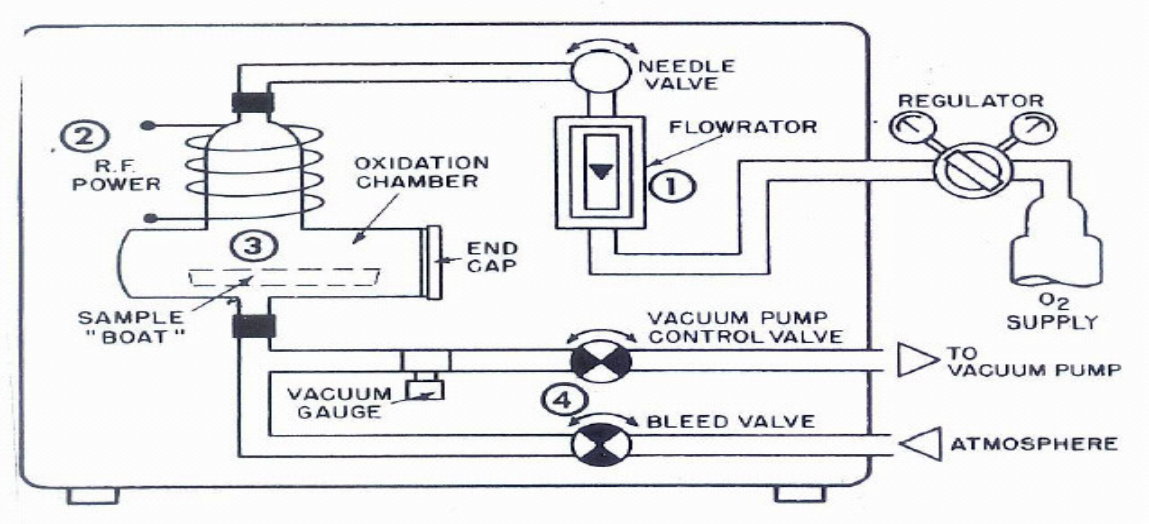


Figure 2.4: Schematic diagram of low temperature asher.

In some cases, the organically-associated inorganic elements in the coal may also interact with each other during plasma ashing to form new minerals (Given, 1984; Benson and Holm, 1985).

The organically-bound elements such as Ca, Mg and Na can also react with organic sulphur to form trace artifact compounds such as bassanite ($CaSO_4.1/2H_2O$), kieserite ($MgSO_4.H_2O$) and thenardite (Na_2SO_4) (Given, 1984; Benson and Holm, 1985).

Other trace minerals (potassium alum ($KAl(SO_4)_2.12H_2O$) and metabasaluminite ($Al_4SO_4(OH)_{10}$) that are also suggested to be artifacts of the plasma ashing process, were detected by XRD (Ward, 1991). Foscolos et al. (1989) found that the low-temperature ash (LTA) from the untreated Greek lignite coal contained ammonium-iron sulphate.

Brown et al. (1959), Nelson (1953), Ward (2001a) and Hicks and Nagelschmidt (1943) heated coal samples to 370°C in the presence of air, to oxidise the organic fraction in the coal prior to the determination of the mineral matter. From their studies they found that coal minerals including siderite, other clays and pyrite start to decompose and result in the alteration of their crystal structures. As a result of mineral decomposition during heating of coal at 370°C, the mass percentage of ash remaining after heating gave unreliable results of the mineral matter content in coals tested.

Nawalk and Friedel (1972) and Ward (1974) noted that the use of hot, concentrated hydrogen peroxide to oxidise organic matter has a negative impact on the crystal structure of carbonates in coals. They suggest that carbonate minerals present in the coal sample dissolve in the organic acids that formed when hydrogen peroxide reacted with organic matter during the oxidation process. Pyrite may also cause spontaneous decomposition of the peroxide and cessation of oxidation. Due to the inevitable reactions between minerals and peroxide, the use of hot peroxide to remove organic matter is not a suitable alternative method for the determination of mineral matter in coals.

2.5.2 Mineral matter determination by chemical analysis

Radmacher and Mohrhauer (1955) used a solution of mineral acid (hydrochloric and hydrofluoric acids) to digest mineral matter present in a high-rank coal sample. The coal sample was weighed before and after digestion with the mineral acids. They concluded that the proportional mass loss represented the content of the mineral matter contained in the coal sample.

The percentage of mineral matter in coals can also be determined by calculation, using the combination of the ash yield of the coal and the proportions of other key inorganic constituents in the coal samples. The simple formulae that were proposed by Parr (1928) and King et al. (1936), are based on the coal's ash yield and total sulphur content and are applied for calculating the concentration of mineral matter from other analytical data. The formula of Parr (1928) was modified to include pyritic sulphur and chlorine, rather than just the total sulphur content (Given and Yarzab, 1978). In the formula of King et al. (1936), known as the King-Maries-Crossley expression or KMC, the carbonate carbon, chlorine, pyritic and sulphate sulphur contents of the coal and the proportion of sulphur retained in the coal ash, as well as the percentage of ash are used to determine the proportion of mineral matter contained in the coal sample. The two formulae are given in Table 2.4.

Table 2.4: Formulae for calculating mineral matter percentages from other analytical data

Parr formula

$MM = 1.08\ A + 0.55\ S$ (original version) (Parr, 1928) (2.2)

$MM = 1.13\ A + 0.47\ S_{pyr} + 0.5\ Cl$ (modified version) (Given and Yarzab, 1978) (2.3)

King-Maries-Crossley (KMC) formula

$MM = 1.13\ A + 0.5\ S_{pyr} + 0.8\ CO_2 + 2.85\ S_{SO4} - 2.85\ S_{ash} + 0.5\ Cl$

(King et al., 1936) (2.4)

Where:

MM	= percentage of mineral matter in coal
A	= percentage ash yield from coal
CO_2	= percent carbonate carbon dioxide yield from coal
S_{pyr}	= percent pyritic sulphur in coal
S_{SO4}	= percent sulphate sulphur in coal ash
S	= percent total sulphur in coal
Cl	= percent chlorine in coal
S_{ash}	= percent total sulphur in ash

2.5.3 Determination of the non-mineral inorganics in low-rank coals using a chemical fractionation technique

A chemical fractionation technique which was developed by Miller and Given (1979) and later modified by Benson and Holm (1985) was used to quantify the concentration of non-

mineral inorganics such as ion-exchangeable cations, acid-soluble elements and insoluble elements in coals. In the chemical fractionation method, water is used in the first leaching step to selectively remove elements that dissolved in pore waters during coalification (Ward, 1991; Ward and French, 2004). The water-leached coal is then treated with ammonium acetate to extract exchangeable ions from carboxylates within the organic matter. In the last step of the selective leaching, a solution of hydrochloric acid is used to dissolve all the elements present in metallic salts of carboxylic acids or chelates within the coal. The leached residual coal was ashed by a low-temperature oxygen-plasma asher, without decomposition of minerals present in the original coal. Ward (1991) used chemical fractionation to investigate non-mineral inorganics present in Mae Moh coal samples.

The flow diagram for selective leaching of Mae Moh coal samples is given in Figure 2.5.

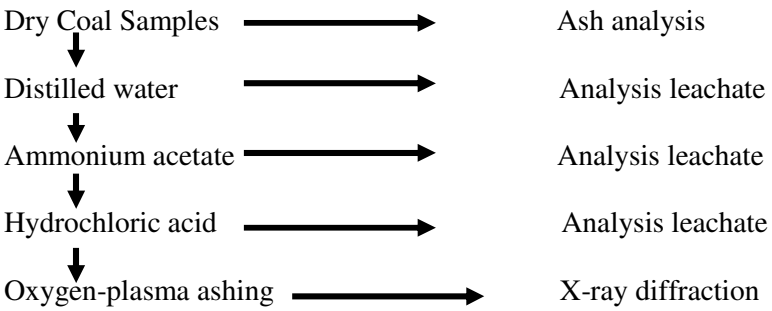


Figure 2.5: Selective leaching scheme used for analysis of Mae Moh coal samples (Ward, 1991).

From results given in Table 2.5, it is clear that the majority of sodium present in the coal sample dissolved in distilled water when water was used as the lixiviant during the sequential leaching step testing. This implies that most of the sodium ions dissolved in the pore water within the coal (Ward, 1991). Results also revealed that calcium occured mostly in ion-exchangeable form (possibly associated with carboxylate compounds and partly in the pore waters and an acid-soluble form). High proportions of sulphur and iron reported to the leached residual coal samples after the selective leaching steps. This suggests that iron and sulphur occur as mineral (pyrite).

The chemical fractionation results reported by Benson and Holm (1985) showed that significant amounts of Ca, Mg and Na present in the lignite coal samples dissolved in ammonium acetate solution during leaching experiments.

Miller and Given (1978), Benson and Holm (1985) and Benson (1987) concluded that the majority of these elements occur in ion-exchangeable form in the lignite coal samples.

Table 2.5: Proportion of selected elements in Mae Moh coals released by different leaching steps (Ward, 1991)

Elements	% elements removed by water	% elements removed by ammonium acetate	% elements removed by hydrochloric acid	% insoluble in the leached coal
Na	75.10	20.90	8.50	0.00
Ca	30.70	43.60	25.00	0.10
Fe	0.10	0.00	44.80	55.00
S	19.40	1.40	1.50	77.70

Results given in Table 2.6 are for the oxidised Mae Moh coal from Thailand. Pyrite was found in most samples to be partially oxidised during storage prior to chemical fractionation experiments. It can be seen that the oxidised coal contained significantly higher proportions of water-soluble S, Fe and Ca in comparison with the unoxidised coal (Tables 2.5 and 2.6). Ward (1991) suggested that sulphuric acid, formed during oxidation of pyrite, reacted with calcium from carbonate minerals and iron from the oxidised pyrite during the selective leaching steps.

Table 2.6: Proportion of selected elements in Mae Moh coals released by different leaching steps after pyrite oxidation (Ward, 1991)

Elements	% elements removed by water	% elements removed by ammonium acetate	% elements removed by hydrochloric acid	% insoluble in the leached coal
Na	45.60	9.40	29.40	15.60
Ca	73.30	11.50	5.00	10.20
Fe	20.70	0.00	38.60	40.70
S	37.00	2.70	5.90	54.40

As mentioned earlier, low-rank coals contain high concentrations of organically-bound cations in comparison with high-rank coals (Miller and Given, 1978; Benson and Holm, 1985; Benson, 1987; Ward, 1991).

In this study it is suggested that metallic salts of carboxylic acids present in coal will release small amounts of elemental Ca, Na or Mg that may react with some aluminium silicates and assist in lowering the melting points of these silicates.

The organically-bound cations, inorganic elements dissolved in the pore waters as well as dissolved salts interact with each other to produce trace artifacts in low-temperature plasma ashing of higher-rank coals. The chemical fractionation technique (coupled with low-temperature ashing of the coal) significantly improves the accuracy of the mineral matter content in lower-rank coals than just using the direct application of low-temperature ashing techniques (Ward et al., 2001a). Although the leachates produced from CHF experiments done by Ward (1991) were not submitted for Cl analysis, the only major mode of occurrence of chlorine according to Huggins and Huffman (2004), is in the form of chloride in the moisture associated with the macerals in coal. Chlorides can readily volatilise from coals during heat treatment.

2.5.4 Proximate analysis of coal

Proximate analysis is a routine analytical method which is used to determine the relative amounts of light organic compounds (volatile matter) and fixed carbon (non-volatile organic material) present in coals. It is also used to quantify the amount of moisture in the coal, and gives a measure of the inorganic components that are left as a residue or ash after the burning off of the organic matter from the coal (SABS 924, ISO 589), ash content (ISO 1171) and volatile matter (ISO 562).

Volatile matter in the coal represents light organic components, excluding the moisture content, released from either the organic matter or mineral matter when coal is heated at an elevated temperature under oxidising conditions (Ward, 1984). If the concentration of volatile material in the coal is to be utilised to classify coals for a particular application, correction for that derived from inorganic sources (carbonates and clays) must be made in order to obtain accurate results (Ward, 1984). The determination of the concentration of volatile matter in coals involves heating the coal under rigidly specified conditions. The standard methods required for the determination of volatile matter content in coal vary from one country to another. According to the A.S.T.M. (1979), the coal sample must be transferred into a platinum crucible in a vertical electric furnace, and heated to 950°C.

However, for British and Australian Standards, coal must be added to the cylindrical silica crucible in a muffle furnace of specified conditions and heated to 900°C for 7min (Standard British, 1973; Standard Australian, 1979). The results for the same coal, using different procedures from various countries, give slightly different results. A modified A.S.T.M. procedure, involving two stages, of heating, is essentially required for low rank coal or sparking coals in order to improve the accuracy of the results (Ward, 1984).

Coals contain four possible forms of moisture, namely: (1) surface water (extraneous water) which is held as films on the surface of coal particles; (2) hygroscopic moisture (water inside the capillaries of the coal substance); (3) decomposition water (water which is incorporated in some of the organic compounds) and (4) mineral moisture (water of crystallisation that is bonded to clay in the coal). The total moisture content of the sample is the difference between the mass of the sealed sample as received from the mine or stockpile and the dry sample (Ward, 1984).

The following known methods can be used to fully dry samples from the mine in order to determine total moisture in coals (Ward, 1984):

A known mass of the sample is dried at 105-110°C in a minimum free-space oven in the presence of the flowing nitrogen and a relative mass is obtained. This method is suitable for the determination of the total moisture as well as the inherent or air-dried moisture in coals of all ranks. It is possible that samples of low-rank coals may undergo oxidation during heating.

For the determination of the moisture content of high-rank coals, a known mass of coal as received in the laboratory is heated to 105-110°C in a laboratory oven in the presence of air and the relative loss of mass is determined.

When coal is heated at elevated temperature in the presence of air or oxygen, the organic fraction of the coal is released as carbon dioxide and water vapour, while mineral matter transforms to form the non-combustible inorganic residue which is termed ash. Ash makes up a smaller mass fraction of coal in comparison with mineral matter concentration (Ward, 1984).

In coal utilisation, coals with low ash content are preferable to coals with a high ash proportion. A smaller amount of ash in the coal will need less energy when compared with coal with greater mass of high ash material, during either the combustion or gasification process. In addition, a smaller amount of waste (ash) will be generated from the low-ash coal combustion or gasification process.

During the determination of ash present in the coal, both the specified temperature and time are required to obtain accurate ash content.

Methods that are employed for the determination of ash content in coals are as follows:

In British and Australian practice, a known mass of the sample of coal to be analysed is heated slowly from room temperature to 815°C until a constant mass of ash (non-combustible residue) is attained (Standard British, 1973; Standard Australian, 1979). In some cases, two stages of heating, namely: using the temperature of 500°C for a certain period of time and then heating coal at 815 °C in the second furnace, are needed.

In America, the nature of the minerals present in the coal sample determines the type of procedure that is suitable for the determination of ash content present in the coal (A.S.T.M., 1979). For calcite and pyrite-rich coals, a two-stage process is required in order to prevent the reaction between sulphur, calcium and aluminium silicate forming mineral artifacts in the ash. In this procedure, coal particles are slowly heated to 500°C for 1h; then to 750°C for 2h, and kept at 750°C until the mass of ash formed during heating becomes constant.

Carbon retained in the coal material after the removal of the volatile matter is termed the fixed-carbon. For the production of coke from the coal, the fixed carbon content is used as an index or as the indicator of the solid combustible material that remains in coal-burning equipment after the volatile matter has been removed (Ward, 1984). For the classification of coals, the fixed carbon can also be used as an index of the coal rank. There is no direct analytical procedure that is used to determine the concentration of fixed carbon present in the coal.

The formula for the calculation of the percentage of fixed carbon (FC) in coals is as follows:

$$FC = 100 - (\text{moisture content} + \text{volatile matter content} + \text{ash content}) \quad (2.5)$$

2.5.5 Ash analysis

The proximate analysis, which was fully described in Section 2.5.4, shows the ash content present in the coal sample, but it does not indicate the elemental composition of the inorganic species in the ash.

Coal ash obtained during the combustion of coal at elevated temperatures consists almost entirely of the transformed aluminium silicate products, quartz and trace amounts of the untransformed or partially oxidised coal minerals including carbonates, sulphides, etc. (Ward, 1984). The analytical techniques including Atomic Absorption Spectroscopy (AAS), Inductively Coupled Plasma (ICP), X-ray Fluorescence Spectroscopy (XRF) and Optical Emission Spectroscopy (OES) are used to quantify elements present in ash. Coal ash typically contains Fe, Al, Mg, Mn, V, Ti, Si, Ca, Na, K, P, S and Cr and is reported as oxides (Fe_2O_3, Al_2O_3, MgO, MnO, V_2O_3, TiO_2, SiO_2, CaO, Na_2O, K_2O, P_2O_5, SO_3 and Cr_2O_3). The chemical composition of coal ash is used to predict the types of minerals present in coal ash, to calculate the fouling factor and slagging factor for the determination of fouling and slagging propensity of coals (Ward, 1984; Benson, 1987 and van Alphen, 2005). The metal oxides can also be used in the calculation of the iron index, slagging index and acid base ratio.

The following slagging indices, which are generally based on ash elemental analysis (oxide - %) and ash fusion temperature are used to predict the slagging propensity of a coal:

- Base/Acid ratio (B/A)

$$B/A = \frac{Fe_2O_3 + Na_2O + K_2O + CaO + MgO}{SiO_2 + Al_2O_3 + TiO_2} \quad (2.6)$$

- Slagging factor (R_s)

$$R_s = B/A * \% TS \quad (2.7)$$

%TS = Total Sulphur

Other factors that contribute significantly to the slagging of mineral matter during coal combustion were developed by Attig and Duzy (1969). He found that the developed slagging factor worked quite well for Eastern coals produced from the USA but was not applicable to Western coals.

- Iron Index (F_i)
- $F_i = \%Fe_2O_3 * B/A$ (2.8)

Attig and Duzy (1969) developed a fouling index relating the ash composition to the formation of deposit in the boiler during coal combustion of Eastern coals.

The fouling factor, which is termed, R_{Fi} is given as:

R_{Fi} = (B/A) * %Na_2O (based on A.S.T.M. ash). (2.9)

Attig and Duzy defined an additional fouling factor, after including sodium emanating from minerals that is likely to volatilise in the flame during heating. It is given by:

R_{Fi} = (B/A) * % water soluble Na_2O.

2.5.6 Determination of minerals in coal and coal ash by X-ray diffraction (XRD) analysis

X-ray diffraction is an established technique which is used to qualify and quantify crystalline phases that are made up of atoms or molecular groups arranged in a regular three-dimensional pattern in solids. Minerals present in solids can be characterised by their unique combination of atoms and molecules, as well as their unique d-spacings. XRD has the capability for measuring d-spacings of the individual mineral present in the solid sample from the combination of internal planes in mixtures (Ward and French, 2004). During XRD analysis of the pulverised solid samples, an X-ray detector (scintillometer) measures the intensity of the diffracted rays from the powdered sample with a smooth surface of even texture, which has been placed in a flat holder at the centre of the rotating goniometer at 2θ to produce a diffractogram. The XRD pattern obtained in this way is matched with the pattern of the reference or standard mineral, in order to identify the mineral present in the sample.

The XRD techniques can produce results of higher accuracy for coals if it is applied to low-temperature ash samples with high concentrations of minerals produced from the coal by low-temperature oxygen-plasma ashing, described previously in Section 2.5.1. (Gluskoter, 1965; Miller et al., 1979; Ward, 1986, 1999, 2002; Ward and French, 2004; Foscolos et al.; 1989). Although some mineral artifacts are formed in the LTA sample during oxygen-plasma ashing, a sample of LTA contains high proportions of minerals that will provide reliable results of minerals during XRD analysis. Also, it has no signs of organic matter that can dramatically affect the quality of the XRD results (Glukoter, 1965; Miller et al., 1979; Ward, 1986, 1999, 2002; Ward and French, 2004; Foscolos et al., 1989).

A number of researchers have developed several methods to determine the proportions of minerals in the coal and ash samples using the XRD technique (Rao and Gluskoter, 1973; Ward, 1977, 1978, 1989; Russell and Rimmer, 1979; Renton, 1986).

Klugg and Alexander (1974) added a known mass of the internal standard (spike) to the LTA sample produced from the coal sample by oxygen-plasma ashing, and subsequently compared the intensity of the sample peaks with the intensity of the peaks of the spike added. In addition, the distribution of dominant minerals present in the individual coal seams of the Illinois Basin, USA was studied by Rao and Gluskoter (1973), Ward (1977) and Harvey and Ruch (1986) using the XRD data for the spiked LTA samples and clay-fraction concentrates.

In their studies they found that a calibration curve for each mineral component needs to be prepared prior to evaluation of minor minerals in the spiked samples. They suggested that variations in methodology, as well as differences in crystallinity of the mineral, preferred orientation in the sample mount, as well as differential absorption of X-rays by minerals in the mixture may significantly affect the quality of the diffractogram of the sample. This may also result in substantial variations in the estimated percentages of minerals in the same analysed samples. In their conclusion they proposed that a standard quantitative XRD procedure for the determination of the concentrations of minerals in the LTA sample is required in order to obtain accurate results from the different laboratories.

Rietveld (1969) developed a technique for using the full profile XRD pattern of X-rays to refine the crystal structure of a mineral or other crystalline phase in the samples with the advent of a computer-based data collection and processing system. His approach has been used more recently to evaluate the concentrations of minerals in a powdered mineral mixture. Extension of Rietveld methodology allows a calculated XRD profile of each mineral phase to be generated from its refined crystal structure and the sum of all calculated patterns to be fitted to the observed XRD profile of a multi-mineral mixture by least-squares analysis to find the optimum phase scales. The optimum phase scales obtained in this way are subsequently used in the determination of the proportion of different minerals contained in the analysed sample (O'Connor and Raven, 1988; Taylor, 1991; Bish and Post, 1993; Ward and French, 2004).

A personal computer software system which is referred to as SIROQUANT® was described by Taylor (1991). SIROQUANT® uses X-ray diffraction patterns and Rietveld techniques to quantify the proportions of up to 25 different minerals contained in the mixture form.

Different crystallographic parameters for each mineral present in the sample are simply interactively adjusted within the programme to produce diffraction patterns of high quality, and also to allow for variations due to atomic substitution, laying disorder, preferred orientation and other factors in the standard pattern used. For the application of SIROQUANT® analysis, a library of XRD files that contains expected minerals in the sample must be prepared; in some cases the high level of background radiation caused by the organic matter needs to be removed from the diffractograms of samples (Taylor, 1991).

2.5.7 Determination of the glass content and glass composition in coal ash using X-ray diffraction techniques

The XRD analysis combined with other quantitative methods can be applied to quantify not only the crystalline phase, but also the non-crystalline, amorphous or glassy phases that are typically present in the coal ash and slag samples (Ward and French, 2004). Coal ash contains dominant components of non-crystalline aluminosilicate glass, crystalline minerals (quartz, mullite, anorthite, etc.) and to a lesser extent unburnt carbon particles.

The majority of glass which is the major component of coal ash, is highly reactive and is used in chemical reactions such as the pozzolanic reaction in cement or zeolite production. In some other cases of coal ash utilisation including soil/plant waste stabilisation, glass significantly enhances the retention of trace elements through encapsulation or adsorption during leaching. Although the glass in ash has the capability of adsorbing some trace elements that may have a negative impact on the environment, glass in ash may also be expected to break down with prolonged exposure, releasing elements that can be leached into surrounding environmental systems (Ward and French, 2004).

Ward and French (2004) developed a method for the determination of the glass content and composition using the XRD results, SIROQUANT® software, XRF analysis and stoichiometry of the crystalline phase in the ash sample, where glassy material humps (broaden pattern) in the diffractrograms indicate the presence of glass or amorphous material.

A SIROQUANT® system has the capacity to determine the concentrations of crystalline phases as well as the proportion of amorphous or non-crystalline material contained in the coal ash. To obtain the results for amorphous material using SIROQUANT®, the evaluation of

the diffractograms produced from the powder ash samples with a known concentration of the crystalline spike, must be done (Ward and French, 2004).

In conclusion, routine SIROQUANT® processing can be used to determine the percentages of the spike added to the XRD traces along with the other crystalline components. The proportion of all the crystalline components including the spike is normalised to 100%. If the sample contained a significant proportion of amorphous material, the concentration of the spike in this normalised estimate will be higher than the proportion of the spike added before XRD analysis (Ward and French, 2004).

Ward and French (2004) found that the chemical composition of the bulk ash obtained by XRF analysis, the weight abundances of the crystalline phases as well as knowledge of the stoichiometric chemistry of the phases that were identified by XRD, can be used to determine the overall chemical composition of glass contained in the coal ash sample. The concentration of the unburnt carbon in the coal ash was not included in the calculation of the glass composition when using the normalised results for the coal samples studied. The electron microprobe results for identified minerals can be used in the calculation of glass composition, instead of using the assumed stoichiometric compositions of minerals.
A flow sheet for the estimation of glass composition for fly ash from bulk chemistry and quantitative XRD results is shown in Figure 2.6.

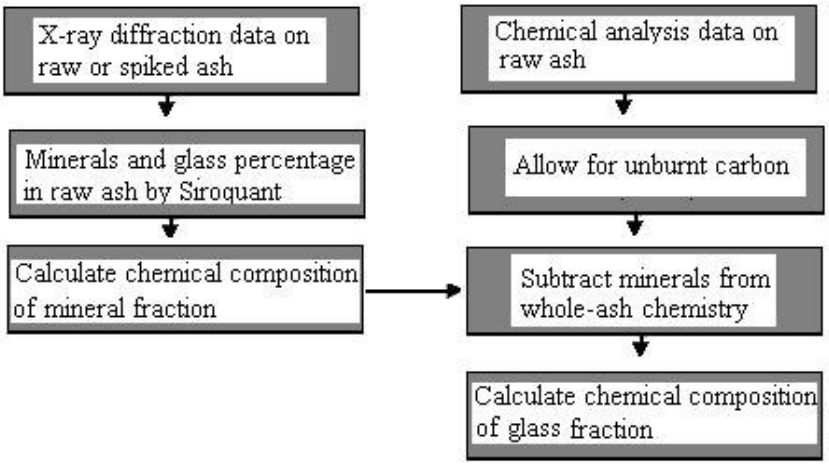


Figure 2.6: Estimation of glass composition for fly ash bulk chemistry and quantitative XRD data (Ward and French, 2004).

During the coal combustion or gasification process, it is imperative to better understand the mineral matter behaviour at elevated temperatures and pressures in order to manage the

clinker formation in the boilers or gasifiers, as well as the fouling problem. Traditionally, the slagging or fouling indices that are based on the elemental oxides, thermodynamic modeling based upon the ash chemistry, or direct examination of the end products, either from the gasifier or the boilers, are used to better understand the mineral matter behaviour at elevated temperatures (Ward, 1984; Ward and French, 2004). Dynamic high-temperature X-ray diffraction analysis in conjunction with SIROQUANT® can be used to study coal mineral matter reactions at elevated temperatures under both oxidising and reducing conditions (French et al., 2001; Ward and French, 2004). In addition, the proportions of crystalline phases, amorphous materials (solid and liquid) formed during high temperature X-ray diffraction analysis, can also be qualified and quantified.

2.5.8 Mineral matter qualification and quantification by scanning electron microscopy (SEM)

Scanning electron microscope techniques can be applied to either polished sections of coals or broken coal surfaces to determine mineral matter contained in the coal samples (Creelman and Ward, 1996; Ward and French, 2004). A scanning electron microscope with a light element energy dispersive spectrometer (EDS) and a back-scattered electron (BSE) detector provides comprehensive chemical composition and imaging of the selected individual mineral grains in the polished sections of coals (Creelman and Ward, 1996; Ward and French, 2004).

A combination of SEM and image analyser (computer controlled scanning electron microscopy, CCSEM) is used to evaluate the nature and distribution of minerals in the coal sample (Straszheim and Markuszewski, 1990; Galbreath et al., 1996; Gupta et al., 1999). The CCSEM technique is widely applied for the determination of association, size, composition and abundance of minerals contained in the coal sample which is used in various processes, including combustion and gasification. In the CCSEM analysis, the electron beam is stepped across the selected polished sections in an SEM operating in back-scattered electron (BSE) mode, to evaluate minerals present in the selected coal grains. The size of mineral identified is then measured from the geometry of the selected area with an elevated BSE signal, and subsequently the energy-dispersive X-ray spectrum is acquired from the centre of the selected area. The particles from the selected area are classified into several mineral categories in accordance with the relative abundance of the detected elements. In order to determine percentages of the different minerals present in the coal, the volumetric and weight

proportions of the different minerals are calculated (Straszheim and Markuszewski, 1990; Galbreath et al., 1996; Gupta et al., 1999).

Creelman and Ward (1996) noted that the QEM*SEM (quantitative evaluation of materials by scanning electron microscopy) technique can be used for determination of the association of the chemical elements at the individual analysis points on a coal polished section from the output of several X-ray analysers directed at each point in a controlled scan under the SEM. QEM*SEM which was originally designed to determine the proportions of base and precious metals in ores for the mining industry, can also be used to measure size and shape distributions of mineral particles present in the coal. QEM*SEM was modified by Commonwealth Scientific and Industrial Research Organisation (CSIRO) of Australia and is termed QEMSCAN. This equipment can be used in coal utilisation to determine mineral-mineral associations, particle size, mineral compositions and texture of particles in the coal samples (Creelman and Ward, 1996).

2.5.9 Chemical composition of mineral matter and organic matter by electron microprobe (EMP) techniques

The electron microprobe technique is an accurate method that is used to determine the chemical compositions of minerals in coals. As an example, Patterson et al. (1994, 1995) applied electron microprobe techniques for the determination of the chemical composition of different carbonate mineral phases in a range of Australian coal seams. In their studies they found that Australian coals contain pure siderite, pure calcite and dolomite. In some cases siderite was found contaminated by significant amounts of Mg and Ca; ankerite was contaminated by significant amount of Fe. It was found that the presence of Mg and Ca in the siderite is possibly attributed to the deposition of the initial minerals (ferroan, dolomite and ankerite) during plant permineralisation associated with the Foord seam in Canada (Zodrow and Cleal, 1999).

Although the electron microprobe technique is a powerful tool for quantification of inorganic elements that are present on the surfaces of different minerals, this technique can also be applied for determination of chemical proportions of both light organic elements and inorganic elements in the organic matter (macerals) in coals. Bustin et al. (1993), Bustin et al. (1996), Gurba (1998) and Mastalerz and Gurba (2001) applied special analytical techniques

for determination of direct light-element concentrations present in the individual macerals in the coal polished sections using the electron microprobe.

These techniques can also analyse sub-micron particles of the inorganic elements that are intimately associated with organic fraction (macerals) in the coal. In some cases, these researchers found that significant proportions of organically-bound calcium, sulphur, aluminium, iron and silicon occur as exchangeable ions attached to carboxylates and elements in metallic salts of carboxylic acids, are present in the different macerals (Bustin et al., 1993; Bustin et al., 1996; Gurba, 1998; Mastalerz and Gurba, 2001). An objective of this present study is to determine the concentrations of the organically-bound inorganic elements in Sasol coals. The determination of the proportions of these elements in coals using electron microprobe techniques may assist in understanding interactions during slagging and fouling.

2.6 Ash Fusion Temperature analysis of coal

It is noted in Section 2.2 that coal consists of not only organic matter, but also of mineral matter which transforms at elevated temperatures to form high-temperature inert metal oxides or ash glass. During the mineral matter transformation at elevated temperatures, the ash fusion of the individual mineral or non-mineral inorganic elements contributes significantly to liquid formation (Ward, 1984; Benson, 1987).

In the laboratory ash fusion temperature test, a cone of ash or a moulded sample of pulverised ash in the form of cube or a pyramid is heated gradually to determine the initial deformation temperature (IDT), softening temperature (spherical) (ST), hemispherical temperature (HT), and fluid temperature (FT) (Ward, 1984; Cumming, 1986). The flow or fluid temperature of the heated ash is reached when the fused ash particles collapse to form a flat button. The temperature values of the above-mentioned temperatures obtained from the ash fusion temperature analysis are critical factors that can be used by the operators or engineers at the combustion or gasification plants to select coals for particular applications as well as to design appropriate boilers or gasifiers.

Huggman and Huggins (1983), Cumming (1986) and Benson (1987) indicated that the ash sample used in the laboratory ash fusibility test had a different chemical composition and particle morphology compared to the fly ash or deposits obtained from the different locations in the boiler.

Variations in the chemical and physical properties of these two samples of ashes result in a discrepancy of the ash fusion temperature values obtained from the laboratory experiments. In addition, Huffman and Huggins (1983) revealed from their research studies that liquid phase formation occurs below the IDT and that the IDT does not represent the solidus temperature.

In most cases, the operators carefully control the operating parameters in the gasification process, including temperature and oxidising agents to manage the physical properties (permeability and particle size distribution) of clinkers. The gasifiers or boilers must be operated at temperatures that are below the bulk melting point of the mineral matter, to avoid massive clinkers or slag. In the present study, the ash fusion temperature was measured as part of coal characterisation.

2.7 Organic matter identification

2.7.1 Ultimate analysis

The ultimate analysis is the fundamental type of routine chemical analysis to determine the concentrations of carbon, nitrogen, hydrogen, sulphur and oxygen in a coal sample (Ward, 1984). The organic matter of coal is essentially made up of carbon, hydrogen, nitrogen, sulphur and oxygen. All of these elements are also found in the coal mineral matter, with the exception of nitrogen. Carbon is also contained in carbonates, sulphur in sulphides and sulphate, and oxygen and hydrogen in hydrous clay minerals (Ward, 1984). Inherent moisture (IM) present in coals mainly consists of hydrogen and oxygen. The concentrations of carbon, hydrogen and oxygen in the organic matter in coals can also be used as indices of rank and as parameters in coal classification (Ward, 1984).

2.7.2 Maceral analysis using electron microscope techniques

Traditionally, a reflected light optical microscope is used to identify various macerals in the polished coal sections in the normal way using oil immersion.

Subsequent to maceral analysis, the electron microprobe technique that was previously described in Section 2.5.9 can be applied for the determination of the direct chemical compositions of the light-elements (C and O) present in the individual macerals in the coal

polished sections (Bustin et al., 1993; Bustin et al., 1996; Gurba, 1998; Mastalerz and Gurba, 2001).

The proportion of organically-bound inorganic elements present in the individual maceral can also be determined using the electron microprobe. As an example, individual points on the identified macerals in carbon coated polished sections were analysed by a Cameca SX-50 electron microprobe equipped with the Windows-based SAMx® operating system and interface software to determine proportions of C, N, O, S, Fe, Ca, Al, Fe (Gurba, 1998; Ward et al., 2005). The accelerating voltage for the electron beam was 10kV and filament current was 20 nA, with a magnification of 20,000x giving a beam spot size on the sample of around 5 to 10mm in diameter. Standards for S, Fe, Ca, Al, Fe and O that were supplied with the equipment, as well as an independently analysed sample of anthracite received from Canada which was used as the standard for carbon in their studies for the equipment calibration. The detection limit for nitrogen present in the coal macerals, when using electron microprobe under above-stated conditions was found to be 0.5% (Mastalerz and Gurba; 2001). Goldstein et al. (1992) found that the minimum detectability limit of various inorganic elements such as Na, Mg, Al, Si and Ca in the minerals using the electron microprobe with an WDS detector ranges from 0.01 to 0.02%.

2.8 Mineral reactions at elevated temperatures

Mineral matter (included mineral, excluded mineral and the organically-bound inorganic elements) occur in coal in different modes of occurrences (Ward and French, 2004). During coal combustion or gasification, the included minerals and excluded minerals experience different temperatures and they react differently to form ash particles (Attalla et al., 2004; van Alphen, 2005). As defined previously, included minerals are finely dispersed within the coal matrix and can undergo both reduction and oxidation during coal combustion/gasification (Srinivasachar et al., 1990a, b). It is proposed that these minerals are most likely responsible for the inevitable sintering of ash particles that result in clinker formation in the gasifier.

Furthermore, included minerals may have a lower melting point and may account for the volatilisation of the inorganic constituents in the locally-reducing conditions of the burning char during pulverised or coarse coal combustion.

As defined previously, the excluded minerals may be in the form of ultra-fine material on the surface of coal or rock fragments (siltstone or sand stone) originating from contamination of the mined product by roof or floor strata. They are also liberated from the organic fraction of coal during milling or pulverisation. These minerals can readily oxidise to form metal oxides during coal combustion (Ward, 2004).

According to Ward and French (2004), mineral matter, including minerals and other inorganic constituents present in coal, interact with each other and also with the organic fraction at elevated temperatures during combustion, gasification and coking of coal. Subsequent to coal gasification or combustion, mineral matter transforms to fly ash and bottom ash, fuses and crystallises to form slag deposits, vaporises and condenses to form deposits and interacts with each other or internal boiler components to produce corrosion.

At elevated temperatures, the organically-associated inorganic elements in low-rank coals may react differently from elements in the crystalline or true mineral form.

Kawamoto et al., (1994) conducted research work on types of carbons using different carbon contents to determine the effects of carbon content on the melting rate of carbonate minerals (Na_2CO_3, Li_2CO_3, $MgCO_3$, $BaCO_3$ and $CaCO_3$). In their study they found that the melting rate of carbonate minerals increases as the carbon content decreases. This indicates that there may be an effect of residual carbon content on the melting of mineral matter in the coal to form slags or clinkers.

2.8.1 Excluded mineral mechanisms

As was mentioned earlier in this section, the excluded minerals experience more oxidising combustion conditions than included minerals; this may enhance the rate of fusion, enlarge the clinker size and also reduce the volatilisation of inorganic elements during coal combustion or gasification.

The possible reaction mechanisms of the excluded coal minerals that take place during combustion are discussed below:

It is well documented that quartz (SiO_2) is often regarded as essentially non-reactive in combustion processes, although it undergoes a series of transitions on heating (Bryers, 1986; Watt, 1969; Ward and French, 2004; van Alphen, 2005). At room temperature, quartz is known as low quartz or a quartz, but upon heating to 573°C, it changes to other polymorphs, α-quartz, β-quartz (573-870°C), β_2–tridymite (870-1470°C) and β_2–cristobalite (1470°C-high temperatures) to form a liquid. β_2-tridymite melts at 1670°C; whereas β_2-cristobalite melts at temperatures greater than 1713°C. Watt (1969) mentioned that in the last two transformations of quartz, the structure of its polymorph opens and reacts with alkali ions to form carnegieite and nepheline.

According to Ward and French (2004), tridymite and cristobalite may be formed by solid-state reactions, but the low rate at which reactions take place often allows much of the original quartz to persist through combustion processes.
Quartz is a hard mineral and it contains coarse grains, which may be responsible for an abrasion and erosion hazards in the furnace operation. Finer-grained quartz, which is often associated within the carbonaceous matter in coal, can be produced as residues during the burning of char. In addition, the residues of quartz formed during coal combustion can build up to reduce the heat transfer capacity of the combustion system (Ward, 1984).

At temperatures of between 425°C and 525°C, kaolinite ($Al_4Si_4O_{10}(OH)_8$) in the coal starts to lose hydroxyl water and dehydration is complete at around 800°C. An amorphous material which is termed metakaolinite is formed. The three final products of the transformation of kaolinite which are formed at 950-1000°C, are gamma-alumina (Al_2O_3), mullite ($3Al_2O_3.2SiO_2$) and cristobalite (SiO_2) with a silicon spinel ($2Al_2O_3.3SiO_2$) occurring as an intermediate. As the temperature of the boiler increases to about 1600°C, mullite and cristobalite appear to persist as solid phases (Grim, 1962; Bryers, 1986; Unsworth et al., 1987b; Ward and French, 2004; van Alphen, 2005). The final transformation products melt at temperatures greater than 1600°C, which is much higher than the maximum temperatures of the existing boilers.

The loss of hydroxyl water from illite ($K_{1.5}Al_4(Si_{6.5}Al_{1.5})O(OH)_4$) starts at about 400°C and may continue to about 900°C, forming spinel and mullite at around 950-1050°C. Grim (1962) found that the dehydration of illite is very slow in comparison with kaolinite.

On heating illite, Grim and Bradley (1940) found that spinel is formed at 850°C; as the temperature increased to about 1200°C the amount of spinel also increased.

These investigators suggested that the octahedral sheet of the illite lattice carrying the alumina, magnesium oxide and iron goes into the spinel formation; the alkalis and the silica from the tetrahedral layers yield an amorphous glass. They also found that at 1300°C the spinel dissolved in the glass; mullite appeared at 1100°C and persisted to at least 1400°C. During their investigation, no evidence of quartz was found at elevated temperatures. Ward and French (2004) similarly reported that illite and other clays, excluding kaolinite, fuse at around 1200°C to 1350°C to form glassy components, resulting in relatively low ash fusion temperatures and possible slag development.

Srinivasachar et al. (1990b) conducted research on the excluded crystalline illite particles and illite grains included within a carbon matrix in a laboratory scale reactor to address the physical and chemical transformation of illite particles during the combustion process. The results from their studies show that illite starts to decompose at temperatures above 1167°C, losing its crystalline structure and completely transforming to a glass. During their investigation, no vaporisation of the potassium species occurred from the liquid from either the excluded or included illite particles, but formation of cenospheres (ash components that contain unburned carbon particles of different types from coal combustion, unaltered quartz, other mineral grains and hollow silicate spheres that float on water) was observed.

Combustion of synthetic chars containing illite inclusions showed coalescence of these inclusions to form larger ash agglomerates (Srinivasachar et al., 1990b). Comparison of these results with ash particle compositional data obtained from the combustion of a bituminous coal containing illite, showed intermediate compositions indicating interaction between the molten illite and quartz, kaolinite and pyrite (Srinivasachar et al., 1990b). Hence liquid derived from illite is responsible for the dissolution of ash particles during the pulverised coal combustion process. Similarly, in this thesis it is proposed that potassium or sodium from the illite particles present in coarse coal, together with the included pyrite particles, contribute to the sintering of mineral matter during the gasification of the coarse coal at elevated temperatures and pressures.

It is well documented that trace amounts of excluded carbonate minerals including calcite ($CaCO_3$), dolomite ($CaMg(CO_3)_2$), siderite ($FeCO_3$), ankerite ($(Fe, Ca, Mg)CO_3$)) are found in most bituminous coals.

Bryers (1986), Ward (1984), Bogwardt and Bruce (1986), Raask (1984) and Ward and French (2004) indicated that calcite decomposes at elevated temperatures of around 1000°C to form quicklime (CaO).
This lime may react with water and sulphur oxides to form portlandite ($Ca(OH)_2$) and anhydrite ($CaSO_4$) respectively. At low temperatures, CaO also reacts with sulphur oxides to form bassanite ($CaSO_4.1/2H_2O$). At high temperatures CaO interacts with reactive aluminium silicates, such as meta-kaolin ($Al_2O_3.2SiO_2$) to form gehlenite ($Ca_2Al_2SiO_7$) and anorthite ($CaAl_2Si_2O_8$), the latter fusing at about 1400°C to 1500°C. They also found that dolomite decomposes in a two-stage process at elevated temperature to form lime and periclase (MgO).

van Alphen (2005) used a Drop Tube Furnace (DTF) to study the high temperature transformation of minerals present in South African pulverised fuel during heating. In this study, the selected coal was screened to produce coal fractions which were suitable for the experiments. Each coal fraction was added into the DFT and subsequently combusted at different temperatures and under both oxidising and reducing conditions to obtain fly ash for analysis. The results obtained from this study were also used to validate the fly ash model. The experimental results showed that the excluded calcite in South African fuel transformed into calcium oxide; excluded dolomite transformed into Ca-Mg-oxide. The excluded quartz and excluded orthoclase remained excluded in the fly ash and did not readily interact with the other mineral phases. The excluded pyrite transformed into Fe-oxide or Fe-O-S melts.

It is known that mineral matter containing high concentrations of alkali elements in low-rank coals are responsible for the slagging and fouling of inorganic species at elevated temperatures (>1000°C) (Raask, 1985; Benson, 1987). In contrast these problems are potentially lower in fluidised bed combustion (FBC) operating at much lower temperatures (ca. 700-900°C). Vuthaluru and Ke Zhang (2001) performed testwork with sand, South Australian lignite calcite ($CaCO_3$), Ca-treated coal and magnesium ($MgCO_3$) to investigate the role of Ca and Mg in agglomeration and defluidisation during coal combustion. Combustion tests were carried out in the laboratory-scale spouted bed combustion system operating at 800°C.

Experiments were performed with the crushed coal sample (in the range 1.4-3.35mm) from Bowmans coal from Australia.

A known mass (100g) of a bed material (calcite, magnesite and sand) was added into the fluidisation vessel from an opening at the top end of the reactor. Coal was then fed into the combustor using a screw feeder at a rate of 500 g h^{-1}. Ash samples were collected in the cyclone and ash-coated bed particles were collected from the combustor and analysed by electron microprobe and XRD.

The results from the experiments revealed that tests with calcite (as the bed material) indicated no agglomeration and defluidisation tendencies for longer operating periods (12h at 800°C). Mg-bearing compounds were found to be superior in terms of controlling defluidisation in comparison with other bed materials. They also found high concentrations of Ca (either in coal or in the bed material) to delay and decrease the severity of agglomerates formed under the above-mentioned operating conditions. High concentrations of Ca and Mg in ash significantly enhanced the presence of anhydrite, calcite, lime, periclase, and dolomite, talc, and feldspar phases; and reduced the cementing material (low temperature eutectics). The researchers of this investigation concluded that the reaction mechanism mentioned above is responsible for the reduction of agglomerate formation and fouling problems observed with the use of Ca/Mg-based bed materials and Ca-treated coal.

Bailey (1999) heated the excluded particles of pure mineral and sink fraction of coal (obtained by density separation) to combustion temperatures of 1100°C and 1600°C in order to understand the behaviour of siderite particles during coal combustion. The results from his investigation revealed that excluded siderite (containing various levels of Ca, Mg and $MnCO_3$) fragmented during heating without the formation of liquid. The author also used the FeO-MgO-CaO ternary phase diagram in order to predict the behaviour of excluded siderite grains under combustion conditions, clearly indicating that the excluded siderite is unlikely to form sticky or completely molten particles at 1600°C, unless MgO < 5wt %, CaO < 37.5 wt % and ($MnO + FeO_n$) > 60wt %. The chemical compositions of the different collected sintered particles of ash also agreed with this prediction. From his visual observation, residues from excluded siderite particles are found to be sticky at higher temperatures (1380°C compared to ~1080°C for pyrite (Bailey, 1999).

The excluded pyrite (FeS_2) present in coals breaks down to form iron oxides (hematite, maghemite and magnetite) during coal combustion (Srinivasachar et al., 1990). These authors

also mentioned that pyrrhotite (FeS) particles, from the high temperature transformation of pyrite under reducing conditions, melts at 1227°C to form an iron oxysulphide droplet (Srinivasachar et al., 1990). Ward and French (2004) indicated that pyrite can undergo an exothermic reaction; burns due to interaction of its oxygen and sulphur before forming an iron oxide residue. During the heating of pyrite in the presence of carbon, the released iron can react with active inorganic elements or substances to form a range of minerals, including spinel, magnesioferrite, calciumferrite, srebrodolskite and brownmillerite.

Briggs and Lindsay (1986) selected a few samples of pure minerals, including clays, pyrite and calcite in order to study minerals that are responsible for the slagging of mineral matter when they transform at elevated temperatures. In this study, a known mass of individual minerals or mixtures of minerals was placed in the crucibles and heated. As expected, pyrite transformed to pyrrhotite, calcite to quicklime and carbon dioxide, while clay transformed to silicate liquid during heating. They found that with a mixture of either illite or montmorillonite in the presence of pyrite and calcite, liquid formed at temperatures of 600-650°C. When illite or montmorrilonite was totally replaced by kaolinite, the liquid formed at higher temperatures of 750-760°C.

A list of the most common phases reported in various high temperature materials, emanating from the coal combustion process, is given in Table 2.7. Decomposition and melting temperatures of the selected coal minerals and high temperature metal oxides formed during coal combustion are given in Table 2.8. Knowledge of these minerals, in relation to the mineral matter characteristics of the original coal, provides a basis for a better understanding of the interactions or reaction mechanisms that take place between the different mineral matter components at the high temperature associated with coal utilisation.

Table 2.7: Principal minerals identified in high temperature phases associated with coal utilisation ……(compiled from various sources) (slightly modified after Ward and French, 2004)

Mineral	**Composition**
Quartz	SiO_2
Cristobalite	SiO_2
Tridymite	SiO_2
Metakaolin	$Al_2O_3.2SiO_2$
Mullite	$Al_6Si_2O_{13}$
Sanidine	$KAlSi_3O_8$
Albite	$NaAlSi_3O_8$
Anorthite	$CaAl_2Si_2O_8$
Corundum	Al_2O_3
Pyrrhotite	$Fe_{(1-x)}S$
Oldhamite	CaS
Anhydrite	$CaSO_4$
Aragonite	$CaCO_3$
Vaterite	$CaCO_3$
Portlandite	$Ca(OH)_2$
Lime	CaO
Periclase	MgO
Wuestite	FeO
Hematite	Fe_2O_3
Maghemite	Fe_2O_3
Magnetite	Fe_3O_4
Spinel	$MgAl_2O_4$
Magnesioferrite	$MgFe_2O_4$
Calcium Ferrite	$CaFe_2O_4$
Srebrodolskite	$Ca_2Fe_2O_5$
Brownmillerite	$Ca_4Al_2Fe_2O_{10}$

Table 2.7 (a): Principal minerals identified in high temperature phases associated with coal utilisation …… (compiled from various sources) (slightly modified after Ward and French, 2004)

Mineral	**Composition**
Wollastonite	$CaSiO_3$
Gehlenite	$Ca_2Al_2SiO_7$
Merwinite	$Ca_3Mg(SiO_4)_2$
Melilite	$Ca_4Al_{12}MgSi_3O_{14}$
Whitlockite	$Ca_3(PO_4)_2$

Table 2.8: Decomposition and melting temperatures of selected coal minerals and combustion ash products (Goblirsch et al., 1984)

Mineral	**Composition**	**Decomposition and Melting points (°C)**
Kaolinite	$Al_2Si_2O_5(OH)_4$	800-1000[d], 1810
Illite	$K_{1.5}Al_4(Si_{6.5}Al_{1.5})O_{20}(OH)_4$	400-1167[d], 1200-1350
Pyrite	FeS_2	800[d], 1171
Marcasite	FeS_2	800[d]
Apatite	$Ca_5F(PO_4)_3$	>1230
Aragonite	$CaCO_3$	875[d]
Calcite	$CaCO_3$	925[d]
Dolomite	$CaMg(CO_3)_2$	775[d]
Ankerite	$(Fe, Ca, Mg)CO_3$	725[d]
Siderite	$FeCO_3$	525[d]
Rutile	TiO_2	1827
Quartz	SiO_2	1710
Anhydrite	$CaSO_4$	1450
Szomolnokite	$FeSO_4.H_2O$	480[d]
Thenardite	Na_2SO_4	885
Arcanite	K_2SO_4	1069

Table 2.8 (continued): Decomposition and melting temperatures of selected coal minerals and combustion ash products (Goblirsch et al., 1984)

Mineral	**Composition**	**Decomposition and Melting points (°C)**
Glauberite	$Na_2Ca(SO_4)_2$	900
Vanthoffite	$Na_6Mg(SO_4)_4$	800
Keiserite	$MgSO_4.H_2O$	1120[d]
Pyrrhotite	$Fe_{(1-x)}S$	1025
Lime	CaO	2570
Wuestite	FeO	1369
Hematite	Fe_2O_3	1567
Magnetite	Fe_3O_4	1592
Cristobalite	SiO_2	1740
Corundum	Al_2O_3	2052
Mullite	$Al_6Si_2O_{13}$	1850
Sanidine	$KAlSi_3O_8$	1512
Leucite	$KAlSi_2O_6$	1650
Albite (plagioclase)	$NaAlSi_3O_8$	1100
Nepheline	$NaAlSiO_4$	768-1250
Nosean	$Na_2Si_2O_5$	874
Nosean	Na_2SiO_3	1088
Nosean	Na_4SiO_4	1018
Anorthite	$CaAl_2Si_2O_8$	1553
Wollastonite	$CaSiO_3$	1554
Gehlenite	$Ca_2Al_2SiO_7$	1590

Note: d – decomposes

Excluded minerals are unlikely to interact with each other in the bulk gas, due to the low probability of collision (Bryers, 1996). Attalla et al. (2004) indicated that during coal combustion or gasification, excluded minerals undergo fragmentation and transformation to residual ash. They also stated that a limited amount of vaporisation of the inorganic species occurs from mineral matter experiencing high temperatures. At high temperatures the excluded minerals can also undergo fusion and subsequently solidification, depending on the melting points of the individual minerals present in the coal.

Based on the results from the literature review on the excluded mineral mechanisms, various minerals (pyrite, and illite, and to a lesser extent calcite) can be expected to react with kaolinite at elevated temperatures to form silicate glass, resulting in slagging of ash during pulverised coal combustion. The literature review on the reaction mechanisms of the included minerals that interact differently from excluded minerals, is given in the following section.

2.8.2 Included mineral mechanisms

During coal combustion the included minerals generally reach peak temperatures in excess of the surrounding gas temperature and react quickly by coalescence, due to the close proximity to one another (Attalla et al., 2004). The inorganic species in the heated particles of the included minerals may undergo reduction and may volatilise partially.

Attalla et al. (2004) and van Alphen (2005) found that fly ash particles produced by different mineral matter transformations during pulverised coal combustion have different particle sizes. Residual ash was formed from the excluded minerals; the included minerals produced finer ash particles by coalescence of the included minerals during combustion. Attalla et al. (2004) also indicated that vaporisation of the inorganic species from sub-micron grains of the included minerals, and from metallic salts of carboxylic acids, together with the subsequent condensation of the inorganic volatiles during cooling, are responsible for the formation of sub-micron ash (in the range of 0.01 to 1 micron).

As stated earlier, according to Quann and Sarofim (1986) low rank coals contain significantly higher concentrations of the alkaline earth metals that are atomically dispersed, present as cations on the carboxylic and phenolic groups. Neville et al. (1981) stated that almost all of the organically-bound cations present in low-rank coals vaporise at 2627°C as sub-micron fumes totaling 1.9 to 9.6 wt% of the total mass of ash produced during coal combustion. The sub-micron ash particles contain MgO, Na_2O and CaO. In bituminous coals, metals occur in discrete minerals which decompose during char oxidation to form refractory metal oxides such as SiO_2, FeO, CaO and MgO. Srinivasachar et al. (1990a, b) stated that if included silica is fine and well dispersed within the coal matrix, it can be reduced to sub-oxide (SiO) and volatilises during combustion.

Srinivasachar et al. (1990a) found that the included pyrite particles react with clays (aluminium silicates) at an elevated temperature of about 1227°C to form iron-potassium aluminosilicate melt during coal combustion, whereas the excluded pyrite particles fragment and oxidise to form smaller particles of either magnetite or hematite

The model that was developed by van Alphen (2005) predicts that fine included kaolinite present in the carbon fraction is released during combustion to form fine excluded kaolinite fly ash particles. Included kaolinite can coalesce with calcite, dolomite and /or pyrite to form kaolinite/calcite, kaolinite/dolomite and kaolinite/pyrite ash particles respectively. A small proportion of the included kaolinite can coalesce with quartz to form quartz60kaolinite40 (60% heated quartz reacted with 40% high temperature transformation product of kaolinite) and quarz80kaolinite20 (80% heated quartz particles reacted with 20% high temperature transformation product particles of kaolinite) ash phase particles. The author also concluded that the majority of kaolinite is released on combustion; a small proportion of the included kaolinite coalesces with pyrite, calcite and dolomite and to a lesser extent with quartz.

2.9 Sintering studies of coal ash

The sintering of solid material normally occurs when loose or compacted powders of the solid particles are subjected to heat treatment at elevated temperatures. The solid particles with substantially low melting points start to partially melt. In the solid-state sintering process, the solid particles contact each other and subsequently form a new solid material with different shape and size. A reduction of the net surface energies of the solid-vapour and solid-solid interfaces is responsible for the sintering process during heating. The heated solids may shrink, due to the rearrangement of particles, resulting in a change of pore shape, grain size and shape (Kingery et al., 1976).

According to Al-Otoom et al. (2000) the inevitable sintering of ash (which is associated with the coal combustion process) is responsible for different operational problems such as: bed agglomeration, ash deposition on gas circuits, heat exchanger tubes as well as ash build-up and bridging on hot gas filtration systems. Raask (1985) found that the viscous flow mechanism dominates during the sintering of coal ash at elevated temperatures. A model for the viscous flow mechanism was developed by Frenkel (1945), equating the change in the surface energy with the energy dissipated by the flow of material.

In his studies, the author suggested that crystalline material can behave like an amorphous material under the influence of surface tension. The equation of the viscous flow mechanism of coal ash sintering is given as follows:

$$1-(\epsilon / \epsilon_0) = 9\gamma/4\eta r_0 t \qquad (2.10)$$

(Frenkel, 1945)

Where η is the apparent viscosity, γ is the surface tension, and ϵ and ϵ_0 are the pore volume at time t = t and at time t = 0 respectively.

Zagar (1975) applied Frenkel's equation for determination of the change in the porosity with time. The results from the equation showed that the range of applicability of Frenkel's equation is limited to a small time period in the initial stages of sintering. In an attempt to enhance the accuracy of the model of the viscous flow mechanism, at a later stage it was modified by Lemaitre et al. (1976).

The modification of the Frenkel's equation was based on the hypothesis that the viscosity of the material changes linearly with time at a constant temperature during sintering by the following equation:

$$\eta = \eta_0 (1+\alpha t) \qquad (2.11)$$

(Lemaitre et al., 1976)

Where η_0 is the initial viscosity

α is a rate constant for the change of viscosity with time. The results from the modified Frenkel's equation indicated that the material lost its excess surface energy by dissipating this energy into the deformation of this material, subsequently becoming less amorphous in behaviour during sintering. They also found that viscosity increases with time. Al-Otoom et al. (2000) noted that a new technique for the measurement of the sintering kinetics of coal ash was developed. The technique involves the use of the pressure-drop of a gas across the ash pellet, providing more information about changes that occur within the pellet during sintering. The measurement of pressure-drop of the airflow through the pellet can also be used to determine the sintering temperature of the ash pellet, as well as the rate of change of its porosity with time.

A number of researchers used the technique that involves slowly heating an ash pellet and subsequently measuring the electrical resistance across the pellet, to determine the sintering temperature of the coal ash (Raask, 1985; Conn, 1984; Cumming et al., 1986; Tangsathitkulchai, 1986). It was found that the electrical sinter point of ash, which is referred to as the sintering temperature of coal ash, was always below the initial deformation temperature of the ash as determined in the A.S.T.M. ash fusion temperature test (Cumming et al., 1986).

Jung (1996) heated samples of low-rank coal ash at elevated temperatures to gain a better understanding of the ash sintering characteristics. In his studies, several factors including ash composition, ash particle size distribution, sintering temperature and reducing and oxidising conditions (that are believed to contribute significantly to sintering) were evaluated. The results (employing the electrical resistance method) indicated that the sinter point of coal ash particles substantially decreased as the particle size distribution of coal ash was decreased. The author also found that the strength of the sintered coal ash significantly increased when increasing the sintering temperature.

Crushing strength measurements were used by Barnhart and William (1956), Gibb (1981), Conn (1984) and Tangsathitkulchai (1986) to determine the sintering temperature of the coal ash. The strength measurements for the coal ash were favourably compared to a known slagging factor of the coal ash. In contrast, the strength values for the coal ash were not correlated with the measured electrical sinter point.

Nowok (1996) noted that densification occurred when a large fraction of the sample pores were completely filled with liquid formed during a liquid-phase sintering process. In this sintering phase, the majority of solid particles melted to form a liquid.

The author of this thesis proposed that sintering reactions between the included fluxing elements-bearing minerals (calcite, pyrite, ankerite and dolomite), as well as the organically-bound inorganic elements and kaolinite in coal may take place to form high temperature aluminium silicate minerals under reducing and oxidising conditions during the gasification of coal.

It was also suggested by the author of this thesis that fluxing elements-bearing minerals (calcite, dolomite, ankerite and pyrite) that are associated with kaolinite in the coarse coal particles, could initiate the sintering and slagging processes at elevated temperatures and pressures during coal gasification. The proposed mechanisms are as follows:

Organic calcium + Organic sulphur → Calcium sulphate (Bassanite) T= >120°C

Bassanite ($CaSO_4.1/2H_2O$) + Kaolinite ($Al_2Si_2O_5(OH)_4$) → CaO.metakaolinite + SO_2

T= > 400°C

Pyrite + kaolinite → Pyrite(kaolinite) T = > 700°C

Pyrite +calcite + kaolinite → (Pyrite, Calcite)Kaolinite T = > 900°C

Dolomite + kaolinite → Dolomite (kaolinite) T = > 1000°C

Calcite + kaolinite → Calcite (kaolinite) T = > 1100°C.

The (pyrite) kaolinite, (pyrite, calcite) kaolinite, (dolomite) kaolinite and (calcite) kaolinite products of the included fluxing elements-bearing minerals and kaolinite formed in the above proposed reactions denote Fe-aluminium silicate, Fe-Ca-aluminium silicate, Ca-Mg-aluminium silicate and Ca-aluminium silicate glasses respectively.

As stated earlier in the present study, the effects of these minerals and elements on the sintering of coal ash during gasification were determined using the various analytical techniques (XRD, XRF, QEMSCAN, SEM-EDS, CCSEM and EMP).

2.10 Formation of glass phases in coal ash

During pulverised coal combustion, mineral matter (silicate minerals, carbonate minerals, sulphide minerals and organically-bound inorganic elements) may interact at elevated temperature to form ash particles. Due to the availability of silicates in the coal, the ash particles contain mainly amorphous or glass-like material. The factors that influence the glass formation from the liquid are the concentrations of dissolved inorganic elements, the rate of crystallisation of inorganic species and the cooling rate of the liquid (Kingery et al., 1976). According to Benson (1987), a number of researchers studied the physical and chemical properties of crystals from the molten solution in order to be able to manage the glass properties.

According to Kingery et al. (1976) and Ward (2004) the alkali silicates melt readily during the combustion of coal; alkali atoms provide the neutrality by occupying random positions throughout the structure of molten silicates. A sufficient quantity of either alkali or alkaline earth elements, added to the glass structure significantly affects the structure of silicate due to the increased oxygen to silicon ratio. The modification of a silicate structure, by the addition of alkali and alkaline earth elements can eventually lead to crystallisation of inorganic species from the solution to form new crystals (Kingery et al., 1976).

2.11 Crystallisation of the dissolved inorganic elements from the ash-derived melt

In liquid-phase sintering, which is the last stage of the sintering process, much of the solid mass may melt. Solid particles with relatively higher melting points (greater than the flame temperature of burning material) will remain undissolved in the melt. These particles may undergo rearrangement, if they have sufficient mobility for effective densification through the sintering process. On cooling the melt, the dissolved species may start to precipitate preferentially or crystallise to form artificial minerals.

According to Kalmanovitch (1983) the phase diagram CaO-FeO-Al_2O_3-SiO_2 can be used to predict the crystallisation path of coal ash melts during the liquid-phase sintering process. In his method, the ash composition was normalised to the four components CaO-FeO-Al_2O_3-SiO_2. The liquidus temperature was estimated and the composition of the residual liquid phase calculated by following the crystallisation path.

Suzuki et al. (1997) used limestone and sewage sludge incineration ash as feedstock for the production of glass-ceramic. In his laboratory experiments, the mixture of limestone and sewage sludge incineration ash (that consisted of high proportions of silica and alumina and trace amounts of hematite, sulphur and carbon) were heated to 1450°C to form a melt. The glass-like material formed by cooling of this melt was reheated at different temperatures (in the range of 800-1100°C) for various times ranging from 1h to 2h. The authors found that carbon readily reacted with sulphur trioxide produced during heating to form elemental sulphur, which interacted with ferric oxide at 800°C to form a colloidal ferrous sulphide.
Their studies revealed that ferrous sulphide behaved as a nucleant during crystallisation of anorthite from the molten solution.

In this present study, ferrous sulphide from the transformation of coal pyrite, as well as from the interaction of organic sulphur and iron-bearing inorganic species during gasification, may act as a nucleant during the crystallisation of anorthite, from the liquid derived from possible high temperature reaction between fluxing elements-bearing minerals (calcite, dolomite, ankerite and pyrite) and aluminium silicate minerals.

2.12 FactSage modeling

In this study, the thermodynamic package FactSage was used to predict the equilibrium phases in the lower part of the gasifier, where the temperature decreases from the peak in the coal combustion region towards the grate. This model runs on a personal computer (PC) operating system under Microsoft Windows® and consists of a series of information, database, calculation and manipulation modules that enables one to access and manipulate pure substances and solution databases. Additional information is available at www.FactSage.com.

FactSage not only enables calculation and manipulation of phase diagrams, but has been established mainly in the field of complex chemical equilibrium and process simulation. For example, with FactSage it is possible to access both Fact (slag, matte, salt, ceramic and aqueous) and alloy databases, import and export streams and mixtures and also import Chem-Sage data files. Another advantage of FactSage is that it can take carbon-mineral reactions into account and the gas composition and atmosphere can also be varied. The FactSage solution database contains critically evaluated thermodynamic data for SiO_2-CaO-Al_2O_3-Cu_2O-FeO-MgO-MnO-Na_2O-K_2O-TiO_2-Ti_2O_3-Fe_2O_3-ZrO_2-CrO-Cr_2O_3-NiO-B_2O_3-PbO-ZnO (Bale, et al., 2002). In addition, Jak et al. (1998), (2000) and (2003) found in their studies that the FactSage can be used to predict liquidus temperatures of coal ash slag. They also stated that the addition of CaO and FeO as fluxing agents to the coal mineral matter, as well as the aluminium to silicon ratios in the coal, has a significant impact on liquidus temperature of the slag during coal combustion. The change in liquidus temperature of coal ash slag can result in the formation of anorthite and mullite, depending on concentrations of CaO and FeO added to the coal during coal-conversion processes. The most-used module for this study was Equilib, where the Gibbs energy minimisation component of FactSage was utilised. It calculated the concentrations of chemical species when specific elements or compounds reacted or partially reacted, in order to reach a state of chemical equilibrium.

CHAPTER 3
EXPERIMENTAL PROCEDURES

3.1 Introduction

Various experimental methods were used to test the hypotheses that were formulated in Chapter 1, regarding actions and interactions of and between minerals and non-mineral inorganic elements in coal. These are expected to transform or interact with each other at elevated temperatures and pressures to form sintered particles or melt. The experimental procedures used in this study are given in this chapter.

The Run of Mine (ROM) coal samples from six different mines situated in the Mpumalanga province in South Africa contained rock fragments (sandstone, siltstone, mudstone and carbonaceous shale) in addition to the coal itself. These ROM samples were characterised using several analytical techniques to determine fluxing elements that are expected to be responsible for the sintering and slagging of mineral matter (refer to Figure 3.1 for an overview). A blend sample of coarse coal particles (>4-120mm coal fraction; suitable for the gasification process) from the various coal sources was firstly characterised to better understand the chemical and mineralogical characteristics. Subsequently, each sample from the individual mine was tested in a high temperature and pressure autoclave under reducing conditions to better understand transformation of minerals and the organically-bound inorganic elements to new minerals or sintered ash particles.

Samples of “turn-out” test material were taken from a Sasol-Lurgi Fixed Bed Dry Bottom (FBDB) gasifier, using the sampling procedure developed by Bunt (2006). A number of different clinker particles, heated rock fragments and partially burned carbonaceous shale fragments were selected from the gasification ash on the basis of their texture, colour and size. The approach taken here to hand-pick coal and ash particles for characterisation was not used for sampling of these gasifiers in the past. Homogenised coal and gasification ash samples, as was done in the past, were also characterised.

Since the turn-out was done by extracting the gasifier contents from the bottom of the gasifier, only variations along the vertical axis could be determined. Gasifier dig-out is a method that can provide axially as well as radially resolved information.

A simple diagram of the hypotheses tested in this study as well as the experimental procedures followed is shown in Figure 3.1. The experimental procedures are described in detail in this chapter.

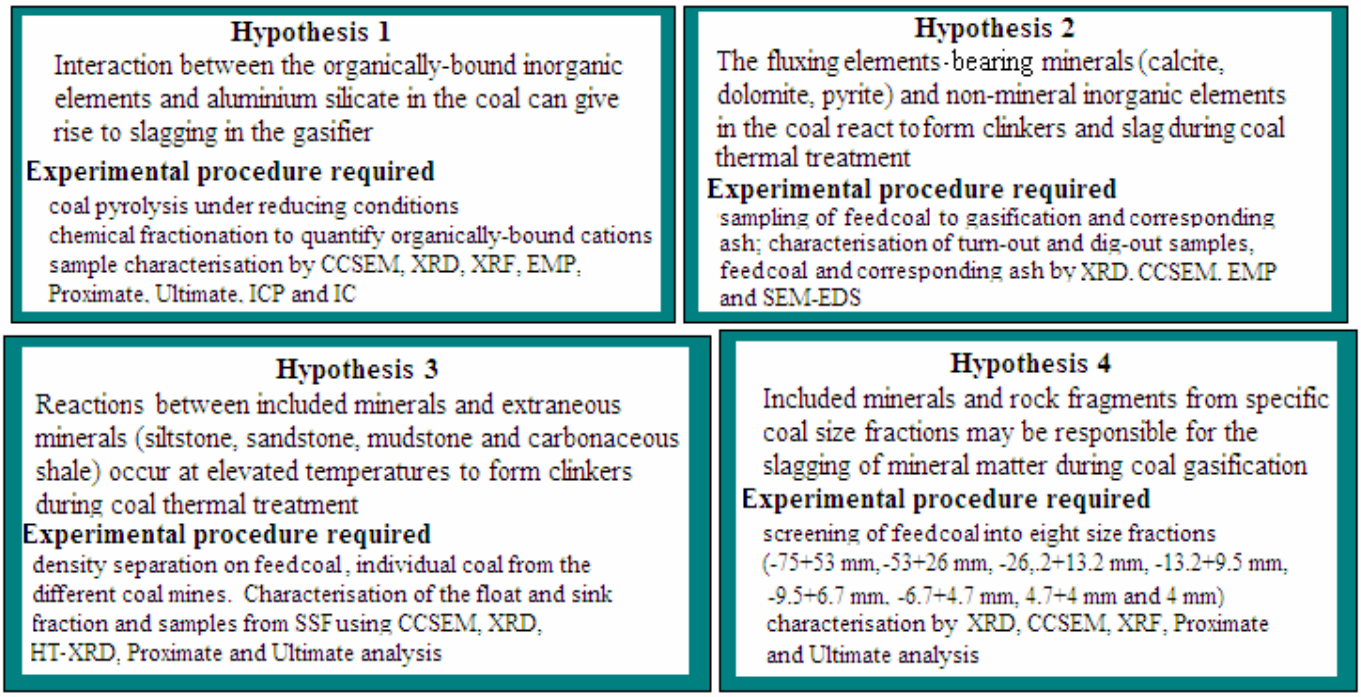


Figure 3.1: Hypotheses tested and experimental procedures used in this study.

3.2 Mineralogical analysis across the screened coal fractions

Based on the results reported by Matjie et al. (2006), coarse ash from the gasification process contains Ca-Fe-Ti-K aluminosilicate glass, anorthite and mullite crystals that could be derived from the included minerals in the carbon matrix and from rock fragments. To evaluate the compositions of included minerals and rock fragments from the different size fractions, the representative feed coal stock to the gasification process (a blend from the different mines) was screened into eight size fractions ranging from <75+53mm to <4mm as shown in Figure 3.2. The screened size fractions were crushed to 100% passing 1 mm for the mineralogical investigations. The mineralogy of each screened coal fraction was determined using CCSEM, XRD and chemical analyses (proximate, ultimate and XRF ash elemental). The calculated mass-% size distribution (mass retained) is illustrated in Figure 3.2. A high proportion (>55 mass-%) of the coal feedstock is concentrated in the <53+13.2mm size fractions (Figure 3.2).

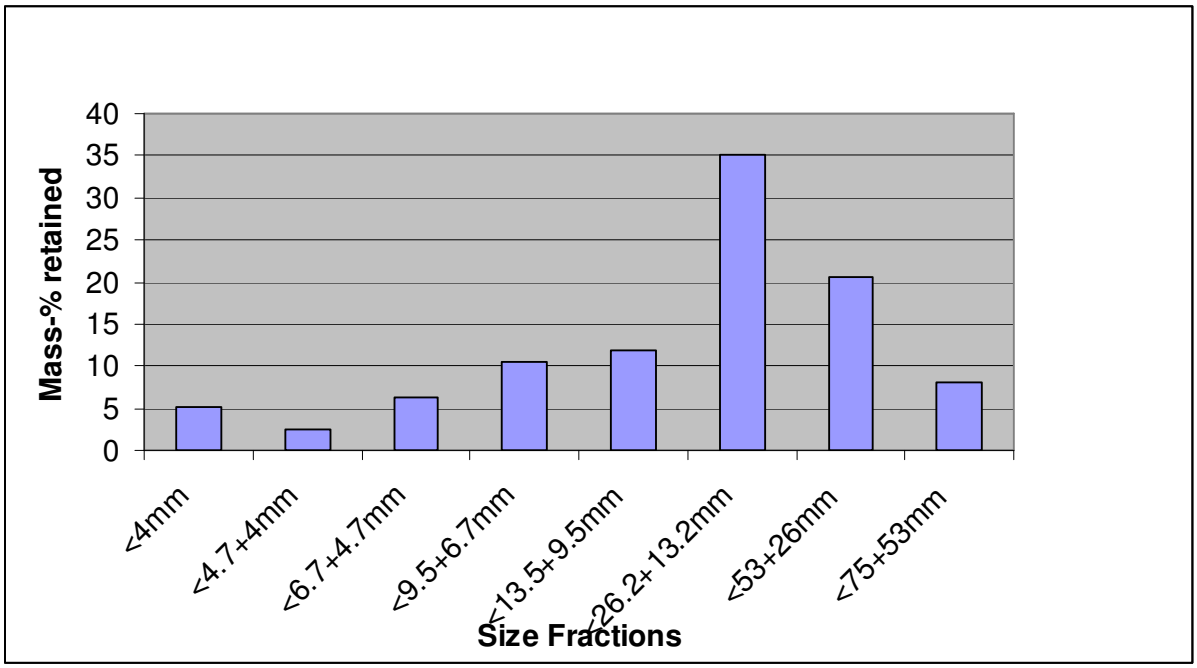


Figure 3.2: Mass-% size distribution (mass-% retained).

3.3 Density separation of Sasol coals

3.3.1 Density separation on the feed coal to the coal-conversion process

The feed coal to the coal-conversion process is a blend of coals from the different Highveld coal mines, with a wide particle size distribution (PSD) and containing extraneous rock ("stone") fragments. A representative sample of the bulk feed coal taken from a commercial gasifier was crushed and pulverised to obtain 100% passing 1 mm material. The pulverised coal sample was separated into three density fractions (Table 3.1) using mixtures of toluene and bromoform (see Figures 3.3 and 3.4 for examples of higher-density and lower-density materials).

Representative samples of the three density fractions produced from the sink-float techniques were submitted to van Alphen Consultancy for CCSEM analysis, to Sasol Syngas and Coal Research for petrography analysis, to Set Point Laboratories for ash elemental analysis and to Coal and Mineral Technologies (CMT) (Pty) Ltd for proximate, ash fusion temperature and ultimate analyses. Additionally, 25mm polished sections were prepared for electron microprobe analysis at the University of Johannesburg (UJ). Electron microprobe analysis was used to accurately determine the elemental proportions of selected minerals.

In parallel, the -1mm particles of the crushed feed coal were screened by 0.25mm sieve to produce fine coal fractions (100% <0.25mm particles) as well as coarse coal fractions (100% >0.2mm particles). Each fraction was separated by float-sink techniques into a low-density ("floats") fraction and a high-density or "sinks" fraction. The density of the separation medium used in this study was 1.56g/cm^3. The mineral matter in the individual size and density fractions was isolated using low-temperature oxygen-plasma ashing; the resulting LTA residues subjected to Rietveld-based X-ray diffraction analysis using procedures described by Ward et al. (2001) and also by the high-temperature XRD using procedure described by French et al. (2001).

Table 3.1: Mass (g) and mass-% distribution for the density fractions of Sasol Coal Supplier (SCS) blend

Density Fraction	**Mass (g)**	**Mass-%**
<1.5g/cm^3	296.8	32.5
>1.5 to <1.8g/cm^3	458.83	50.2
>1.8g/cm^3	158.14	17.3
Total	913.77	100.0

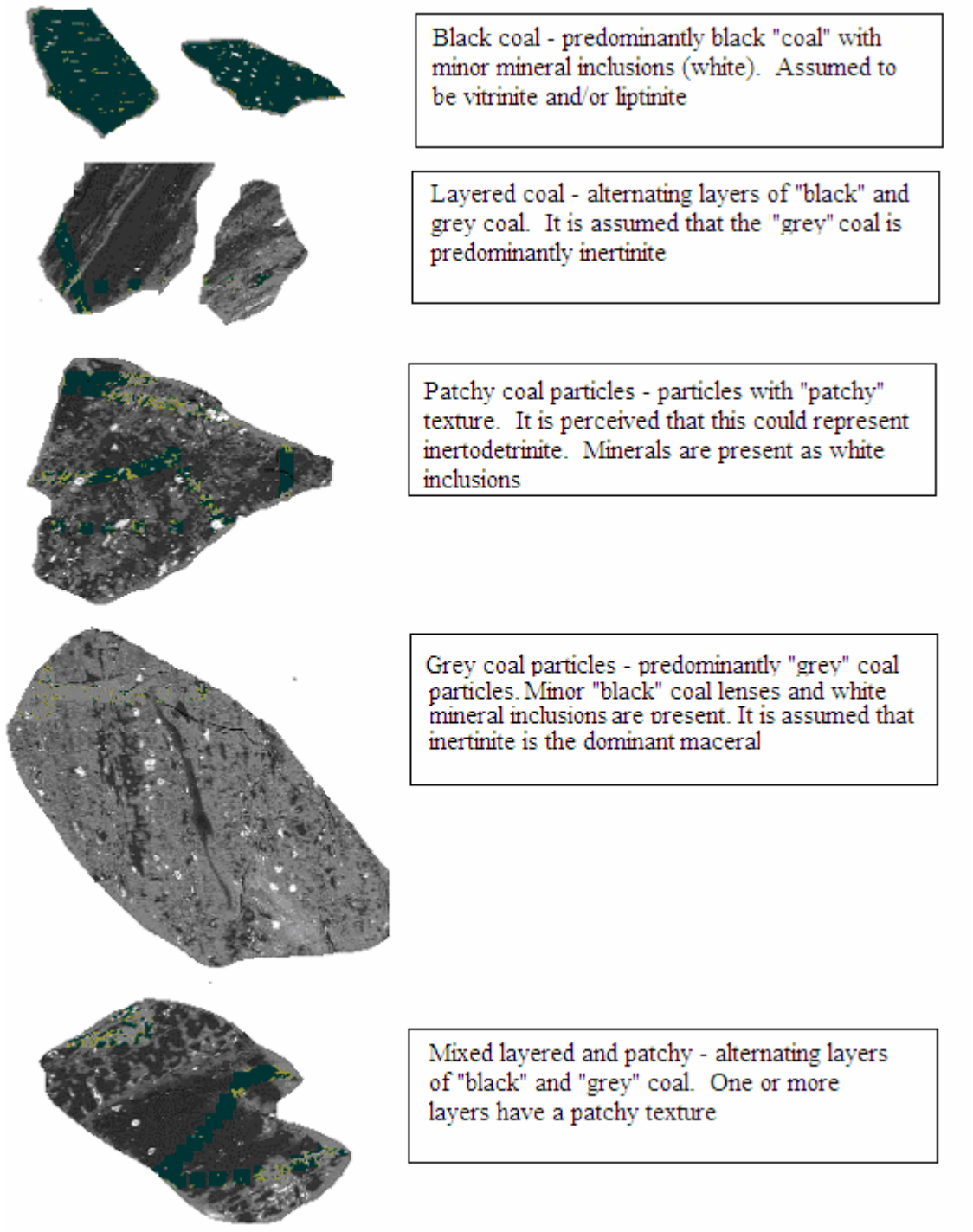


Figure 3.3: Optical images of float coal particles hand-picked from the float fractions (<1.5g/cm^3 to <1.8g/cm^3). The average width of the images is 6.7mm.

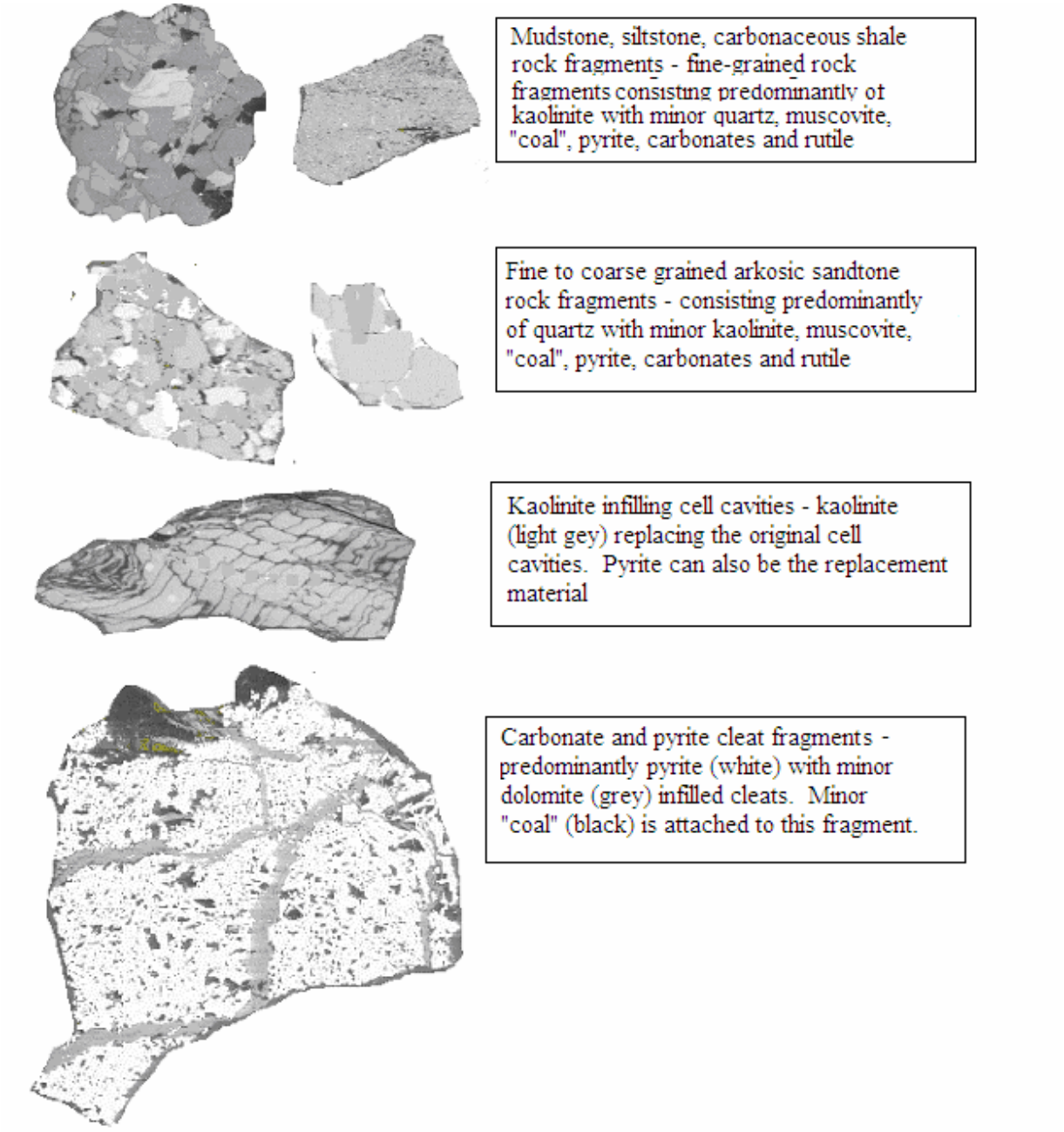


Figure 3.4: Optical images of rock fragments or stone taken from the sink fractions (>1.8g/cm^3). The average width of the samples shown in the images is 6.7mm.

3.3.2 Density separation on coal from the individual mines

As was stated in the previous section the coal feedstock contains minerals that are associated with the carbon matrix and also with the extraneous rock fragments. The proportions of fluxing elements-bearing minerals and organically-bound inorganic elements (that are expected to cause the slagging process during gasification) could significantly depend on particle size, mode occurrence of mineral matter in the coal and the density of the coal.

To test these effects for coals from different mines, coal samples were taken from the coal belt of each coal mine using the procedure developed by the operators from the mine. In the experimental procedure 50kg coal sample was taken from the coal belt every 15min. Approximately 100kg coal sample was separated using a mixture of tetra-bromo ethane and benzene at a density of 1.8g/cm^3 to produce float and sink fractions.

The sink and float fractions produced in this manner were separately crushed and pulverised to obtain 100% passing 1mm. The prepared samples of the composites from the different mines, float and sink fractions were subsequently submitted for proximate, ultimate, elemental analyses and ash fusion analyses. The proximate, ultimate and elemental analyses of the original sample, float and sink fractions were used in van Alphen Consultancy Coal Quality Predictor (CQP) model to predict the mineral proportions of the composite feed coal, calculated feed coal based on float and sink fractions, float and sink fractions. The model is also based on the elemental analysis of the mineral matter present in the coal. The composite samples were measured by CCSEM.

3.4 Pyrolysis of coal samples from Highveld coal mines

Pyrolysis experiments were conducted on six coarse coal samples mined from different collieries situated in the Mpumalanga province in South Africa. The coal samples were tested in a high pressure and temperature autoclave using the following procedure:
Coarse coal particles from the different coal mine (i.e. mines 1 to 6), as well as the blended feed coal (termed "Feed 32") for the coal-conversion process, were tested. Due to the confidentiality issues related to the real names of some South African coal mines, coal samples taken from these mines are termed coal samples 1 to 6. For each test, 1.2kg of coarse coal was pyrolysed at a maximum temperature of 600^{o}C and pressure of 26bars under nitrogen gas for one hour. The flow-rate of nitrogen gas used in this study was 40ml/min (at room temperature and 26bars pressure). The experimental setup is shown in Figures 3.5 and 3.6.

The volatile matter produced during the pyrolysis experiment was condensed in a round bottom flask and the excess gas bubbled through a series of scrubbing solutions, each containing 700ml of distilled water (as shown in Figure 3.6). The first scrubbing solution was removed after the pyrolyser had reached 200^{o}C. The second, third and fourth scrubbing

solutions were removed after the coal sample had reached 300°C, 400°C and 600°C respectively. The coal and corresponding char samples were subsequently pulverised to 100% passing 212µm and these samples were submitted for chemical and mineralogical analyses. All scrubbing solutions, the gas liquor (condensed volatile matter) as well as the blank solution (distilled water) were analysed by Inductively Coupled Plasma Mass Spectrometry (ICP-MS). Ions that are contained in these liquid samples were determined by ion chromatography (IC).

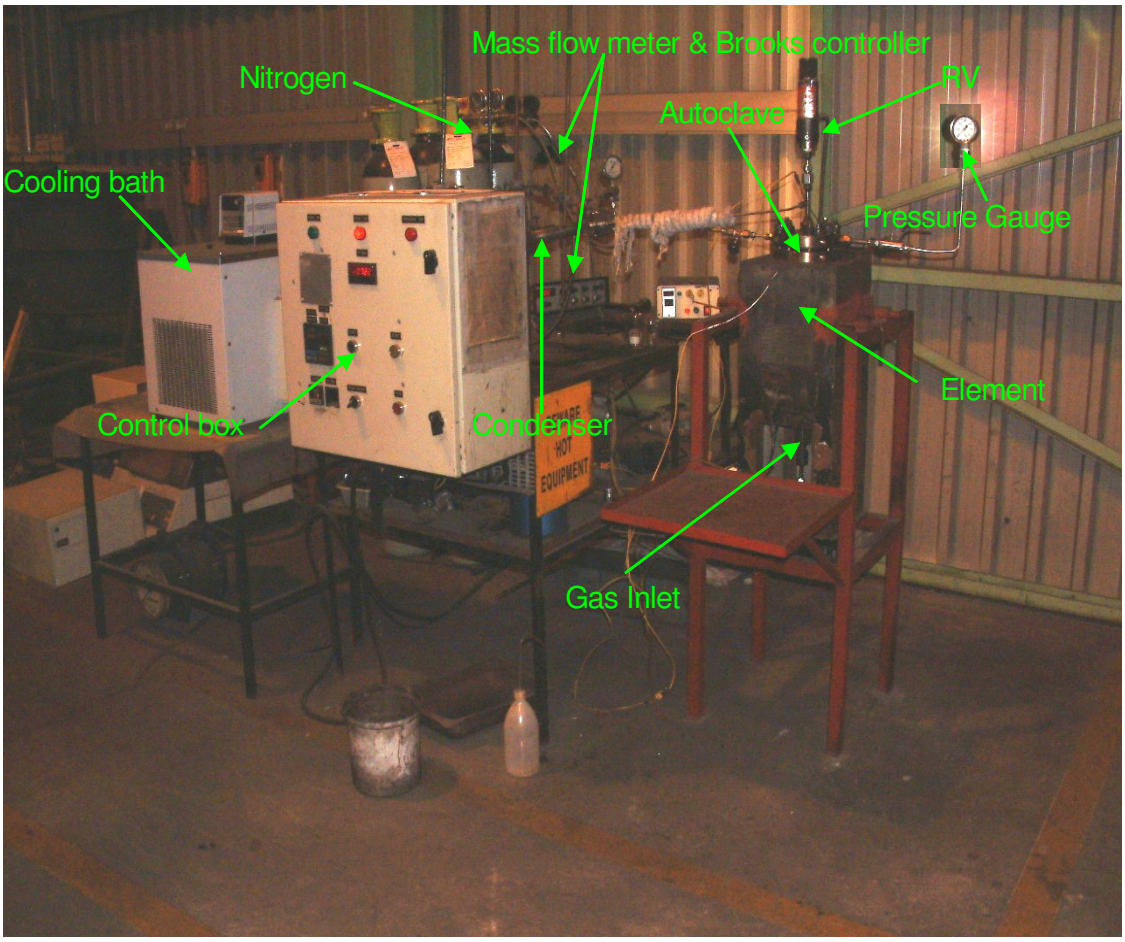


Figure 3.5: Photograph showing the high temperature autoclave for pyrolysing coal.

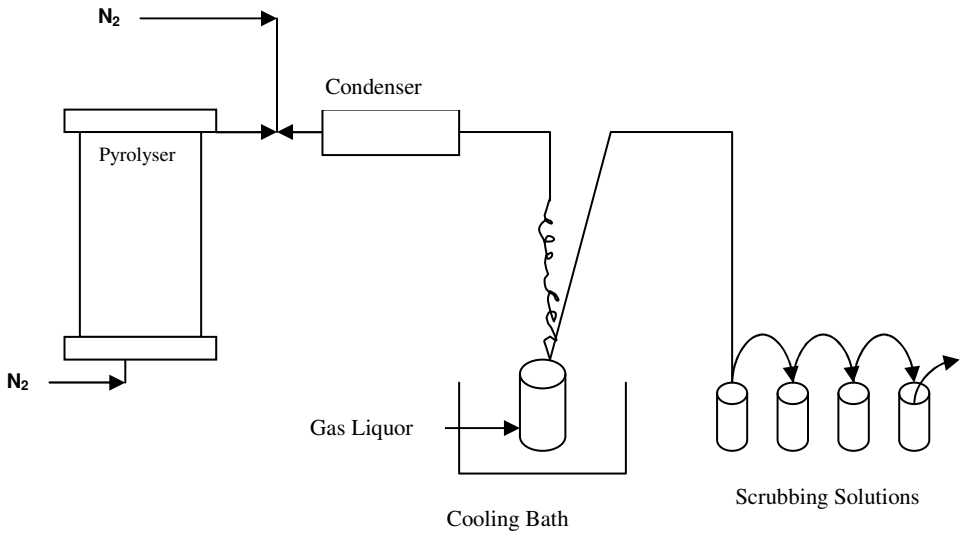


Figure 3.6: Schematic showing the experimental setup for the pyrolysis tests with four water scrubbers.

3.5 Coal and ash sampling methodology - gasifier

In order to evaluate the chemical, mineralogical and physical properties of coal as well as mineral characteristics of the minerals, glasses and elements present in the coarse gasification ash, representative coal and ash samples from a gasifier were required in this study.

A sampling plan was developed to prepare representative coal and ash samples for this investigation from a commercial gasifier. This gasifier was constructed like the other gasifiers that are being used in the gasification process, but it was assigned to the gasifier tests. In this procedure, the wet coarse coal entering the top of the gasifier was sampled from the conveyor belt on an hourly basis over a 24h period. Approximately 20kg of the coal was acquired for each sample taken. A 50kg sample of corresponding gasification ash was collected from the bottom of the gasifier every three hours for an equivalent 24h period. At the end of the 24h period, the entire composite samples (approximately 480kg coarse coal and 400kg coarse gasification ash) were separately crushed and ground to obtain 100% passing 1mm. Before crushing, the coarse ash fraction, clinker particles were hand-picked from this sample, based on their visual appearance.

Representative fractions of the crushed coal feedstock and coarse ash (100% <1mm particles) were submitted to Sasol Technology Research and Development (Materials Characterisation Group) for (1) qualitative and quantitative XRD analyses and to (2) van Alphen Consultancy for CCSEM analysis (van Alphen, 2000). Proximate, ultimate and XRF ash elemental analyses were also undertaken to support the XRD and CCSEM analysis.

3.5.1 Sampling methodology of composite turn-out samples, coarse coal and ash particles taken from the coal-conversion process facility

In order to understand coal mineral matter that gives rise to the slagging and clinker formation within Sasol gasifiers, it was necessary to take coal and ash samples at different levels along the (height) of the gasifier. Since the gasifiers operate under high pressure, it is not feasible to obtain samples while the gasifier is operating. Fortunately, in 2005 a gasifier was shut-down, enabling samples to be acquired from different depths from within the gasifier. Thirty two samples of "turn-out" test material were taken from another gasifier (Figure 3.7), using the sampling procedure developed by Bunt (2006). This gasifier typically contains c.a. 100 tons of material, thus if the ash grate was rotated at its lowest speed and every increment sampled every 0.5h, then 32 x 3m^3 samples would be obtained in total. This implied that each sample taken represented a composite of the material in every 0.26m x 4m (height x diameter) slice of the gasifier, given that the gasifier is c.a. 9m high. From the 32 samples taken from the gasifier, 4 gasifier "ash"samples and the original coal (Table 3.2) were selected and analysed by CCSEM and XRD to determine the mass-% variation in mineral and phase proportions formed at the different temperatures.

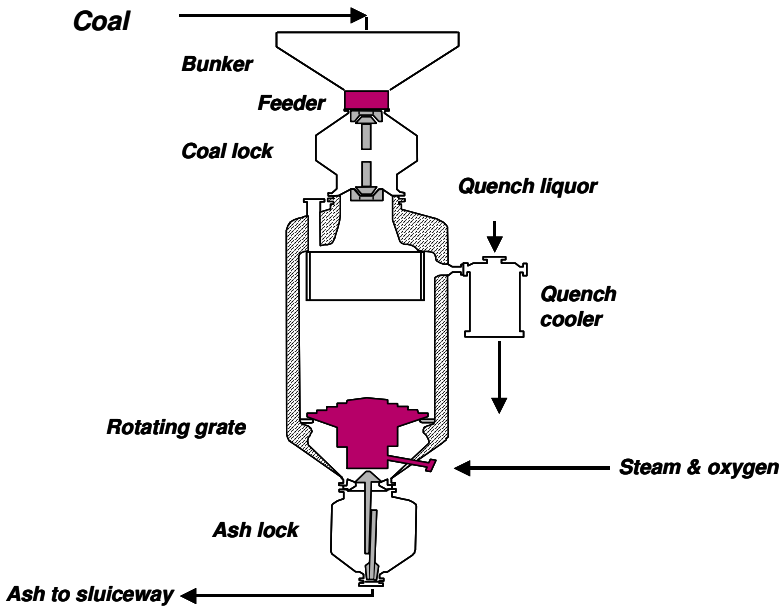


Figure 3.7: Schematic showing the Sasol-Lurgi Fixed Bed Dry Bottom (FBDB) gasifier.

Table 3.2: Table showing sample number, zones of the gasifier and approximate temperature of the sample

Samples number	Zones of the gasifier	Approximate temperature of sample (^{o}C)
32T	Top of gasifier	25
24T	Drying zone	400
16T	Pyrolysis	700-900
8T	Gasification	1000-1350
1T	Bottom of gasifier	1100-1350

Note: T: turn-out

The author of this thesis selected a number of different clinker particles, heated rock fragments and partially burned carbonaceous shale fragments from the selected turn-out samples based on their colour, texture and size (Figure 3.8). For each group, individual specimens were selected and regions of interest were identified and cut into 20mm sections (Figure 3.9). The sections were placed in a 30mm mould. Epoxy resin was added and allowed to cure for 12h. The hardened sections were ground and polished, exposing a cross-section surface for analysis. To ensure good sample conductivity and image quality (under the SEM), the polished sections were carbon-coated. Thin sections, polished sections and polished thin sections were prepared from these particles for optical and electron microscope studies.

Selected polished thin sections were further analysed in a Cameca SX-50 electron microprobe, using procedures described by Patterson et al. (1994).

On a hand-specimen scale, many of the samples could be seen to contain partially burnt carbonaceous shale and other rock fragments, set in a fine-grained glassy matrix (Figures 3.10a and 3.10b). The fragments commonly showed reaction rims around the contact with the matrix; these rims presumably developed as they became incorporated into the clinker while moving through the gasifier. Under the microscope some fragments still displayed their original sedimentary texture, with granular silt- and sand-sized particles surrounded by partly fused matrix material (Figure 3.10b). The matrix containing these fragments was seen (under the microscope) to consist mainly of elongated feldspar crystals, set in a very fine grained, essentially glassy vesicular groundmass (Figures 3.10c and 3.10d).

The off-cuts from the sections, representing duplicates of the clinker and ash particles studied under the microscope, were pulverised, and analysed by XRD using a Philips X'pert diffractometer system. The percentages of the individual crystalline phases (minerals) in each sample were determined using the Rietveld-based Siroquant software system (Taylor, 1991), with XRD data for a poorly crystalline metakaolin component incorporated in each task to evaluate the proportion of non-crystalline (amorphous) or glassy components (Ward and French, 2006). The results obtained from this approach were checked by separate tests involving the addition of a weighed-in ZnO spike to some ash samples (Ward and French, 2006), which confirmed that the metakaolin provided a consistent basis for evaluation of the amorphous content.

The chemical composition of each powdered sample was also determined by XRF spectrometry, based on the sample preparation procedures of Norrish and Chappell (1977). The abundance of the individual crystalline phases as indicated by the XRD analysis, combined with their respective stoichiometric compositions, was used to estimate the overall chemical composition of the crystalline components. The overall composition of the glassy (amorphous) phase in each case, was then estimated by subtracting the proportion and inferred composition of the crystalline phases from the bulk ash composition, following procedures described by Ward and French (2006).



Figure: 3.8: Photographs of ash clinkers, heated rock fragments, partially burned carbon and coal particles (selected from the turn-out samples) based on their size and colour.
Top row: small and medium heterogeneous clinkers with black and white colours taken from the gasification ash exiting the gasifier.
Second row: small, medium and large heterogeneous clinkers with black and white colours taken from the gasification ash exiting the gasifier.
Third row: large heterogeneous clinkers with black and white colours and partially burnt carbonaceous siltstone taken from the gasification ash exiting the gasifier.
Fourth row: partially burnt carbonaceous siltstone, partially burnt carbonaceous shale and coal particles taken from the gasification ash exiting the gasifier and coal feedstock.
Fifth row: coal particles taken from the coal feedstock.



Figure 3.9: Photographs of the polished sections of the selected clinkers, coal, partially burned carbon, and heated rock fragment particles from the turn-out samples.

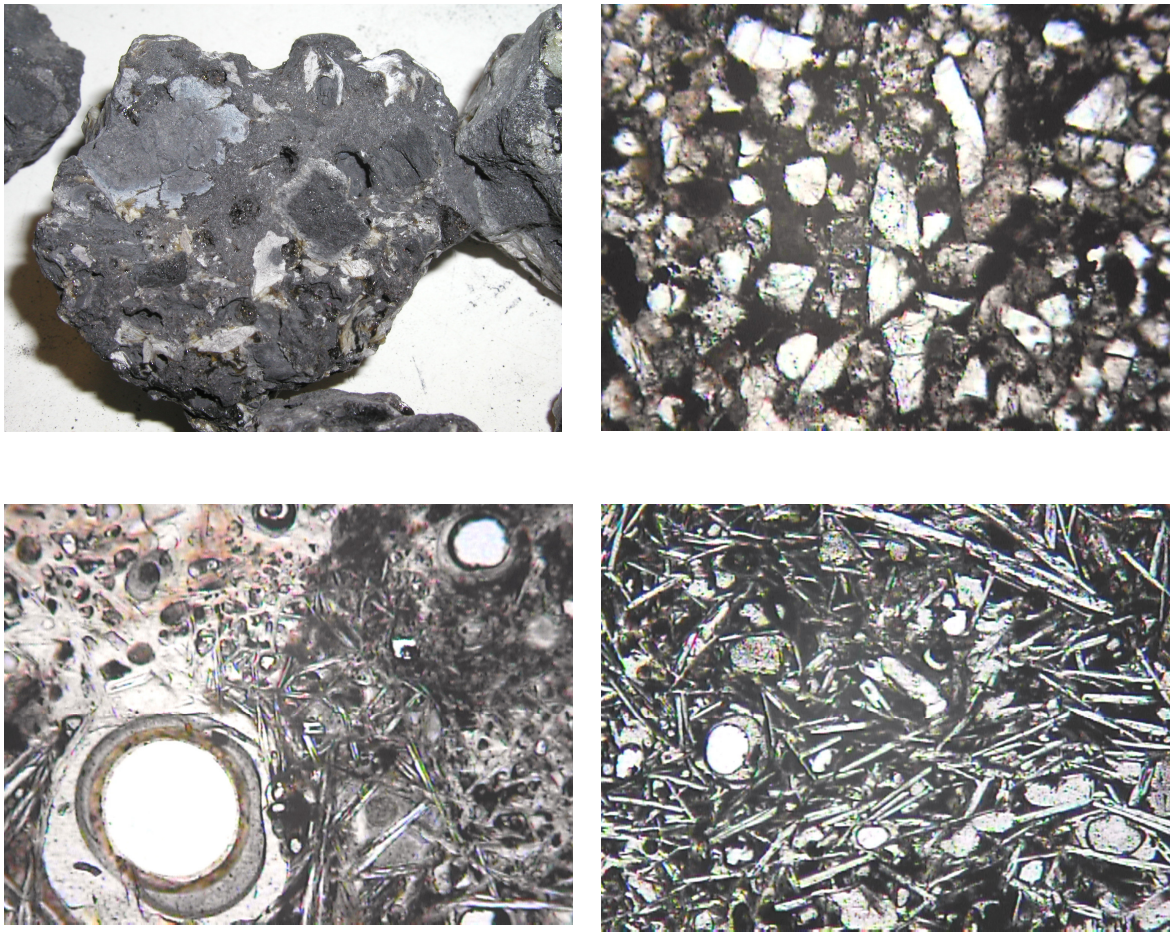


Figure 3.10: Textures of clinker materials (optical images). Top left (Figure3.10a): Clinker fragment from gasifier (width approximately 7cm), showing partly burnt carbonaceous shale particles with light-coloured reaction rims set in a fine sintered to glassy matrix. Other images: Thin-section photomicrographs (open polars, field width 1.4mm) of detrital quartz grains in fused siltstone fragment Figure 3.10b (top right), and vesicles (gas cavities) and elongate feldspar crystals in fine glassy groundmass Figures 3.10 c and d (lower left and right.)

3.5.2 Sampling methodology of dig-out samples, coarse coal and ash particles taken from the coal-conversion process facility

One of Sasol gasifiers used in a coal gasification process to produce syngas and ash as a by-product was shut down in 2007 due to normal maintenance of the gasification process facility. The opportunity was used to dig out the gasifier to obtain samples. Before the commencement of sampling of coal and ash particles as well as the removal of coal lock from the gasifier, water quenching of the burning coal inside the gasifier was used to cool the gasifier. Water was allowed to pass through the coal-bed and ash-bed in the gasifier until it exited the ash lock at the bottom of the gasifier. The water quenching was repeated several times until it was safe to dig out the gasifier.

The gasifier was dug out by mining it from the top, loading the coal into a drum which was lifted out of the gasifier using cranes. Samples of coal and ash particles (Table 3.3) were taken from the water cooled gasifier at 1m vertical intervals. The procedure as described in Paragraph 3.5.1 was followed to select a number of different clinker particles, heated rock fragments and partially burned carbonaceous shale fragment and coal lumps, for SEM-EDS analyses. Representative sub-samples of all thirteen samples dug out from the gasifier were ground to obtain 100% passing 212µm. The ground coal and ash samples were submitted for proximate, ultimate, XRF and XRD analyses.

Table 3.3: Table showing sample number, zones of the gasifier and approximate temperature of the samples taken from the gasifier during the dig-out tests

Samples number	Zones of the gasifier	Approximate temperature of sample (^{o}C)
1D	Drying (Top of skirt)	25
3D	Drying	350
5D	Pyrolysis	400-900
6D	Pyrolysis	400-900
7D	Pyrolysis	400-900
9D	Gasification	900-1000
11D	Combustion (Bottom of gasifier)	1350

Note: D: dig-out

3.6 Methods and instrumentation

Since the objective of this study was not to develop analytical characterisation methodologies for all samples generated from the pyrolysis experiment, ROM samples, turn-out and dig-out samples from the coal-conversion process, but rather to use the "standard" analytical techniques, no detailed preamble will be provided. However, the reader is referred to Sections, 2.5.2-2.6, 2.7.1and 2.7.2 in Chapter 2 in which a detailed review of the coal and ash analyses employed in this study is given. From a study structure perspective, the characterisation methodologies used will be discussed in four general categories, based on the chemical, mineralogical, petrographical and physical properties which impact on slagging and sintering of mineral matter during coal-conversion processes.

In this study, the chemical analysis of coal and ash samples involving proximate analysis (as described in Section 2.5.4), ultimate analysis (as described in Section 2.7.1) and ash analysis (as described in 2.5.5), were used to qualify and quantify inorganic elements present in these samples. The mineralogical analysis (as described in Sections 2.5.6-2.5.7) of coal and ash sample was used to identify and quantify crystalline phases present in the coal and ash samples analysed in this study. A low temperature oxygen-plasma ashing technique developed by a number of authors (Glukoter, 1965; Miller et al., 1979; Ward, 1986, 1999, 2002; Ward and French, 2004 and Foscolos et al., 1989) to oxidise organic matter present in coals at low temperature, without altering the coal minerals was also used in this study. A standard petrographic technique was applied to determine types and concentrations of maceral in the coal samples tested in this study. The laboratory instruments as well as methods followed in this study are briefly described in this section.

3.6.1 Chemical fractionation method

The chemical fractionation analysis which was described in Section 2.5.3 was followed to determine: (1) the concentration of non-mineral inorganic elements within macerals, (2) inorganic elements dissolved in the pore waters and (3) the dissolved inorganic salts in the coals.

The procedure involved the three sequential leaching procedures performed on a coal sample that was pulverised to -200mesh. Chemical fractionation is used to selectively extract elements from the coal based on solubility, which reflects their association in the coal. Briefly, the technique involves: (1) treating the coal with water to remove water-soluble elements such as sodium in sodium sulphate or those elements that were most likely associated with the groundwater in the coal (Benson and Holm, 1985). This is followed by (2) an extraction with ammonium acetate (1M concentration, 70°C) to remove elements such as sodium, calcium, and magnesium that may be bound as salts of organic acids. The residue of the ammonium acetate extraction is then extracted (3) with hydrochloric acid (1M concentration, 70°C) to remove acid-soluble species such as iron and calcium that may be in the form of hydroxides, oxides, carbonates, and organically-coordinated species. The components remaining in the residue after all three extractions are assumed to be associated with the insoluble mineral species such as clays, quartz and pyrite. The leach liquor samples, leached coal residues from the chemical fractionation analysis, as well as the feed coal samples from the different coal mines were submitted for chemical and mineralogical analyses.

3.6.2 Proximate analysis

The proximate analysis uses standard methods to measure the percentage of moisture (SABS 924, ISO 589), ash content (ISO 1171) and volatile matter (ISO 562). The difference between these three percentages and the dry mass of the original sample (100%) is referred to as the fixed carbon.

3.6.3 Ultimate analysis

The A.S.T.M. D5373 procedure for ultimate analysis was used to determine the proportion of carbon, hydrogen and nitrogen present in the coal. The sulphur content in the coal is determined by A.S.T.M. D4239 and the oxygen content is calculated by the difference.

3.6.4 Ash analysis by XRF

An XRF spectrometer (ARL9800XP SIM-SEQ) was used to determine the elemental compositions. For quantification, the intensity of characteristic lines of the element to be analysed was measured. Coal ash contains typically Fe, Al, Mg, Mn, V, Ti, Si, Ca, Na, K, P, S and Cr, which are reported as oxides by default (Fe_2O_3, Al_2O_3, MgO, MnO, V_2O_3, TiO_2, SiO_2, CaO, Na_2O, K_2O, P_2O_5, SO_3 and Cr_2O_3).

For XRF analysis, each coarse solid sample (coal and ash particles) was initially ground to 100% passing 212 µm. The powdered sample was then calcined at 850°C in air for 4h in order to remove all organic compounds and water originally contained in the sample. The calcined sample was then converted into a solid solution by fusion with lithium tetraborate ($Li_2B_4O_7$).

The prepared solid solution and standard (NIMN from Mintek) were placed in the sample holders. The sample holder was then placed in the sample compartment of an XRF spectrometer. The intensity of a characteristic line of element to be determined was measured and concentration of the element in the sample was calculated from the intensity measured (Matjie, 1997).

3.6.5 Elemental analysis by ICP-AES

A Vista AZ CCD simultaneous Inductively Coupled Plasma Atomic Emission Spectroscopy (ICP-AES) instrument was used to determine concentrations of elements present in the gas liquor samples. The sample was shaken or stirred well before and an aliquot was weighed into a clean borosilicate glass beaker. The sample was spot-treated with 30 vol. H_2O_2. The beaker was then placed on a sand bath at 100°C. The sample was not completely dried. It was removed from the sand bath and 10ml of 56% HNO_3 and 2ml of 10% Br in $HC_2H_3O_2$ were added to the heated sample. The mixture was subsequently placed on the sand bath at 100°C and taken to incipient dryness. To the dried sample, 5ml of 56% HNO_3 was added and again taken to incipient dryness. This step was repeated twice more. Finally 5ml of 32% HCl was added to the resulting solution and warmed. The sides of the beaker were washed down; after cooling, it was diluted to the desired volume. Subsequently, the concentration of the element present in the liquid sample was determined using the ICP-AES instrument.

A method number, 010-002 AICP-aqua-Regia 010-002, is briefly prescribed as follows: Five standards with appropriate concentrations, using a ratio 1:1 of the mixture 32% HCl and 56% HNO_3 as diluents, were prepared.

The ICP-AES spectrometer was allowed to warm up for 20min and a wavelength calibration was performed at the beginning of the session. A wavelength resloping procedure was performed at every 50^{th} sample of each analytical condition, as previously determined. A calibration for every element to be determined, using the prepared standards, was performed and the calibration curve of each element was checked. Finally the samples were analysed and the concentrations of the elements present in these samples were reported as ppm, g/l or %.

3.6.6 Electron microprobe analysis

For determination of the chemical composition of amorphous material and crystalline phases, the electron microprobe technique as described earlier in Section 2.5.9 was used. In addition, the author of this thesis suggests that this equipment could be used to determine the proportions of the organically-bound inorganic elements in the individual coal macerals. The author also proposes that the proportions of the organically-bound inorganic elements (magnesium, potassium, titanium) in the coal macerals, that were not determined by the electron microprobe in the past, must be undertaken in this study. Some of these elements could also be responsible for the slagging process during coal-conversion processes.

Polished sections were prepared from six lump coal samples produced by six Highveld coal mines, South Africa. The sections were prepared to embrace the range of coal macerals in each sample, as indicated by the macroscopic appearance (lithotype) of selected particles.

The surfaces of the polished sections, as shown in Figure 3.9, were coated with a thin layer of carbon and loaded into a Cameca SX-50 electron microprobe analyser equipped with the Windows-based SAMx operating system and interface software. The elemental chemistry of the individual macerals in each sample was analysed in this instrument using special light-element techniques, following procedures described more fully by Bustin et al. (1993) and Ward et al. (2005).

Individual points on the various macerals in each coal were analysed under operating conditions described by Ward et al. (2005).

The accelerating voltage for the electron beam was 10kV and the filament current 20nA, with a magnification of 20,000x giving a beam spot size on the sample of around 5 to 10µm in diameter. As discussed by Bustin et al. (1993), an independently analysed anthracite sample was used as the standard for carbon in the analysis process.

A range of mineral standards was used for the other elements. The detection limit of nitrogen in the coal, determined by Mastalerz and Gurba (2001) using accelerating voltage of 10kV, beam current of 20nA and counting time of 20s during electron microprobe analysis, was found to be 0.5%. However, the detection limits of other inorganic elements present in the coal macerals were not reported.

The percentages of carbon, oxygen, nitrogen, sulphur, silicon, aluminium, calcium, magnesium, potassium, titanium and iron were measured for each point, with a note on the type of maceral represented in each case. The results of the individual analyses were tabulated in spreadsheet format. Although care was taken to analyse only "clean" macerals and avoid areas where visible minerals were also present, the area analysed for some points unavoidably included significant proportions of mineral components (e.g. quartz, clay, and pyrite) as well as the organic matter. Points that apparently included mineral contaminants (e.g. points with high [> 0.5%]) Si or points with particularly high percentages of both Fe and S) were excluded from consideration; so, too, were points that included some of the mounting epoxy resin (e.g. epoxy filling empty cell structures), indicated by unusual oxygen and high nitrogen contents.

As mentioned in Section 3.6, a number of different clinker particles and partially burned carbonaceous shale fragments were selected from the gasification ash on the basis of their colour and size. Thin sections, polished sections and polished thin sections were prepared from these particles for optical and electron microscope studies (as shown in Figure 3.9). The same prepared sections of the selected clinkers and heated rock fragments were analysed by electron microprobe to determine the chemical composition and relative abundance of the amorphous or glassy material, as well as the crystalline phases present in coarse gasification ash. Minerals such as diopside ($CaMgSi_2O_6$), pyrite (FeS_2), apatite ($Ca_5F(PO_4)_3$), hematite (Fe_2O_3), rutile (TiO_2) and sanidine ($KAlSi_3O_8$) supplied with the electron microprobe were used as standards for silicon, calcium, magnesium, sulphur, iron, phosphorus, titanium, potassium and aluminium during the electron microprobe analysis of the selected clinkers and heated rock fragments.

3.6.7 Determination of mineral matter in the coal by low temperature asher

Representative portions of coal samples from the six coal mines were finely powdered. A representative portion of each powder was subjected to low-temperature oxygen-plasma ashing using an IPC 4-chamber asher, as outlined in Australian Standard 1038, Part 22. The mass percentage of low-temperature ash representing the proportion of mineral matter in the coal was determined in each case.

3.6.8 XRD analysis

Coarse samples (coal, char and ash) to be analysed were initially ground using a ball mill in order to obtain -212µm particles. The powdered sample was transferred to a suitable sample holder (preferably made of aluminium) and the sample in the holder was tamped gently, but thoroughly, with the edge of a glass slide. It was important to fill the sample holder; thereafter the surplus sample was sliced off with a glass slide (approximately 50x70mm and 5mm thick), whilst simultaneously compressing the sample in the holder. The above procedure was repeated until a suitable surface (a smooth surface of even texture) was obtained. The pulverised coal and char samples prepared in this way were analysed by XRD using an X'Pert PRO PANalytical (Philips) – Unit 2 diffractometer system.

The XRD system: X'Pert PRO PANalytical (Philips) – Unit 2 was used to analyse the samples. The experimental parameters were as follows:

Goniometer:	PW3050/60 (Θ / Θ configuration)
X-ray detector:	X'Celerator (Solid State, RTMS)
X-ray tube:	Cobalt target, ceramic, LFF-type; λ Co Kα = 1.7889 Å
Voltage:	40KV
Amperage:	40mA
Prog. Divergence Slit:	1.0º (fixed)
Anti-scatter Slit:	2.0º
Scan from:	5º 2Θ
Scan to:	135º 2Θ
Soller slits:	0.02 Rad
Scanning:	Continuous.
Duration of scan for quantitative XRD analysis:	6-14h

The qualitative XRD analysis was carried out using the Graphics & Identification programme. The percentages of the individual crystalline phases (minerals) in each sample were determined using the Rietveld-based Siroquant software system (Taylor, 1991). In order to determine the proportion of amorphous material in the samples, calcium fluoride was used as an internal standard.

In parallel, the mineralogy of low temperature ash from the coal samples and the pulverised ash from the coal-conversion process were analysed by X-ray powder diffraction using a Phillips X'pert diffractometer with copper Kα radiation; the minerals present were identified by reference to the ICDD Powder Diffraction File. Quantitative analyses of mineral phases in the LTA and ash were made using SIROQUANT™, commercial interpretation software written by CSIRO based on the Rietveld XRD analysis technique (Taylor, 1991).

3.6.9 High-temperature X-ray diffraction (HT-XRD)

The -1mm particles of the crushed feed coal were screened into fine (100% <0.25mm) and coarse (100% >0.25mm) fractions. Each fraction was separated by float-sink techniques into a low-density ("floats") fraction, and a high-density ("sinks") fraction. The density of the separation medium used in this study was 1.56g/cm^3. The mineral matter in the feed coal, as well as the individual size and density fractions, were isolated using low-temperature oxygen-plasma ashing. The resulting LTA residues were subjected to Rietveld-based X-ray diffraction analysis using procedures described by Ward et al. (2001) and also to HT-XRD analysis using procedures described by French et al. (2001).

3.6.10 Determination of clay mineral in the coal

The clay fraction (less than 2µm effective diameter) of each sample was isolated by ultrasonic dispersion in sodium hexametaphosphate (Calgon) and subsequent settling. The clay fraction was further investigated by X-ray diffraction of oriented aggregates, using glycol and heat treatment. The relative proportions of the different clay minerals in this fraction for each sample were determined by the method of Griffin (Carver, 1971).

3.6.11 Computer controlled scanning electron microscope (CCSEM) (van Alphen, 2005)

CCSEM at Technology Service International (TSI, Eskom), is a SEM configured to automatically and rapidly determine the minerals in coal and phases in fly ash and slag deposits. Samples of pulverised coal or fly ash were mixed with iodinated epoxy resin and allowed to cure. The cured 30mm mount was polished, exposing individual particles in cross-section.

The CCSEM analytical procedure is as follows:

- Appropriate magnification based on particle sizes was selected. The polished section was divided into regularly spaced analytical fields of view or frames.
- The sample was positioned at the first field of view and a back-scattered electron image (BSI) acquired. BSI (Figure 3.11) is based on atomic number contrast and ensures that coal and minerals can be identified by image processing routines.
- The image was processed and the regular grid of analytical points established for each field of view.
- The electron beam was positioned at each analytical point and a 100msec X-ray spectrum acquired (Figure 3.12). The elemental composition of the phase was derived from the X-ray spectrum.
- The sample was positioned at the next field of view and the process repeated until all the fields of view had been analysed.

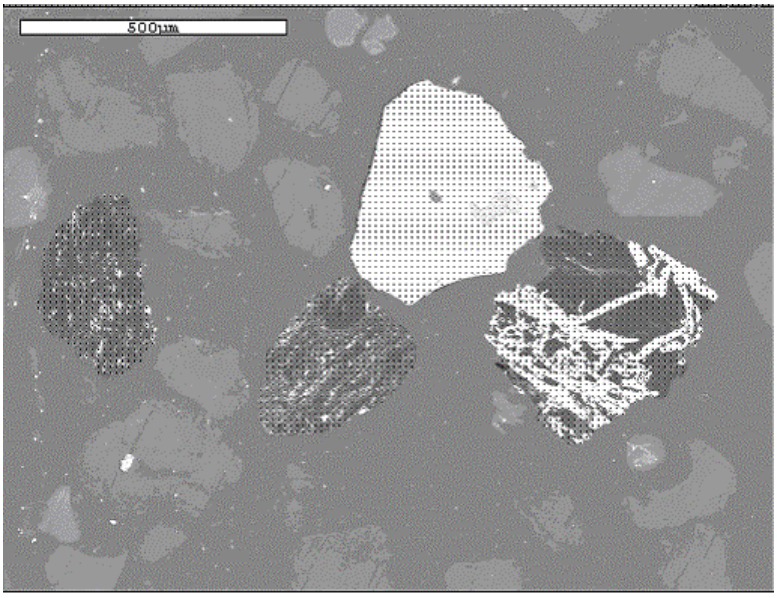


Figure 3.11: Processed back-scattered electron image of pulverised coal with the regular grid of analytical points superimposed (black dots).

The scale bar represents 50µm and the estimated point spacing is 11.21µm. In this image the coal is black, the epoxy resin is grey and the mineral matter is white.

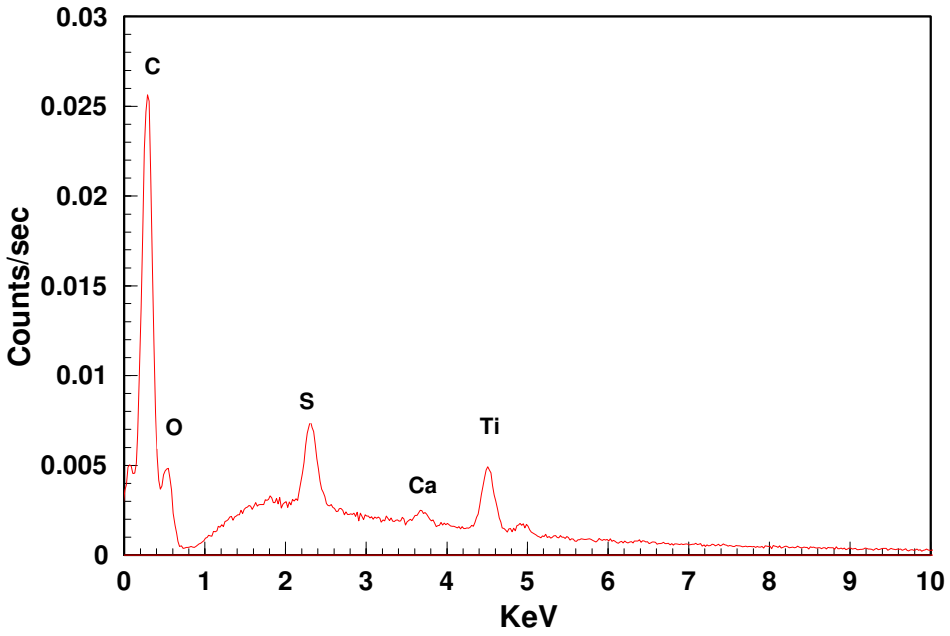


Figure 3.12: Typical X-ray spectrum of coal.

The development of mineral identification rules based on the principles of fuzzy logic is crucial for CCSEM analysis. The rules are listed in an ASCII file (*.sui) and are developed by examining the polished section and identifying the minerals present prior to undertaking an automated CCSEM analysis. The file developed is unique and can be used for subsequent CCSEM analysis.

Mineral nomenclature for pulverised fuel is based on the typical minerals found in pulverised fuel (van Alphen, 2005). In context of pulverised fuel, the CCSEM mineral "coal" describes a C-rich phase (Figure 3.11), describing the organic-rich fraction of pulverised coal. Coarse ash and clinker phase identification is based on the elemental composition, while nomenclature is based on the perceived coal mineral source.

The major outputs from CCSEM analyses are:

- Mass-% mineral or phase proportions in pulverised fuel or fly ash, respectively. Mineral proportions (volume-%) are determined by dividing the number of analytical points for each phase by the total number of analysed

points. The mass-% can be calculated by multiplying the volume-% by the density of the phase.

- The oxide elemental composition can be calculated from the mass-% mineral proportions.
- Association characteristics of minerals in coal and phases in fly ash.
- Size variation of the different minerals.
- Proportion of included minerals compared to proportion of extraneous minerals. From a slagging perspective, included minerals (within the coal which is undergoing gasification) can be expected to be exposed to higher temperatures and more reducing conditions, compared to extraneous mineral particles. This difference in localised environment may affect mineral transformations.

3.6.12 QEMSCAN analysis

As stated earlier in Section 2.5.8, QEMSCAN equipment can be used to determine mineral-mineral associations, particle size, mineral compositions and texture of particles in the coal and ash samples. In this study the polished sections and polished thin sections of coal and ash samples (as shown in Figure 3.9) were placed into the sample compartment of QEMSCAN for characterisation.

As illustrated in Figure 3.13, the electron beam of the QEMSCAN interacts with a sample during scanning, generating secondary X-rays with distinct energy levels that can be interpreted in terms of type and amount of element present. Combinations of elements and relative proportions are interpreted on-line and used to automatically identify a mineral or phase present. Typically 100,000 individual X-ray identifications per hour can be achieved automatically. This procedure is therefore similar to CCSEM, but with a higher degree of automation.

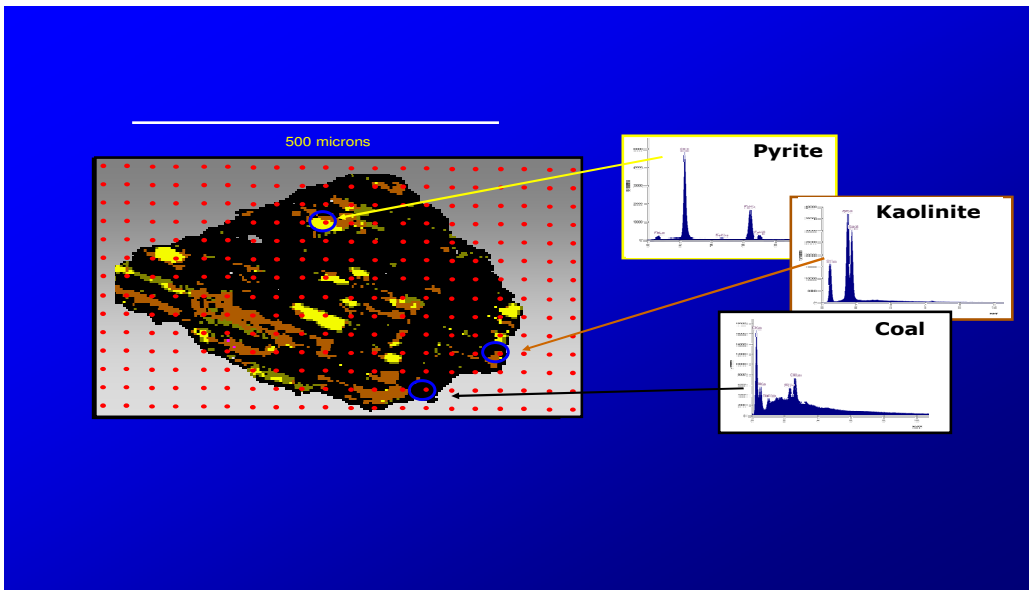


Figure 3.13: Identification of minerals in coal particles by QEMSCAN (Butcher, 2006).

3.6.13 Petrographic analysis

Coal and ash samples, crushed to -1mm, were prepared as per routine preparation for petrography following ISO standard 7404-2. A maceral group analysis as per ISO 7404-3 was conducted on sample 32T, considered as the gasifier feed coal, as well as on six coal samples from the six different mines.

The samples were obtained and prepared to minimise contamination and 500 sampling points were determined for each sample. The particle falling directly under the cross hair was categorised, applying a 50x50µm field of view. Large particles were classified several times, if meeting the requirements above. All particles -30µm were not counted, due to reduced ability to observe these small particles accurately. As more than 10 categories were required and the point counter only measured up to 10 variables at a time, certain measurements were recorded separately on paper, ensuring that 500 particles were counted per block.

Reflectance analysis was conducted before (or very shortly after), the particle type analysis, in order to limit the potential impact of the oil on reflectance readings. Initially, every second sample was analysed and additional samples were analysed where significant changes in trends were determined.

3.6.14 Ash Fusion Temperature analysis

The standard method ISO 540 was used to demonstrate the fusion properties of laboratory prepared coal ash. The ash was heated to 1600°C in an oxidising atmosphere. The results of an AFT analysis consist of four temperatures, namely: (1) initial deformation temperature (DT), (2) softening temperature (ST), (3) hemispherical temperature (HT) and (4) flow temperature (FT).

3.6.15 Particle size distribution

The representative coal feedstock to gasification process, prepared by blending coals from the different mines, was screened into eight size fractions using the screen aperture sizes: 75mm, 53mm, 26mm, 13.2mm, 9.5mm, 6.7mm, 4.7mm and 4mm. Each fraction of coal was ground to 100% passing lmm, before submitting the prepared samples for chemical analysis (XRF, proximate and ultimate analyses) and mineralogical analysis (XRD and CCSEM analyses).

3.6.16 FactSage modeling

As stated by Matjie et al. (2006), the thermodynamic package was used to predict the equilibrium phases in the lower part of the gasifier (where the temperature decreases from the peak in the coal combustion region towards the grate). The FactSage modeling was undertaken to support XRD, CCSEM and QEMSCAN results for char and ash samples produced in this study. The fluxing elements such as sodium, potassium, calcium, magnesium and iron as ferrous oxide in the coal may possibly react with aluminium silicates in the coal and give rise to the slagging process during coal conversion processes, under either reducing or oxidising conditions. This possibility was examined by calculating the equilibrium speciation of elements between the coal and the solid formed during coal-conversion processes.

For predicted changes during pyrolysis the practical conditions during the pyrolysis experiments were approximated. The equilibrium state was found for a combination of the 1.2kg of coal which was fed to the reactor, with all the nitrogen which entered the reactor in one hour (40ml/min at room temperature and 26bar pressure, giving a total of 2.52mol N_2) and a reaction temperature of 600°C, the maximum temperature attained during pyrolysis.

These conditions would give an upper boundary on the extent of sintering of mineral matter which can be expected.

The thermodynamic package FactSage was used for undertaking the calculations, considering species in the gas phase and liquid phase, as well as solid compounds and solid solutions. The products of pyrolysis of the coal macerals were assumed to be limited to char (heated carbon), CH_4, H_2, H_2O, CO and CO_2 (which could react further to yield other products, such as H_2S, HCl and HF). The assumed chemistry for the pyrolysis calculations was an average of all the coals in this study, given in Table 3.4.

Table 3.4: Assumed coal chemistry for equilibrium calculations

Species	**Mass %**	**Mineral**
H_2O	3	
S	1	
O	8	
C	55	
H	3	
SiO_2	8	quartz
$Al_2Si_2O_5(OH)_4$	10	kaolinite
FeS_2	1	pyrite
$KAl_2(OH)_2AlSi_3O_{10}$	4	muscovite
$CaCO_3$	2	calcite
$MgCa(CO_3)_2$	3	dolomite
NaCl	0.82	halite
$Ca_5F(PO_4)_3$	0.44	fluoroapatite

CHAPTER 4

RESULTS AND DISCUSSION - COAL ANALYSIS

In this chapter, the results obtained from the detailed characterisation of coals from mines in the Highveld coalfield as well as the feed coal are discussed as the basis for a better understanding of the mineralogical and chemical properties of the individual components in the feedstocks used for coal conversion processes.

4.1 Chemical analyses of coals from six different Highveld coal mines and feed coal to the coal conversion process

4.1.1 Proximate analysis

Proximate analysis data (Table 4.1) show that the samples yield 30-34% volatile matter on a dry ash free (daf) basis. The inherent moisture content of the coals ranged between 2.9% and 3.8% and the total sulphur content from 0.7% to 1.1%. The ash yield of the samples tested (air-dried basis) ranged between 22.1% and 29.7%.

Table 4.1: Proximate analyses (air dried basis) of the coals tested

Mine Number	1	2	3	4	5	6
Moisture (%)	3.30	2.90	3.20	3.40	3.00	3.80
Ash (%)	24.50	29.00	29.70	27.20	26.80	22.10
Volatile matter (%)	21.70	22.90	21.30	21.50	22.40	23.10
Fixed carbon (%)	50.50	45.20	45.80	47.90	47.80	51.00
Total sulphur (%)	1.10	1.00	0.80	1.00	1.10	0.70
Volatile matter (daf basis, %)	30.10	33.60	31.70	31.00	31.90	31.20

4.1.2 Ultimate analysis

Ultimate analysis data (Table 4.2) indicate that the coals contain high proportions of carbon (ranging from 77 - 80% daf), with relatively low concentrations of sulphur (0.9%-1.6% daf), nitrogen (2-2.2% daf) and hydrogen (ranging from 4-4.6% daf). The oxygen content of the coals (daf basis) was found by calculation to range from 12-16%.

Table 4.2: Normalised ultimate analyses of the coals tested (dry, ash-free basis)

Mine Number	**1**	**2**	**3**	**4**	**5**	**6**
Carbon (%)	79.90	78.50	77.10	77.80	79.00	77.90
Hydrogen (%)	4.36	4.55	4.07	4.12	4.59	4.29
Nitrogen (%)	2.12	2.00	1.97	2.00	2.08	2.00
Total sulphur (%)	1.55	1.41	1.15	1.50	1.62	0.92
Oxygen (% by difference)	12.10	13.50	15.7	14.60	12.70	14.90

4.1.3 XRF analysis

The normalised proportions of inorganic elements in the coal samples, derived from XRF analysis of the whole-coal samples, are given in Table 4.3. The XRF technique used is regarded as only semi-quantitative for sulphur, hence the sulphur contents are not reported. The results given in Table 4.3 also indicate that there are some variations in the chemical composition of the coal used in the study. These differences in compositions are attributed to the particle size of the coarse coal samples, which ranged from 13.2mm to 2.36mm, possibly producing heterogeneity that affected the sampling process.

The XRF analysis of the feed coal sample to gasification indicated that this sample contains 52.2% SiO_2, 26.2% Al_2O_3, 4.0% Fe_2O_3, 1.5% TiO_2, 0.7% P_2O_5, 8.1% CaO, 3.7% MgO, 0.7% Na_2O, 1.1%K_2O and 1.9% S (normalised XRF results, excluding carbon and volatiles).

Table 4.3: Inorganic oxide percentages (wt %) from normalised XRF analysis of whole-coal samples

Mine Number	1	2	3	4	5	6
SiO_2	57.16	55.38	55.91	52.20	57.43	55.68
Al_2O_3	24.96	30.21	27.78	29.40	26.70	25.31
Fe_2O_3	5.13	2.34	1.88	2.42	3.58	2.59
TiO_2	1.21	1.26	1.42	1.64	1.17	1.33
P_2O_5	0.32	0.76	0.53	0.86	0.89	0.68
CaO	7.49	6.54	8.26	9.27	7.03	10.60
MgO	1.67	1.42	2.02	1.84	1.23	2.06
Na_2O	0.89	0.76	1.06	1.07	0.85	1.06
K_2O	0.85	0.95	1.02	1.29	1.13	0.54

4.2 Petrographic analysis of coals from different Highveld coal mines

Petrographic analysis (Table 4.4) indicates that coals characterised in this study are inertinite-rich, with 64-77% inertinite and 19-30% vitrinite components on a mineral-free basis. It is clear from the results given in Table 4.4 that mines 5 and 6 contain slightly higher proportions of vitrinite and liptinite and lesser proportions of inertinite than the other coal samples analysed. The results from this table also show that the coals have a mean maximum vitrinite reflectance, measured on telocollinite, of around 0.70-0.75%. According to ISO 11760, the coals can be classified as medium-rank C bituminous coals.

Table 4.4: Petrographic analysis of coal samples from the different mines (vol. %, mineral free)

Maceral Group	1	2	3	4	5	6
Vitrinite (%)	19.2	25.8	20.5	20.6	31.6	27.1
Liptinite (%)	3.5	3.7	3.2	3.4	5.4	5.4
Inertinite (%)	77.3	70.6	76.3	76.1	64.0	67.5
Rv_{max} (%)	0.72	0.70	0.75	0.72	0.70	0.70

4.3 Mineralogical analyses of LTA of coals from the different mines and feed coal

4.3.1 Mineralogy of LTA residues

Table 4.5 summarises the percentages of the individual minerals in each LTA of coals produced from the different coal mines, based on the powder XRD and SIROQUANT evaluation. Figures 4.1 and 4.2 illustrate the X-ray diffractograms of the LTA from each coal sample.

The results shown in Table 4.5 indicate that the coal sample from mine 4 contains a slightly lower proportion of mineral matter in comparison with the other coal samples analysed. The proportions of low-temperature (oxygen-plasma) ash in the coal samples were found to be 24.60-43.90 wt%, compared to the (high-temperature) ash yields of 22.10-29.70wt%, as determined by proximate analysis. The difference is largely because many of the minerals (kaolinite, calcite, dolomite, pyrite, siderite and illite) in the coal samples decompose at the high temperatures associated with ashing in proximate analysis, but remain stable under plasma-ashing conditions (Tables 4.1 and 4.5).

As indicated in Table 4.5 and Figures 4.2-4.3, the LTA derived from the six coals was made up mainly of kaolinite (44-51%), with a lesser proportion of quartz (15-22%), mica (4.5-7.4%) and dolomite (6.4-15%) and minor proportions of siderite ($FeCO_3$), calcite ($CaCO_3$), pyrite (FeS_2), anatase (TiO_2), and the aluminophosphate mineral, goyazite ($SrAl_3(PO_4)_2(OH)_5.H_2O$). It is interesting to note that the LTA of samples 1 and 6 contain no illite ($K_{1.5}Al_4(Si_{6.5}Al_{1.5})O_{20}(OH)_4$), whilst the LTA of coal samples from mines 2, 3, 4 and 5 contain admixed illite, ranging in abundance from 2 to 5.7%. A small proportion of bassanite ($CaSO_4.½H_2O$), which was probably derived from interaction of the organically-associated calcium in the coals with organic sulphur during the low-temperature ashing process, was also noted in the LTA samples of coals.

Further results on the clay fractions, based on the separate oriented aggregate XRD study, are provided in Table 4.6. The results differ from those given in Table 4.5, because only the smallest (<2 micron) particles were analysed for the results in Table 4.6. The nature of the sub-micron clay minerals (illite, smectite ($Na_{0.33}(Al_{1.67}Mg_{0.33})Si_4O_{10}(OH)_2$),

illite/smectite and kaolinite) may possibly be significant in clinker formation, as well as in the volatilisation of minor amounts of Al and Si during coal conversion processes.

Table 4.5: Mineralogical analyses of LTA from coal samples from the different mines (wt %)

Mine	**1**	**2**	**3**	**4**	**5**	**6**
LTA	31.90	43.90	33.60	24.60	36.20	34.50
Quartz	17.60	21.50	20.10	18.30	15.20	20.60
Kaolinite	51.40	50.40	50.80	47.60	44.00	49.50
Illite	nd	5.70	5.30	2.20	5.70	nd
Mica	10.40	7.40	4.50	4.50	6.90	7.00
Calcite	2.10	1.20	1.80	4.60	9.80	2.70
Dolomite	10.30	6.40	10.20	15.20	10.00	11.70
Siderite	0.00	1.30	0.30	1.40	0.40	0.90
Pyrite	2.40	1.40	2.60	2.00	1.40	1.60
Bassanite	2.10	1.40	1.90	2.50	2.50	1.60
Goyazite	1.00	1.70	1.40	0.90	3.00	2.70
Anatase	2.70	1.50	1.00	0.80	1.00	1.60

Note: nd: not detected.

The chemical composition of the coal ash expected in each of the coals was calculated from the mineral percentages listed in Table 4.5 and the chemical composition of the individual minerals based either on stoichiometry or on typical analyses of the same minerals published in the literature. The results (Table 4.7), normalised to exclude sulphur (as SO_3), are very similar to the data obtained from direct XRF analysis of the same coals, also normalised to a sulphur-free basis, presented in Table 4.3. Only minor differences are present in most cases, probably reflecting differences in the actual samples analysed in each instance, differences between stoichiometric and actual mineral compositions, as well as errors inherently associated with the two different techniques.

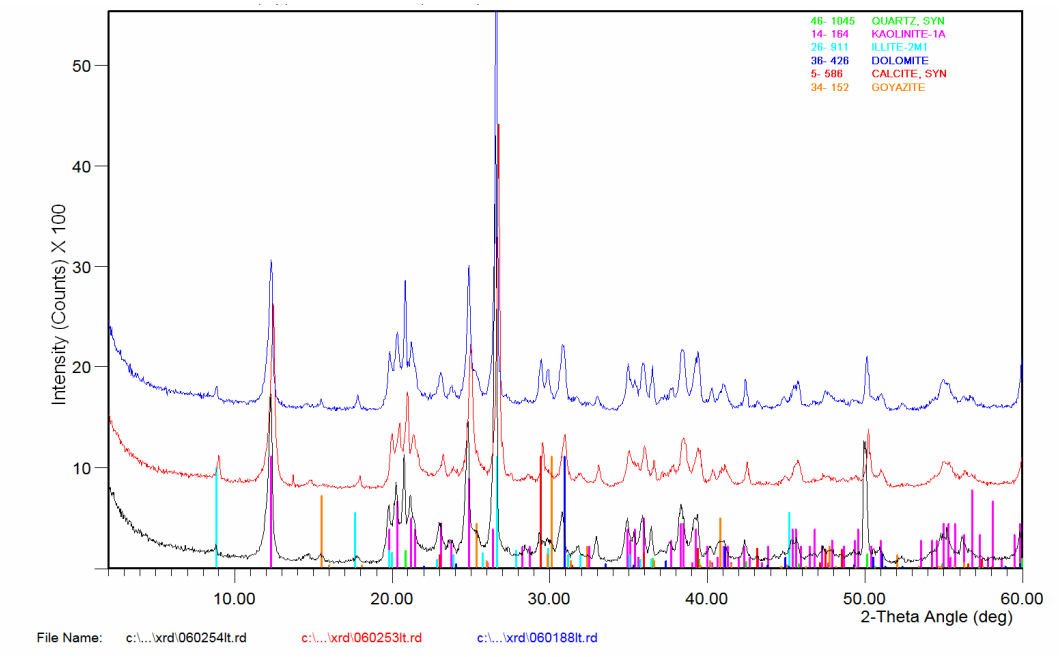


Figure 4.1: X-ray diffractograms of LTA from samples from mines 3 (top), 1 and 5 (bottom).

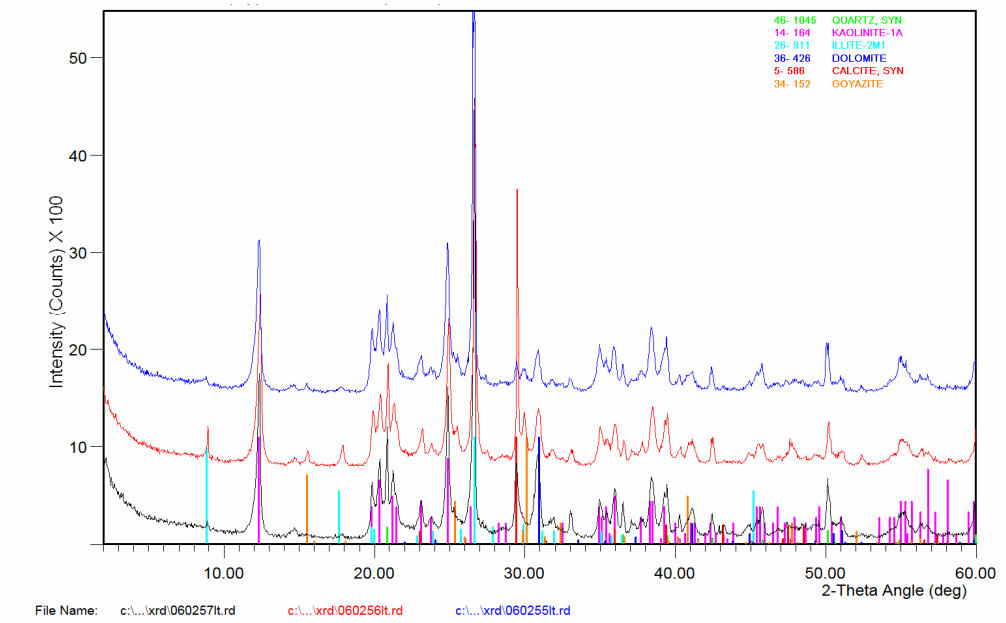


Figure 4.2: X-ray diffractograms of LTAs from samples from mines 2 (top), 4 and 6 (bottom).

Table 4.6: Mineralogy of <2 micron fraction by oriented aggregate XRD

Mine Number	Kaolinite %	Illite %	Expandable Clay %	Nature of Expandable Clay
1	93.00	1.00	6.00	Mainly smectite
2	92.00	3.00	5.00	Mainly irregular I/S
3	93.00	3.00	4.00	Mainly irregular I/S
4	96.00	0.00	4.00	Mainly irregular I/S
5	92.00	3.00	5.00	Regular to irregular I/S
6	90.00	2.00	8.00	Smectite + regular I/S

Note: I/S = interstratified (mixed-layer) illite-smectite

Table 4.7: Inferred ash chemistry (SO_3-free) based on Siroquant results

Mine Number	1	2	3	4	5	6
SiO_2	55.17	59.32	56.18	51.33	57.57	54.02
Al_2O_3	28.86	29.09	27.51	28.18	28.55	26.58
Fe_2O_3	1.91	2.02	1.95	1.46	2.28	2.73
TiO_2	3.22	1.74	1.92	1.23	1.19	0.99
P_2O_5	0.41	0.67	1.10	1.26	0.57	0.38
CaO	6.27	3.93	7.27	12.20	5.98	10.27
MgO	2.69	1.63	3.08	2.70	2.66	4.13
Na_2O	0	0	0	0	0	0
K_2O	1.47	1.61	0.99	1.64	1.20	0.91

4.3.2 Coal Quality Predictor model results for six coals and their density fractions from the different Highveld coal mines

The van Alphen Consultancy Coal Quality Predictor model, which is also based on the chemical analysis (proximate, ultimate and elemental analyses) of the mineral matter and organic matter present in the coal, was used to estimate the proportions of minerals in the composite sample float and sink fractions. The composite feed coal samples were measured by CCSEM. The following general trends of results presented in Tables 4.8-4.10 are noted:

- Mineralogical analysis of coals which was predicted by the CQP model, shows that sample from mine 3 is distinct from the other samples analysed. The elevated proportion of ash yield in sample from mine 3 is attributed to the substantially

higher proportion of kaolinite and quartz present in the rock fragments (mudstone, sandstone and siltstone).

This coal contains significantly higher proportion of calcite along with the lowest proportion of pyrite. Significant proportions of pyrite and calcite in the coal occur as included particles in the carbon matrix and not as coarse cleat fragments. The coal contains a significantly high proportion of secondary aluminium sulphate compared to the other coals. The density results for this coal indicated that this coal probably has the highest proportion of rock fragments, indicating contamination by the stones from the roof and floor during mining.

- The model results also reveal that the sample from mine 1 contains significantly higher proportions of pyrite and siderite/Fe-oxide in comparison with the other coals. A significant proportion of the pyrite occurs as included fine grains in carbon-rich coal particles, in pyrite-rich layers, in carbon-rich particles and is also associated with quartz.
- Samples from mines 5 and 6 contain comparatively high proportions of pyrite and low proportions of kaolinite. In this coal, a significant proportion of the pyrite occurs as coarse pyrite cleat fragments, concentrated in the sink fraction. These two samples also have the highest proportion of coarse calcite particles that occur as cleat fragments. The sample from mine 5 has the highest proportions of quartz and microcline that are attributed to a higher proportion of coarse grained quartz/kaolinite/microcline sandstone rock fragments. The sample from mine 6 had the lowest ash yield with the correspondingly lowest proportion of "stone". The high proportion of extraneous coarse pyrite and calcite in samples from mines 5 and 6 can have an impact on obtaining representative samples if not treated with care during sample preparation. The sample from mine 2 has the highest kaolinite and illite/muscovite content. Excluding quartz, which occurs as the coarse sandstone rock fragments and included particles in the carbon-rich matrix, a high proportion of pyrite, calcite, dolomite and kaolinite occurs as included grains in the carbon-rich coal particles.
- The sample from mine 4 has the same mineralogical and chemical properties as the sample from mine 3.

Significantly higher proportions of illite, kaolinite, muscovite, siderite and quartz, along with a low proportion of carbon-rich particles, reported to the sink fractions (Table 4.10); whereas significantly higher proportions of dolomite, calcite, carbon-rich particles and low

proportions of illite, kaolinite and quartz, reported to the float fractions (4.9). Significant proportions of dolomite and calcite fluxing elements-bearing minerals in samples from mines 3 and 4 can react with kaolinite and illite in the carbon-rich particles at elevated temperatures to form a melt during coal gasification. This melt will result in the clinker formation.

Table 4.8: Proportions of minerals in coal composite from Highveld coal mines determined by CQP (mass %)

Mine	**1**	**2**	**3**	**4**	**5**	**6**
Pyrite/pyrrhotite	2.03	1.10	0.99	1.07	1.09	0.57
Calcite	2.48	2.34	3.09	2.78	1.68	2.43
Dolomite	2.90	3.31	3.68	3.99	2.79	2.96
Apatite	0.22	0.71	0.47	0.66	0.63	0.40
Microcline	0.12	0.24	0.24	0.30	0.18	0.09
Muscovite	0.50	0.99	0.99	1.34	0.82	0.37
Illite	0.74	1.47	1.47	1.98	1.21	0.55
Kaolinite	15.95	21.40	18.12	18.26	15.02	13.80
Quartz	5.11	2.87	3.72	1.56	1.27	3.24
Siderite/Fe-oxide	0.00	0.00	0.00	0.00	0.00	0.00
Rutile	0.37	0.33	0.30	0.42	0.24	0.35
#Coal	69.59	65.24	66.93	67.64	75.06	75.25

Note: #Coal – refers the carbon-rich matrix and represents the macerals

Table 4.9: Proportions of minerals in float fraction of coals from Highveld coal mines determined by CQP (mass %)

Mine	1	2	3	4	5	6
Pyrite/pyrrhotite	2.15	1.11	0.92	1.12	1.64	0.96
Calcite	2.92	2.58	3.59	3.73	2.71	3.66
Dolomite	1.53	1.48	2.18	1.86	1.24	1.67
Apatite	0.21	0.57	0.42	0.63	0.65	0.38
Microcline	0.18	0.25	0.27	0.30	0.26	0.11
Muscovite	0.80	1.02	1.13	1.33	1.17	0.45
Illite	1.18	1.50	1.67	1.97	1.73	0.67
Kaolinite	15.56	21.68	20.19	19.27	17.61	14.62
Quartz	6.07	5.17	6.18	3.83	5.91	5.36
Siderite/Fe-oxide	0.00	0.00	0.00	0.00	0.00	0.00
Rutile	0.27	0.34	0.39	0.40	0.28	0.28
#Coal	69.12	64.29	63.05	65.57	66.81	71.85

Note: #Coal – refers the carbon-rich matrix and represents the macerals

Table 4.10: Proportions of minerals in sink fraction of coals from Highveld coal mines determined by CQP (mass %)

Mine	1	2	3	4	5	6
Pyrite/pyrrhotite	5.31	2.66	2.47	6.48	6.08	9.21
Calcite	2.48	2.35	4.30	5.33	5.47	14.09
Dolomite	1.27	1.03	1.40	1.32	1.54	1.55
Apatite	0.06	0.24	0.26	0.69	0.39	0.44
Microcline	1.09	0.89	0.62	0.65	1.12	0.50
Muscovite	4.74	3.55	2.47	2.94	5.67	2.28
Illite	7.01	5.25	3.65	4.35	8.39	3.38
Kaolinite	37.98	44.94	40.38	40.18	25.24	27.74
Quartz	24.86	23.18	22.05	15.81	31.22	17.43
Siderite/Fe-oxide	2.16	1.36	1.14	1.30	2.49	1.75
Rutile	0.80	0.84	1.03	0.90	0.52	0.68
#Coal	12.23	13.71	20.24	20.05	11.87	20.95

Note: #Coal – refers the carbon-rich matrix and represents the macerals

4.3.3 Mineral matter in feed coal and their transformation at elevated Temperatures

The XRD analysis (Table 4.11) of the low temperature ash sample of the feed coal shows that this coal contains around 35% mineral matter (LTA), made up mainly of kaolinite (53%), quartz (18.2%) and dolomite (11.2%), with minor proportions of illite (5.6%), calcite (2.7%), pyrite (2.8%), and the phosphate minerals apatite ($Ca_5F(PO_4)_3$) (1.0%) and gorceixite ($BaAl_3(PO_4)_2(OH)_5.H_2O$) (1.9%). The presence of a small proportion of bassanite ($CaSO_4.½H_2O$) (2.2%) in the LTA sample produced from the feed coal probably formed from interaction of organically-associated calcium in the coals with organic sulphur during the low-temperature ashing process. Such a mineral assemblage confirmed the previous results for the South African coals that were found by Pinetown et al. (2006).

Data on the different size and density fractions, also summarised in Table 4.11, indicate that the float fractions, with low percentages of LTA, have a mineral assemblage with lesser proportions of quartz and pyrite than the LTA-rich sinks fractions. Dolomite, by contrast, is more abundant in the floats fractions than in the high-density sinks material. Together with the greater abundance of dolomite in the fine fractions than the coarse fractions, this suggests a relatively intimate association of the carbonate minerals with the maceral components. Apart from a greater abundance of illite in the coarse floats material, the clay minerals, the phosphates and the bassanite all appear to be more or less evenly distributed amongst the different size and density fractions.

Table 4.11: Mineralogy of LTA isolated from feed coal and float-sink fractions (wt %)

Sample	Feed Coal	Coarse Floats	Coarse Sinks	Fine Floats	Fine Sinks
LTA	*34.6*	*15.0*	*55.4*	*14.9*	*53.6*
Quartz	18.2	9.3	19.8	11.1	24.7
Kaolinite	53.3	61.0	58.8	62.8	49.0
Illite	5.6	13.8	5.9	4.8	7.3
Calcite	2.7				
Dolomite	11.2	7.8	2.8	10.2	6.5
Pyrite	2.8	1.5	5.5	0.3	4.8
Bassanite	2.2	4.5	5.2	9.3	5.2
Rutile	1.1		0.8	0.3	0.5
Gorceixite	1.9	2.1	1.4	1.3	1.9
Apatite	1.0				

The high temperature-XRD results (Appendix G) for the LTA sample from Sasol coal feedstock to gasification, LTA of the sink fraction (>1.5635g/cm^3) and LTA of the float fraction (<1.5635g/cm^3) indicate that bassanite ($CaSO_4.1/2H_2O$), which was formed from the interaction of the organic sulphur and organic calcium or calcium-bearing minerals (calcite and dolomite) as well as from pyrite, decomposes at a low temperature of 400°C (Table G1). As expected kaolinite loses its water of hydration around 600°C (Table G1) to form amorphous meta-kaolin. Calcite and dolomite that are not pure minerals in the coal, decompose at 600°C (Table G1) and some of their oxides will react with aluminium silicate to form a melt. Interestingly, for all ash samples tested, quartz grains persist to 1300°C and lose their natural structure at 1350°C during HT-XRD analysis. The HT-XRD analysis also reveals that anorthite, which crystallises from the melt, appears at 1100°C and persists to 1400°C (Table G1). For the LTA from Sasol coal feedstock as well as LTA from the float fraction, cristobalite which is formed from clays at elevated temperatures appears at 1200-1400°C (Table G1). The HT-XRD analysis of LTA from the sink fraction indicated that mullite, which is formed from high temperature transformation of either kaolinite or K-feldspar, appears at 900°C and persists to 1250°C.

4.3.4 CCSEM and SEM-EDS analyses of coals

The CCSEM analysis (Table 4.12) confirms that the coal sample analysed in this study contains the major minerals: kaolinite ($Al_2Si_2O_5(OH)_4$), quartz (SiO_2), muscovite/illite ($K_2O.3Al_2O_3.6SiO_2.2H_2O/K_{1.5}Al_4(Si_{6.5}Al_{1.5})O_{20}(OH)_4$), calcite ($CaCO_3$), dolomite ($CaMg(CO_3)_2$) and pyrite ($FeS_2$). Minor and trace minerals are orthoclase, apatite, rutile, and Fe-oxide/siderite ($Fe_2O_3/FeCO_3$), zircon ($ZrSiO_4$), monazite (Ce, La, Th) PO_4 and Nd-Ce-Al-Th-phosphate.

The selected back-scattered electron images taken during CCSEM analysis of the feed coal taken from the coal conveyor belts entering the gasifier (Figure 4.3) highlight mineral attributes. From Figures 4.3 and 4.5 it is clear that the following particle types and associated minerals are present in the coal sample:

Organic-rich coal particles with small concentrations of kaolinite (particle A), quartz (particle A), pyrite (particle A1) and calcite/dolomite inclusions. Fine to coarse dolomite and calcite cleats in predominantly organic-rich particles (particle A2) are common.

- Coarse to fine quartz-rich sandstone rock fragments (particles B, E and E1). Minor kaolinite, microcline, muscovite and fine pyrite inclusions are present.

- Large (>750µm) calcite and pyrite cleat fragments (particle D).
- Fine grained kaolinite-rich mudstone/siltstone rock fragments. Minor muscovite, quartz and orthoclase (particle F) are present.

The black carbon-rich particles shown in Figure 4.3 are vitrinite and the grey carbon-rich phases are inertinite-rich (Ag).

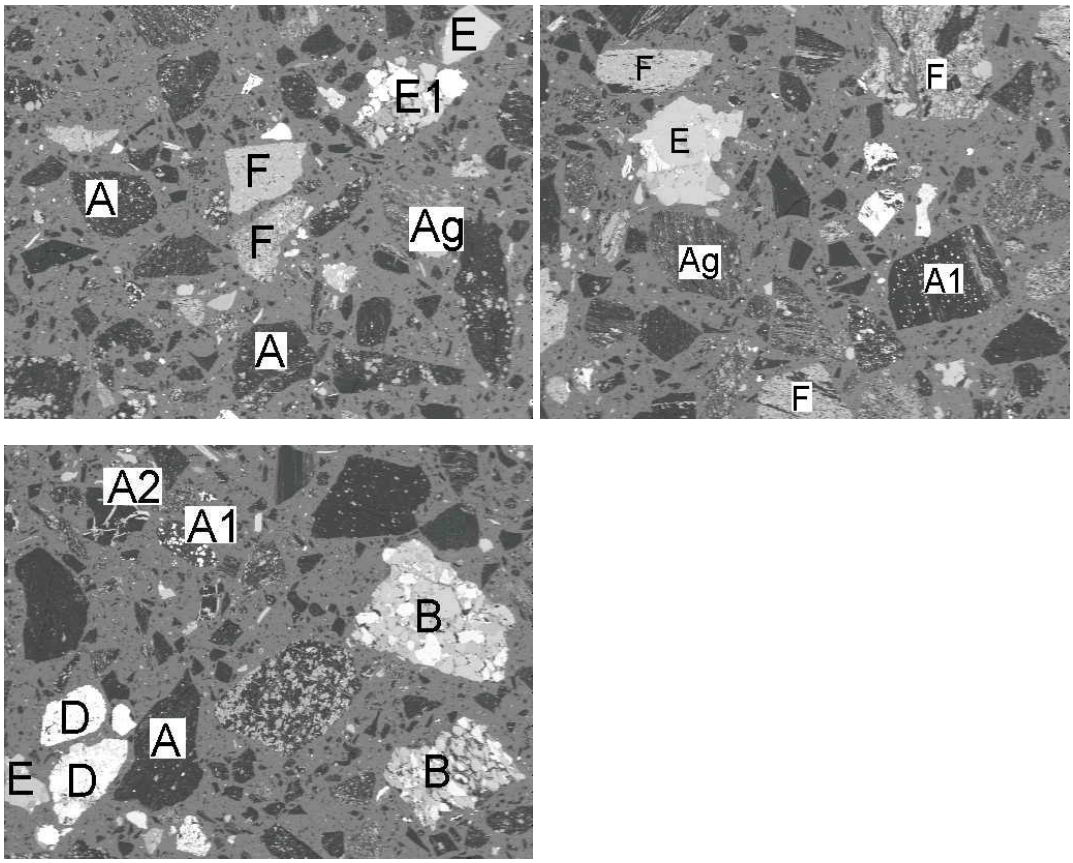


Figure 4.3: Scanning electron micrographs (back-scattered electron images) highlighting mineral attributes and deportment characteristics in Gasifier feedstock. Carbon-rich particles are black, mineral matter is light grey to white and epoxy mounting resin is grey. The width of each image is approximately 3.5mm.

The XRD and CCSEM results (mass percentages of minerals) are presented in Table 4.12. Kaolinite and to a lesser extent quartz, are the major coal minerals (Table 4.12). Pyrite, calcite, dolomite, muscovite/illite and feldspar are minor minerals. The calculated elemental proportions derived from the CCSEM mineral proportions agreed well with the XRF ash elemental proportions, whereas the XRD analysis indicated higher Si, Ti and K and lower Al, Mg and Fe than the XRF results (as reported in Paragraph 4.1.3). The quantitative XRD results given in Table 4.12 are based on the total amounts of the crystalline phases present in the coal sample. The CCSEM results (Table 4.12) are in broad agreement with the QEMSCAN measurements (Paragraph 4.3.5).

Table 4.12: Mineral abundance in coal (mass %)

Mineral	Idealised formula	CCSEM Mass%	XRD analysis
Pyrite	FeS_2	2.10	3.80
Quartz	SiO_2	5.30	28.00
Feldspar	$KAlSi_3O_8$	1.80	nd
Muscovite/illite	$K_2O.3Al_2O_3.6SiO_2.2H_2O$/ $K_{1.5}Al_4(Si_{6.5}Al_{1.5})O_{20}(OH)_4$	2.90	13.00
Kaolinite	$Al_2Si_2O_5(OH)_4$	17.10	34.00
Iron oxide/siderite	$Fe_2O_3/FeCO_3$	0.02	0.60
Calcite	$CaCO_3$	2.10	7.80
Dolomite	$CaMg(CO_3)_2$	2.30	9.00
Ankerite	$(Fe, Ca, Mg)CO_3$	0.09	nd
Apatite	$Ca_5F(PO_4)_3$	0.20	nd
Anatase/rutile	TiO_2	0.40	3.1
Other	Unidentified minerals	0.09	nd
Coal	Organic fraction	65.57	nd
Total		100.0	99.30

Note: nd: not detected

The SEM-EDS analysis (Figure 4.4) of the coal sample taken from the gasifier during the dig-out test confirmed that carbonate cleats (dolomite and calcite) occurred within carbon-rich particles in this coal sample. The typical X-ray spectra of kaolinite and potassium-feldspar contained in the dig-out samples are given in Figures E1and E2 respectively. In most cases, the fluxing elements-bearing minerals such as dolomite and calcite are associated with each other in the coal samples analysed in the present study. These results are in good agreement with QEMSCAN results (Figure 4.7). These included minerals that contain the fluxing elements (Ca and Mg) (Appendix E, Figures E3 and E4) are also associated with the included kaolinite. The SEM-EDS analysis (Figure 4.4 and Figure E5) also shows that pyrite grains (white) are included in the carbon particles and some are associated with kaolinite in the coal sample.

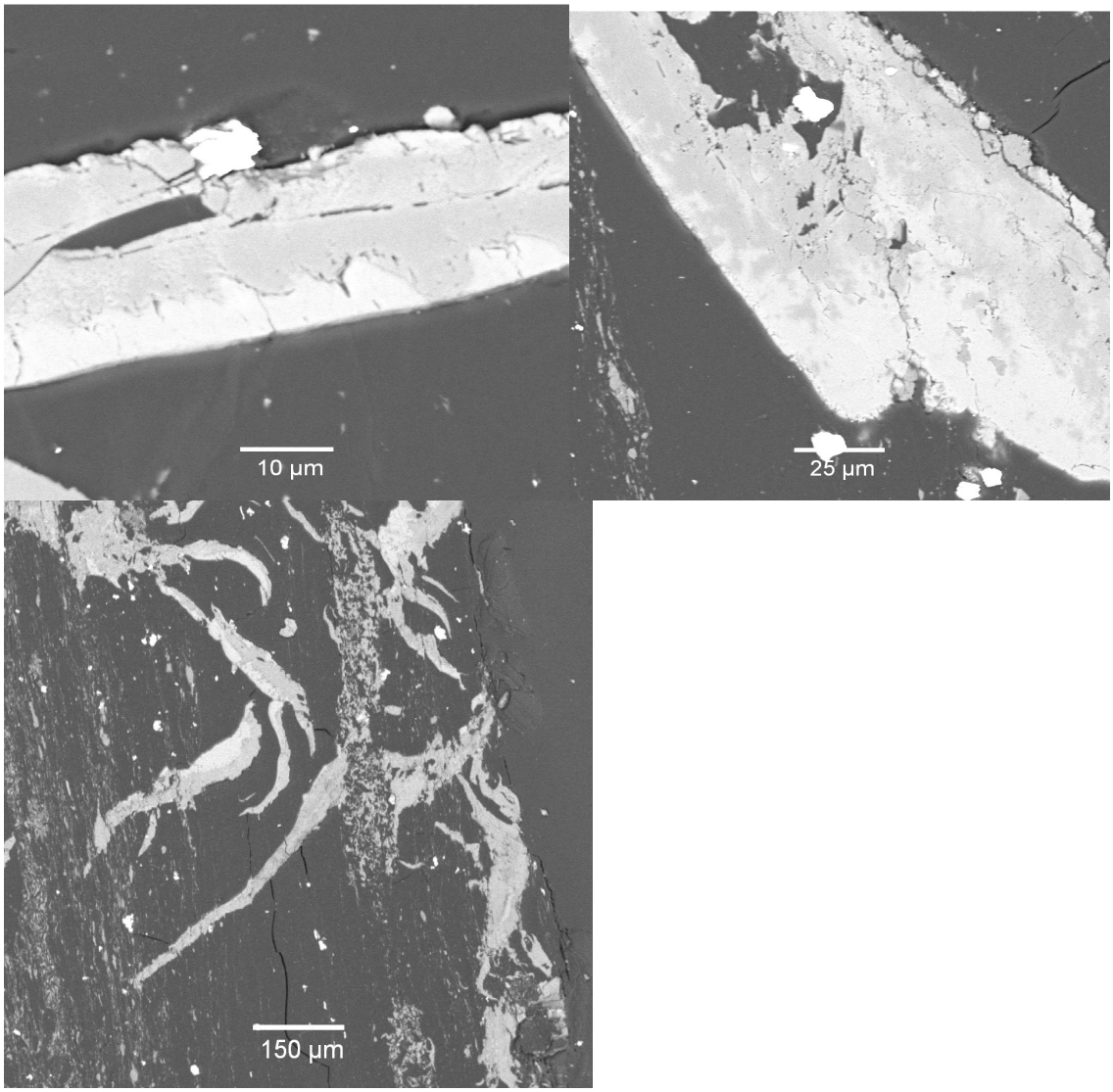


Figure 4.4: The BSE images of feed coal show carbonate cleats (calcite with white colour and dolomite with light grey) between two carbon particles, the bottom image shows included kaolinite associated with dolomite/calcite, kaolinite is also associated with dolomite/calcite/pyrite (white dots). Scale bar of the top left image is 10µm, for the top right image it is 25µm, and for the bottom image it is 150µm.

Figure 4.5 shows that grains of quartz with grey appearance, kaolinite (dark grey), potassium feldspar (light grey) and white pyrite grains are contained in the extraneous rock fragments analysed in this study. Kaolinite in the rock fragments is expected to transform differently in comparison with the kaolinite mineral associated with dolomite/calcite/ pyrite in the coal during coal combustion/gasification.

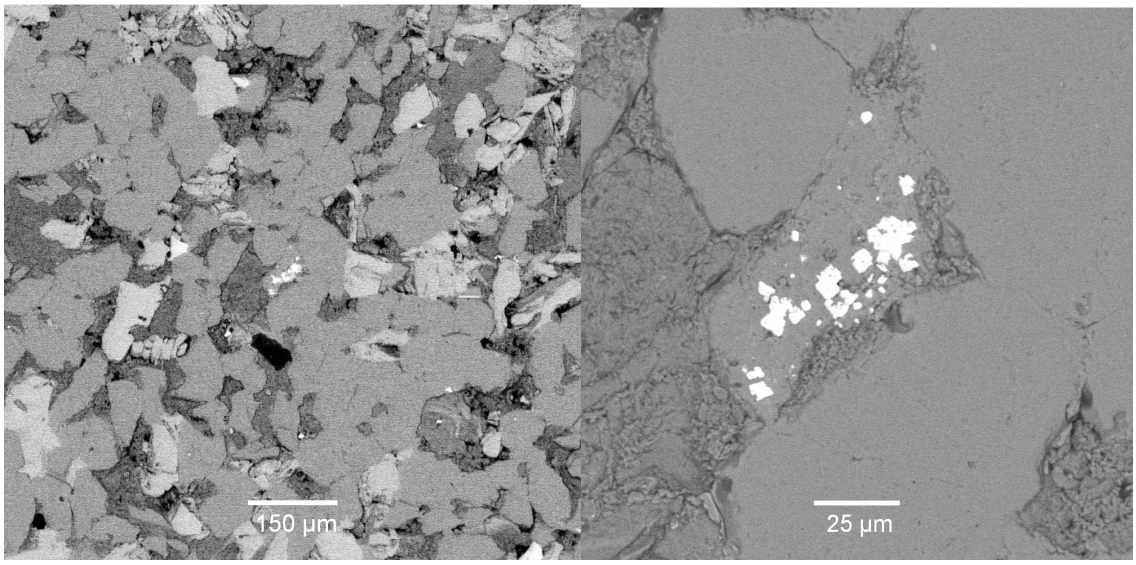


Figure 4.5: Back-scattered electron images of dig-out coal stone (from feed coal): Quartz grains (mid-grey), kaolinite (dark grey), potassium feldspar (light grey) and pyrite grains (white). Scale bar of the first image is 150µm, while for the second image it is 25µm.

4.3.5 QEMSCAN analysis of feed coal

QEMSCAN analysis of sample 32T (feed coal) indicates that high proportions of kaolinite (15.81%), quartz (6.5%), dolomite (2.67%), calcite (2.18%), organic matter (68.76%) and low proportions of pyrite (1.63%), siderite (0.02%), rutile (0.94%), illite (0.42%), apatite (0.07%) and organic sulphur (0.94%) are contained in these samples. The size of the mineral grains in the coal sample 32T analysed in this study ranged from 10 -106 microns

False-colour images of grains of minerals in Figure 4.6 indicate the occurrence of minerals in the coal particles. As shown in this figure, some pyrite particles (yellow) occur as extraneous particles while others are associated with minerals such as kaolinite, quartz and also carbon-rich (black) particles.

From Figure 4.7 the amount of transitions was normalised to a 100%. The iDiscover (QEMSCAN programme) counted the transitions between the minerals that are present in the sample. The transitions were converted to a percentage, meaning that out of the total number of transitions in the sample, a percentage between a specific combination of minerals (in this case between background and a set of minerals) was displayed. This figure shows mineral associations in the coal sample 32T.

The background mentioned in Figure 4.7 is the mounting medium. Depending on the sample type, the mounting medium can vary between wax and epoxy resin. With regards

to the background transitions, the transitions between background and mineral can be seen as a proxy for liberation.

QEMSCAN analysis of the coal sample in this figure shows the following:
Some pyrite particles are strongly associated with both high sulphur coal (organically-bound sulphur) and carbon-rich fraction (maceral). They are also associated with the background, indicating that around 30% of the surface of pyrite grains are excluded.

- All feldspar particles in this coal sample are included (associated with the carbon-rich fraction and not with the background) and are strongly associated with calcite and dolomite. A small proportion of illite is associated with the background, indicating that around <5% of the surface of illite grains is excluded. A small proportion of illite is associated with quartz and organic sulphur, while a significant proportion is associated with kaolinite.
- The apatite grains are strongly associated with calcite and carbon-rich fraction and are not associated with the background, indicating that the apatite grains are included.
- Interestingly, about 30% dolomite particles are associated with calcite grains and a significant proportion (above 50%) with the carbon-rich fraction. The results also show that a small proportion of dolomite grains are associated with the background, indicating that around 3% of dolomite particles are excluded. This mineral association could affect the melting of mineral matter in the coal at elevated temperatures and pressure during coal gasification or combustion.
- Calcite grains (above 50%) are strongly associated with the carbon-rich fraction (see also Figure 4.4) and are also associated with dolomite, kaolinite, quartz and apatite. Due to the presence of the fluxing elements-bearing minerals in the coal, this mineral association could contribute significantly to the sintering and slagging of mineral matter at elevated temperatures during coal gasification or combustion. The calcite particles are also associated with the background, indicating that about 5% of the surface of calcite grains is excluded.
- In most cases, the organic sulphur is associated with carbon-rich particles (macerals) in the coal. The electron microprobe results in Table 4.13 corroborate this result. The organic sulphur particles interacted with the organically-associated calcium in the coals to form bassanite ($CaSO_4.½H_2O$) during the low-temperature ashing process (Table 4.5).

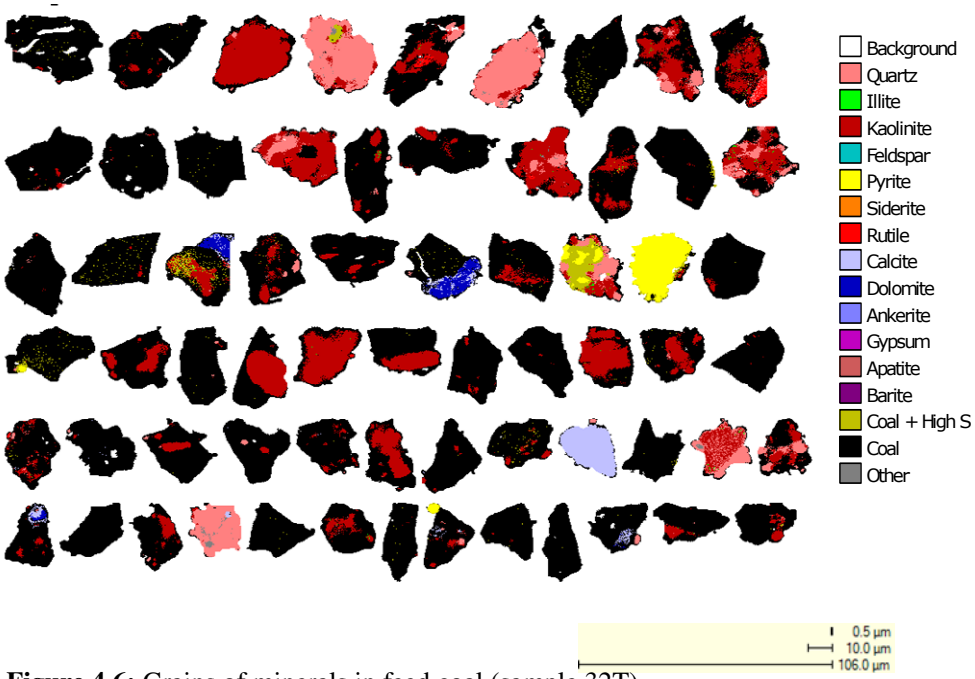


Figure 4.6: Grains of minerals in feed coal (sample 32T).

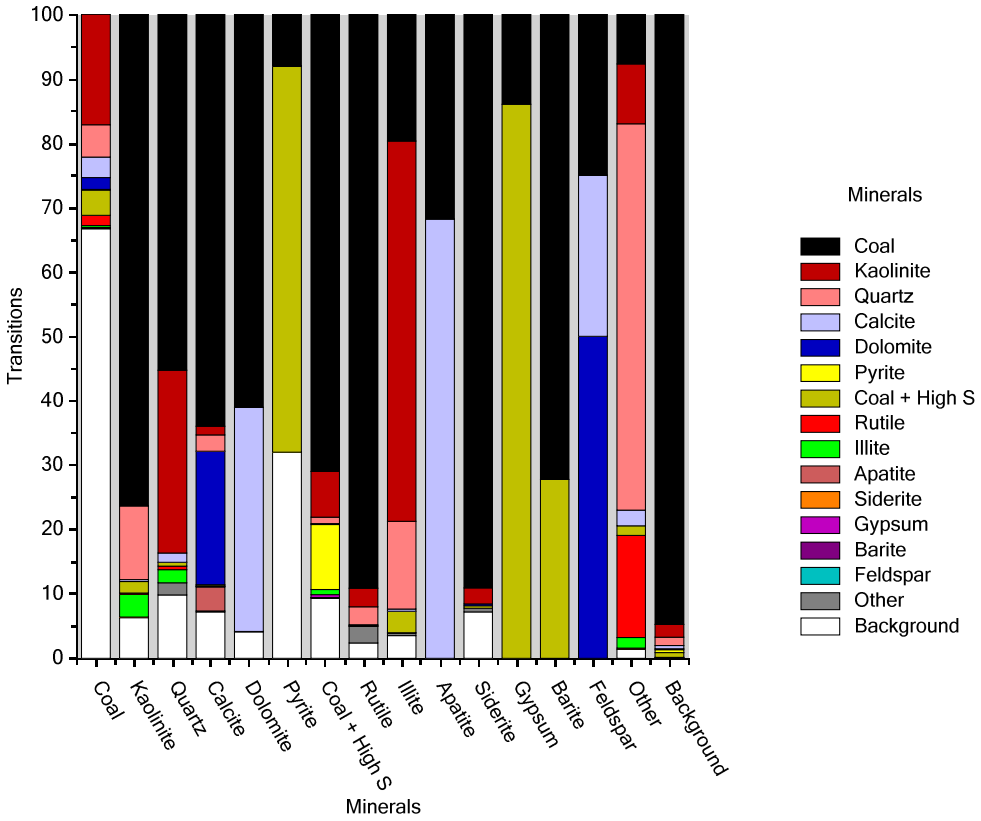


Figure 4.7: Mineral associations of feed coal (sample 32T).

4.4 Elemental composition of individual coal macerals by electron microprobe

As was stated earlier in Chapter 3 of this thesis, the organically-bound inorganic elements, as well as sub-micron minerals in the macerals, could interact with each other or react with aluminium silicates at elevated temperatures under reducing and oxidising conditions to form a melt. The qualification and quantification of this mineral matter in the organic matter (macerals) in the coal samples (using electron microprobe and optical microscope), were used to test the hypothesis (that the interactions between the organically-bound inorganic elements and sub-micron clays at elevated temperatures, give rise to the sintering and slagging of mineral matter during either coal combustion or gasification) which is stated in Chapter 3.

Table 4.13 contains a summary of the results of the electron microprobe analyses of the coal macerals. These results represent the average proportion of each element in each maceral of the respective sample analysed in this study, based on the number of individual points indicated in each case.

Ward (1998, 2005) found that the vitrinite macerals in the Australian coals contained lower carbon and higher oxygen contents than the inertinite macerals. The same author also found that telocollinite (also referred to in some standards as collotelinite) generally has a slightly lower carbon content than the desmocollinite in the same coal sample. Comparison with results presented by Ward et al. (2005) indicates that the carbon content of the telocollinite in most samples (around 75%) is similar to that of the telocollinite in coals from the Bowen Basin of Australia, having a mean maximum vitrinite reflectance of around 0.7%. Similar vitrinite reflectance values are noted in the South African coal samples analysed in the present study.

The telocollinite in sample from mine 6, however, has a slightly lower carbon content (around 70%), yet still has a vitrinite reflectance of 0.7%. The significance of this is not clear at the present time; it may indicate either a slightly low vitrinite carbon percentage for a coal with a similar rank level to the other samples, or it may indicate a slightly high reflectance for the vitrinite in a coal with a slightly lower rank level.

The electron probe analysis of coals revealed that the vitrinite macerals in each individual coal contains significantly higher proportions of the organic sulphur and nitrogen, in comparison with the inertinite macerals in the same coal samples. These results are in agreement with the previous results obtained by Ward et al. (2005) and Gurba (2001). In almost all cases, the proportion of these elements in the vitrinite macerals is approximately twice that in the same sample's inertinite components.

The proportion of organic sulphur in the vitrinite of samples from mines 1, 2, 3 and 5 is around 0.6-0.8%, while samples from mines 4 and 6 have only 0.4-0.5% organic sulphur. The significance of this observation is also not clear at the present time. From the results given in Table 4.13, it is clear that coal macerals contain no organically-bound iron. The absence of any significant iron in these macerals confirms that the sulphur in all cases is organic in nature, and that the higher sulphur levels do not reflect incorporation of sub-microscopic pyrite in the macerals concerned. The difference between these values and the total sulphur content of the coals (Table 4.2), reflects the additional occurrence of pyrite (pyritic sulphur), as indicated by the mineralogical data in Table 4.5.

Despite efforts to avoid including data form points with significant contamination by mineral matter, the vitrinite and semi-fusinite macerals in sample from mine 3, and possibly also sample from mine 4, appear to contain small (approximately equal) proportions of both Al and Si. This may suggest incorporation of an intimate admixture of sub-micron kaolinite or a similar clay mineral into the maceral structure. Lesser, but similarly equal, proportions of Al and Si are noted in the vitrinite of samples from mines 1 and 2. The vitrinite in samples from mines 5 and 6 appears to contain relatively high proportions of Al and only traces of Si, suggesting either incorporation of bauxite-group minerals (gibbsite and/or boehmite), or possibly incorporation of Al as an inorganic element within the vitrinite structure.

Inertinite macerals in some coals analysed contain small proportions (mostly <0.2%) of Ca. Ca is especially abundant in the sporinite and inertinite components of sample from mine 6, probably indicating traces of calcite or dolomite in the pore spaces of those particular macerals. For the vitrinite macerals, the relatively minor amount of Ca may occur within the organic structure.

It is interesting to note that the vitrinite in samples from mines 1, 2, 3 and 4 contains significant proportions (0.3-0.5%) of titanium in comparison with other coal samples analysed in this study. The significant proportion of titanium in these coal samples detected by the electron microprobe, may occur either as the organically-associated inorganic element or evenly distributed sub-microscopic particles in the coal vitrinite. The vitrinites in the other two coal samples possibly contain small proportion of Ti (<0.1%). Interestingly, the electron microprobe results for the selected area of inertinite macerals, show that titanium is however, not present in any of these inertinite components.

According to Li et al. (2006) more detailed electron microprobe analysis, using element mapping techniques, has shown that Ca and Al in other coals form an integral part of the maceral structure, rather than representing fine (but discrete) included mineral particles. These techniques have however, not been applied to the coals of the present study, nor to Ti in other coal samples.

Table 4.13: Elemental composition of macerals in coal samples from the different mines by electron microprobe analysis

Maceral	Pts	C%	N%	O%	Mg%	Al%	Si%	S%	K%	Ca%	Ti%	Fe%
Mine 1												
TC	23	73.24	2.38	18.97	0.01	0.06	0.06	0.65	0.00	0.10	0.55	0.02
DSC	12	74.82	2.46	17.39	0.01	0.10	0.11	0.67	0.01	0.10	0.44	0.00
SF	15	84.40	0.98	10.21	0.01	0.02	0.04	0.30	0.01	0.07	0.02	0.00
FUS	16	85.73	0.84	8.68	0.03	0.06	0.09	0.25	0.01	0.13	0.01	0.00
Mine 2												
TC	23	74.34	2.29	18.00	0.03	0.10	0.07	0.79	0.01	0.13	0.38	0.00
DSC	22	78.56	1.94	14.71	0.01	0.09	0.12	0.58	0.01	0.06	0.22	0.00
SF	7	88.28	0.23	7.07	0.07	0.01	0.01	0.24	0.01	0.07	0.01	0.00
FUS	15	89.28	0.75	6.31	0.07	0.02	0.02	0.36	0.01	0.15	0.01	0.00
Mine 3												
TC	15	73.17	2.41	19.83	0.01	0.41	0.33	0.76	0.05	0.06	0.38	0.00
DSC	12	74.49	2.31	18.62	0.01	0.40	0.25	0.77	0.08	0.07	0.41	0.00
SF	10	81.04	1.66	13.03	0.02	0.22	0.25	0.42	0.02	0.08	0.01	0.00
FUS	14	83.11	1.00	11.41	0.02	0.00	0.01	0.36	0.00	0.11	0.02	0.00
Mine 4												
TC	23	77.32	1.93	16.02	0.01	0.10	0.10	0.39	0.03	0.06	0.42	0.00
DSC	17	77.67	2.10	15.24	0.01	0.17	0.16	0.40	0.02	0.07	0.45	0.00
SF	12	85.46	0.81	9.16	0.02	0.01	0.01	0.19	0.01	0.09	0.01	0.00
FUS	14	86.36	0.99	8.43	0.04	0.01	0.02	0.18	0.01	0.17	0.01	0.00
Mine 5												
TC	33	75.39	2.10	17.96	0.01	0.24	0.07	0.80	0.01	0.09	0.03	0.00
DSC	19	76.47	2.19	16.80	0.01	0.17	0.09	0.87	0.01	0.08	0.09	0.00
SP	1	79.70	1.89	15.00	0.02	0.54	0.53	1.14	0.02	0.04	0.03	0.00
SF	6	86.26	0.94	9.48	0.06	0.06	0.08	0.34	0.01	0.17	0.01	0.00
FUS	8	89.22	0.43	7.39	0.04	0.09	0.07	0.37	0.01	0.12	0.00	0.00
IDT	2	90.90	1.52	5.77	0.02	0.13	0.13	0.33	0.00	0.12	0.02	0.00
Mine 6												
TC	29	69.51	2.67	23.38	0.02	0.19	0.06	0.46	0.01	0.12	0.07	0.00
DSC	21	70.06	2.55	22.06	0.02	0.20	0.08	0.47	0.01	0.17	0.06	0.00
CUT	2	76.49	1.61	16.03	0.01	0.18	0.01	0.35	0.00	0.12	0.02	0.00
SP	4	77.04	1.84	14.28	0.02	0.29	0.09	0.36	0.00	0.93	0.02	0.00
SF	18	80.39	1.25	12.64	0.02	0.04	0.03	0.22	0.01	0.14	0.01	0.01
FUS	12	85.05	0.72	9.40	0.06	0.10	0.10	0.17	0.00	0.26	0.01	0.00
IDT	5	90.13	0.68	4.23	0.02	0.02	0.01	0.20	0.00	0.43	0.01	0.00

Key: TC = telocollinite, DSC = desmocollinite, SP = sporinite, CUT = cutinite, SF = semifusinite, FUS = fusinite, IDT = inertodetrinite. Pts = number of points analysed for indicated maceral.

4.5 Chemical fractionation method

Two South African low-grade, medium rank C bituminous (SAMB) feed coals (Highveld feed coal 1 and Highveld feed coal 2) to the conversion coal processes, were used in this study. Samples 1 and 2 were obtained from the same source and have similar chemical and physical properties. However, Highveld feed coal 1 was obtained from the top of the gasifier after its operation had ceased and had been exposed to temperatures of <400°C, while Highveld feed coal 2 was obtained from the conveyor belt entering the gasification plant, before heat treatment.

The preliminary results obtained from chemical, mineralogical and physical analyses of the two feed coals and residual coal particles from the pyrolysis experiments, using the conventional analytical techniques and results from ICP-OES analysis of each leachate obtained from the sequential leaching procedure, are discussed in this section.

4.5.1 Proximate analysis of feed coal before and after sequential leaching

Proximate analysis data (Table 4.14) indicate that the two Highveld feed coals before leaching (unleached coal 1(UC1) and unleached coal 2 (UC2)) had 19-22% volatile matter, 3.1-3.4% air-dried moisture content and an ash yield between 25% and 31%. Total sulphur content ranged from 1.0-1.5%. These results are in agreement with those previously found by (Pinheiro et al., 1998-1999; Matjie et al., 2006; DME, 2006). No significant changes were observed in the moisture and volatile matter contents after sequential leaching.

As might be anticipated, the ash yield of these samples decreased after ammonium acetate and acid leaching steps, due to removal of the relevant soluble inorganic components. No significant changes were observed in the volatile matter yield after sequential leaching. The fixed carbon content increased slightly after ammonium acetate and acid leaching, likely as a result of the reduction in ash percentage. The sulphur content was reduced after water leaching and then remained fairly constant through the ammonium acetate and acid leaching stages. This may in part reflect removal of iron sulphates derived from oxidation of pyrite in the coal samples, or alternatively removal of sulphate ions in the pore water derived from other sources.

Table 4.14: Proximate analyses (air-dried basis, %) of Highveld coal samples before and after sequential leaching with water, ammonium acetate and hydrochloric acid

	Samples	Moisture (%)	Ash (%)	Volatile Matter (%)	Fixed Carbon (%)	Total Sulphur (%)
Coal 1	HUC	3.10	30.70	19.60	46.60	1.41
	H_2O	3.20	29.50	20.30	47.00	1.17
	NH_4OAc	3.10	27.50	19.30	50.10	1.15
	HCl	3.10	26.00	19.50	51.40	1.02
Coal 2	HUC	3.40	25.10	21.90	49.60	1.03
	H_2O	3.30	24.80	22.90	49.00	0.94
	NH_4OAc	3.60	22.70	21.70	52.00	0.96
	HCl	4.00	20.60	21.80	53.60	0.96

Note: HUC = Highveld coals before sequential leaching test
H_2O = after water leaching;
NH_4OAc = after ammonium acetate leaching and
HCl = after hydrochloric acid leaching

4.5.2 Ultimate analysis of feed coal before and after leaching

The normalised ultimate analysis (Table 4.15) indicated that these coals had 77-80% carbon dry and 3.70-4.10% hydrogen with relatively low concentrations of sulphur (1.44-2.13%) and around 2% nitrogen. The oxygen content of the coals ranged from 13-14%. These results are in agreement with those previously found by (Pinheiro et al., 1998-1999; Matjie et al., 2006; DME, 2006). A minor increase in the carbon and hydrogen was noted after ammonium acetate leaching. Due to the presence of ammonium acetate in the residual coal particles, nitrogen contents were slightly higher after this leaching stage. The slight variation in the concentration of oxygen during the sequential leaching could perhaps be attributed to the dissolution of salts of carboxylic acids from the coals.

Table 4.15: Normalised ultimate analyses (dry ash-free basis, %) of Highveld coal samples before and after sequential leaching with water, ammonium acetate and hydrochloric acid

	Samples	Carbon	Hydrogen	Nitrogen	Sulphur	Oxygen
Coal 1	HUC	78.99	3.93	2.02	2.13	12.93
	H_2O	79.63	3.76	2.07	1.74	12.81
	NH_4OAc	78.72	3.80	2.49	1.66	13.33
	HCl	77.98	3.67	2.21	1.44	14.70
Coal 2	HUC	78.80	4.10	1.99	1.44	13.68
	H_2O	78.94	3.89	1.97	1.31	13.88
	NH_4OAc	79.40	3.95	2.54	1.30	12.81
	HCl	77.14	3.89	2.24	1.27	15.46

4.5.3 The normalised XRF and ICP-OES analyses for HTA samples produced from the coal samples 1 and 2 before and after the sequential leaching

The ICP-OES analyses of the High Temperature Ash (HTA) of coal samples 1 and 2 are shown in Appendix A, Table A2 and Table A3. In all cases, the normalised proportions of inorganic elements (XRF analysis) in the HTA, produced after heating the two coals (HUC1 and HUC2) at 815°C were very similar, thus confirming the applicability of the ICP data for samples (Table 4.16). Sulphur results are not reported, as the XRF method used was regarded as only semi-quantitative for sulphur. The ashes analysed by ICP-OES provided results on the Ba and Sr concentrations; these elements were not included in the typical XRF major elemental analysis routine.

It is clear from the results given in Tables 4.16 and 4.17, that HTA from coal 1 contained significantly higher proportions of iron and silicon oxides than HTA of coal 2. The variation in chemical composition of these two coals can be attributed to variations in the quality of coal with the depth of the seams. In most cases, results given in Tables 4.16 and 4.17 indicated that the percentages of some major elemental oxides for samples 1 and 2 are very similar from both ICP-OES and XRF analyses. However, the most abundant elements in the feed coals (as expressed as SiO_2 and Al_2O_3), are approximately 2% higher in the results from XRF than by ICP-OES analysis. Although there is a slight discrepancy of concentrations of both SiO_2 and Al_2O_3, these differences do not significantly affect the trends in the data series. The primary constituents in the SAMB feed coals are SiO_2,

Al_2O_3, CaO, Fe_2O_3, MgO and TiO_2. Minor proportions (<0.6%) of K_2O, Na_2O, P_2O_5, SrO, BaO and Mn_3O_4 were also present, along with a SO_3 content between 4.5 and 5.7%.

A decrease in the content of the inorganic elements present in the original coals during sequential leaching with water, ammonium acetate and hydrochloric acid solutions may be attributed to the decomposition of other coal minerals, dissolution of ions from moisture, as well as the loss of volatiles upon heat treatment. Carbonate minerals (dolomite and calcite), along with other organically-bound calcium and sulphur may dissolve in solutions of lixiviants (ammonium acetate and hydrochloric acid) during the leaching steps and therefore a significant decrease in the calcium, magnesium and sulphur data would result. Matjie et al. (2008) also found that the proportions of MgO, SrO and BaO correlated quite well with the proportion of CaO, suggesting on the basis of other studies (Ward et al., 1999) that they may be associated with the carbonate minerals in the Highveld coal samples.

Significant reductions in the concentrations of BaO, MgO, SrO and CaO upon leaching, as shown in Table 4.17, confirmed that Ba, Mg, Sr and Ca dissolved in the lixiviants used during the sequential leaching experiments. In addition, Miller and Given (1978); Benson and Holm (1985) and Benson (1987) showed that significant proportions of the Ca, Mg and Na in the lignite coal samples dissolved in ammonium acetate solution during the leaching experiments. These elements occurred mostly in ion-exchangeable form (possibly associated with carboxylate compounds and partly in the pore waters and an acid-soluble form) (Miller and Given, 1978; Benson and Holm, (1985); Benson, 1987). The electron probe analysis of Highveld coals reported in this section, confirmed the presence of calcium, iron and magnesium that are either in the form of salts of carboxylic acids (organically-bound inorganic elements) or associated with carbon-rich particles in the coal macerals.

Trace amounts of fluxing elements such as K, Sr and Fe that may also reduce ash fusion temperature (AFT) of mineral matter in the coal, were leached out from some coal samples evaluated in this study (Table 4.16). As expected, lower AFT's are due to the presence of fluxing elements-bearing minerals that have reacted with organically-associated inorganic elements and clays and may also be attributed to increased basic oxide levels and low SiO_2/Al_2O_3 ratios. The chemical fractionation results (Tables 4.16-4.18) also reveal that concentrations of Na_2O, SO_3 and P_2O_5 in HTA samples of the coals

decreased substantially during the sequential leaching steps of these coals. The dissolution of sodium in distilled water implies that most of the sodium ions were dissolved in the pore water within the coal. These results are in line with previous results that were found by Ward (1991).

A significant decrease of sulphur in the leached coal particles may be attributed to the formation of acidic ammonium sulphate through the reaction of organic sulphur or pyrite with ammonium acetate, as well as sulphuric acid formation because of the reaction of the partially oxidised pyrite and water. Ward (1991) suggested in his studies that sulphuric acid formed during oxidation of pyrite reacted with calcium from carbonate minerals and iron from the oxidised pyrite during the selective leaching steps. A slight reduction in the concentration of phosphorus from coals can be attributed to the reaction between phosphate minerals in the coal and ammonium sulphate produced from the ammonium acetate solution, as well as from HCl during the sequential leaching experiments.

Table 4.16: Inorganic oxide percentages from normalised XRF and ICP-OES analyses of HTA samples of Highveld coal sample 1 before and after leaching (wt %)

	ICP-OES Data				**XRF Data**			
	HUC1	**WL HLC1**	**AAL HLC1**	**HClL HLC1**	**HUC1**	**WL HLC1**	**AAL HLC1**	**HClL HLC1**
	%	**%**	**%**	**%**	**%**	**%**	**%**	**%**
SiO_2	54.68	54.69	62.01	61.09	56.74	56.68	61.65	61.09
Al_2O_3	24.60	24.89	28.3	30.83	26.37	26.66	29.12	31.6
Fe_2O_3	5.61	5.22	5.54	3.84	5.89	5.37	5.61	3.66
TiO_2	1.46	1.48	1.67	1.84	1.51	1.54	1.64	1.83
BaO	0.15	0.16	0.17	0.3	*	*	*	*
SrO	0.20	0.21	0.12	0.17	*	*	*	*
P_2O_5	0.26	0.3	0.32	0.24	0.34	0.34	0.38	0.28
CaO	5.61	6.02	0.53	0.32	5.92	0.36	0.57	0.32
Mn_3O_4	0.04	0.04	0.01	0	0.04	0.04	0.01	0.01
MgO	1.94	2.14	0.35	0.29	2.14	2.33	0.43	0.38
SO_3	4.5	4.06	0.32	0.22	*	*	*	*
Na_2O	0.4	0.23	0.07	0.1	0.45	0.13	0	0.07
K_2O	0.55	0.55	0.58	0.76	0.59	0.57	0.59	0.77
Total					100	100	100	100

Note: HUC1 = Highveld coal 1 before sequential leaching test
HLC1 = Highveld coal 1 after sequential leaching test
WL = Water leaching;
AAL …= Ammonium acetate leaching
HClL = Hydrochloric acid leaching
* = BaO, SrO and SO_3 were not determined

Table 4.17: Inorganic oxide percentages from normalised ICP-OES and XRF analysis of HTA samples of Highveld coal sample 2 (wt %)

	ICP-OES Data				XRF Data			
	HUC1	WL HLC1	AAL HLC1	HClL HLC1	HUC1	WL HLC1	AAL HLC1	HClL HLC1
	%	%	%	%	%	%	%	%
SiO_2	46.84	48.06	56.12	64.88	45.51	46.55	56.04	64.28
Al_2O_3	26.22	26.44	30.64	27.41	26.19	25.94	31.56	28.13
Fe_2O_3	4.32	4.35	4.84	4.59	4.25	4.19	4.88	4.50
TiO_2	1.38	1.42	1.65	1.77	1.35	1.39	1.63	1.74
BaO	0.30	0.31	0.35	0.10	*	*	*	*
SrO	0.47	0.47	0.38	0.06	*	*	*	*
P_2O_5	0.87	0.85	1.02	0.06	0.86	0.85	1.01	0.1
CaO	9.84	10.11	2.10	0.16	9.73	9.88	2.03	0.17
Mn_3O_4	*	*	*	*	0.06	0.06	0.03	0.01
MgO	2.80	2.86	0.87	0.25	2.80	2.83	0.84	0.29
SO_3	5.69	3.96	1.08	0.10	*	*	*	*
Na_2O	0.51	0.38	0.13	0.07	0.37	0.37	0.11	0.08
K_2O	0.70	0.73	0.80	0.56	0.68	0.71	0.79	0.57

Note: HUC2 = Highveld coal 2 before sequential leaching test
HLC2 = Highveld coal 2 after sequential leaching test
WL = Water leaching;
AAL = Ammonium acetate leaching
HClL = Hydrochloric acid leaching
* = Mn_3O_4, BaO, SrO and SO_3 were not determined

4.5.4 Mineralogical analysis of unleached and leached coal particles

Table 4.18 indicates the percentages of the individual minerals in each LTA, based on powder XRD and SIROQUANT evaluation. Figures 4.8-4.9 illustrate the X-ray diffractograms of the LTA from coals 1 and 2 of the feed coal and the residual material from sequential leaching with water, ammonium acetate and hydrochloric acid solutions.

As presented in Table 4.18, feed coals 1 and 2 were found to have 36.4% and 28.4% mineral matter (LTA) respectively. These results are in line with the heat treatment (<400°C) of coal 1; some moisture and volatiles were removed from sample 1 during heat treatment, resulting in an increase in mineral matter content. The feed coal's minerals are primarily made up of kaolinite ($Al_2Si_2O_5(OH)_4$, 52-55%), lesser proportions of quartz (SiO_2, 16-26%) and the fluxing elements-bearing mineral dolomite ($CaMg(CO_3)_2$, 8-12%). Minor proportions of the fluxing elements-bearing mineral calcite ($CaCO_3$), illite ($K_{1.5}Al_4(Si_{6.5}Al_{1.5})O_{20}(OH)_4$), the fluxing elements-bearing mineral pyrite (FeS_2), the fluxing elements-bearing mineral siderite ($FeCO_3$), the sulphate mineral bassanite

($CaSO_4 \cdot ½H_2O$) and the alumino-phosphate mineral goyazite ($SrAl_3(PO_4)_2(OH)_5.H_2O$) are present. A small proportion of rutile (TiO_2) was also present in the LTA samples of these coals.

The silicate and carbonate minerals dominate in the feed coals and their mineral assemblage is consistent with similar data obtained from the analysis of other South African coals (Pinetown et al., 2007).

In coal 1, the quartz content slightly increased after the ammonium acetate leaching stage (from 23.5 to 26.3%) and the kaolinite content slightly increased after the ammonium acetate (from 52.6 to 60.9%) and hydrochloric acid leaching stages (from 60.9 to 68.9%). An increase in the moisture content from 3.3% after water leaching, to 4.0% after the ammonium acetate leaching stage was observed. The results of coal 2 indicated that an outlier (3.0%) in the rutile content in the residual coal particles after the water leaching stage was most probably due to an analytical error. A slight increase in the volatile matter content in coal 2 from 19.3 to 19.5% after the acid leaching, may account for the increased quartz content (from 21.2 to 27.8%) after the acid leaching stage and increased kaolinite content (from 49.6 to 64.5%) after the ammonium acetate leaching stage.

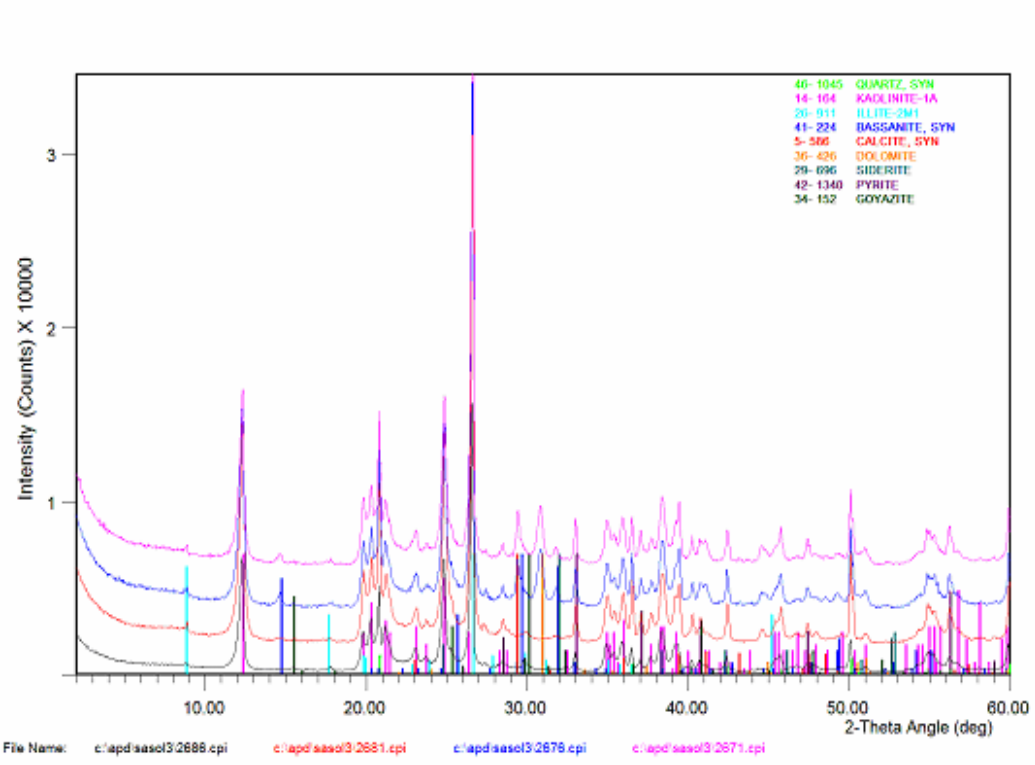


Figure 4.8: X-ray diffractograms of LTA from Sample 1 Feed coal (top) to water, ammonium acetate and HCl leaching (bottom).

Table 4.18: Mineralogical analysis data for coal LTA samples (wt% of LTA)

Sample		*LTA*	Qtz	Kaolin	Illite	I/S	Cal'ite	Dol'it-e	Sid'ite	Pyrite	Rutile	Goy't-e	Bas'te
1	Feed	36.4	25.7	52.9	3.0		2.3	8.3	0.5	4.8	0.6		1.8
	WL	36.0	23.5	52,6	3.7		1.3	8.8	1.1	4.1	0.7		4.2
	AAL	31.9	26.3	60.9	2.9	4.7				4.4	0.8		
	HClL	23.9	22.7	68.9	2.6					3.5	0.9	1.5	
2	Feed	28.4	16.1	54.4	3.5		3.8	11.4	2.1	3.5	0.7	2.4	2.1
	WL	30.8	18.2	49.6	3.7		5.2	12.0	0.7	2.9	3.0	1.7	3.0
	AAL	26.3	21.2	64.5	3.6			1.0	1.2	3.2	0.9	2.1	2.2
	HClL	29.5	27.8	61.2	2.0	4.6				3.5	0.8		

Note: WL= water leaching; AAL =ammonium acetate leaching and HClL = hydrochloric acid leaching
Qtz =Quartz; Kaolin = Kaolinite; I/S = Illite/smectite; Cal'ite= Calcite; Dol'ite = Dolomite;
Sid'ite = Siderite;
Goy'te=Goyazite;..Bas'te=Bassanite;

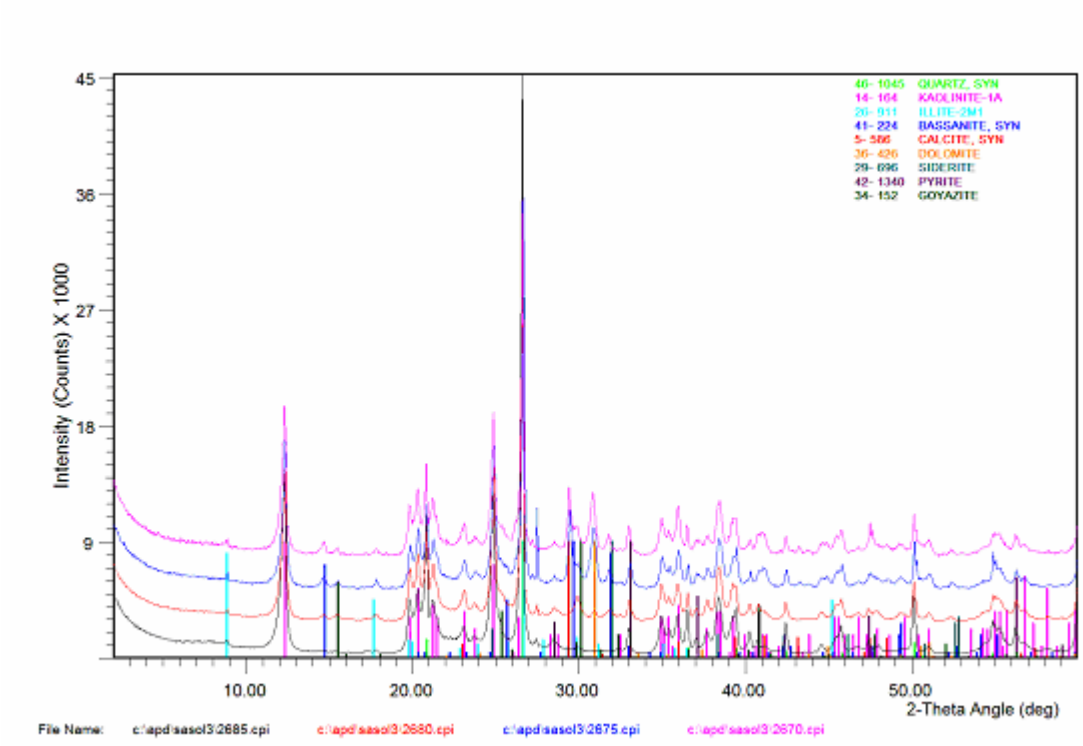


Figure 4.9: X-ray diffractograms of LTA from Sample 2 Feed coal (top) to water, ammonium acetate and HCl leaching (bottom).

4.5.5 Water leaching

Table 4.14 shows that water leaching reduced the ash yield of HUC1 by 1.2% and that of HUC2 by 0.3%. The primary non-mineral inorganic element found in the leachate of the SAMB coals was Na, along with minor proportions of Ca, K, Mg and Si (Table 4.19). The dissolution of sodium, calcium, potassium, silicon and magnesium in distilled water used as the lixiviant during the sequential leaching step testing, implies that most of the sodium ions dissolved in the pore water within the coal. These results are in line with the previous results (Ward, 1991; Govender, 2005). Cr, Mn, Fe, Al, V and Ti were found not to be present in the leach liquor after water leaching. The pH of the slurry and leachate, before and after leaching, did not differ for these samples evaluated by CHF in this study. This implies that iron-containing minerals such as pyrite and siderite in the coal tested were not partially oxidised.

4.5.6 Ammonium acetate leaching

From the results for the coal samples, before and after sequential leaching, given in Table 4.14 it can be seen that subsequent to water leaching, ammonium acetate leaching further reduced the ash yield of coal 1 by 2.0% and that of coal 2 by 2.1%. The leach liquors produced from the sequential leaching of the residual coal particles, after the water leaching with ammonium acetate solution, contained a significantly higher concentration of Ca and to a lesser extent Mg, Na, K, Mn and Si (Table 4.19). The pH values of the leach liquors produced from ammonium acetate leaching of these two coals, slightly increased from the pH value of 7.00 to 7.40, perhaps because of the presence of alkali elements (K and Na) as well as Ca in the leach liquors. Benson and Holm (1985) and Benson (1987) also found that significant amounts of Ca, Mg and Na present in the lignite samples dissolved in ammonium acetate solution during leaching experiments and the researcher suggested that these elements occur mostly in ion-exchangeable form (salts of organic acids in the coal). The elements removed by ammonium acetate leaching are likely to be present in the coal as the salts of carboxylic acid groups.

4.5.7 Hydrochloric acid leaching

The acid leaching step further reduced the ash yield of the residual leached coal particles of coal 1 by 1.5% and of the residual leached coal particles of coal 2 by 2.1% (Table 4.14) removing much more of Cr, K, Fe, Al, V, Ti and Si than the previous lixiviants (Table 4.19). Trace amounts of the remaining Mg, Na and Ca were also removed from the residual coal particles by hydrochloric acid leaching. Some of these elements could be derived from sub-

micron illite, illite/smectite, sub-micron clay and carbonate minerals that were removed during the HCl leaching step.

Miller and Given (1978), Benson and Holm (1985), Ward (1991) and Benson (1987) found in their studies that the HCl leaching stage, the last step of CHF, significantly removes elements that are present in the coal in the form of carbonates, hydroxides, oxides and organically-coordinated species. Contrary to the previous results for lignite coal samples that were found by Miller and Given (1978), Benson and Holm (1985), Ward (1991) and Benson (1987), trace proportions of Si, Al, V and Ti dissolved in hydrochloric acid during sequential leaching of Highveld coals. These elements could be derived from the sub-micron clays containing trace amounts of Ti and V, which were removed during the HCl leaching step.

Table 4.19: Concentration of elements detected in the leachate of coal samples that were subjected to sequential leaching (ppm) with water, ammonium acetate and hydrochloric acid

Sample	Lixiviant	Al	Ca	Fe	Cr	Mg	Na	K	Si	Mn	Ti	V
1	H_2O	0	62	0	0	13	61	4	2	0	0	0
	NH_4OAc1	0	1886	0	0	188	138	19	2	4	0	0
	NH_4OAc2	0	2786	0	0	869	16	4	4	14	0	0
	NH_4OAc3	0	433	0	0	122	5	2	5	4	0	0
	HCl1	819	492	677	17	46	22	54	227	6	1	2
	HCl2	651	36	23	9	13	13	61	11	1	2	1
2	H_2O	0	26	0	0	5	123	6	2	0	0	0
	NH_4OAc1	0	3000	0	0	587	128	25	3	13	0	0
	NH_4OAc2	0	1398	2	0	590	12	3	2	7	0	1
	NH_4OAc3	0	349	0	0	143	7	2	4	4	0	0
	HCl1	769	261	828	13	45	11	33	152	6	0	2
	HCl2	456	21	200	1	14	7	31	161	0	0	0

Note: L1= leach liquor produced after sequential leaching of HUC1
L2 = leach liquor produced after sequential leaching of HUC2
NH_4OAc1, NH_4OAc2, NH_4OAc3 = Ammonium acetate leaching steps 1, 2 and 3
HCl1, HCl2 = Hydrochloric acid leaching steps 1 and 2.

4.5.8 Physical analysis:Ash Fusion Temperatures (AFT)

The ash fusion temperatures of the Higveld coal samples, as expressed by the initial deformation temperatures, varied from 1150 to >1500°C (Table 4.20) with flow temperatures being 40 to 110°C higher. From the results given in Table 4.20, it is clear that the AFT values of these coals remained constant before and after the water leaching step. The AFT values increased to >1500°C after the ammonium acetate and hydrochloric acid leaching steps, related to the loss of fluxing elements (such as Ca, Mg and Fe) (Table 4.16 and Table 4.17) and the removal of carbonates (calcite, dolomite and siderite) as shown by XRD data (Table

4.18). Electron microprobe analyses of macerals from similar coals (Table 4.12) suggest that Ca, Al and possibly Mg may also occur as inherent components of the individual macerals and these might also have been removed by ammonium acetate and acid treatment. Such observations are in agreement with those of Van Dyk et al. (2005), who suggested that acid leaching removes potentially harmful minerals from the coal, leading to a rapid increase in the ash fusion temperatures.

Table 4.20: AFT's (°C) of the feed coal and residual coal particles after sequential leaching with water, ammonium acetate and hydrochloric acid

Lixiviants	Samples	ID	ST	HT	FT
Sample 1	HUC	1310	1320	1330	1350
	H_2O	1310	1320	1330	1340
	NH_4OAc	>1550	>1550	>1550	>1550
	HCl	>1550	>1550	>1550	>1550
Sample 2	HUC	1320	1360	1390	1430
	H_2O	1340	1360	1390	1430
	NH_4OAc	>1550	>1550	>1550	>1550
	HCl	>1550	>1550	>1550	>1550

Note: HUC1 and HUC2 = Highveld coal 1 and Highveld coal 2 before sequential leaching test
HLC1 and HLC2 = Highveld coal 1 and Highveld coal 2 after sequential leaching test
ID = Initial deformation temperature,
ST = Spherical temperature
HT = Hemispherical temperature,
FT = Flow temperature

The relationship of these changes in mineralogy and chemistry to the ash fusion characteristics is illustrated in Figure 4.10, where the initial deformation temperatures after each treatment are seen to be inversely related for each coal to the total proportions of CaO, MgO and Fe_2O_3 in the ashes of the relevant coal residues.

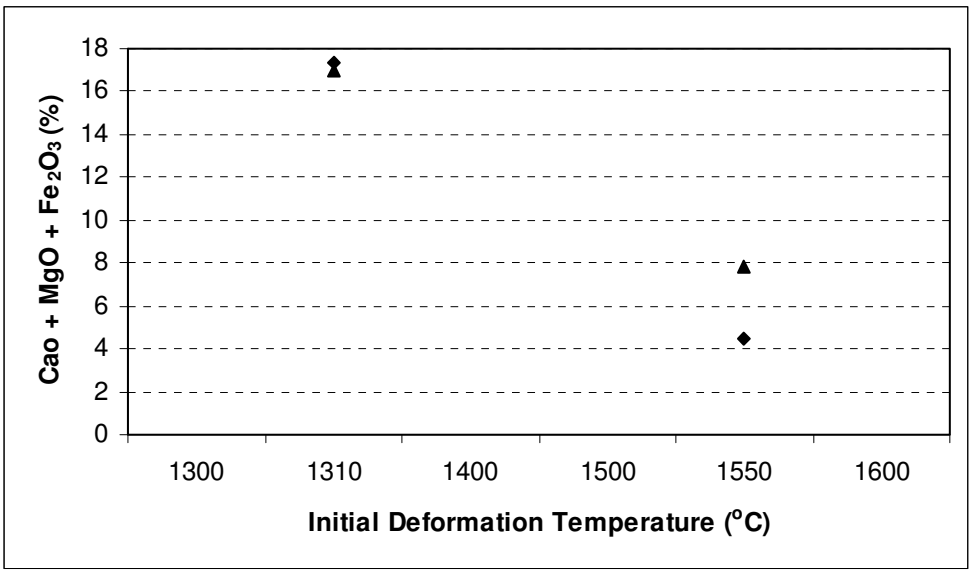


Figure 4.10: Relation between deformation temperature and proportion of CaO, MgO and Fe_2O_3 in coal ashes after each leaching process. Sample with deformation temperatures >1550ºC have been plotted at 1550ºC (from ICP data).

4.6 Distribution of inorganic elements in the minerals and macerals

The CCSEM results (Table 4.12) Petrography analysis (Table 4.4) and Electron microprobe results (Table 4.12), were used to calculate amounts of inorganic elements in the minerals and macerals present in the coals analysed in this study. Appendix F (Table F1) shows calculated total amounts of inorganic elements from minerals present in the Highveld coals obtained when using CCSEM analysis of coals. It can be seen from the results given in Table F2 that significantly higher amounts of Al, Si, Ca and Fe and to a lesser extent Ti, P, Mg and K are contained in the minerals present in the coals. As expected, small amounts of C and H are contained in the minerals in the coal. Nitrogen was not found to be present in the coal minerals.

From the results given in Table F1 it is clear that macerals in the coal contain small amounts of Mg, Al, Si, S, Ca and Ti. Macerals in the coals evaluated in this study contain about 0.4-1% organically-bound inorganic elements (Mg, Al, Si, S, Ca and Ti). Table F2 shows calculated concentrations of inorganic elements in the minerals present in Highveld coals, and Table F1 indicates calculated concentrations of the organic elements and inorganic elements in all coal macerals (the concentrations of elements in these two tables total 100%). As expected, significant amounts of C, H, N and O are reported to the organic matter (macerals). Some of these inorganic elements can interact with each other at elevated temperatures and

pressures and subsequently volatilise in the form of gases during coal pyrolysis. Whereas other inorganic elements in the macerals, as well as fluxing inorganic elements from mineral associations in the coal, could significantly contribute to sintering and slagging of mineral matter at elevated temperatures during coal gasification.

CHAPTER 5
RESULTS AND DISCUSSION - COAL SIZE AND DENSITY FRACTIONS ANALYSES

In this chapter the analytical results for coal size and density fractions produced from the feed coal are presented and discussed.

5.1 Characterisation of coal size fractions of feed coal by chemical analyses

5.1.1 Ultimate analysis of coal size fractions

Table 5.1 shows that the proportion of carbon varies between 77.02-80.12% as the size of coal particles decrease from -53+26.2mm to -4mm. The results for the coal size fractions also reveal that there are slight variations in proportions of hydrogen and nitrogen. Interestingly, the -75+53mm fraction contains high concentration of the total sulphur and to a lesser extent in the -53+26mm size fraction**.**

Table 5.1: The ultimate analysis of coal size fractions feed coal (dry, ash-free basis) (wt%)

Coal size fractions	**-75 +53mm**	**-53 +26.2mm**	**-26.2 +13.2mm**	**-13.2 +9.5mm**	**-9.5 +6.7mm**	**-6.7+ 4.7mm**	**-4.7 +4mm**	**-4mm**
Carbon (%)	78.14	78.65	79.57	80.12	80.38	79.90	77.02	80.03
Hydrogen (%)	3.72	4.06	4.04	4.00	3.89	4.00	4.04	3.98
Nitrogen (%)	2.06	2.10	2.14	2.14	2.10	2.08	2.14	2.15
Total sulphur (%)	4.58	1.84	1.22	0.99	1.18	1.21	1.01	1.00
Oxygen (%) by difference.	11.49	13.35	13.03	12.74	12.45	12.81	15.79	12.84

5.1.2 Proximate analysis of coal size fractions

In contrast, Table 5.2 shows that there is no notable difference in concentrations of inherent moisture, ash, volatile matter and fixed carbon in the coal size fractions analysed in this study.

Table 5.2: The proximate analysis of coal size fractions

Coal size fractions	-75 +53mm	-53 +26.2	-26.2 +13.2mm	-13.2 +9.5mm	-9.5 +6.7mm	-6.7+ 4.7mm	-4.7 +4mm	-4mm
IM (%)	4.6	4.4	4.9	4.9	4.8	4.7	4.8	4.7
Ash (%)	26.4	28.9	23.8	23.4	24.7	23.3	24.1	22.7
VM (%)	22.1	21.2	21.6	21.2	21.2	21.3	21.3	22.0
FC (%)	46.9	45.5	49.7	50.5	49.3	50.7	49.8	50.6

The XRF analysis (Table 5.3) indicates that the coarser fraction (-75+53mm) contains a higher proportion of sulphur (in line with Table 5.1) and to a lesser extent in the -53+26mm size fraction in comparison with other coal size fractions analysed in this study. The significantly higher sulphur proportion in the -75+53mm and -53+26mm size fractions is associated with a high Fe content (Table 5.3), indicating that pyrite is concentrated in these two coarse coal size fractions. Similarly, other fluxing elements such as Ca and Mg are concentrated in the -75+53mm fraction. The presence of these fluxing elements in this coal size fraction can be expected to enhance the sintering and slagging of mineral matter at elevated temperatures and pressures, subsequently resulting in clinker formation during coal gasification/combustion. A high proportion of phosphorus (which could possibly be present as apatite) is also present in the -75+53mm coal size fraction.

Table 5.3: Inorganic oxide percentages (wt %) from XRF analysis of coal size fractions

Coal size fractions	-75 +53mm	-53 +26.2mm	-26.2 +13.2mm	-13.2 +9.5mm	-9.5 +6.7mm	-6.7+ 4.7mm	-4.7 +4mm	-4mm
SiO_2	10.90	16.20	13.40	13.60	13.70	12.60	13.00	11.50
Al_2O_3	4.90	6.90	6.60	7.10	6.80	6.50	6.80	6.60
Fe_2O_3	3.93	1.61	1.07	0.95	0.87	0.79	0.81	0.86
TiO_2	0.23	0.41	0.38	0.38	0.39	0.36	0.38	0.35
P_2O_5	0.89	0.17	0.22	0.24	0.27	0.26	0.26	0.26
CaO	4.68	2.66	2.00	1.87	1.87	1.87	1.90	2.12
MgO	1.20	0.80	0.80	0.80	0.50	0.50	0.50	0.50
Na_2O	0.02	0.05	0.04	0.07	0.04	0.04	0.04	0.05
K_2O	0.19	0.30	0.24	0.25	0.25	0.24	0.24	0.23
SO_3	3.05	1.27	0.94	0.82	0.72	0.70	0.62	0.53

5.2 Mineralogical analysis of coal size fractions

5.2.1 CCSEM analysis of coal size fractions

Figure 5.1 illustrates back-scattered electron images with the prominent differences between the eight size fractions that were crushed before analysis. The appearance of the carbon-rich organic phase in these back-scattered electron images (with atomic number contrast) is black to dark grey and minerals are light grey to white.

The results in Figure 5.1 also show that, with exception of the -75+53mm size fraction, the remaining size fractions contain similar minerals. However, the -75+53mm size fraction has a higher proportion of pyrite associated with coarse-grained sandstone, coarse pyrite cleat fragments and coarse calcite cleat fragments. The characteristics of selected particles of coal and rock fragments shown in Figure 5.1, are described as follows:

- Particle 1 - pyrite (white) is associated with coarse grained quartz-rich (grey) sandstone;
- Particle 2 - coarse calcite cleat (grey) is associated with organic fraction;
- Particle 3 - fine-grained kaolinite and quartz siltstone rock fragment;
- Particle 4 - coarse grained quartz rich sandstone rock fragment;
- Particle 5 - fine calcite/dolomite (grey) cleats transecting carbon matrix (black);
- Particle 6 - kaolinite-rich (grey) mudstone rock fragment, included microcline and muscovite (elongated grain) minerals are present;
- Particle 7 - coarse microcline-rich fragment;
- Particle 8 - complex intergrowth of calcite/dolomite in a carbon-rich matrix (black);
- Particle 9 - large predominantly dolomite (grey) inclusions in carbon-rich matrix (black);
- Particle 10 - medium grained sandstone rock fragment with equal proportions of kaolinite (grey), quartz (light grey) and minor proportions of microcline (white).

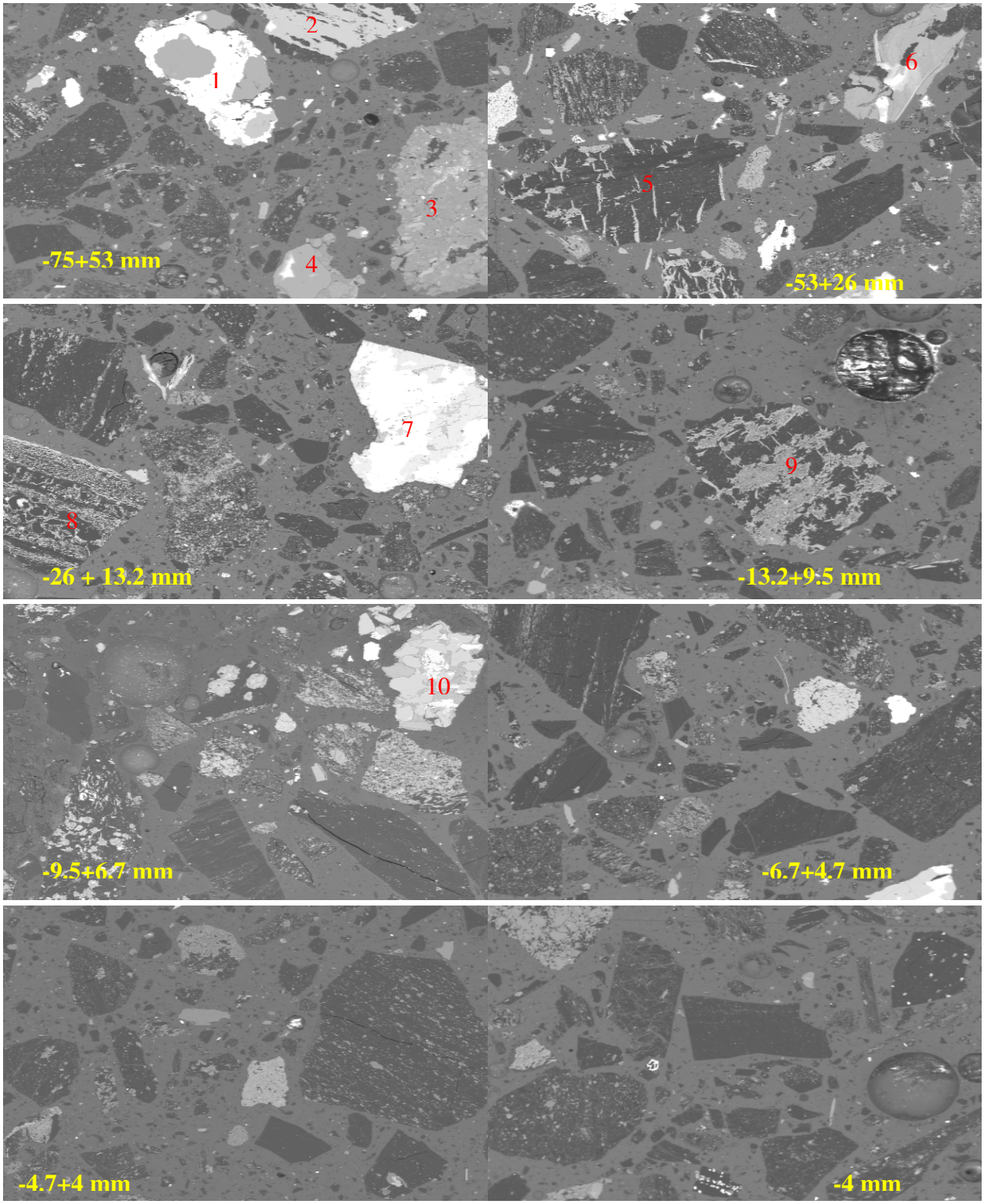


Figure 5.1: Back-scattered electron images of the eight size fractions. The particle characteristics and variation in proportions of minerals are illustrated. The width of the each image field is approximately 6.3 mm.

a) Concentrations of minerals in coal size fractions (mass-%)

The CCSEM technique was used to determine concentrations of minerals present in the individual coal size fractions. The calculated mass-% mineral distribution is summarised in Table 5.4. The results given in Table 5.4 confirm that the -75+53mm size fraction contained significantly higher proportions of fluxing elements-bearing minerals such as pyrite, dolomite and calcite and a corresponding low proportion of kaolinite (in line with the XRF results in Table 5.3). The apatite mineral, which could also play a significant role to lower the ash fusion temperature of mineral matter at elevated temperatures, concentrated in the coarse coal fraction (the-75+53mm size fraction). High concentrations of the carbonate minerals, as well as pyrite in the sink fraction (<1.8g/cm^3) that were also detected by CCSEM, corroborated these results (Table 4.11). Quartz was also found to be somewhat concentrated in the coarse coal particles and remained fairly constant as the coal fractions decreased from the -26.2+13.2mm to-4.7+4mm in comparison with other coal fractions analysed in this study. This favourably corresponds to the observed variations in Al_2O_3, SiO_2, Fe_2O_3, CaO and MgO contents (Table 5.3).

Table 5.4: Mineral proportions for the individual size fractions (mass-%)

Coal size fractions	**-75 +53mm**	**-53 +26.2mm**	**-26.2 +13.2mm**	**-13.2 +9.5mm**	**-9.5 +6.7mm**	**-6.7+ 4.7mm**	**-4.7 +4mm**	**-4mm**
Pyrite	6.2	1.7	1.9	1.1	1.5	0.9	0.9	1.4
Quartz	7.2	9.6	5.2	6.9	6.2	5.2	5.9	4.8
Microcline	0.8	0.8	0.6	0.5	0.5	0.2	0.3	0.2
Muscovite/ Illite	1.0	2.3	1.2	4.5	1.8	1.0	1.6	1.0
Kaolinite	8.1	15.7	14.4	11.6	13.6	14.8	15.5	13.6
Anatase	0.1	0.2	0.1	0.1	0.1	0.1	0.2	0.2
Ankerite	0.1	0.1	0.1	0.1	0.1	0.1	0.1	0.1
Siderite	0.1	0.1	0.0	0.0	0.0	0.0	0.0	0.2
Calcite	5.2	3.2	1.9	1.8	1.8	1.8	2.1	3.1
Dolomite	4.4	4.0	2.8	2.9	2.9	2.7	3.1	2.1
Apatite	0.9	0.0	0.4	0.2	0.2	0.1	0.2	0.1
Other	0.6	0.4	0.3	0.6	0.7	0.2	0.4	0.2
Coal (carbon)#	65.3	61.7	71.0	69.7	70.6	72.9	69.9	73.1

Table 5.5 illustrates the mineral distribution across the individual size fractions. The mineral distribution across the individual size fraction was calculated by using the proportion of mineral in the individual size fraction (Table 5.4) and the calculated mass-% size distribution (mass retained) in Figure 3.2. The individual mineral distributions were compared with the mass-% distribution across the size fractions or particle size distributions (PSD). The results indicated that a comparatively high proportion of pyrite (25.6%) and to a lesser extent calcite (16.9%) and dolomite (11.3%) are concentrated in the -75+53mm size fraction. The -26.2+13.2mm size fraction contains a high proportion of other minerals, along with low proportions of quartz and muscovite/illite. As the size of coal particles decreases from the -13.2+9.5mm to -4.7+4mm, proportions of other minerals, and carbon also decrease, with the exception of kaolinite.

Table 5.5: Percent mineral distribution across size fractions (wt%)

Coal size fractions	**-75 +53mm**	**-53 +26.2mm**	**-26.2 +13mm**	**-13.2 +9.5mm**	**-9.5 +6.7mm**	**-6.7 +4.7mm**	**-4.7 +4mm**	**-4mm**
Pyrite	25.60	17.80	34.50	6.50	8.00	3.00	1.00	3.60
Calcite	16.90	26.60	27.50	8.50	7.70	4.50	2.00	6.30
Dolomite	11.30	26.20	30.50	11.00	9.80	5.30	2.30	3.50
Kaolinite	4.80	23.40	36.80	10.00	10.50	6.80	2.70	5.00
Quartz	8.90	29.90	27.90	12.40	10.00	5.00	2.10	3.70
Microcline	10.70	28.50	37.30	9.60	8.90	2.50	1.10	1.50
Muscovite/ illite	4.20	25.50	23.30	28.80	10.10	3.30	2.00	2.90
Coal (carbon)#	7.70	18.40	36.30	12.10	10.90	6.70	2.40	5.40

Note: #Coal-refers the carbon-rich matrix and represents the macerals

b) Characterisation of particles of the screened coal fractions

To determine proportions of extraneous mineral matter, as well as the included mineral matter (mineral matter that is associated with the carbon matrix or present in the coal macerals), the same back-scattered electron images of particles taken during the CCSEM analysis of coal fractions were used to classify particles into the different texture groups described in Figures 3.8-3.9. The area-% proportions of these particle types are summarised in Table 5.6 and percent distribution across the size fractions in Table 5.5.

From the results given in Table 5.6, it can be seen that the proportion of included minerals slightly increased with a decrease in the coal size fractions. The -75+53mm size fraction contains comparatively higher proportions of sandstone rock fragment, pyrite cleats, carbonate cleats and a smaller proportion of siltstone/mudstone rock fragment in comparison with other coal size fractions analysed in this study.

Table 5.6: Area-% proportions of the major particle types

Coal size fractions	**-75 +53mm**	**-53 +26.2mm**	**-26.2 +13mm**	**-13.2 +9.5mm**	**-9.5 +6.7mm**	**-6.7 +4.7mm**	**-4.7 +4mm**	**-4mm**
Coal rich particles (MM <60 vol-%)	76.80	73.60	85.20	86.30	83.50	92.50	91.90	92.90
Siltstone/ mudstone rock fragment	2.90	16.00	10.00	11.10	10.90	6.30	5.80	4.30
Sandstone rock fragment	8.90	7.90	2.00	1.20	3.70	0.50	1.10	0.90
Pyrite cleats	5.90	2.20	0.60	0.20	0.20	0.00	0.10	0.10
Carbonate cleats	3.00	0.10	2.00	1.00	1.00	0.40	1.00	1.80
Carbonate and pyrite cleats	2.50	0.00	0.00	0.10	0.50	0.20	0.00	0.00
Kaolinite and pyrite cell cavities	0.00	0.10	0.20	0.00	0.10	0.10	0.00	0.10

Table 5.7 shows that the -75+53mm coal fraction contains a low proportion of the carbon-rich particles and a marginally higher proportion of the extraneous carbonate and pyrite cleats. Interestingly, pyrite and kaolinite cell cavities were not contained in this coal fraction, but significantly higher proportions of pyrite and kaolinite cell cavities (23.50% and 57.80% of the total) were found in the -53+26mm and -26+13.2mm size fractions respectively. The

absence of the pyrite and kaolinite cell cavities in the -75+53mm coal fraction could imply that this fraction may contribute little to the sintering and slagging of mineral matter during coal gasification or combustion.

High proportions of the siltstone/mudstone rock fragments (32% and 34% of the total) are contained in the two largest fractions (-75+53mm and -53+26mm). In excess of 40% of the sandstone is in the -53+26mm size fraction. Significantly higher proportions (39.70% and 38.40%) of the extraneous pyrite cleat fragments are in the -53+26mm and -75+53mm size fractions respectively, when compared to other coal size fractions analysed in this study. The results from Table 5.7 also reveal that a substantially higher proportion of the carbonate cleat fragments (52%) are concentrated in the -26+13.2mm size fraction, when compared to other size fractions analysed.

Table 5.7: Percent particle type distribution across size fractions

Coal size fractions	**-75 +53mm**	**-53 +26.2mm**	**-26.2 +13mm**	**-13.2 +9.5mm**	**-9.5 +6.7mm**	**-6.7 +4.7mm**	**-4.7 +4mm**	**-4mm**
Coal-rich particles (MM <60 vol-%)	7.50	18.20	36.00	12.30	10.60	7.10	2.60	5.70
Siltstone /mudstone rock fragment	2.30	32.00	34.20	12.90	11.20	3.90	1.30	2.20
Sandstone rock fragment	19.50	43.80	19.30	3.90	10.70	0.90	0.70	1.20
Pyrite cleats	39.70	38.40	17.40	2.00	2.00	0.10	0.20	0.20
Carbonate cleats	18.00	2.00	52.40	9.10	8.00	2.00	1.80	6.80
Carbonate and pyrite cleats	71.50	2.80	0.0	3.30	19.00	3.30	0.00	0.00
Kaolinite and pyrite cell cavities	0.00	23.50	57.80	0.0	9.40	3.60	0.90	4.80

c) Liberation characteristics of minerals of the screened coal fractions

In order to describe the liberation characteristics of minerals in the coal size fractions, all coal size fractions produced by dry screening (excluding the -4.7+4mm size fraction) were ground to 100% passing 1mm. A sample of the -4.7+4mm size fraction was pulverised to 100% passing 212µm. As expected, pulverising coal samples should technically liberate mineral matter that is associated within the carbon matrix (coal macerals). The CCSEM and QEMSCAN analyses of coal revealed that the average size of mineral grains in South African coals is less than 20µm. In order to obtain 100% mineral liberation during coal pulverising, the coal must be pulverised to 100% passing 20µm. To minimise the impact of excessive pulverising only the coarse particles are included in the CCSEM liberation analysis. The results from the minerals' liberation study can provide the proportions of the included minerals that are presumed to be responsible for the initiation of the melting of mineral matter under reducing and oxidising conditions during coal combustion or gasification. Partially excluded mineral particles could presumably attach to the melt and form small and large clinkers in the gasifier.

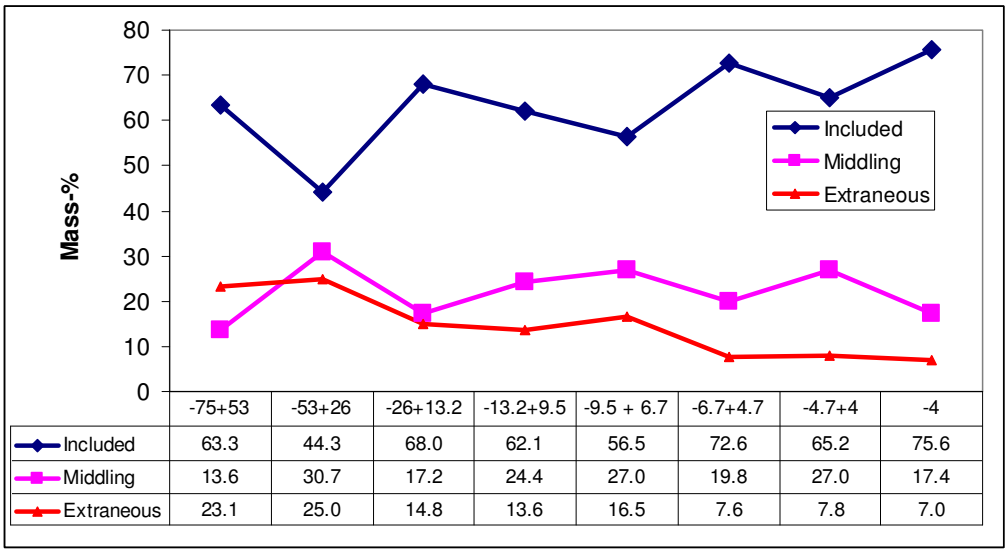
In this study the liberation groups are defined as follows:

- Included liberation group – mineral matter proportion is less than 20 vol.-percent and the organic coal fraction exceeds 80 vol.-percent;
- Middling liberation group – mineral matter proportion is between 20 to 60 vol.-percent and organic coal fraction is between 40-80 vol.-percent. This is analogous to the carbominerite microlithotype group;
- Extraneous liberation group – mineral matter proportion exceeds 60 vol.-percent and proportion of organic coal fraction is less than 40 vol.-percent. This is analogous to the minerite microlithotype group.

CCSEM analysis shows on average that (based on their minerals) 61.5 mass-percent of the coal particles in the coal samples are classified as "included", 22.0 mass-percent are "middlings" and 16.6 mass-percent are "extraneous". In addition, the results reveal that the majority of minerals (about 50.8%) in the coal sample are present as "extraneous" particles, while the remaining mineral particles (49.2%) occur as "middling" and "included" particles. The proportions of particles produced during the pulverising of the different coal size fractions, as well as the percent mineral proportion for each liberation group, are depicted in

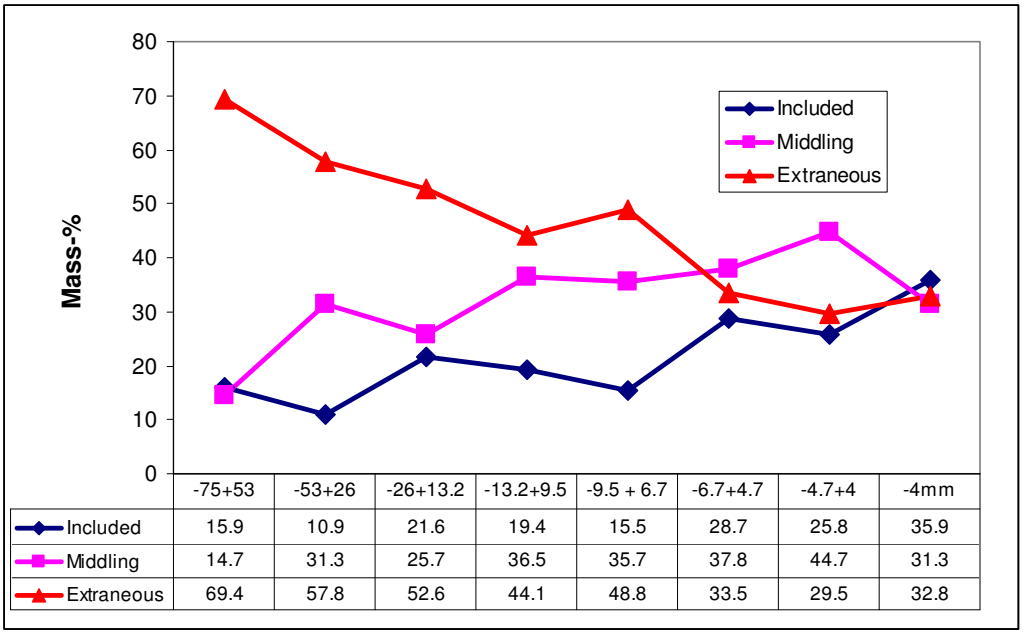
Figures 5.2 and 5.3. Figure 5.2 shows that there is a slight increase in the concentrations of the "included"type particles, with a decrease in the coal size, excluding the -53+26.2mm, 13.2+9.5mm and -9.5+4.7mm size fractions. Excluding the -9.5+4.7mm size fraction, the proportion of extraneous particles gradually decreases with a decrease in the coal size fractions. There is a gradual increase in the proportion of the "included" particles and corresponding decrease in the proportion of "extraneous" particles with a decrease in the size fractions (Figure 5.2). From Figure 5.3 it is clear that a higher proportion (37.8% of total mineral proportions) of the minerals are "extraneous" particles, in the coarser size fractions (>13.2mm), whereas a higher proportion of the minerals are "included" and "middling" particles in the finer size fractions.

Run of mine coal samples consist of coarse "stone" and organic-rich particles with varying proportions of the included minerals. During the mining activities and further sample preparation using physical methods such as screening and crushing, the carbon-rich particles (coal maceral particles), with varying proportions of the included minerals, will possibly break into smaller fragments; whereas, some stones or rock fragments will not readily break into smaller fragments. This is a plausible explanation for the trends observed in Figures 5.2 and 5.3 and the distribution of extraneous rock fragments, pyrite cleat fragments and calcite cleat fragments (Table 5.7).



	-75+53	-53+26	-26+13.2	-13.2+9.5	-9.5 + 6.7	-6.7+4.7	-4.7+4	-4
Included	63.3	44.3	68.0	62.1	56.5	72.6	65.2	75.6
Middling	13.6	30.7	17.2	24.4	27.0	19.8	27.0	17.4
Extraneous	23.1	25.0	14.8	13.6	16.5	7.6	7.8	7.0

Figure 5.2: Overall particle liberation characteristics.



	-75+53	-53+26	-26+13.2	-13.2+9.5	-9.5 + 6.7	-6.7+4.7	-4.7+4	-4mm
Included	15.9	10.9	21.6	19.4	15.5	28.7	25.8	35.9
Middling	14.7	31.3	25.7	36.5	35.7	37.8	44.7	31.3
Extraneous	69.4	57.8	52.6	44.1	48.8	33.5	29.5	32.8

Figure 5.3: Percent mineral distribution across the different liberation group.

In the same manner, the liberation characteristics of the individual minerals can be determined (Table 5.8). It is interesting to note that 72% of the pyrite present in the coal occurs as extraneous particles, whereas 13.2% and 15.3% of pyrite in the coal are included and middling particles respectively (Table 5.8). In line with this, the CCSEM analysis of coal particles indicates that pyrite predominantly occurs as extraneous coarse cleat fragments and is associated with coarse to medium grained sandstone (Table 5.7). A low proportion of pyrite, which is associated with kaolinite, is present in the coal. A significant proportion of calcite in the coal occurs as coarse calcite-rich cleat fragments; however, the siltstone/mudstone rock fragments contain a large proportion of kaolinite. A low proportion (23.4%) of calcite occurs in the "included" particles, whereas 26.6% of calcite occurs in "middling" particles. From Table 5.8 it can be seen that a small proportion of dolomite in the coal occurs as extraneous particles, whereas dolomite predominantly occurs as included and middling particles. A high proportion (45.7%) of apatite occurs as inclusions in the organic-rich matrix.

A high proportion of quartz (63%), microcline (85%) and muscovite/illite (66%) occur as extraneous particles. This is as expected, since quartz, microcline and muscovite/illite are common constituents of arkosic sandstone rock fragments.

The included minerals (kaolinite/quartz/calcite/dolomite/pyrite) in carbon-rich particles ("included" and "middling") can presumably interact with one another to lower the ash fusion temperature of mineral matter at elevated temperatures and result in slag/clinker formation

during coal gasification or combustion. In addition, the fluxing elements-bearing minerals (pyrite, dolomite and calcite) that are associated with clays (kaolinite, illite) in the rock fragments (sandstone and mudstone/siltstone) can also reduce the ash fusion temperature of mineral matter at elevated temperatures, to form a melt which will presumably result in slag/clinker formation during the heat treatment of coal.

Table 5.8: Average liberation characteristics of individual minerals

Particles	Included	Middling	Extraneous
Pyrite	13.20	15.30	71.50
Calcite	23.40	26.60	49.90
Dolomite	44.00	43.70	12.30
Apatite	45.70	22.10	32.20
Kaolinite	22.50	31.00	46.50
Quartz	16.80	20.50	62.80
Microcline	4.00	11.20	84.80
Muscovite/illite	12.10	22.10	65.80

5.3 Characterisation of density coal fractions by analytical techniques

As was stated in the previous section, the coal feedstock to the coal-conversion process, contains minerals that are associated with the carbon matrix and also with the extraneous rock fragments. The proportions of fluxing elements-bearing minerals and organically-bound inorganic elements (that are expected to cause the slagging process during gasification) could significantly depend on particle size, mode of occurrence of mineral matter in the coal and the density of the coal particles. To test this, coal samples were taken from the coal belt of each coal mine using the procedure developed by the operators from the mine. In the experimental procedure a 50kg coal sample was taken from the coal belt every 15min. Approximately 100kg coal sample was separated, using a mixture of tetra-bromo ethane and benzene at a density of 1.8g/cm^3 to produce float and sink fractions. The proportions of float and sink fractions were 83-93% and 7-17% respectively.

The sink and float fractions produced in this manner were separately crushed and pulverised to obtain 100% passing 1mm. The prepared samples of the composites from the different mines' float and sink fractions were subsequently submitted for proximate, ultimate,

elemental and ash fusion analyses. The proximate, ultimate and elemental analyses of the float and sink fractions were used to predict the mineral proportions of the calculated feed coal, based on the van Alphen Consultancy Coal Quality Predictor model. The model is also based on the elemental analysis of the mineral matter present in the coal.

5.3.1 Petrographic results for float (<1.5g/cm^3), middling (1.5-1.8g/cm^3) and sink (>1.8g/cm^3) fractions

The maceral and microlithotype group analysis results obtained are summarized in Table 5.9 and Table 5.10. The maceral and microlithotype results presented in Tables 5.9 and 5.10 follow the expected trends. The float coal fraction (<1.5g/cm^3) contains significantly higher proportions of vitrinite, liptinite, reactive semi-fusinite, inert semi-fusinite+fusinite and sclerotirite in comparison with the sink fraction. Note that the average vitrinite density is 1.3g/cm^3, liptinite is 1.25g/cm^3 and inertinite is 1.5g/cm^3 (Falcon and Snyman, 1986). As expected, significant proportions of mineral matter (quartz, clays, carbonates, pyrite) as stated in (Table 5.10) reported in the sink fraction (>1.8g/cm^3).

From the results given in Table 5.10, it is clear that the middling fraction (1.5–1.8g/cm^3) contained higher proportions of quartz, clay, carbonates and pyrite minerals in relation to the float fraction (<1.5g/cm^3).

Table 5.9: Maceral group analysis on coal samples (%vol)

Density fraction	Vitrinite	Liptinite	RSF	ISF	Fus/Scl	Mic	Inertodet	Qtz/ Cly	Carbs	pyrite	Others
<1.5g/cm^3	39.60	4.40	13.20	31.60	1.40	1.00	7.80	0.40	0.00	0.60	0.00
1.5-1.8g/cm^3	6.40	2.80	8.20	40.60	1.80	1.80	23.20	12.60	0.80	1.80	0.00
>1.8g/cm^3	2.40	0.80	0.60	9.00	0.60	1.00	19.80	47.60	6.20	8.00	4.00

Note: RSF = reactive semi-fusinite, ISF = inert semi-fusinite, Fus/scl = fusinite & sclerotinite
Mic= micrinite, Inertodet = reactive and inert inertodetrinite, Total reactive macerals = vitrinite+liptinite+RSF

Table 5.10: Particle type analysis (microlithotype group analysis) on coal samples (%vol)

Density fraction	Vitrite	Intermed	SF/Fus	Indet	Saprop -elic	Carb-argilite	Carb-ankerite	Carbopy rite	Minerals >60%
<1.5g/cm^3	23.80	20.60	45.80	7.80	0.40	0.80	0.60	0.40	0.00
1.5-1.8g/cm^3	1.60	6.60	50.20	26.60	0.80	7.20	5.60	1.00	0.40
>1.8g/cm^3	1.40	1.00	7.20	11.20	0.00	18.60	5.20	8.80	46.6

Note: Intermed = mixed coal particles vitrinite, inertite and liptite
SF/fus = semi-fusite+fusite, Indet = inertodetrite, Sapropelic = liptinite rich particles
Carbominerite = organic and inorganic mineral matter associations, Carbargilite = coal + 20-60% clays/quartz included, Carbankerite = coal 20-60% carbonate minerals included, Carbopyrite = coal 5-20% pyrite included

5.3.2 Chemical analysis of density fractions

The ultimate and proximate results for the density coal fractions obtained from Coal and Mineral Technologies are summarized in Tables 5.11 and 5.12. The ultimate analysis of the float fraction shows that this fraction contains significant concentrations of C, H and S as compared with the sink fraction. As expected, the float fraction contains a lower ash content of 9.1% and significantly higher proportion of volatile matter, whilst the sink fraction contains a substantially higher ash content of 62.60% and a low content of volatile matter.

Table 5.11: Ultimate analysis of density coal fractions (dry, ash-free basis)

Coal density Fractions	Carbon (%)	Hydrogen (%)	Nitrogen (%)	Total Sulphur (%)	Oxygen (%)
<1.5g/cm^3	78.25	4.33	2.05	0.68	14.69
>1.5-1.8 g/cm^3	75.87	3.49	1.95	0.70	17.99
>1.8g/cm^3	63.28	3.39	1.69	6.21	25.42

Table 5.12: Proximate analysis of feed coal and density coal fractions

Coal density fractions	IM %	Ash %	VM %	FC %
Float (<1.5g/cm^3)	3.40	9.10	28.70	58.80
Middling (>1.5-1.8 g/cm^3)	4.60	23.70	21.90	49.8
Sink (>1.8g/cm^3)	2.00	62.60	16.70	18.70

Note: IM ……Inherent moisture
VM …..Volatile matter
FC……Fixed carbon

From the results given in Tables 5.13 and 5.14, it is clear that there is a general increase in the proportion of SiO_2, Fe_2O_3 and K_2O with an increase in density and mineral matter proportions. In contrast, there is a general decrease in the proportion of Al_2O_3, TiO_2, P_2O_5, CaO, MgO and Na_2O with an increase in density and mineral proportions (Table 5.13). These trends emphasize that SiO_2, Fe_2O_3 and K_2O have a strong mineral affinity; whereas Al_2O_3, TiO_2, P_2O_5, CaO, MgO and Na_2O have a strong carbon/organic affinity, either as included minerals and/or organically-bound inorganic elements. This could imply that these elements may interact differently at elevated temperatures during coal gasification or combustion.

Table 5.13: XRF analysis of the feed coal and density coal fractions (wt%)

Sample number	Float <1.5 g/cm^3	Middling >1.5-1.8 g/cm^3	Sink >1.8g/cm^3
SiO_2	44.20	50.40	56.70
Al_2O_3	30.90	29.50	21.40
Fe_2O_3	2.40	2.00	5.70
TiO_2	2.20	1.50	1.10
P_2O_5	1.50	1.00	0.40
CaO	8.60	7.90	6.80
MgO	3.10	2.80	1.30
K_2O	0.70	0.70	0.90
SO_3	5.70	4.20	7.00
Na_2O	1.00	0.50	0.30
Total	100.00	100.00	100.00

5.3.3 Mineralogical analyses of float, middling and sink fractions from feed coal

Data on the different size and density fractions, also summarised in Table 4.11, indicate that the float fractions, with low percentages of LTA, have a mineral assemblage with lesser proportions of quartz and pyrite than the LTA-rich sinks fractions. Dolomite, by contrast, is more abundant in the floats and middlings fractions than in the high-density sinks material. This, together with the greater abundance of dolomite in the fine fractions than the coarse fractions, confirms a relatively intimate association of the carbonate minerals with the maceral components (in line with Table 5.8). Apart from a greater abundance of illite in the coarse floats material, the clay minerals, the phosphates and the bassanite, all appear to be more or less evenly distributed among the different size and density fractions.

- **CCSEM analysis of the float, middling and sink fractions**

The BSE images (Figure 5.4) of coal particles from the float, middling and sink fractions clearly show the substantial differences between these three density coal fractions. As before, in these back-scattered electron images, the appearance of carbon is black to dark grey and that of mineral matter is light grey to white.

Interestingly, the CCSEM analysis using BSE has successfully distinguished a “black” carbon phase and a “grey” carbon phase (Figure 5.4). This is specifically noted in the <1.5g/cm^3

density fraction. It is therefore proposed that this grey level discrimination is attributed to the variation in the density of macerals, ranging from 1.25g/cm^3 for liptinite, 1.3g/cm^3 for vitrinite and 1.5g/cm^3 for inertinite. Each density fraction has distinct particle characteristics (Figure 5.4). This illustrates the efficiency of density separation used in this study to produce float and sink fractions from the feed coal.

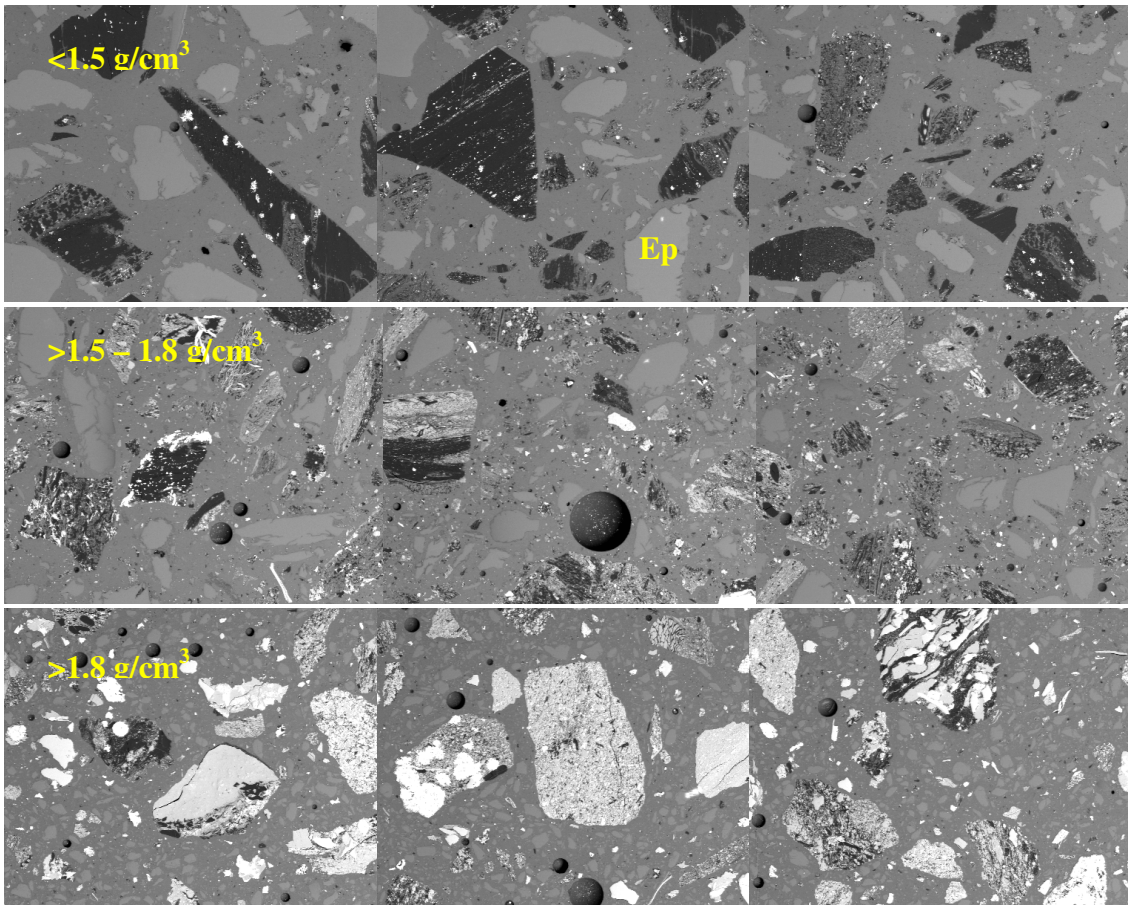


Figure 5.4: Back-scattered electron image of the three density fractions. The particle characteristics and variation in proportions of minerals are depicted. The width of each image is approximately 6.3mm. The large light grey particles (Ep) are included crushed iodinated epoxy resin particles.

- **Proportions of minerals present in the density coal fractions**

The mass-% mineral distribution as reported by CCSEM for the individual density fractions and the calculated total sample is summarised in Table 5.14. The concentration of the individual minerals present in Table 5.14, as well as the mass of the density fraction given in Table 3.1 were used to calculate the percent mineral distribution across the density coal fractions.

From Table 5.14 is clear that the proportions of minerals, with the exception of apatite, ankerite or siderite increases with an increase in density of the coal fractions. As expected, the ash yield of these density coal fractions increase. As expected, the organic fraction (macerals) significantly decreases with an increase in density of the coal fraction.

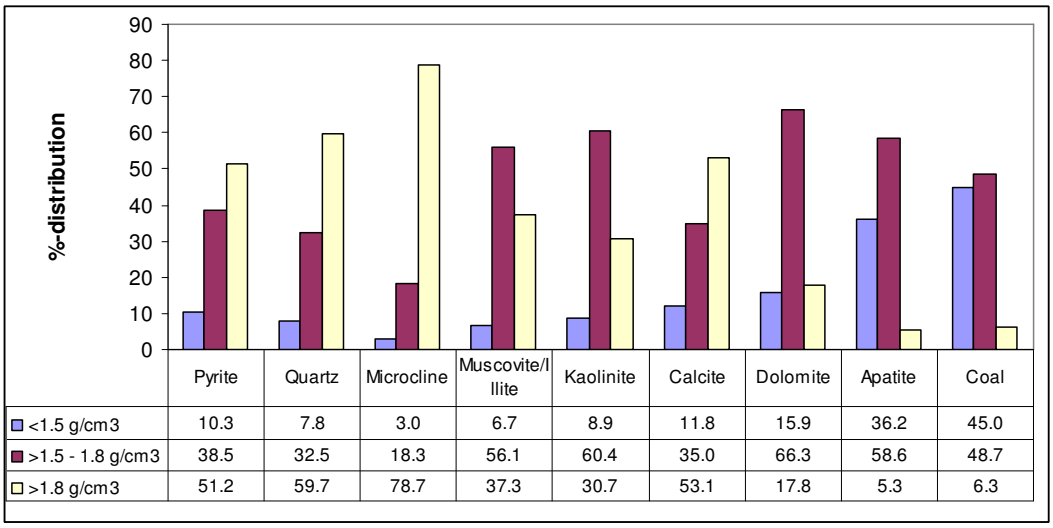
Table 5.14: Proportions of minerals in the float and sink fractions determined by CCSEM (mass percentage)

Mineral	Idealised formula	Float fraction <1.5 g/cm^3	Middling >1.5 - 1.8 g/cm^3	Sink Fraction >1.8g/cm^3
Pyrite	FeS_2	0.60	1.40	5.40
Quartz	SiO_2	1.30	3.60	19.20
Feldspar (Microcline)	$KAlSi_3O_8$	0.00	0.20	2.30
Muscovite/illite	$K_2O.3Al_2O_3.6SiO_2.2H_2O$/ $K_{1.5}Al_4(Si_{6.5}Al_{1.5})O_{20}(OH)_4$	0.40	2.20	4.30
Kaolinite	$Al_2Si_2O_5(OH)_4$	5.10	22.30	33.00
Anatase/rutile	TiO_2	0.10	0.20	0.30
Iron oxide/siderite	$Fe_2O_3/FeCO_3$	0.00	0.00	0.10
Calcite	$CaCO_3$	0.90	1.80	7.80
Dolomite	$CaMg(CO_3)_2$	1.50	4.00	3.10
Ankerite	$(Fe, Ca, Mg)CO_3$	0.00	0.10	0.10
Apatite	$Ca_5F(PO_4)_3$	0.20	0.20	0.10
Other	Unidentified minerals	0.30	1.30	0.60
#Coal	Organic fraction	89.50	62.70	23.70
Total		100.00	100.00	100.00

Note: #Coal = refers the carbon-rich matrix and represents the macerals

Figure 5.5 shows the percent mineral distribution as function of density. Based on the results given in Figure 5.5, it is clear that high proportions of fluxing elements-bearing minerals (pyrite and calcite), with the exception of dolomite, report to the sink fraction (>1.8g/cm^3). Dolomite, which is the alternative source of the fluxing elements such as Ca and Mg, concentrated in the middling fraction (1.5-1.8g/cm^3 density fraction). This trend is attributed to significantly higher proportions of pyrite and calcite that occur as extraneous particles in the coal. However, a higher proportion of dolomite occurs as finer cleats between carbon-rich particles present in the middling coal fraction (1.5-1.8g/cm^3 density fraction). The high proportion of pyrite in the >1.8g/cm^3 density fraction is in line with the XRF analysis given in Table 5.13, showing a higher Fe content of this density fraction.

The >1.8g/cm^3 density fraction contains a significantly higher proportion of quartz, which is from rock fragments such as coarse to fine-grained arkosic sandstone. High concentrations of microcline/feldspars are contained in the >1.8g/cm^3 density fraction. As expected, kaolinite and muscovite/illite occur as fine included grains in the carbon matrix and are concentrated in the inertinite-rich particles (1.5-1.8g/cm^3 density fractions). In addition, a significant proportion of apatite is associated with the inertinite-rich particles (1.5-1.8g/cm^3 density fraction) and to a lesser extent with vitrinite-rich particles (<1.5g/cm^3 density fraction). Some preliminary results for the float and sink fractions found in this study are in line with previous results for density fractions of other South African coals that were found by Snyman et al. (1983).



	Pyrite	Quartz	Microcline	Muscovite/Illite	Kaolinite	Calcite	Dolomite	Apatite	Coal
<1.5 g/cm3	10.3	7.8	3.0	6.7	8.9	11.8	15.9	36.2	45.0
>1.5 - 1.8 g/cm3	38.5	32.5	18.3	56.1	60.4	35.0	66.3	58.6	48.7
>1.8 g/cm3	51.2	59.7	78.7	37.3	30.7	53.1	17.8	5.3	6.3

Figure 5.5: Mass % distribution of minerals in the density fractions.

CHAPTER 6

RESULTS AND DISCUSSION - COAL PYROLYSIS

The analytical results for the char samples and the samples of gas liquor from the pyrolysis experiments are discussed in this section. As stated earlier in Chapter 3 of this thesis, the coal samples were heated to 600^{o}C at greater than 20bar for one hour under reducing conditions.

6.1 Chemical and mineralogical analyses of char samples

6.1.1 XRF analysis of char samples

The normalised XRF analyses of the char samples of coals taken from the six different mines (as produced in the pyrolysis experiments) are given in Table 6.1. The XRF analysis of coals from the six different coal mines was discussed in Chapter 4 of this thesis. The XRF technique used is semi-quantitative for sulphur, hence the sulphur contents are not reported in Table 6.1. Also, the results given in Table 6.1 reveal that there are significant variations in chemical compositions of the char samples produced. The significant differences between these chemical compositions are attributed to the coarse size of the coal samples ranging from 13.2mm to 2.36mm (and hence significant heterogeneity) in this study.

Table 6.1: XRF analyses of char samples obtained from the pyrolysis experiments

	Char-1	**Char-2**	**Char-3**	**Char-4**	**Char-5**	**Char-6**
Sample Number	*%*	*%*	*%*	*%*	*%*	*%*
SiO_2	57.90	56.94	55.80	51.86	53.23	53.40
Al_2O_3	26.50	30.01	27.90	29.30	27.80	24.82
Fe_2O_3	4.50	2.77	2.75	3.31	4.72	4.27
TiO_2	1.40	1.34	1.43	1.45	1.44	1.33
P_2O_5	0.40	1.13	1.12	1.55	1.54	1.83
CaO	6.10	5.24	7.94	9.11	8.10	10.89
MgO	1.10	1.03	1.43	1.35	1.33	1.83
Na_2O	0.60	0.62	0.71	0.73	0.72	0.92
K_2O	0.80	0.92	0.92	1.35	1.13	0.71

6.1.2 Mineralogical analysis of corresponding char samples

The mineralogical composition of corresponding chars tested in this study is given in Table 6.2. During the pyrolysis experiments, some minerals present in the coal partially transformed, with trends observed being in line with those summarised by Tomeczek and Palugniok (2002). Pyrite transformed to pyrrhotite. The kaolinite is expected to lose its bound water around 550^{o}C to form amorphous meta-kaolin. The high proportion of non-crystalline inorganic material in the char samples confirms the partial transformation of kaolinite to form meta-kaolinite during the pyrolysis experiments. Furthermore, the included minerals as well as the organically-bound inorganic elements could partially react with aluminium silicates (kaolinite and muscovite) at low temperatures under reducing conditions to form partially sintered particles. The XRD results for the char samples indicate that anhydrite formed during pyrolysis, probably from the interaction of the organic sulphur (and sulphur from the decomposition of pyrite) with organic calcium or with the included calcium-bearing fluxing elements-bearing minerals (calcite and dolomite).

In this study the thermodynamic package FactSage was used for undertaking the calculations, considering species in the gas phase, liquid phases and both solid compounds and solid solutions. It is clear from the results given in Table 6.3 that the FactSage model predicted the formation of high-temperature transformation products (anorthite ($CaAl_2Si_2O_8$), pyroxene (Mg, Fe)Si_2O_6, pyroxene ($CaMgSi_2O_6$)) of coal minerals (Table 3.4) at 600°C during coal pyrolysis under the reducing conditions. These calculated equilibrium phases that are generally observed only at temperatures of greater than 1000°C are not in good agreement with those of XRD. For example, Bryers (1986), Ward (1984) and Raask (1984) in their studies found that anorthite ($CaAl_2Si_2O_8$) formed when CaO reacted with reactive aluminium silicates such as metakaolin at high temperatures (1000-1200°C). The XRD analysis (Table 6.2) of the char samples from the pyrolysis experiments shows the presence of high proportions of coal minerals such as quartz and trace amounts of kaolinite, muscovite, dolomite, calcite and rutile as well as amorphous material in the char samples.

Table 6.2: Mineralogical composition of the corresponding char of coals mentioned in Table 4.5

Sample Number	Char-1 Mineral %	Char-2 Mineral %	Char-3 Mineral %	Char-4 Mineral %	Char-5 Mineral %	Char-6 Mineral %
Quartz	7.60	8.50	7.50	6.10	5.00	4.90
Kaolinite	1.70	2.50	1.60	0.80	1.30	1.20
Pyrite	0.00	0.00	0.00	0.00	0.00	0.00
Muscovite	1.30	2.00	1.20	1.30	1.20	-
Calcite	2.10	2.80	2.30	3.70	2.70	2.50
Dolomite	0.20	0.40	0.80	0.40	0.70	0.90
Pyrrhotite (Fe_7S_8)	1.40	0.80	0.60	0.60	0.60	0.50
Rutile	0.20	0.10	0.30	0.10	0.10	0.10
Anhydrite	0.20	0.60	0.30	0.30	0.30	0.30
Carbon and non-crystalline phases content	85.30	82.20	85.40	86.70	88.10	89.60

6.2 Pyrolysis results of the volatilised inorganic species

In this study, concentrations of inorganic elements in the gas liquor (determined by ICP-MS and IC) were used to calculate the amounts of inorganic elements vaporised during coal pyrolysis under conditions stated in Chapter 3. The IC analysis of all the gas liquor (pH values of 8.2 to 9.2) showed 800-1964ppm chloride, 64-91ppm bromide, 26-53ppm iodide, 0.01-0.04ppm fluoride, 800-1124ppm sulphate, 36-397ppm bicarbonate, 12 ppm carbonate, 6539-26000ppm ammonium, 28-40ppm sodium, 2ppm potassium, 0.2ppm magnesium, 6-14ppm boron, 5-7ppm calcium, 0.44-0.8ppm iron, 5.4-7.4ppm silicon, 0.2-1ppm aluminium and low concentrations of trace elements. The presence of these elements in the gas liquor clearly confirms volatilisation of these inorganic species during the pyrolysis of Highveld coal at a peak temperature of 600°C and pressure of 26bar. For all gas liquor samples analysed in this study, phosphate was not detected by IC, which implies that the volatilised trace phosphorus in the gas liquor is likely in the form of organic species.

Figures 6.1a to Figure 6.1g show the amounts of silicon, aluminium, iron, calcium, sodium, phosphorus and sulphur collected from the off-gas during pyrolysis. In these figures,

"distilled water" indicates the blank analysis, "200°C", "300°C", "400°C" and "600°C" the product of dissolution of gaseous products in distilled water for treatment up to the temperatures indicated, while "GL" is the condensed phase (water and organic liquid) for the whole pyrolysis treatment.

Of the coal samples tested, mine 5 coal followed by mine 6 coal released more volatile Si than all the other coals tested (Figure 6.1a); this was similar for Al and Fe (Figure 6.1b and c). Figure 6.1 gives the total amounts of the volatilised elements. These elements do not volatilise as inorganic species (based on the FactSage calculations and literature results) and must involve organic compounds.

Tar samples produced during the pyrolysis of the coal samples from the Highveld coal mines were analysed using FT-IR analysis to identify organometallic compounds in these samples. The FT-IR results for the tar samples revealed that these samples contain an aliphatic hydrocarbon, carboxylic acid, carboxylic acid salt, alcohol, epoxide, aromatic type of compound and metal carbonyls. Likely organometallic compounds in coal were summarised by Koppenaal and Manaham (1976) and include transition metal carbonyls, arene carbonyls, metal alkyls, organo hydrides and metal chelates. Recent results demonstrate that these compounds contribute to volatilisation: Zhang et al. (2006) showed (by X-ray photo-electron spectroscopy) that the sulphur, silicon, iron and sodium which are present in condensed volatile matter are organically bound. In addition, it was reported that the concentrations of silicon, aluminium and iron present in particulate matter (PM_1) particles (particles smaller than 1µm) after combustion in a drop-tube furnace were proportional to the amounts of these elements which are bound organically in the coal (Zhang et al., 2006).

The situation is different for the halogens in coals as given in Tables 6.3 and 6.4. The equilibrium calculations predict substantial volatilisation of chlorine (as HCl) and flourine (as HF); this is in line with the observation that as much as half of the chloride content of coal can be released as HCl, even at 300°C (Herod et al., 1983). In addition, some evaporation of NaCl may have occurred, since this has been shown to start at 597°C (Tomeczek and Palugniok, 2002), just below the peak temperature in these tests. In line with these predictions, the amounts of chlorine in the chars were significantly lower than in the coals (Table 6.3). The amounts of chlorine and fluorine in the coal and the corresponding char from the pyrolysis of mine 1 and mine 3 coals summarised in Table 6.4 were calculated by using

concentrations of chlorine and fluorine measured in these coals and the corresponding chars. In contrast with the FactSage (equilibrium) predictions, a smaller extent of volatilisation of fluorine than chlorine was observed during the pyrolysis of coal (Table 6.4). This could be attributed to the presence of fluorine as fluoroapatite in feed coal (Table 3.4), which decomposes at temperatures higher than 600°C.

Table 6.3: Predicted equilibrium compositions when 1.2kg coal with the composition as given in paragraph 3.4 equilibrates with 2.52mol N_2, at 600°C

Gas composition (major species and selected minor species shown); amount of gas is 21.5 mol

Species	Vol%
H_2O	30.98
CH_4	27.10
H_2	15.13
N_2	11.67
CO_2	10.23
H_2S	2.30
CO	1.85
HCl	0.60
NH_3	7.92E-02
HF	4.89E-02
COS	9.04E-03
HCN	6.59E-06
NaCl	5.23E-06
$FeCl_2$	4.41E-06
KCl	2.44E-06
$KFeCl_3$	2.26E-06
CS_2	2.02E-06
SiF_4	4.71E-08
$NaAlF_4$	1.55E-10
SiO	6.11E-23

Solids

Species	Mass (g)
Char (heated carbon)	566.4
Anorthite ($CaAl_2Si_2O_8$)	116.3
Quartz	59.1
Na feldspar ($NaAlSi_3O_8$)	33.8
Leucite ($KAlSi_2O_6$)	26.3
Pyroxene $(Mg,Fe)Si_2O_6$	21.4
Pyrrhotite	6.6
Pyroxene ($CaMgSi_2O_6$)	3.7
Hydroxyapatite $[Ca_5H(PO_4)_3]$	5.3
NaCl	2.3

Table 6.4: Amounts of halogens (Cl and F) in the 1200 g of coals and in 969 g of corresponding char from mine 1 and in 974 g of char from mine 3 before and after pyrolysis

Halogen	Mass of Cl and F in coal from Mine 1 (g)	Mass of Cl and F in char from coal Mine 1 (g)	Mass of Cl and F in coal from Mine 3 (g)	Mass of Cl and F in char from coal Mine 3 (g)
Cl	0.11	0.04	0.20	0.09
F	0.18	0.11	0.16	0.15

6.3 Calculated equilibrium volatilisation of cations in inorganic compounds from coal

The predicted equilibrium compositions of inorganic compounds are summarised in Table 6.3. As this shows, the dominant gaseous species are H_2O, CH_4, H_2, N_2, CO_2, H_2S, CO and HCl; the equilibrium vapour pressures of species containing Na, Fe, Al and K (chlorides), and Si (SiF_4 and SiO) are very low, with little removal of these elements predicted. In contrast, much of the fluorine and chlorine in the coal is removed to the gas phase, as HF and HCl. Of the 6g Cl in the coal, 4.6g is predicted to be removed by the gas phase, and all of the 0.2g F in the coal. This is in line with the chemical analyses of the char (as found experimentally), which indicate removal of the bulk of the halides by the gaseous pyrolysis products (Table 6.4). Similarly, of the 18.4g of S in the coal, 15.9g is predicted to be removed by the gas, partly as a result of decomposition of pyrite to pyrrhotite, but largely through the formation of volatile H_2S from the sulphur in the coal macerals. The predicted removal of Fe, Na, Si and Al is much smaller, at 80µg Fe, 26µg Na, 0.3µg Si, and approximately 1ng Al in comparison with the experimental results shown in Figure 6.1.

The low partial pressures of the species which contain Fe, Na, Si and Al are not unexpected. For example, the equilibrium constant of the reaction $SiO_2+4HF(g) = SiF_4(g)+2H_2O(g)$ is $K=(p_{SiF_4}\, p_{H_2O}{}^2)/(a_{SiO_2}\, p_{HF}{}^4)=30.9$ at 600°C. From the equilibrium gas composition, the partial pressure of HF is found to be 0.0125atm and that of H_2O 7.95atm. For equilibrium with pure SiO_2 that gives an equilibrium partial pressure of SiF_4 of 1.2×10^{-8}atm, which agrees with the volume percentage of SiF_4 as given in Table 4.39. Similarly, the formation of SiO would require a much higher temperature; at 600°C the equilibrium constant of the reaction $SiO_2+0.5C=SiO+0.5CO_2$ is $K= (p_{SiO}\, p_{CO_2}{}^{0.5})/(a_{SiO_2}\, a_C{}^{0.5})=2.5\times10^{-23}$, giving an equilibrium partial pressure of SiO of just 1.6×10^{-23} atm. Similar calculations for the Al- and Fe-bearing species support the predicted low equilibrium concentrations of volatile species of these elements in the pyrolysis product gas.

Note that volatilisation of all of these species is suppressed by increased oxygen levels in the inputs, since H_2O and CO_2 are co-products when respectively SiF_4 and SiO (as examples) are formed. Hence drying of the coal by removing the 3% water before the reactions occur, would favour greater volatilisation of Fe, Si and Al. However, this effect is quite small, since the major part of the hydrogen and oxygen in the off-gas originates from the coal macerals, not from the coal moisture.

To test this idea, the equilibrium for coal with no moisture and with the bound water removed from the kaolinite and muscovite before equilibration, was also calculated. For this case, the water vapour content of the product gas decreased to 26.4% and the CO_2 to 6.5%, and the HF content increased to 0.063%. The result though was only a slight increase in the SiF_4 content to 1.8×10^{-7}%, with 7.7×10^{-23}% of SiO - far too small to account for the observed volatilisation of silicon from the coal.

Based on these results, it does not appear possible for Fe, Na, Al and Si to be removed from the coal as volatile inorganic compounds during pyrolysis; this is in line with other results published in the literature (for example, Yan et al., 1999; Zhang et al., 2006). Yet the experimental results do indicate significant volatilisation of these elements. The only possibility appears to be that these elements are carried by volatile organic compounds. This suggestion is supported by the experimental observation that, in most cases, the largest part of the volatilised elements reports to the gas liquor (mixture of organic phase and aqueous phase), rather than being scrubbed out by the water scrubber.

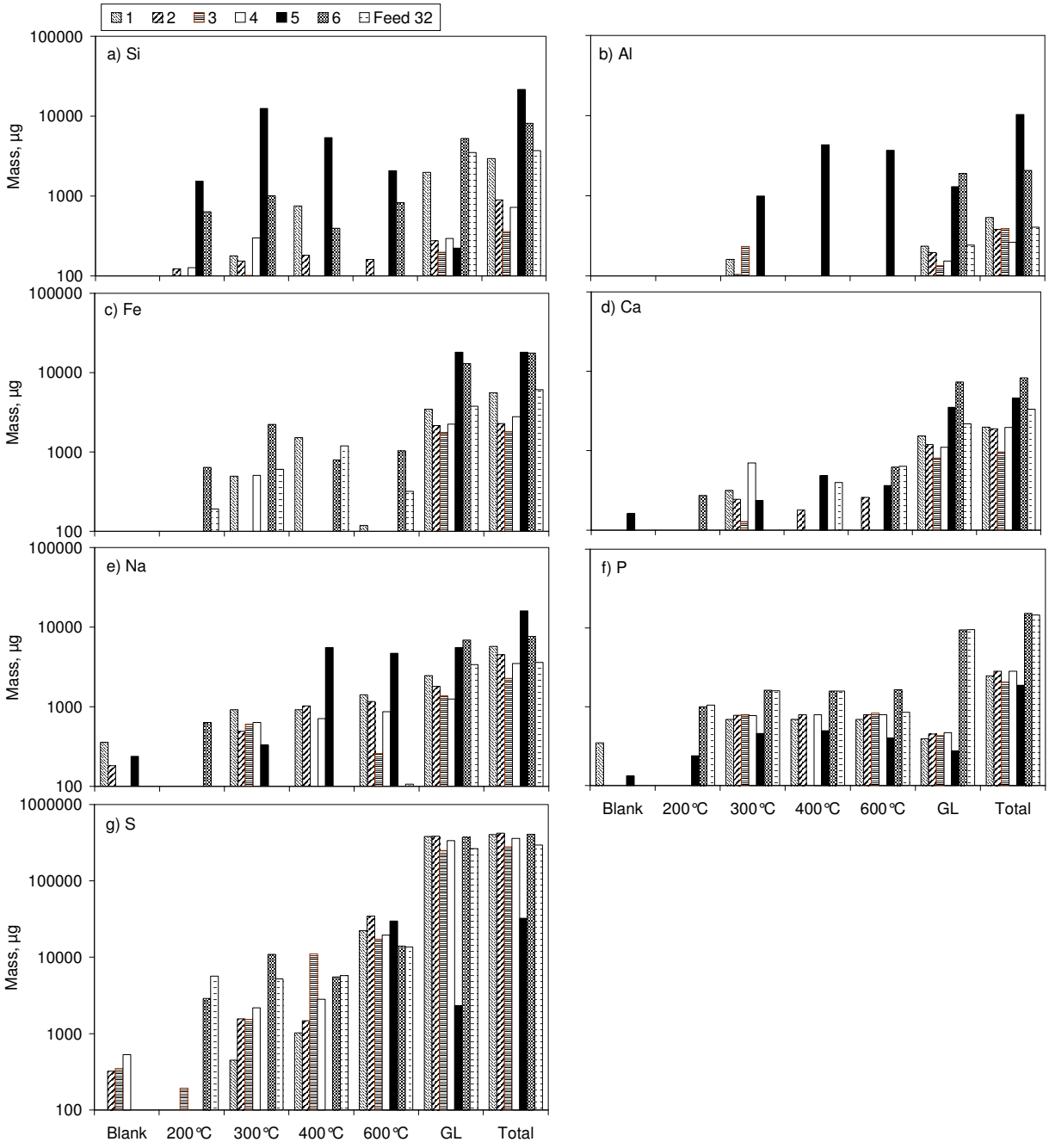


Figure 6.1. Amounts of elements volatilised during pyrolysis at various temperatures of various Highveld coal sources: a) Si; b) Al; c) Fe; d) Ca; e) Na; f) P; g) S.

CHAPTER 7

RESULTS AND DISCUSSION - GASIFICATION ASH ANALYSIS

The analytical results (chemical, physical and mineralogical analyses) for bulk gasification ash and gasification ash particles taken from the gasifier during gasifier test, turn-out and dig-out tests are discussed in this chapter. The main objective of this study was to determine inorganic components in the coal that are responsible for the clinker formation in the gasifier during coal gasification.

7.1 Chemical and mineralogical analyses of ash samples taken from the gasifier sampling methodology

7.1.1 Chemical analysis of corresponding ash samples

The chemical results for ash samples produced when using the experimental procedure described in Chapter 3 are summarised in Table 7.1. As noted earlier, a sample of corresponding gasification ash was collected from the bottom of the gasifier every three hours for an equivalent 24h period. At the end of the 24h period, the entire composite sample of coarse gasification ash was crushed and ground to obtain 100% passing 1mm. Before crushing the coarse ash fraction, clinker particles were hand-picked from this sample, based on their visual appearance.

The normalised ash elemental analysis values are reported in Table 7.1 and can be seen to be similar for the two sample types. A difference between the coarse ash and clinker is expected, as the clinker sample was hand-picked from the bulk gasification ash taken from the gasifier. The clinker was formed by physical contact between the heated rock fragment and the melt at elevated temperatures in the gasifier. The significant difference in concentrations of K, S and Ca in coal (Table 4.16) and ash samples could be attributed to significant volatilisation of these elements in the form of either sub-micron oxides ($CaO/CaSO_4$, K_2O) or gas (SO_2, H_2S).

The ultimate analysis (Figure 7.1) of the ash sample shows the expected low concentrations of S, H, N and C when compared with the coal sample. Trace amounts of sulphur in the coal ash can be captured by calcium oxide formed during transformation of either dolomite or calcite at elevated temperatures of greater than 1000°C to form calcium sulphate.

Table 7.1: Normalised XRF analysis of ash clinker and coarse ash samples and loss on ignition (L.O.I.) (wt%)

Sample Number	**Clinker**	**Coarse ash**
SiO_2	53.30	52.20
Al_2O_3	25.30	24.00
Fe_2O_3	5.30	4.90
TiO_2	1.40	1.30
P_2O_5	0.60	0.60
CaO	8.10	7.20
MgO	2.20	2.20
Na_2O	0.40	0.40
SO_3	0.50	0.50
K_2O	1.00	1.00
Total	100.00	100.00
L.O.I.	0.65	4.62

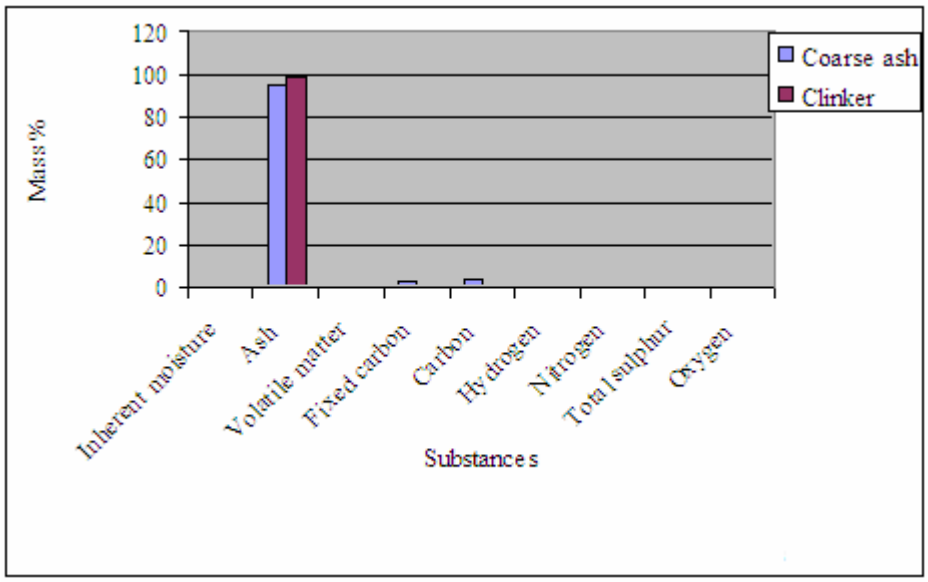


Figure 7.1: Ultimate and proximate analyses of ash particles.

7.1.2 Chemical composition of bulk gasification ash, heated stone and clinker samples from the turn-out test

Chemical analysis (Table 7.2) of samples from the gasifier turn-out indicates a wide variation in the composition of the individual ash, stone and clinker samples evaluated in the study. The main constituents in all cases are SiO_2, Al_2O_3, Fe_2O_3, CaO, MgO and TiO_2, with minor proportions (<1%) of Na_2O, K_2O, MnO, P_2O_5 and SO_3. Measurable concentrations of BaO and SrO occur in many of the coal gasification ash samples. The proportions of MgO, SrO and BaO can be correlated with the proportion of CaO (Figure 7.2), suggesting on the basis of other studies (Ward et al., 1999) that they are associated with the carbonate minerals in the feed coal.

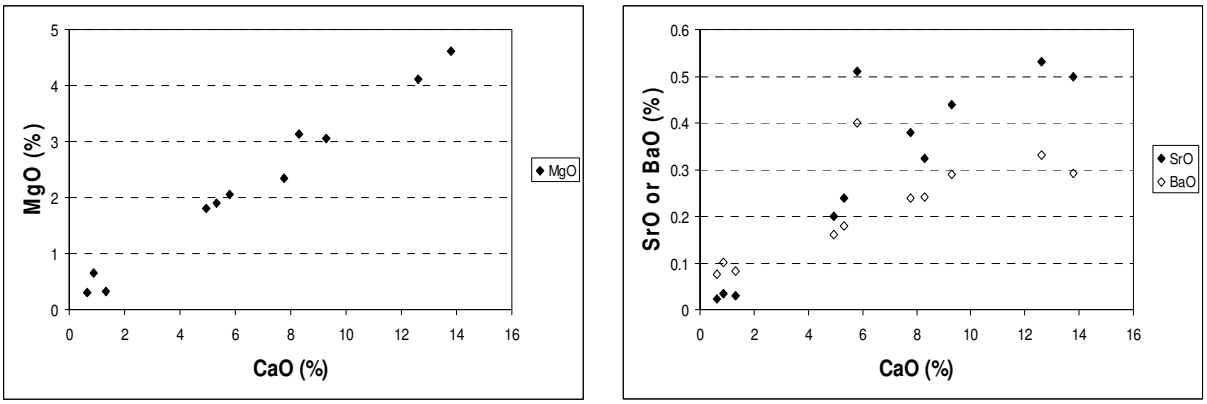


Figure 7.2: Correlation of MgO (left), SrO and BaO (right) with CaO in ash samples studied.

The composition of the bulk ash from the gasifier is similar to the ash chemistry expected from the mineral matter of the feed coal, calculated from the percentages and stoichiometric compositions of the minerals listed in Table 4.11. The abundance of bassanite has given rise to a greater percentage of (inferred) SO_3 in the LTA than that observed in the bulk gasification ash. The difference may reflect the higher temperatures associated with the gasification process, which would be expected to break down any calcium sulphates and convert more of the sulphur to the volatile form.

As discussed more fully below, the wide variations in chemical composition of the clinker samples are also reflected in the mineralogical composition of the materials, as well as the nature of the glasses occurring in the respective sample types.

Each sample typically represents an individual fragment of either coal or carbonaceous shale (stone) that occurred within the coarse feed coal, after being subjected to the high temperatures and pressures of the gasification process. For example, the results given in Table 7.2 indicate that the samples of partially burnt carbonaceous shale (heated stones 1 and 2) have higher concentrations of SiO_2 and K_2O and lower concentrations of Al_2O_3 and CaO than the clinker samples (1, 2, etc) analysed in the study. Based on data from a range of other South African coals and associated rocks (Pinetown et al., 2006), this suggests derivation from a material rich in quartz, feldspar and/or illitic clay minerals, rather than the kaolinite-rich clays and associated carbonate minerals (Table 7.2) associated with the coals themselves.

In most cases the white clinker particles (e.g. 4, 6) contain higher proportions of SiO_2 than the corresponding black or grey clinker particles (e.g. 3 and 5) and lower proportions of Fe_2O_3, CaO, SrO, MgO, K_2O, Na_2O and BaO (Table 7.2). The latter oxides, especially CaO, SrO, Na_2O, K_2O, MgO and Fe_2O_3 (which reacts as FeO), are generally thought to be associated with the sintering of coal ash materials. Briggs and Lindsay (Briggs, 1986) indicate that clay minerals may react with partially-oxidised pyrite and CaO from calcite at 750 -760°C to form silicate glass. Bryers (1986), Ward (1999) and Raask (1984) also indicate that CaO interacts with reactive aluminium silicates such as metakaolin at high temperatures (1000 -1200°C) to form gehlenite ($Ca_2Al_2SiO_7$) and anorthite ($CaAl_2Si_2O_8$), which in turn fuse at about 1400 to 1500°C.

Table 7.2: Chemical composition (wt %) of coal LTA inferred from XRD and of coal gasification ash, clinker and heated rock samples determined by XRF analysis

Oxide	Coal LTA	Bulk gasification ash	Clinker 1	Clinker 2	Clinker 3	Clinker 4	Clinker 5
SiO_2	54.30	49.40	41	48.7	49.8	60.9	49.30
Al_2O_3	28.20	24.40	24	27.9	25.8	23.4	23.70
Fe_2O_3	2.21	4.06	4.39	3.26	5.71	1.16	4.93
CaO	7.79	7.76	13.8	9.28	5.81	4.94	8.29
MgO	2.91	2.34	4.62	3.06	2.05	1.81	3.13
TiO_2	1.30	1.36	1.25	1.45	2.07	1.73	1.46
Na_2O	0.00	0.76	0.61	0.68	0.49	0.45	0.56
K_2O	0.60	0.88	0.67	0.72	1.01	0.54	0.69
MnO		0.05	0.075	0.06	0.05	0.08	0.06
P_2O_5	1.25	0.72	0.896	0.89	0.97	0.39	0.56
SO_3	1.44	0.25	0.221	0.102	0.03	0.09	0.68
SrO		0.38	0.498	0.44	0.51	0.20	0.32
BaO		0.24	0.293	0.29	0.4	0.16	0.24
ZrO_2		0.05	0.048	0.06	0.06	0.05	0.05
LOI		8.20	8.52	3.1	4.82	4.60	7.27
Total	100.00	101.00	100.01	100.00	99.70	101.00	101.00

Oxide	Clinker 6	Clinker 7	Clinker 8	Heated stone 1	Heated stone 2	Heated stone 3	Heated stone 4
SiO_2	61.00	56.50	43.2	76.90	80.01	52.50	57.40
Al_2O_3	28.80	26.50	27.7	9.89	10.70	25.30	25.80
Fe_2O_3	1.20	2.90	3.9	1.53	1.37	9.34	1.07
CaO	0.87	5.31	12.6	1.33	0.63	0.46	0.39
MgO	0.65	1.90	4.11	0.32	0.30	0.43	0.40
TiO_2	0.67	1.20	1.51	1.24	1.10	0.96	1.57
Na_2O	0.34	0.73	0.73	0.40	0.32	0.29	0.29
K_2O	1.25	1.32	0.68	2.19	2.44	1.72	0.90
MnO	0.01	0.04	0.08	0.02	0.01	0.011	0.00
P_2O_5	0.09	0.47	1.06	0.06	0.07	0.07	0.20
SO_3	0.00	0.05	0.04	0.19	0.23	0.29	0.21
SrO	0.03	0.24	0.53	0.03	0.02	0.02	0.11
BaO	0.10	0.18	0.33	0.08	0.08	0.08	0.16
ZrO_2	0.02	0.04	0.04	0.25	0.21	0.02	0.05
LOI	4.61	1.93	4.47	5.08	1.60	8.45	11.32
Total	99.70	99.10	101	99.70	99.20	99.90	99.90

Note: LOI = Loss on Ignition at 1050°C
Samples:
Coal LTA = inferred chemistry of coal ash based on mineralogy of LTA (Table 7.6)
Clinker 1 = A small heterogeneous clinker with black and white colours taken from the gasification ash exiting the gasifier.
Clinker 2 = A medium heterogeneous clinker with white and black colours taken from the gasification ash exiting the gasifier.
Clinker 3 = A large heterogeneous clinker with black colour taken from the gasification ash exiting the gasifier.
Clinker 4 = A large heterogeneous clinker with white colour taken from the gasification ash exiting the gasifier.
Clinker 5 = A largest heterogeneous clinker with black colour taken from the gasification ash exiting the gasifier.
Clinker 6 = A largest heterogeneous clinker with white colour taken from the gasification ash exiting the gasifier.
Clinker 7 = One lump of clinker sample taken from the bottom of the ash-bed area during turn-out sampling.
Clinker 8 = One lump of clinker sample taken from the gasification zone area during the turn-out sampling.
Clinker 9 = A large heterogeneous clinker with white and black colour taken from the gasification ash exiting the gasifier.
Clinker 10 = A largest heterogeneous clinker with white and black colour taken from the gasification ash exiting the gasifier.
Heated stone 1 = One lump of partially burnt carbonaceous shale taken from the gasification ash exiting the gasifier.
Heated stone 2 = One white lump of partially burnt carbonaceous shale taken from the gasification ash exiting the gasifier.
Heated stone 3 = One lump of partially burnt carbonaceous siltstone taken from the bottom of the ash-bed during turn-out sampling
Heated stone 4 = One lump of partially burnt carbonaceous sandstone taken from the gasification zone during turn-out sampling

7.2 Mineralogy of bulk gasification ash and clinker samples from the turn-out test

XRD analysis (Table 7.3) indicates that the bulk gasification ash sample contains around 10% quartz, together with 18% mullite ($Al_6Si_2O_{13}$), 13% anorthite ($CaAl_2Si_2O_8$) and around 50% amorphous glass. Small proportions of cristobalite (SiO_2) and diopside ($CaMgSi_2O_6$) are also present. The cristobalite was probably formed from the amorphous decomposition products of the clay minerals, kaolinite and illite. The remaining available amorphous silica may have reacted with high temperature transformation products (CaO and MgO) of carbonates (calcite and dolomite) to form diopside. The different clinker particles hand-picked from the gasification ash (clinkers 1, 2, 7, 8, 9 and 10) contain similar phases (including glass), although the proportions vary from fragment to fragment depending on factors such as composition and possibly the temperature reached by the fragment in the ash bed.

Samples of the partially burned carbonaceous shale taken from the gasification ash (heated stones 1 and 2), as well as partly burned siltstone and sandstone (heated stones 3 and 4), have higher proportions of quartz, but little (if any) anorthite, cristobalite or diopside. Table 7.3 indicates, for example, that heated stone 1 contains 7.9% illite, 6.4% pyrrhotite and traces of anatase and/or rutile (TiO_2), all of which presumably represent unaltered or partly altered remnants of the original sedimentary material. The presence of remnant illite particles in the heated stone samples is attributed to a combination of factors and processes, including incomplete thermal decomposition of the rock fragments entering the gasifier with the coal, the typical wide range of particle sizes (leading to incomplete fusion of the larger particles), and variations in operating procedures. The pyrrhotite (FeS) in heated stone 3 represents an alteration product of pyrite in the original rock, developed by heating under reducing conditions.

Dynamic high-temperature XRD studies on other materials (French et al., 2001) suggest that mullite and cristobalite form from the residues of clay minerals in the parent coal, especially the kaolinite, by solid state reactions that commence at around 1000°C. Solid-state reactions in calcium-rich mineral matter produce anorthite at similar temperatures, with quartz and/or clay mineral residues being incorporated into the anorthite as part of the process.

When tested at progressively higher temperatures the anorthite begins to react with the melt at around 1200°C, while the mullite and cristobalite in Ca-poor ashes begin to react with the melt at around 1400°C. Cooling of the molten material, especially the slow cooling associated with the gasifier bed, may also be expected to produce crystals of anorthite, as well as the pyroxene mineral diopside, in a manner analogous to the crystallisation of magmas in igneous rock formation.

Table 7.3: Mineralogy of coal gasification ash, clinker and heated rock samples by XRD and Siroquant (wt %)

Mineral	**Bulk coal gasification ash**	**Clinker 1**	**Clinker 2**	**Clinker 3**	**Clinker 4**	**Clinker 5**	**Clinker 6**
Quartz	10.7	3.9	0.2	3.7	10.6	5.5	14.6
Anorthite	13.1	27.0	51.6	19.5	10.4	38.8	2.3
Mullite	17.7	5.7	9.5	13.9	22.1	10.7	29.7
Cristobalite	1.8		1.7	5.5	10.2	4.2	
Diopside	0.7	12.1		1.9	0.9		
Illite							
Anatase							
Rutile							
Calcite							
Dolomite							
Pyrrhotite							
Amorphous*	56.0	51.3	37.0	55.7	45.8	40.8	53.4

Mineral	**Clinker 7**	**Clinker 8**	**Heated stone 1**	**Heated stone 2**	**Heated stone 3**	**Heated stone 4**
Quartz	12.9	1.5	61.8	50.8	21.3	24.9
Anorthite	8.4	62.3	3.2	2.3		
Mullite	17.0	5.8	14.8	7.7	19.7	
Cristobalite		1.0				
Diopside		12.1				
Illite					7.9	
Anatase	0.1				0.6	1.1
Rutile						0.8
Calcite						
Dolomite						0.3
Pyrrhotite					6.4	
Amorphous*	61.6	17.3	20.1	39.2	44.2	73.0

Note: * Includes both non-crystalline glass and any unburnt carbon (char) components

7.2.1 Interpretation of glass composition from XRD and chemical data

Tables 7.4 and 7.5 provide data on the inferred chemical composition of the crystalline minerals and the glass phases in the ash, clinker and heated rock (stone) samples, estimated from the XRD and whole-sample chemical data (Tables 4.11 and 7.2), following the

methodology described by Ward and French (2006). As might be expected from the nature of the materials, a wide range of compositions is implied by these results, especially for the glassy phases. For some samples, such as clinker 1 and heated stone 2, the crystalline and glassy components appear to have similar overall compositions, at least with respect to the major oxides (SiO_2, Al_2O_3 and CaO). For most others, however, such as the bulk gasification ash, heated stone 1 and clinkers 2-6, the glass fraction appears to have a higher proportion of SiO_2 and a lesser proportion of Al_2O_3. The partitioning of CaO within this group varies, although most samples appear to have similar to higher proportions of CaO in the crystalline phases compared to the glassy components. MgO is mostly present in the glass phase only.

Negative percentage values are noted in some instances. These may reflect over-estimation of the abundance of particular crystalline phases (e.g. anorthite), or possibly under-estimation of glass content, by the XRD technique.

As pointed out by Ward and French (2006), the material identified as glass by the XRD technique is not necessarily of uniform composition within the individual ash samples. It may also include particles of crystalline components that are too low in abundance or too small in particle size to be identified separately by X-ray diffraction methods. Some of the crystalline phases, such as mullite, may also have different chemical compositions to the stoichiometric data used in interpreting the XRD results. Although the electron microprobe study has identified some discrete solid particles made up mainly of Fe and Ti (see below), these make up only a small proportion of the relevant ash or slag samples. None of the crystalline phases identified in the samples by XRD techniques would normally be expected to contain iron, titanium, magnesium or sodium; these elements are therefore interpreted from the XRD and bulk chemical data to occur only in the glassy phases of the samples studied.

Table 7.4: Inferred composition (wt%) of mineral and glass fractions for gasification ash and clinker samples

Sample	**Bulk gasification ash**		**Clinker 1**		**Clinker 2**	
	Minerals	**Glass**	**Minerals**	**Glass**	**Minerals**	**Glass**
Fraction	*44.6*	*55.4*	*48.7*	*51.3*	*63*	*37*
SiO_2	53.43	53.98	49.66	40.25	43.55	62.89
TiO_2	0.67	2.13		2.66		4.08
Al_2O_3	38.87	16.62	28.14	24.44	39.99	10.43
Fe_2O_3		7.97		9.36		9.17
MgO		4.59	4.62	5.46		8.61
CaO	6.5	10.01	17.58	12.73	16.46	-1.92
Na_2O		1.49		1.3		1.91
K_2O		1.73		1.43		2.03
P_2O_5		1.41		1.91		2.5
SO_3	0.53	0.07		0.47		0.29
Total	100	100	100	100	100	100

Sample	**Clinker 3**		**Clinker 4**		**Clinker 5**	
	Minerals	**Glass**	**Minerals**	**Glass**	**Minerals**	**Glass**
Fraction	*44.5*	*55.5*	*54.2*	*45.8*	*59.2*	*40.8*
SiO_2	51.26	54.62	59.3	69.19	50.52	56.22
TiO_2		3.98		3.96		3.84
Al_2O_3	38.03	19.1	36.11	10.82	36.31	9.58
Fe_2O_3		10.98		2.65		12.95
MgO	0.79	3.3	0.31	3.78		8.22
CaO	9.91	3.22	4.29	6.23	13.17	2.66
Na_2O		0.94		1.03		1.47
K_2O		1.94		1.24		1.81
P_2O_5		1.86		0.89		1.47
SO_3		0.06		0.21		1.78
Total	100	100	100	100	100	100

Sample	**Clinker 6**		**Clinker 7**		**Clinker 8**	
	Minerals	**Glass**	**Minerals**	**Glass**	**Minerals**	**Glass**
Fraction	*46.6*	*53.4*	*38.4*	*61.6*	*82.7*	*17.3*
SiO_2	51.49	75.47	55.77	59.91	46.49	39.14
TiO_2		1.32	0.26	1.85		9.14
Al_2O_3	47.52	15.38	39.57	19.73	31.85	15.33
Fe_2O_3		2.37		4.86		23.6
MgO		1.28		3.18	2.72	11.86
CaO	0.99	0.85	4.4	6.16	18.93	-14.26
Na_2O		0.67		1.22		4.42
K_2O		2.47		2.21		4.11
P_2O_5		0.18		0.79		6.41
SO_3				0.09		0.24
Total	100	100	100	100	100	100

Table 7.5: Inferred composition (wt%)of mineral and glass fractions for heated stone samples

Sample	Heated stone 1		Heated stone 2		Heated stone 3		Heated stone 4	
	Minerals	Glass	Minerals	Glass	Minerals	Glass	Minerals	Glass
Fraction	*79.8*	*20.2*	*60.8*	*39.2*	*55.8*	*44.2*	*27*	*73*
SiO_2	84.45	71.16	88.8	72.34	55.2	60.3	92.2	55
TiO_2		6.53		2.89	1.1	1	6.7	0
Al_2O_3	14.74	-6.19	10.44	11.9	30.5	24.2		40.1
Fe_2O_3		8.05		3.6	5.3	16.5		1.7
MgO		1.68		0.79		1.1	0.2	0.5
CaO	0.81	3.82	0.76	0.47		1.1	0.3	0.5
Na_2O		2.11		0.84		0.7		0.5
K_2O		11.53		6.41	1.3	2.6		1.4
P_2O_5		0.33		0.17		0.2		0.3
H_2O					0.7	-0.8		
CO_2							0.5	-0.2
S					6	-7.6		
SO_3		0.98		0.6		0.7		0.3
Total	100	100	100	100	100	100	100	100

7.2.2 XRD analysis of the homogenised selected dig-out samples

From Appendix D, Table D1 it is clear that kaolinite, illite and dolomite decreases from sample 1D (top of the gasifier) to sample 11D. This implies that as the temperature of the gasifier increases, minerals in the coal transform to form high temperature transformation products. The presence of mullite, cristobalite, anorthite and diopside ($CaMgSi_2O_6$) in some of the ash samples indicate that these minerals were derived from the mineral transformation at elevated temperatures and pressures during gasification, since these minerals were not present in the feed coal to generate the ash.

XRD analysis also indicates that the proportion of mullite increases from samples 6D-11D. Kaolinite transforms at elevated temperatures of greater than 800°C to form reactive aluminosilicate (metakaolinite) and amorphous quartz (Grim, 1962; Bryers, 1986; Unsworth et al., 1987b; Ward and French, 2004; van Alphen, 2005). As the temperatures of the ash particles increase further to greater than 1000°C, some metakaolinite and amorphous quartz particles further transform to form mullite and cristobalite respectively. Some other amorphous quartz particles react with high temperature transformation products (CaO and MgO) of carbonates (dolomite and calcite) to form diopside. Some reactive metakaolinite can react with either CaO or MgO to form a melt.

On cooling the ash with steam injection at the bottom of the gasifier, anorthite and to a lesser extent mullite begins to crystallise out from the melt (Matjie et al., 2006). The presence of anorthite and mullite in the dig-out samples 6D-11D indicates the interaction of kaolinite and dolomite at high temperatures resulting in a melt formation and anorthite and mullite subsequently being crystallised out from the melt.

As indicated previously, quartz grains which might otherwise react to form feldspar or glass, can also persist as essentially unreacted particles throughout the different stages of the gasification process (Matjie et al., 2008). The XRD results for all of the dig-out samples (showing a significant proportion of quartz) confirmed the previous results.

7.2.3 XRD analysis of the homogenised turn-out samples

The XRD analysis of the turn-out samples taken from the gasifier is summarised in Appendix C, Tables C1and C2. The concentrations of minerals and non-crystalline phases in these samples added up to 100%. The data for these samples indicate the following trends:

- Sample 32T, which is the feedstock for the gasification process, contains mainly kaolinite (6,7%), quartz (6.0%) and dolomite (2%) with minor proportions of muscovite (1.1%), calcite (1.2%), aroganite (1.2%), pyrite (0.4%), rutile (0.3%), greigite (0.2%), gorceixite ($BaAl_3(PO_4)PO_3OH)(OH)_6$) (0.2%). Such mineral assemblage is consistent with similar results for the LTA of the same feed coal presented in Tables 4.11 and 7.3.
- As expected, the total non-crystalline content (80%) of carbon in sample 32 was found to be the highest when compared to the carbon content of other turn-out samples that were exposed to elevated temperatures.
- Dolomite was found to be present in samples 24T and 32T that were taken from the top of the gasifier. In samples from lower in the gasifier, the dolomite had completely transformed to form either magnesium oxide or calcium oxide. These oxides preferentially react with the transformed product of kaolinite to form a melt. Some CaO and MgO reacted with reactive silica from the transformation of kaolinite to form diopside ($CaMgSi_2O_6$). The absence of dolomite and aragonite and a low proportion of kaolinite in sample 16T (heated to 1000°C), could imply that magnesium and calcium

from the transformed dolomite initially reacts with the transformed kaolinite (metakaolinite) to form a melt under reducing and oxidising conditions during coal gasification.

- Calcite persisted at elevated temperatures and is still contained in sample 8T, which was taken from the bottom of the ash-bed in the gasifier. According to Bryers (1986), Ward (1984) and Raask (1984), CaO from calcite reacted with reactive aluminium silicates such as metakaolin at high temperatures (1000-1200°C) to form anorthite ($CaAl_2Si_2O_8$), which in turn fused at about 1400-1500°C. This could imply that some calcite transformed at elevated temperature of greater than 1000°C to form CaO, which preferentially reacted with reactive alumino-silicate to form anorthite under oxidising conditions. The presence of anhydrite, which is a product of calcium oxide and sulphur dioxide, was found to in samples 1T, 8T and 16T.
- According to XRD analysis of the turn-out samples, pyrite transformed to pyrrhotite, magnetite and hematite and contributed minimally to the sintering or slagging mineral matter during coal gasification.
- Kaolinite was found to be present in samples 32T, 24T and 16T and started to transform at elevated temperatures (sample 16T) and completely transformed to a reactive alumino-silicate (metakaolinite) in samples 1T and 8T.
- Interestingly the concentration of quartz in the turn-out samples does not vary significantly. These results confirm that quartz can persist as unreacted particles throughout the different stages of the gasification process.

7.2.4 QEMSCAN images of the clinker samples

QEMSCAN images of the clinker samples taken from the turn-out samples are illustrated in Appendix Figure C1. The pink and green areas that are shown in these images are unreacted quartz and dehydrated kaolinite present in the crystalline phase (anorthite) and glass matrix.

The bottom image of the clinker sample 8T clearly shows heated laminated siltstone/mudstone fragments on the left with pink quartz and green /blue clay (Figure C1). From the top right of the bottom image, the fragment of feldspathic sandstone set in a feldspar rich matrix. The glass to centre left (red) of the bottom image is of a different chemical composition.

These QEMSCAN results revealed that the heated siltstone/mudstone and sandstone rock fragments physically attached to the feldspar-rich matrix, without reacting with the melt during coal gasification. The CCSEM results given in Figures 7.3 and 7.4 are in good agreement with the QEMSCAN results.

7.2.5 CCSEM of coarse ash and clinker mineralogy

Macroscopically, the coarse ash mainly consists of rock fragments ("stone") in a black matrix (Figure 7.3). The black matrix has distinct elongated crystalline laths (dark grey) in the Ca/CaMg/Fe-bearing aluminosilicate glass (light grey) matrix (Figure 7.4). Based on the elemental proportions, these crystalline laths are anorthite ($CaAl_2Si_2O_8$) and the glass is principally the Ca/CaMg/Fe-bearing aluminosilicate glass with varying proportions of Ca, K, Ti, Fe, P and Mg. The anorthite crystals are presumed to have crystallised from the melt during cooling.

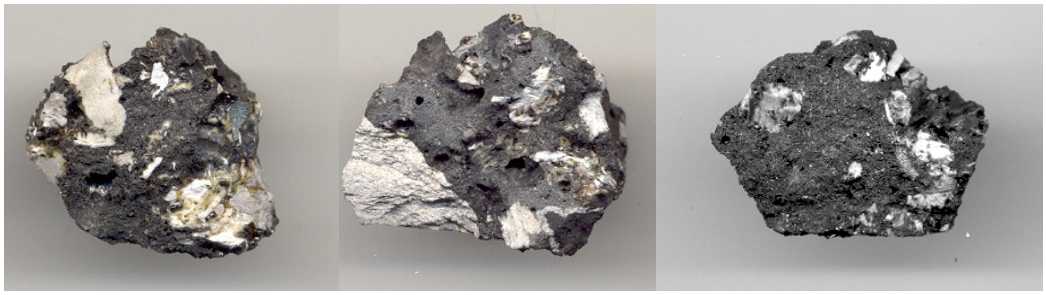


Figure 7.3: Hand-picked clinker fragments: "Stone" fragments (light colour) in black "glass" matrix.

The quartz (Q) grains in the quartz-kaolinite-muscovite-microcline siltstone fragment (Figure 7.4) have defined grain boundaries. The "honeycomb" structures (Ka) were originally kaolinite, which dehydrated (leaving the observed cavities). The light grey interstitial phase is K-bearing aluminosilicate derived from muscovite/illite. Rising steam and the cessation of carbon gasification lowers the temperature and initiates crystallisation of anorthite and to a lesser extent mullite from the melt. As the ash-bed subsides towards the rotating grate, the temperature decreases further and the residual molten material solidifies into a Ca- and Fe-bearing aluminosilicate glass. The interstitial glass is a Ca- and Fe-bearing aluminosilicate with varying proportions of K, Ti, P and Mg.

Simplistically, the Ca/CaMg/Fe-bearing aluminosilicate glass can be classified into four broad types, depending on the proportion of Ca/Mg and Fe. These are:

- Ca-aluminosilicate glass - Ca/Mg content is variable, with trace concentrations of Fe; K and Ti can occur.
- Ca-Fe-aluminosilicate glass - Ca/Mg and Fe content are variable; trace concentrations of K and Ti can occur.
- Fe-aluminosilicate glass - Fe content is variable; trace concentrations of Ca, K, Mg and Ti can occur.
- Silica-rich glass with minor and varying concentrations of Al, Ca, K, Mg, Fe and Ti.

The proportion of Ca/CaMg/Fe-bearing aluminosilicate glass relative to anorthite is extremely variable. On a microscopic scale, anorthite tends to occur in isolated clusters separated by the Ca/CaMg/Fe-bearing aluminosilicate glass devoid of anorthite laths and rock fragments. In addition to anorthite, mullite ($Al_6Si_2O_{13}$) needles in the glass were also identified. These mullite needles are extremely fine and are not common (Figure 7.4).

Minor coarse Fe-oxide/Fe-S-oxide rich, Ca-oxide/CaMg-oxide-rich and carbon-rich particles were identified in the pulverised bulk gasification ash. The Fe-oxide/Fe-S-oxide rich particles and Ca-oxide/CaMg-oxide either occur as extraneous particles or are attached to Ca/CaMg/Fe-bearing aluminosilicate glass.

The Fe-oxide/Fe-S-oxide particles comprise pyrrhotite, Fe-S-oxide and Fe-oxide and represent the transformed products of pyrite (Srinivasachar et al., 1990a; 1990b; Matjie et al., 2006; Bryers, 1986). This mineral originally occurred as coarse pyrite-rich cleat fillings in the coal (Figure 4.3). As the CCSEM cannot distinguish between hematite (Fe_2O_3), magnetite (Fe_3O_4) and wustite (FeO), these phases are grouped as “Fe-oxide”.

The Ca-oxide and CaMg-oxide rich particles are grouped as “Ca-Oxide/CaMg-oxide”. It is concluded that these Ca-oxide/CaMg-oxide particles are transformed coarse calcite/dolomite cleat fillings originally present in the coal (Deer et al., 1992; van Alphen, 2005; Briggs, 1986; Bryers, 1986).

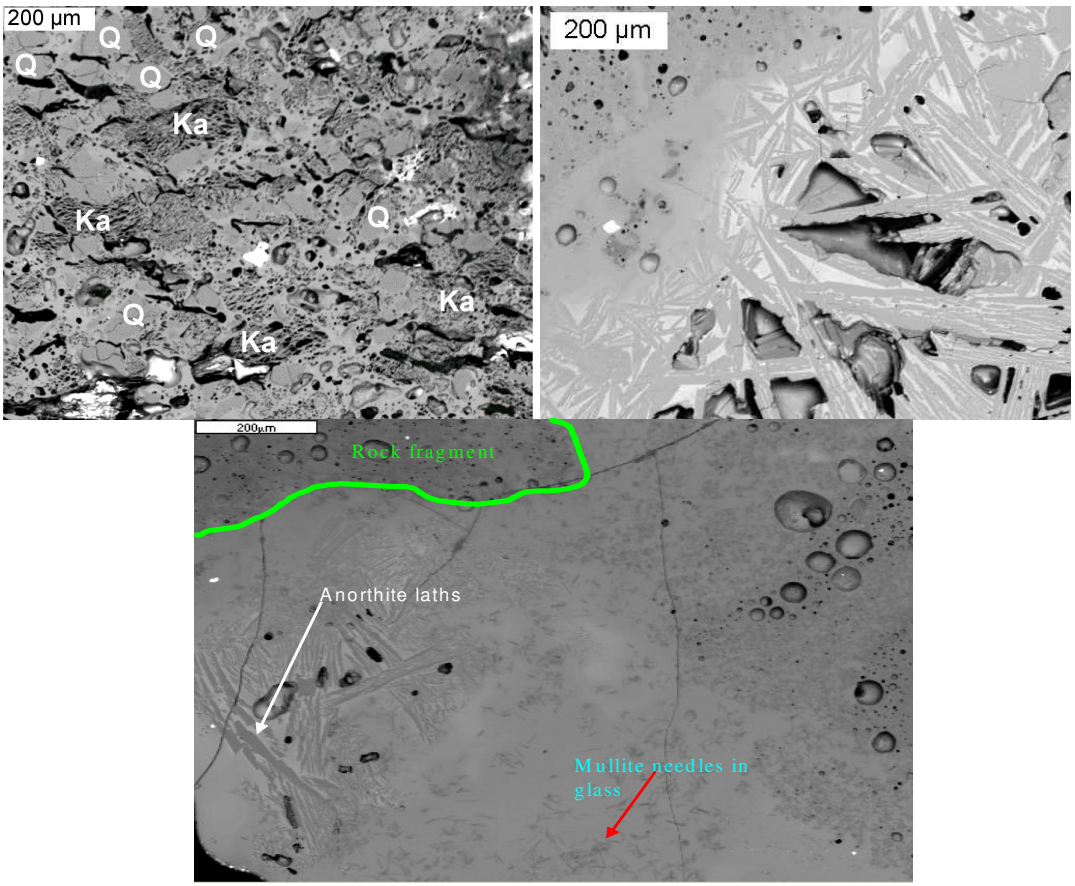


Figure 7.4: Detail of rock fragment (left image) and grey elongated anorthite crystals and Ca- and Fe-bearing glass matrix (light grey). The bottom image shows crystallisation of anorthite and mullite from a melt and physical contact between rock fragment and the melt.

7.2.6 Phase proportions in coarse ash and clinker fragments

The mass percentages of phases in the coarse ash and clinker sample (as measured by CCSEM) are summarised in Appendix B, Table B1. XRD results of the coarse ash and clinkers indicated that the major crystalline phases are: anorthite (27.7%), quartz (37.7%) and mullite (26.6%) in the coarse ash; and anorthite (52%), mullite (23.8%) and quartz (22.3%) in the clinker sample. Minor albite (6.8%), augite (2.5%), hematite (2%) and magnetite (0.3%) are present in the coarse ash; and augite (2%) and hematite (0.2%) in the clinker. Glass phases were not analysed by XRD. The XRF analysis of ash samples (coarse ash and clinker) indicated that these samples contain 52.2% SiO_2, 24.0% Al_2O_3, 5.3% Fe_2O_3, 1.3% TiO_2, 0.6% P_2O_5, 7.2% CaO, 2.2% MgO, 0.4% Na_2O, 1.0%K_2O and 0.5% S (normalised XRF results).

7.2.7 CCSEM analysis of hand-picked coal and clinker particles

Simplistically, the coal feedstock consists of organic-rich coal particles with varying proportions of included minerals, mineral rich rock fragments or "stone" derived from floor, hanging wall and in-seam partings and coarse pyrite-rich and calcite-rich cleat fragments.

CCSEM and XRD analyses (Table 4.3, Table 4.5, Table 4.12 and Figure 4.3) of the coal feedstock to the gasification process indicate that this coal contains major minerals (kaolinite, quartz and dolomite) and minor minerals (pyrite, calcite, muscovite/illite, apatite, microcline and rutile). The grains of kaolinite and quartz occur in organic-rich coal particles and significant proportions of these minerals occur in siltstone, mudstone and sandstone rock fragments (Figure 4.3). In most cases calcite and pyrite mainly occur in cleats in organic-rich coal particles (Figure 4.3). Dolomite is associated with calcite-rich cleats. The K-bearing microcline and muscovite/illite are mainly associated with kaolinite and quartz in the siltstone and mudstone rock fragments (Figure 4.3).

Macroscopically, the coarse ash and clinkers consist of rock fragments ("stone") in a matrix of "glass" (Figure 7.4). The included fluxing elements-bearing minerals such as pyrite, dolomite and calcite react with the included kaolinite to form a melt. On cooling a melt with steam during the coal gasification process, the crystalline phases such as anorthite and to a lesser extent mullite, crystallised out from the melt and amorphous phase (glass) is formed. Some heated rock fragments from the surroundings attach to the melt to form heterogeneous clinkers. The chemical and mineralogical composition of the heated rock fragments in a clinker sample is controlled by the interaction of mineral matter present in the original coal sample.

It was visually observed that the hand-picked clinkers analysed in this study have distinct vesicles or voids with a reddish brown surface. It is proposed that these vesicles are the frozen remnants of steam or air bubbles that passed through the molten clinker. On cooling of the clinkers, the partially oxidised iron or ferrous in the glass further reacted with steam or air to form ferric hydroxides. This produced the "rust" surface colour of the bubbles.

It is clear from Figure 7.5 that randomly-orientated elongated anorthite laths crystallised out from the melt during cooling. The Ca-, Fe-, Mg-bearing aluminosilicate glass with varying

chemical composition was formed. The proportion of glass to anorthite can vary significantly and is localised. Although, not as common as anorthite, thin mullite needles and spinel are present (Figure 7.5). The formation of anorthite through crystallisation implies that dolomite and calcite reacted with aluminium silicate (kaolinite) at elevated temperatures to form a melt. On cooling anorthite crystallised out from the melt. The presence of anorthite and mullite crystals in these clinkers was confirmed by the electron microprobe and CCSEM analyses (Figure 7.5, Figure 7.4 and Figure 7.17). Anorthite laths and Fe- and Mg-bearing aluminosilicates were identified in sample 1T, sample 8T and sample 16T. These samples are below the gasification zone and have been exposed to temperatures exceeding 1000°C.

Fine mullite and corundum needles in glass were identified in sample 1T only (Figure 7.5). These mullite crystals can occur with anorthite (Figure 7.5) or as the only crystalline phase in the glass. Unlike anorthite, the proportion of mullite relative to glass is comparatively low and the mullite needles are smaller than anorthite. The mullite rich areas were in close proximity to remnant rock fragments. The mullite needles in sample 8T (identified by CCSEM) are derived from the reaction of kaolinite and pyrite or dolomite at elevated temperatures. A high ratio of alumina to silica in the melt could enhance the formation of a significant amount of mullite crystals.

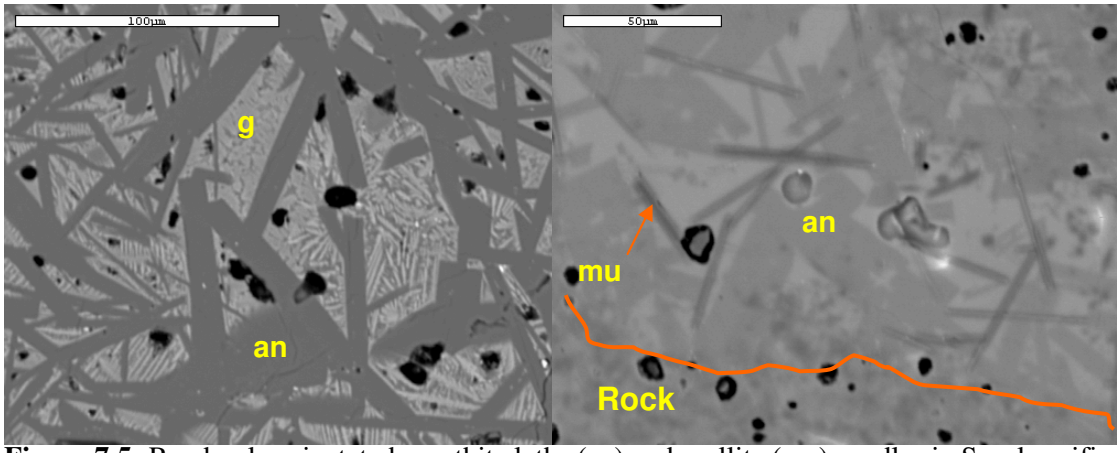
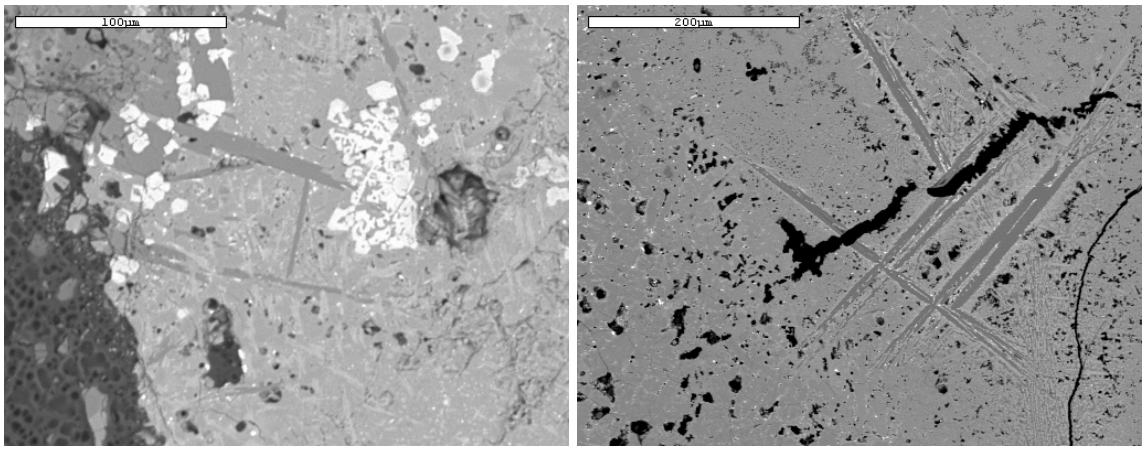


Figure 7.5: Randomly orientated anorthite laths (an) and mullite (mu) needles in Sasol gasification ash. Image on left is from sample 8T and on the right sample 1T. Glass is light grey (g). Note the glass in sample 8T is differentiated into two phases, whereas sample 1T interstitial glass is uniform. Scale bars represent 100µm and 50µm, respectively.

The interstitial glass is enriched in Fe (some iron particles are derived from kaolinite/pyrite association, siderite and ankerite) and to a lesser extent Mg relative to the average field composition. This trend is expected as Fe and Mg cannot be accommodated into the anorthite structure. On further cooling, the Fe and Mg in the interstitial glass reacts with aluminosilicate or oxygen to form the following iron species, Fe-rich Mg-aluminosilicate (pyroxene or amphibole), Fe-rich hercynite ($FeAl_2O_4$) and finally wustite. The Mg reacts with aluminosilicate and alumina to form MgFe-aluminosilicate and Mg-rich spinel ($MgAl_2O_4$) respectively (Figure 7.6). The excess Al will partition into mullite, Mg-rich spinel and corundum (Al_2O_3). The Fe-Mg silicate minerals in the analysed clinkers may have been derived from reactions between fluxing elements-bearing minerals (pyrite, calcite and dolomite) and kaolinite or illite at elevated temperatures during coal gasification. During the transformation of pyrite, which is associated with organic-rich particles in the coal, iron can be formed. The iron may react with inorganic elements or substances to form a spinel such as magnesioferrite ($MgFe_2O_4$), which dissolves in the melt formed from the decomposition products of kaolinite, calcite and pyrite at 750-760°C to form Fe-Mg silicate glass (Briggs, 1986). The increase in Fe and partitioning of the interstitial glass into different Fe-bearing phases is illustrated in Figure 7.6.



igure 7.6: Left hand image (sample 1T) consists of prominent dark anorthite laths and white hercynite in two toned glass. The right hand image is from sample 1S. The glass is differentiated into grey and light grey phases and very small iron-oxide phases (white).

7.2.8 CCSEM analysis of the hand-picked heated rock fragments

The feed coal contains rock fragments such as siltstone, mudstone, carbonaceous shale and sandstone. It is imperative to determine the role of these stones during coal gasification.

The CCSEM and XRD analyses (Table 4.12 and Table 4.11) of these common rock fragments in the coal feedstock indicate that these stones contain major minerals (kaolinite, quartz, muscovite/illite and microcline) and minor minerals (dolomite, pyrite, calcite, zircon, apatite, rutile and monazite). In most cases, the minor minerals in the coal are associated with these rock fragments taken from the turn-out samples 1T, 8T, 16T and 24T (Figure 7.7). The proportion of kaolinite, quartz, muscovite/illite and microcline in the rock fragments vary significantly.

During the thermal treatment of rock fragments, clays (kaolinite, muscovite/illite) started to lose water of hydration at elevated temperatures ranging from 450-1000°C to form reactive aluminium silicates. It is apparent from images of the heated rock fragments that the "kaolinite" in the heated rock fragment particles hand-picked from sample 1T (which has passed through the gasification temperature zones and exited the gasifier) (Figure 7.7) has distinct desiccation cracks attributed to the dehydration (ash sample 1T, Figure 7.7 and Figure 7.8). Some quartz particles in the heated rock fragments show sign of cracks, but still maintain the physical and chemical properties of quartz in the original coal. Interestingly, the elongated muscovite/illite and angular microcline transformed to form a molten K-bearing glass with Al/Si ratios similar to coal muscovite/illite and microcline (Figure 7.8).

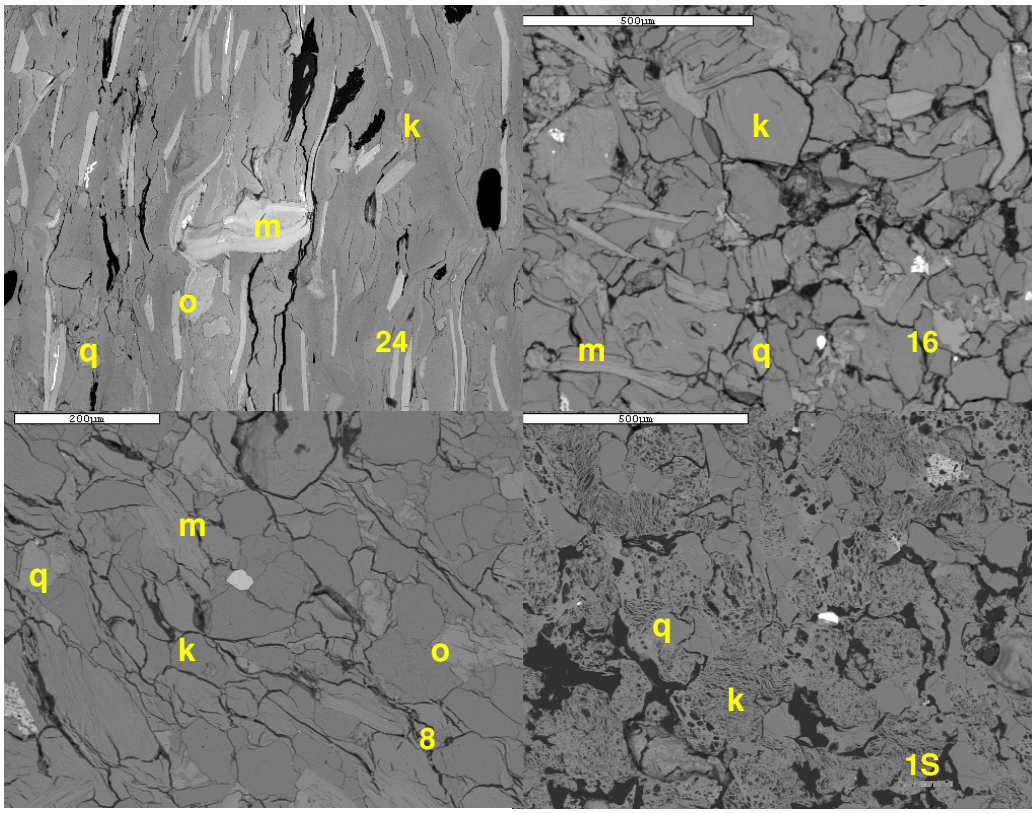


Figure 7.7. Different rock fragments with varying proportions of kaolinite (k), quartz (q), muscovite/illite (m) and microcline (m). Sample numbers (1T (Siltstone), 8T, 16T and 24T) are shown. Scale bar is 200µm.

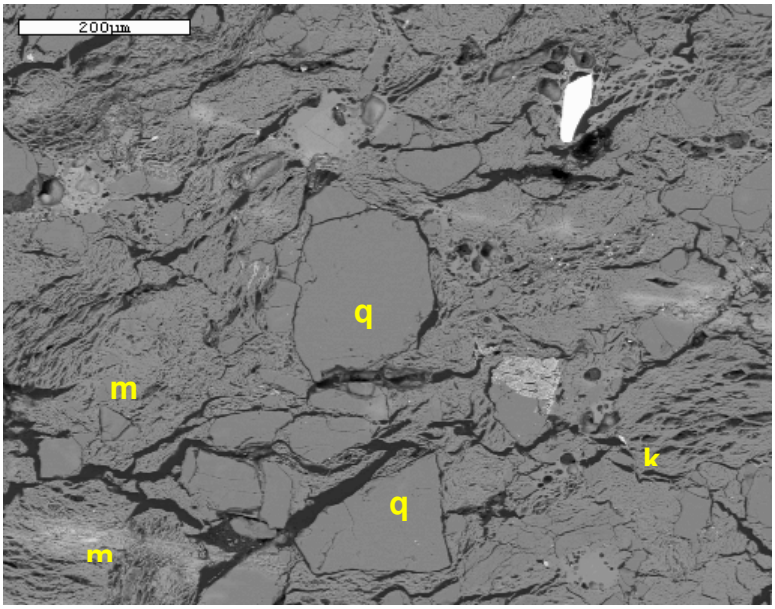


Figure 7.8: Detailed view of rock fragment in sample 1T. Note the dehydrated "kaolinite" (k), angular quartz (q), and molten muscovite/illite (m). Scale bar is 200µm.

It is suggested that significant proportions of mineral matter (non-mineral inorganic elements and minerals) in rock fragments transformed at elevated temperatures in-situ and attached

themselves to the melt to form heterogenous clinkers without chemically participating in the formation of a melt. However, there are some reactive aluminium silicate (metakaolinite) particles and fluxing element-bearing mineral (pyrite) particles in the heated rock fragments that can possibly react with glass to enhance the formation of mullite. There are examples of rock fragments reacting with the glass and perhaps influencing the formation of mullite (Figure 7.9).

CCSEM analysis shows that, on average, particles of the heated rock fragments taken from the coarse ash produced from the gasification process are significantly finer than particles of rock fragments hand-picked from the feed coal. The fragmentation of rock fragments into smaller particles can possibly be attributed to the decomposition of minor carbonate and sulphide minerals, as well as the dehydration of clays in the rock fragment during coal gasification.

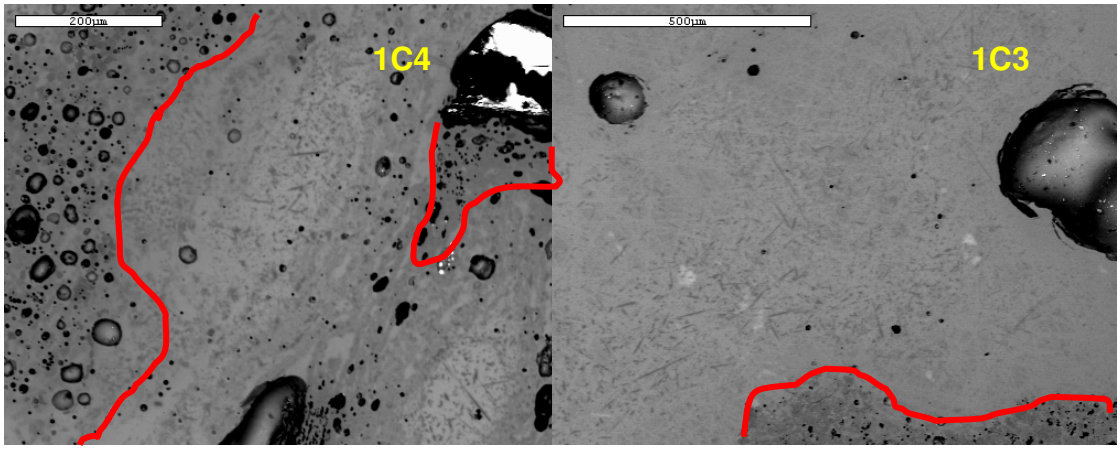


Figure 7.9. Fine dark mullite needles in light grey glass matrix. Not the high proportion of remnant rock fragments associated with mullite.

7.2.9 Transformation of carbonate and pyrite at high temperatures

Heated rock fragment particles that were hand-picked from sample 24T, taken from the turn-out experiment, contain a single large (>10mm) calcite-rich cleat fragment with minor transecting pyrite in filled cleats (Figure 7.10). These extraneous calcite and pyrite-rich cleats in the rock fragment particle transformed partially. The temperature of this rock fragment was below the decomposition temperatures of calcite and pyrite.

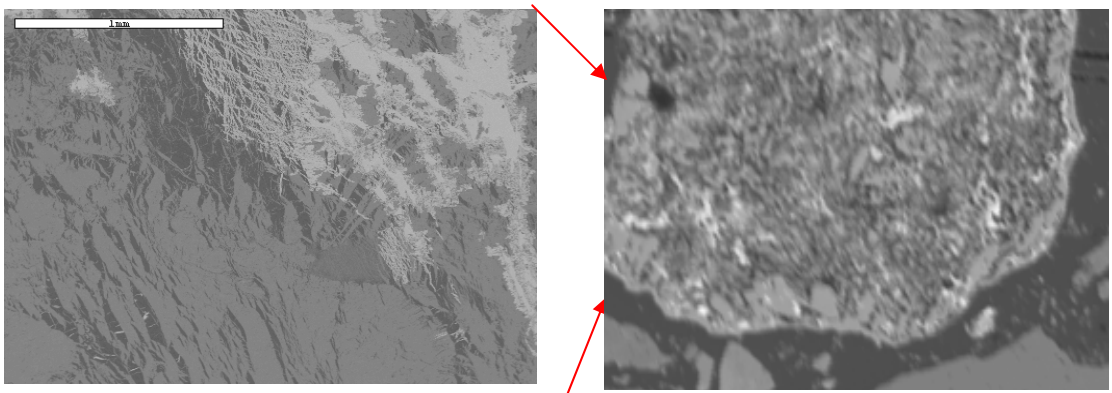


Figure 7.10: Large calcite (Ca) and pyrite rich extraneous cleat fragment. An example of partially transformed calcite/dolomite cleat fragment in the coarse ash is represented on the right hand side. Size of the scale bar is 1mm.

The heated rock fragment particle of sample 8T, shown in Figure 7.11, comprises the Fe-oxide/ Fe-S-oxide/pyrrhotite that are high temperature transformation products of the extraneous pyrite. The spherical light grey grains in the heated rock fragment particle are pyrrhotite, the grey phase is Fe-S-oxide and the dark grey is Fe-oxide. The heated rock fragment particle attached to the particle of clinker consists of anorthite crystals and glass particles. There is no evidence of reaction between the partially oxidised pyrite and dehydrated kaolinite.

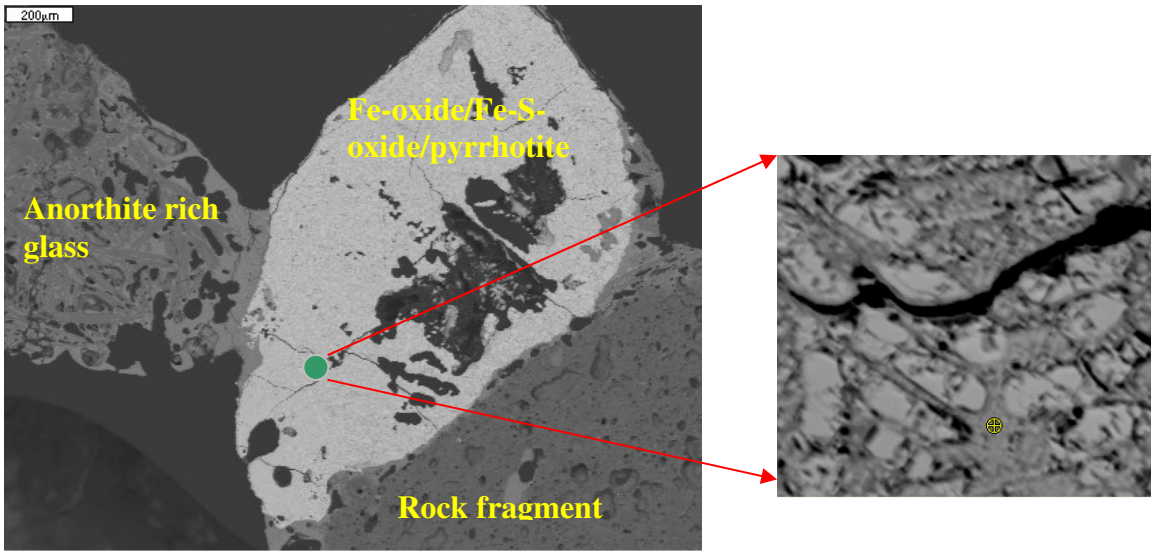


Figure 7.11: Large extraneous "Fe-oxide/Fe-S-oxide/pyrrhotite" particle attached to rock fragment and anorthite rich glass fragment in the coarse ash: scale bar is 200µm). The scale bar of Fe-oxide/ Fe-S-oxide/pyrrhotite is 20um.

In conclusion, the CCSEM results for the heated rock fragments reveal that a significant proportion of minerals in these stones transformed in-situ during gasification. Kaolinite dehydrated at elevated temperatures to form reactive aluminosilicate. Quartz cracked, forming small quartz fragments. The muscovite or illite in the rock fragment transformed at elevated temperatures to K-bearing glass with an Al/Si ratio similar to muscovite/illite or microcline present in the original feed coal. Almost all the extraneous pyrite particles in the coal transformed at elevated temperatures to form iron oxide particles during coal gasification.

7.2.10 Characterisation of the homogenised turn-out samples taken from the gasifier

Figure 7.12 and Appendix C, Table C2 show the concentrations of phases in the turn-out samples taken from the different zones of the gasifier determined by CCSEM. From the results given in Figures 7.12 and 7.13 it is clear that the proportions of phases increase from sample 24T, which was taken before the pyrolysis stage, to sample 1T, which is the gasification ash exiting the gasifier. As expected, the proportion of interstitial and matrix glass has increased from 4.2 mass-% in sample 24T to 30.3 mass-% in sample 1T (Figure 7.12).

It is interesting to note that the proportion of metakaolinite, which is the high temperature transformation product of kaolinite, as well as the proportion of CaO/MgO in the turn-out samples decrease; while glasses of kaolinite (carbonate) increase significantly during coal gasification (Figure 7.13). This supports the suggestion that carbonates (dolomite and calcite), which are associated with kaolinite in the coal, reacted with each other and kaolinite at elevated temperatures and pressures to form a melt resulting in glasses and crystalline phase formation during coal gasification. Interestingly, a low proportion of iron-bearing phases derived from the reaction between kaolinite and pyrite was formed in the turn-out samples (Figure 7.14). From these results it can be concluded that a major proportion of carbonates (dolomite, siderite and calcite) that are associated with kaolinite, lower the ash fusion temperature of kaolinite at elevated temperatures forming a melt; whereas a small proportion of pyrite particles that are associated with kaolinite also contributes to sintering or slagging of mineral matter at elevated temperatures during coal gasification.

There is a marginal decrease in the quartz content. Figures 7.7 and 7.8 show that the quartz grains in the bulk gasification ash, heated stone and clinker samples are typically irregular, broadly equidimensional particles, essentially pure and probably represent unreacted fragments inherited from the coal and non-coal (sandstone, siltstone, carbonaceous shale) components in the feedstock to the gasification process. This implies that quartz, at the existing operating temperatures of the gasification process, does not participate in the chemical reactions.

Extensive CCSEM investigations of gasifier ash have shown that muscovite and orthoclase in rock fragments alter in-situ and do not necessarily participate in glass formation (Matjie et al., 2006). This is confirmed by the consistent proportion of orthoclase and muscovite glass.

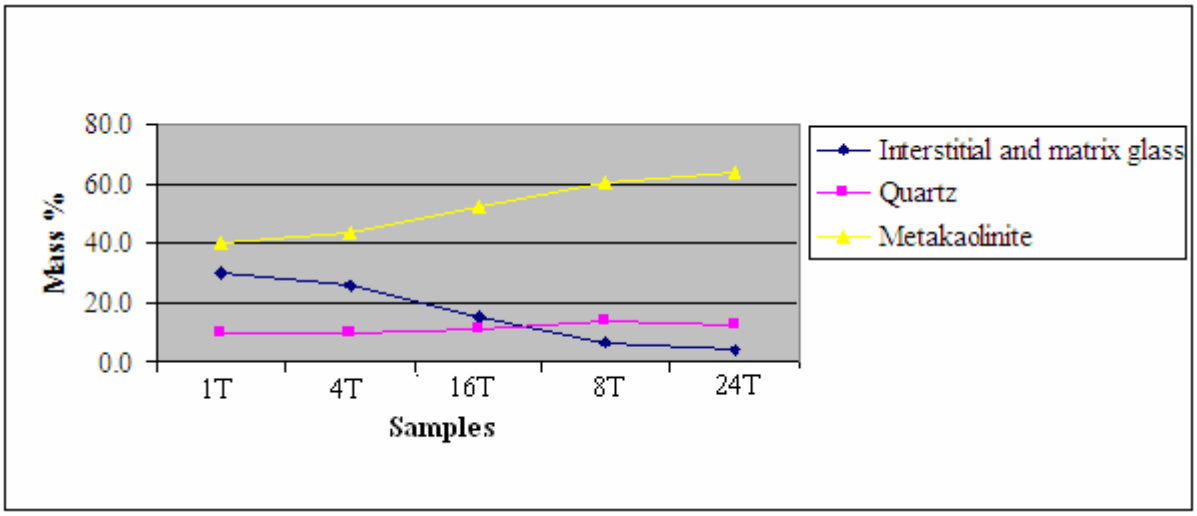


Figure 7.12: Proportions of glass, quartz and metakaolinite.

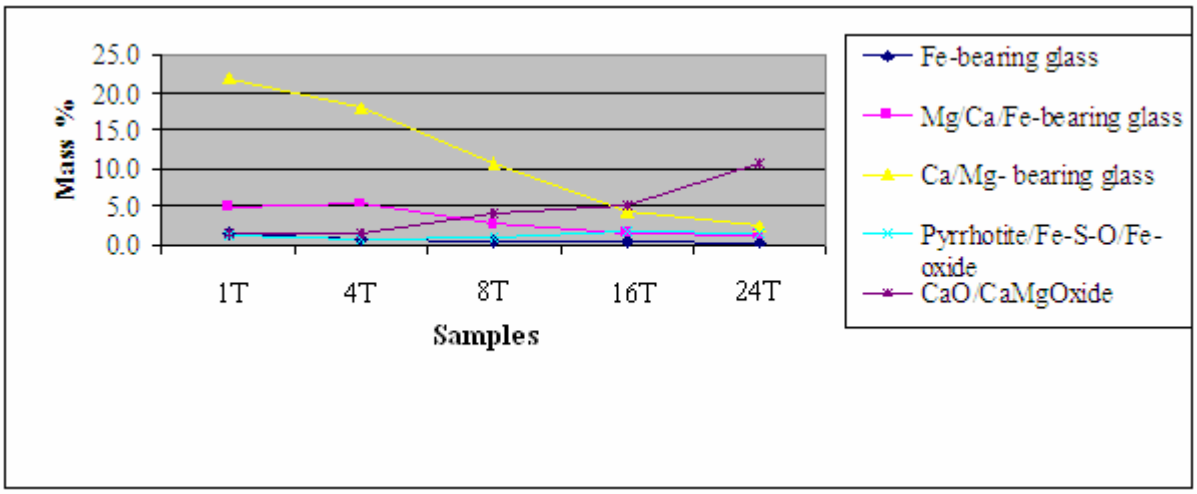


Figure 7.13: Proportions of silicates and metal oxides in the turn-out samples.

Based on the CCSEM results for the turn-out samples, it is clearly that carbonates (dolomite or ankerite, siderite and calcite) that are associated with kaolinite, lower the ash fusion temperature of kaolinite at elevated temperatures, forming a melt. Anorthite and mullite crystallised out from the melt, resulting in formation of different glasses. Interestingly, a low proportion of iron-bearing phases derived from the reaction between kaolinite and pyrite was formed in the turn-out samples. This could imply that some extraneous pyrite and pyrite particles associated with carbon matrix, contribute little to sintering or slagging of mineral matter at elevated temperatures during coal gasification. The hypothesis (the included minerals are accountable for clinker formation in the gasifier) was successfully tested in this study.

7.2.11 SEM-EDS analysis of the hand-picked clinkers and heated rock fragments from the selected dig-out samples

The back-scattered electron images (Figures 7.14 and 7.15) of the clinker particles, taken from sample 7D during the dig-out test, indicate that these ash particles (formed at elevated temperatures in the gasifier) contained two high temperature transformation phases (anorthite and mullite). This implies that high temperature transformation products of the included dolomite and calcite minerals that were associated with kaolinite reacted with the reactive high temperature transformation product (meta-kaolinite) of kaolinite at elevated temperatures to form a melt. On cooling the melt with steam, anorthite and mullite crystallise out from the melt resulting in the formation of glasses containing a different chemical composition. The electron microprobe and CCSEM results for the turn-out ash particles corroborated reports in this study.

The heated rock fragments containing some devolatilised kaolinite particles, partially transformed quartz, unaltered quartz grains and potassium feldspar being present in the gasifier attached to the cooling melt during crystallisation of anorthite and mullite to form clinkers (Figures 7.14 and 7.15). The presence of the mullite and anorthite crystals in the heated rock fragments implies that some fluxing elements-bearing minerals, including calcite and dolomite present in the stone, reacted with kaolinite at elevated temperatures to form an in-situ melt of the heated rock fragments (Figure 7.15).

Although iron as ferrous (Fe^{2+}) from pyrite reduces the ash fusion temperature of mineral matter in coal during thermal treatment, the majority of iron from the extraneous pyrite particles contributes little to the sintering and slagging of mineral matter during coal gasification. The CCSEM and SEM-EDS results (Figures 7.10, 7.11 and 7.14) for ash samples treated in this study, confirmed that some extraneous pyrite particles transformed at elevated temperatures to pyrrhotite and hematite, without reacting with the high temperature transformation products of kaolinite to form a melt. Some of the iron species may react with the available metal oxide to form spinel such as hercynite ($FeAl_2O_4$), ferrianspinel ((Fe, Mg)Al_2O_4) phases, or magnesioferrite ($MgFe_2O_4$) (Figure 7.14, Figure 7.6). Other iron particles from trace amounts of siderite, iron from ankerite and iron from the kaolinite and pyrite association in the coal can contribute significantly to the sintering and slagging of mineral matter during coal-conversion processes.

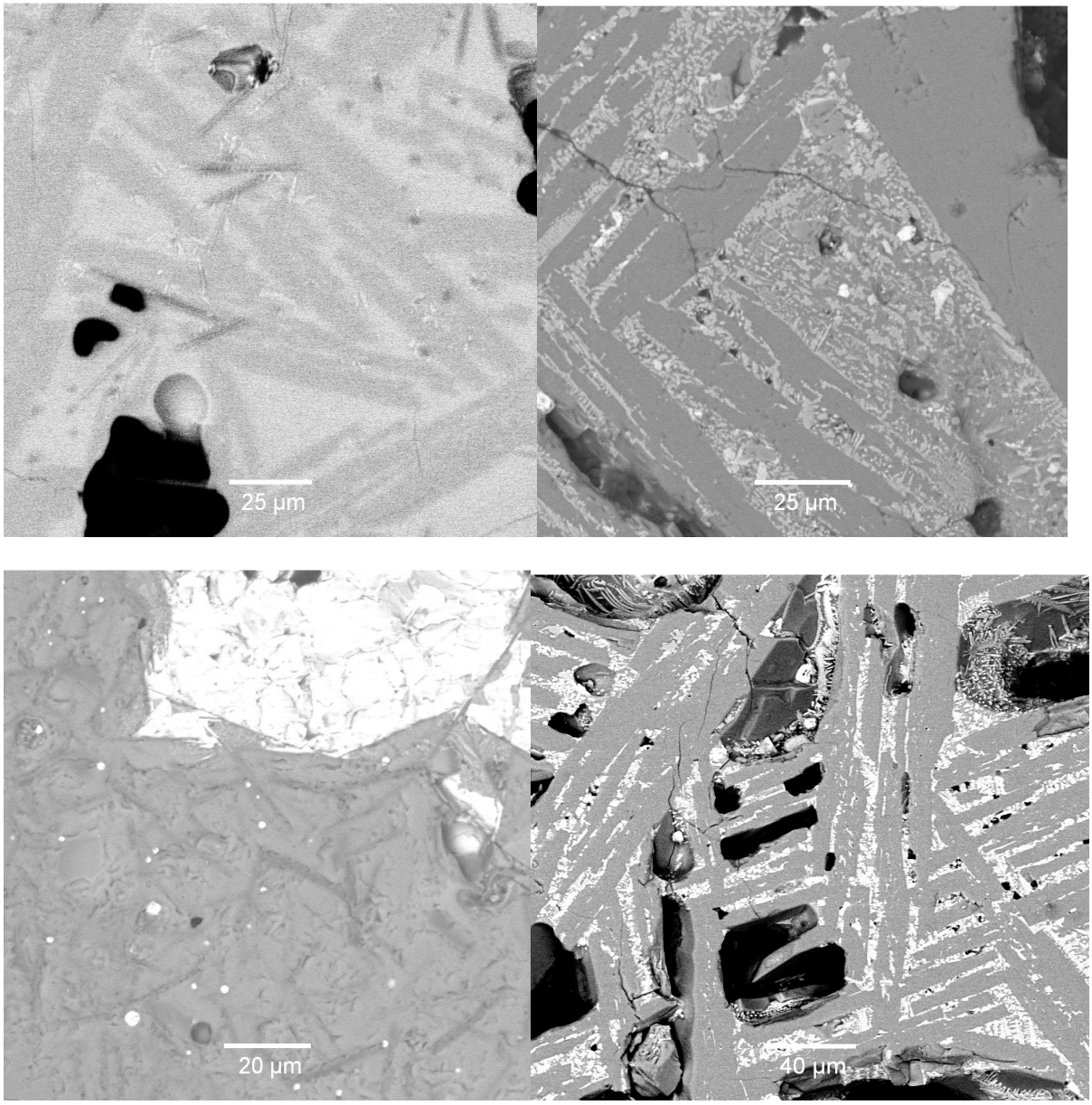


Figure 7.14: Back-scattered images of dig-out clinkers 6D and 7D: the left top image of clinker 7D: shows anorthite and mullite (dark) needles crystals and right top image shows anorthite crystals (dark grey). Scale bar for the top images is 25µm. The bottom images of clinkers 7D and 6D show mullite and anorthite crystals. The left bottom image of clinker 7D shows white dots of iron oxide. Scale bar for the left bottom image is 20µm and for the second bottom image is 40µm.

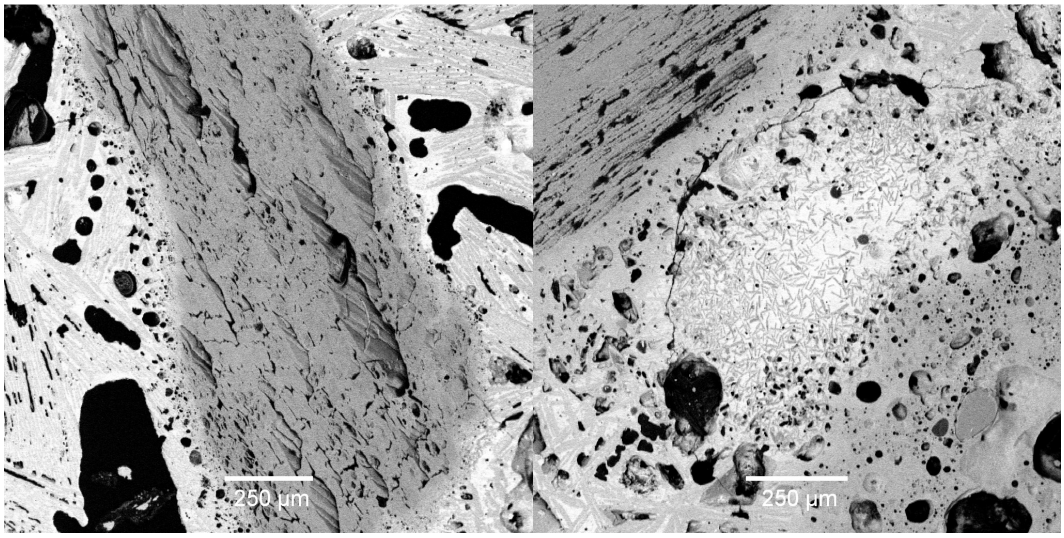


Figure 7.15: First BSE image of the heated stone 6.7D shows devolatilised kaolinite; and the second image (right) of heated stone 6.11D shows heated carbonaceous shale attached to anorthite and mullite crystals in the heated stone. Scale bar for the images is 250µm.

7.2.12 Determination of glass and mineral compositions in the gasification ash particles by electron microprobe analysis

Electron microprobe analysis was used to determine the chemical composition of the principal crystalline and glassy phases in polished sections and polished thin sections of selected lump clinker samples. Images illustrating the textures in a typical sample, showing the modes of occurrence of quartz, feldspar and glassy phases, are provided in Figure 7.16. The chemical composition of the quartz, feldspar and aluminosilicate glass for a wider range of samples, based on the microprobe study, is given in Table 7.6.

- **Quartz and feldspar crystals**

The quartz grains in the bulk gasification ash, heated stone and clinker samples are typically irregular, broadly equidimensional particles, probably representing unreacted fragments inherited from the coal and non-coal (sandstone, siltstone, carbonaceous shale) components in the feedstock to the gasification process. Figure 7.16a, for example, shows a series of silt-sized quartz grains each around 10µm in size. Table 7.6 indicates that the quartz particles are essentially pure, with usually more than 98% SiO_2. Traces of Al_2O_3, Fe_2O_3, CaO and TiO_2 are also present in some cases.

Although both potassium feldspar and anorthite (Ca feldspar) were noted in the bulk coal gasification ash sample (Table 7.6), the feldspar crystals in the other heated stone and clinker samples were found to be essentially pure anorthite. As indicated in Table 7.6, most of the feldspars analysed have chemical compositions close to that of stoichiometric anorthite, which is 44.3% SiO_2, 35.6% Al_2O_3 and 20.1% CaO. A small concentration (up to around 0.5%) of Na_2O is also indicated in some cases, occurring in solid solution. Measurable concentrations of Fe_2O_3, MgO and TiO_2 reported in some samples may represent inclusions within the feldspar crystals.

Potassium feldspar, in the form of microcline, is commonly present in the non-coal rocks associated with South African coal seams (Pinetown et al., 2006). The potassium feldspar noted in the bulk coal gasification ash (Table 7.6) may thus represent residual particles originally of detrital origin. The euhedral shape of the anorthite crystals (Figure 7.16B), however, and their textural relationship to the associated glassy matrix, suggest that most of the anorthite crystals are formed in the gasification ash from the molten state, in a manner analogous to the crystallisation of igneous rocks from magmatic materials. The textural features suggest that melting and subsequent crystallisation has taken place and that solid-state reactions resulting in feldspar formation, identified in combustion-based studies (Benson, 1987; French et al., 2001; Jung, 1996; Reifenstein, 1999), are less significant in the fixed-bed gasification process.

- **Aluminosilicate glass**

The aluminosilicate glass in the coal gasification ash and clinker samples, as determined by electron microprobe analysis (Table 7.6), varies considerably among the samples studied. Based on averages for a number of individual points, the proportion of SiO_2 in the glass ranges from around 20% to around 70% and Al_2O_3 from 15 to 35%. Although one or two samples have higher values, the proportion of Fe_2O_3 in the glass is mostly less than 10% and CaO mostly less than 5%. MgO, TiO_2 and K_2O are also significant components of the glass in a number of the samples studied.

Table 7.6: Composition of main mineral fragments and glass matrix in coal gasification ash samples (wt %), as determined by electron microprobe analysis

	Pts	SiO_2	TiO_2	Al_2O_3	Fe_2O_3	MgO	MnO	CaO	Na_2O	K_2O	P_2O_5	SO_3	Total
Quartz													
Bulk gasification ash	7	98.98	0.01	0.29	0.20	0.01	0.01	0.01	0.02	0.15	0.01	0.02	99.71
Clinker 1	2	100.43	0.02	0.04	0.01	0.00	0.01	0.00	0.00	0.00	0.02	0.01	100.53
Clinker 2	4	99.73	0.05	0.07	0.02	0.00	0.01	0.01	0.01	0.01	0.01	0.01	99.93
Clinker 7	8	98.39	0.09	0.14	0.03	0.01	0.02	0.01	0.01	0.01	0.02	0.02	98.75
Clinker 9	5	94.37	0.63	3.19	0.19	0.09	0.00	0.20	0.06	0.08	0.11	0.01	98.93
Clinker 10	3	99.20	0.02	0.04	0.04	0.00	0.01	0.02	0.00	0.01	0.04	0.01	99.38
Heated stone 3	4	100.16	0.02	0.02	0.11	0.00	0.01	0.02	0.01	0.02	0.00	0.01	100.38
Feldspar K-feldspar													
Bulk gasification ash	1	63.73	0.04	18.41	0.11	0.01	0.00	0.00	0.41	16.13	0.00	0.01	98.86
Anorthite													
Bulk gasification ash	1	42.42	0.09	33.87	0.10	0.12	0.03	20.60	0.02	0.04	0.13	0.09	97.51
Clinker 1	7	43.74	0.16	34.40	0.38	0.38	0.03	18.48	0.36	0.08	0.10	0.01	98.12
Clinker 2	7	44.22	0.11	34.41	0.37	0.25	0.01	18.20	0.54	0.13	0.07	0.02	98.32
Clinker 7	4	43.17	1.28	27.84	2.94	4.16	0.06	16.50	0.47	0.44	0.79	0.09	97.74
Clinker 8	7	44.56	0.29	32.27	1.22	0.99	0.01	17.81	0.76	0.29	0.23	0.04	98.46
Clinker 9	30	45.19	0.36	31.32	1.03	1.17	0.02	16.73	0.76	0.25	0.25	0.04	97.12
Clinker 10	7	44.37	0.14	34.13	0.40	0.25	0.02	17.85	0.49	0.14	0.09	0.02	97.91
Si-Al glass													
Bulk gasification ash	14	58.37	0.42	20.90	9.41	0.43	0.02	4.80	0.16	2.86	0.03	0.16	97.55
Clinker 1	20	44.60	2.75	14.21	4.22	13.02	0.26	13.09	0.43	1.72	1.48	0.12	95.89
Clinker 2	20	47.92	1.46	33.45	3.97	3.87	0.04	3.77	0.38	1.45	1.49	0.04	97.85
Clinker 7	20	70.18	2.94	21.01	0.82	0.47	0.02	0.47	0.28	1.30	0.04	0.02	97.55
Clinker 8	35	22.23	2.37	33.73	16.88	18.08	0.14	4.86	0.13	0.09	0.55	0.02	99.10
Clinker 9	8	58.45	2.20	21.72	1.39	2.48	0.03	4.07	0.23	0.64	0.52	0.07	91.80
Clinker 10	16	56.56	1.13	28.70	2.61	1.43	0.05	2.77	0.39	1.61	0.49	0.11	95.84
Heated stone 3	54	54.83	0.24	15.80	1.74	2.11	0.01	3.12	3.46	0.98	0.06	1.38	83.72

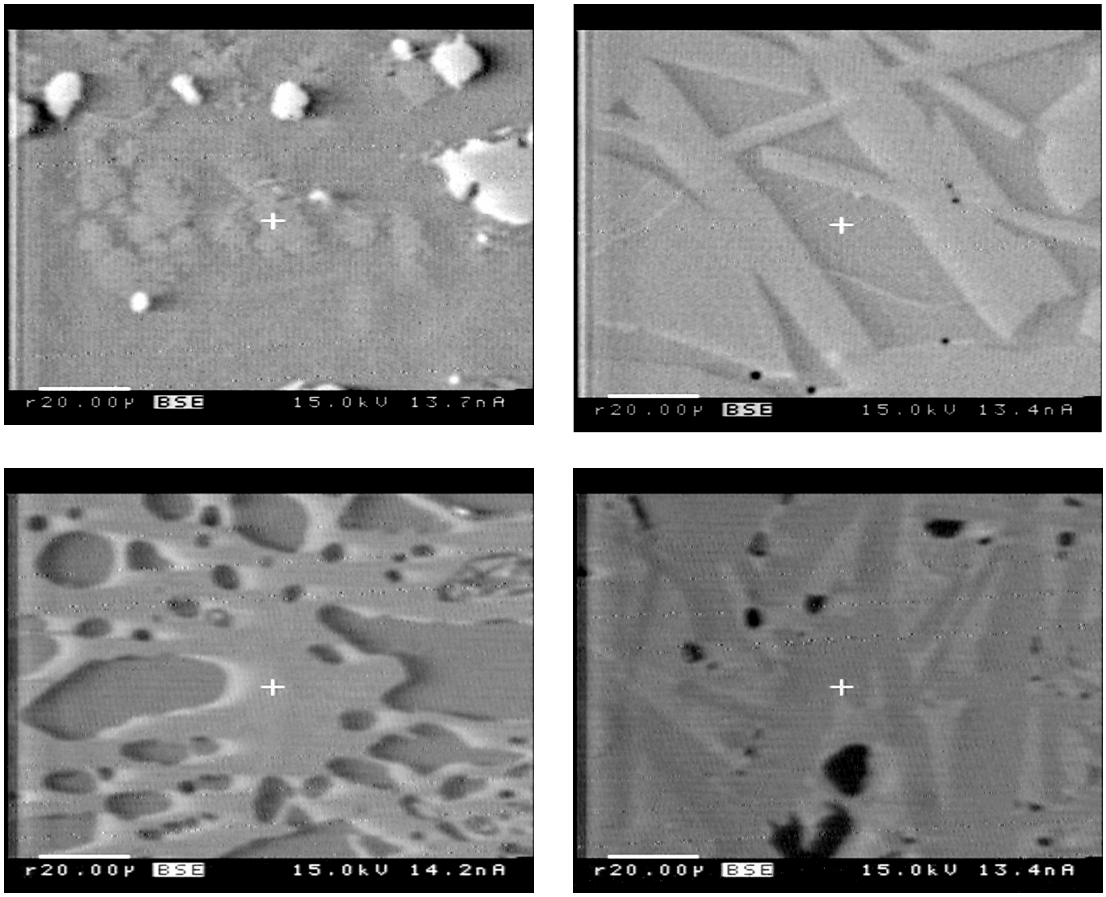


Figure 7.16: Electron microprobe images of slag samples (back-scattered electron mode) in Clinker 2. Top left: quartz particles (mid grey) set in glassy matrix; top right: elongate anorthite crystals (light grey) with interstitial glass; bottom left: homogeneous vesicular glass; bottom right: anorthite crystals (mid grey) with vesicles (black) in interstitial light grey glass. Scale bar in each case represents 20µm.

Figure 7.17 indicates the correlation between the proportions of the main oxides in the aluminosilicate glass for each sample, based on averaging a number of points as indicated in Table 7.6 and the proportions of the same oxides, inferred from the bulk chemistry of each sample and the quantitative XRD data (Table 7.5). Although there is considerable scatter, the overall trend for SiO_2, Fe_2O_3 and CaO suggests a positive correlation, with many of the individual points falling close to the diagonal representing equality for the two different types of evaluations. However, the overall trend for Al_2O_3 seems to be almost the opposite, with a negative correlation; notwithstanding this apparent trend, over half of the points still fall close to the equality line.

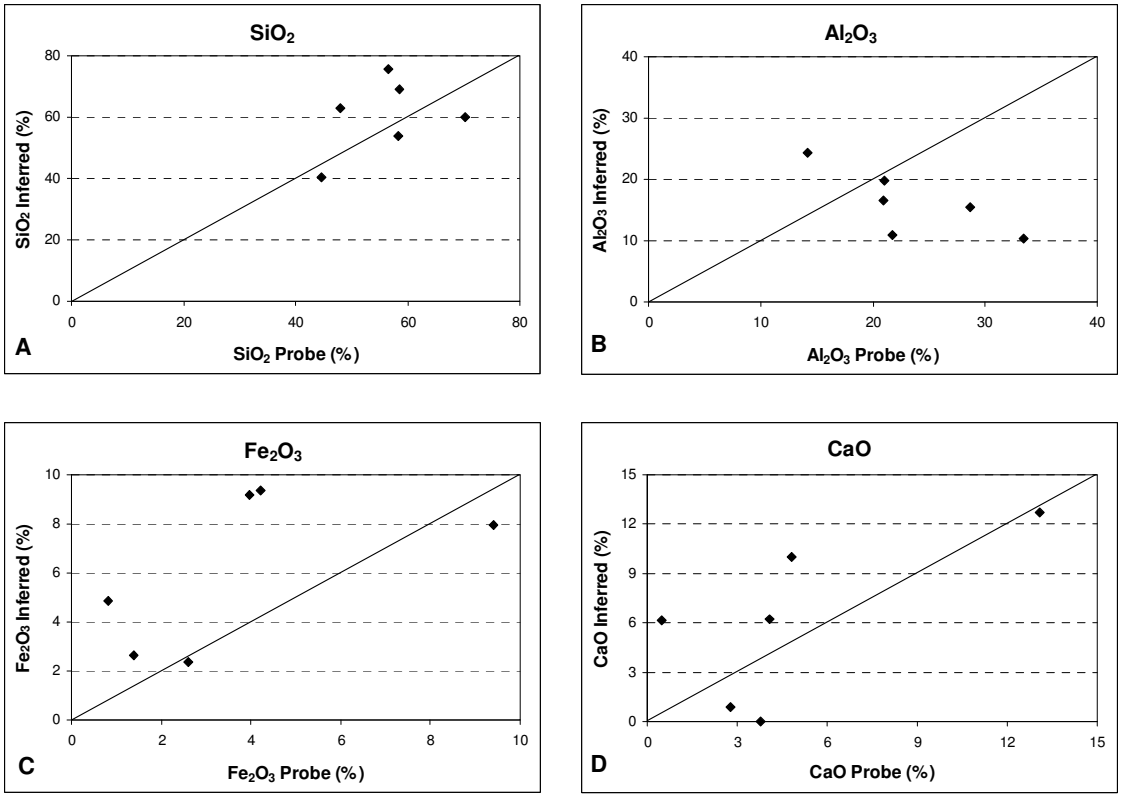


Figure 7.17: Correlation between key oxide percentages in aluminosilicate glass as determined by electron microprobe analysis (Table 7.6) and inferred percentages of same oxides in glass fraction interpreted from bulk composition and XRD analysis (Tables 7.4 and 7.5). A: SiO_2; B: Al_2O_3; C: Fe_2O_3; D: CaO.

- **Other particles and phases**

A range of other particles and glassy phases is also present in the samples; the composition of some of these is indicated in Table 7.7. They include particles identified as corundum (with almost 100% Al_2O_3) and particles (probably representing rutile or anatase) that consist almost entirely of TiO_2. Small proportions of SiO_2 and/or Al_2O_3 in some particles may represent inclusion of glass or other phases in the analysed field. Other phases, with roughly equal proportions of SiO_2 and Al_2O_3 have been tentatively identified as metakaolin, probably derived from kaolinite in the feed coal. Although mullite is identified in the various materials by XRD, the lack of contrast between this mineral and the associated aluminosilicate glass makes it difficult to identify and analyse the mullite composition separately by microprobe techniques. The individual mullite crystals are also likely to be sub-micron in size, so that the spot size embraced in any microprobe analysis would inherently include at least some of the associated glassy matrix as well.

An alumino-phosphate phase is also indicated by the microprobe data. Although departing from the stoichiometric composition of crandallite (13.6% CaO, 37.1% Al_2O_3, 34.0% P_2O_5, 15.3% H_2O), this material probably represents a product of the gorceixite-group material identified in the LTA of the feed coal (Table 4.11).

A range of phases rich in iron and magnesium are also indicated in Table 7.7. Some of these may represent discrete hercynite ($FeAl_2O_4$) or ferrianspinel ($(Fe,Mg)Al_2O_4$) phases, while others, such as in sample clinker 10, represent Fe-Mg silicate components, apparently occurring in a more glassy form. The Fe-Mg silicate minerals in the clinkers analysed in this study may have been derived from reactions between fluxing elements-bearing minerals (pyrite, calcite, and dolomite) and kaolinite or illite at elevated temperatures during coal gasification.

Phases consisting of iron and sulphur are also present, with a composition close to that of pyrrhotite (FeS, 63.6% Fe, 36.3% S) rather than pyrite (FeS_2, 46.6% Fe, 53.4% S). These are probably reaction products of pyrite in the original feed coal.

In conclusion, the bulk gasification ash, heated stone and clinker samples produced by the gasification process contain fragments of heat-altered rock materials, set in an often vesicular, partly crystalline glassy matrix. Quartz and possibly K-feldspar in the feed coal or admixed non-coal rocks may pass unaltered into the bulk gasification ash, along perhaps with titanium or iron-titanium oxides and aluminophosphate minerals. Extraneous pyrite particles also react to form pyrrhotite as part of the gasification process. Although products of solid-state reactions may be preserved in some of the heat-altered fragments, anorthite that has crystallised from molten aluminosilicate material is contained within a glassy matrix in a manner analogous to the formation of igneous rocks.

In the next chapter, the FactSage results for the selected clinker and heated rock fragment particles obtained, after using the area SEM-EDS analysis of these particles, are discussed.

Table 7.7: Composition of other coal gasification ash components (wt %) as determined by electron microprobe

	Pts	SiO_2	TiO_2	Al_2O_3	Fe_2O_3	MgO	MnO	CaO	Na_2O	K_2O	P_2O_5	SO_3	Total
Corundum													
Clinker 8	2	0.03	0.00	99.02	0.19	0.00	0.01	0.07	0.00	0.00	0.00	0.03	99.36
Metakaolin													
Clinker 8	5	49.57	0.50	42.08	0.87	0.17	0.00	0.11	0.34	0.35	0.08	0.06	94.13
Ti-oxide													
Clinker 7	2	2.84	93.33	0.77	0.19	0.02	0.01	0.07	0.02	0.08	0.02	0.01	97.37
Clinker 10	3	11.61	82.81	4.23	0.62	0.15	0.02	0.14	0.14	0.69	0.08	0.03	100.50
Heated stone 3	1	0.19	98.21	0.19	0.17	0.00	0.00	0.00	0.01	0.03	0.00	0.00	98.78
Al-phosphate													
Clinker 9	6	3.89	0.13	24.18	0.52	1.75	0.02	26.13	0.45	2.41	27.39	0.01	86.88
Fe Mg-rich													
Clinker 2	1	13.05	13.66	6.10	59.27	3.84	0.44	1.85	0.26	1.07	1.33	0.29	101.14
Clinker 8	5	0.38	47.45	0.27	49.45	2.05	0.75	0.59	0.02	0.10	0.04	0.17	101.27
Clinker 9	2	1.01	1.06	23.09	68.05	8.01	0.07	0.11	0.01	0.03	0.05	0.00	101.49
Clinker 10	9	40.23	3.60	10.00	23.33	15.06	0.30	4.77	0.27	0.75	2.08	0.28	100.66

CHAPTER 8
RESULTS AND DISCUSSION - FACTSAGE MODEL

In the next section (8.1) the FactSage results for high-temperature equilibria of the inorganic material from the feed coal, float fraction, sink fraction as well as selected clinker and heated rock fragment particles are discussed.

8.1 FactSage Model

8.1.1 FactSage results for the feed coal

The expected equilibrium phases in the coal ash were predicted by using the "Equilibrium" module of FactSage (Bale et al., 2002), considering as possible phases: liquid slag, several solid-solution phases (including spinel, anorthite, monoxide, wollastonite, pyroxenes and olivine) and all pure compound solids between the inputs. In first calculations, to show broad trends, the following oxide composition was assumed: 56.0% SiO_2, 26.1% Al_2O_3, 9.1% CaO, 3.4% FeO, 3.0% MgO, 1.1% TiO_2, 0.9% K_2O and 0.4% Na_2O (note that it is effectively assumed that all the pyrite in the coal is oxidised to FeO in the lower regions of the gasifier). The composition is the average of the gasifier ash originating from the coal minerals and the rock fragments. By using this composition, it is effectively assumed that there is full interaction between the coal minerals and the rock fragments. In fact, there is only partial interaction, as was explored in further calculations.

Based on other models of the gasifier, the temperature at the ash grate is predicted to be 335°C, with the peak temperature in the combustion zone being some 1390°C, with the gas composition changing from an O_2-H_2O mixture at the ash discharge point to H_2O-CO_2 in the combustion zone. This does imply that much of the iron would be in the trivalent form at equilibrium. Since FeO is a strong fluxing agent for silica, oxidation to Fe^{3+} would affect the formation of liquid slag. However, in the calculations presented here, it was assumed that all the iron is present as FeO.

The presence of glass (supercooled molten silicate) indicates that the ash and clinker formed from phases which included a large amount of liquid slag. Hence, the equilibrium calculations were performed for the temperature range 1100-1400°C, where a substantial amount of liquid

slag was predicted. The results are given in Figure 8.1. As Figure 8.1 shows, the mineral matter of the coal is predicted to be largely molten at the peak temperature (1390°C), with anorthite the main solid phase upon cooling below 1300°C (the "anorthite" was modelled as the $CaO.Al_2O_3.2SiO_2$-$Na_2O.Al_2O_3.6SiO_2$ solid solution, here containing 93-94% of $CaO.Al_2O_3.2SiO_2$). In comparison with this, CCSEM or XRD did not detect any appreciable levels of cordierite ($2MgO.2Al_2O_3.5SiO_2$) or leucite ($KAlSi_2O_6$), but confirmed the occurrence of glass, anorthite, mullite and quartz. Comparing the CCSEM, EMP, SEM-EDS results (Figure 7.4, Figure 7.5, Figure 7.6, Figure 7.16,,Figure 7.14, Figure 7.15) to FactSage model (Figure 8.1), it is proposed that rising steam and oxygen quenched the molten slag, preventing the crystallisation of cordierite, effectively freezing the structure which had been present at temperatures estimated to be between 1220°C and 1390°C. This is confirmed by the occurrence of crushed ash fragments ranging from pure glass, with no evidence of any anorthite crystals, to fragments in which anorthite is the dominant phase (Figure 7.4). Note that the quartz in the coarse ash originated from coarse-grained sandstone rock fragments or included quartz in siltstone/mudstone rock fragments, not from crystallisation during cooling of the ash slag. Hence, the observation of quartz in the coarse ash is consistent with the proposal that the phases in the ash represent the structure as quenched from temperatures above 1220°C, where quartz and cordierite are not stable under equilibrium conditions.

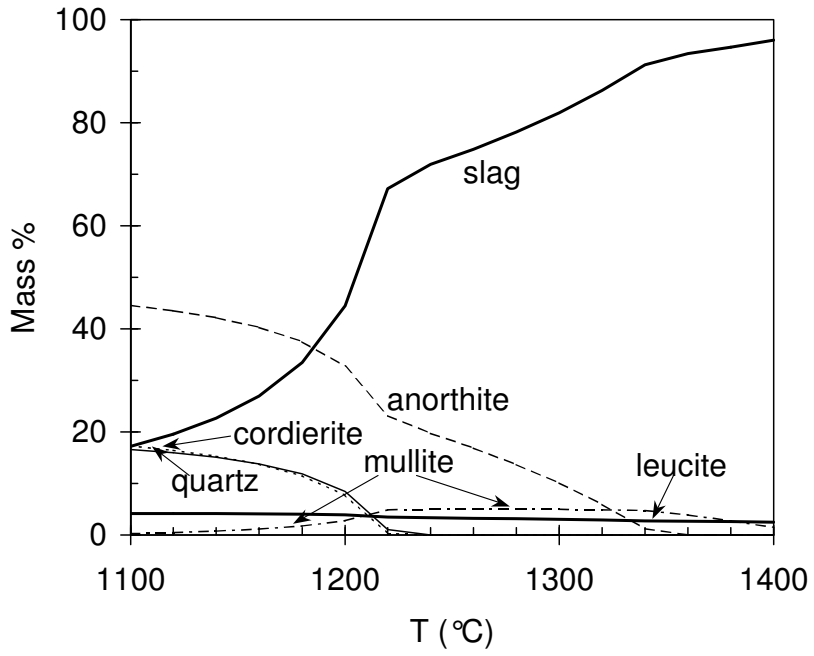


Figure 8.1: Predicted mass percentages of phases in ash (composition 56.0% SiO_2, 26.1% Al_2O_3, 9.1% CaO, 3.4% FeO, 3.0% MgO, 1.1% TiO_2, 0.9% K_2O and 0.4% Na_2O).

8.1.2 Predicted equilibrium phases in the float and sink fractions of the feed coal

As was stated earlier in this study, the included minerals in the coal are responsible for the clinkering and slagging of mineral matter during coal gasification, hence the equilibrium phases in the float fraction (containing a significantly higher proportion of included minerals) and sink fraction were calculated by FactSage. The chemical compositions of ash samples of the float and sink fractions used in the calculation were given in Table 5.13.

The FactSage results (Figures 8.2 and 8.3) indicate broadly similar trends, with anorthite and mullite the dominant high-temperature solid phases, but with higher proportions of anorthite and a smaller proportion of slag in the float fraction in comparison with the sink fraction. Significant proportions of Fe deriving from the pyrite mineral and Si from silicate minerals in the rock fragment present in the sink fraction, contribute to the predicted fayalite and ilmenite. These minerals (and cordierite) are not generally observed in the gasifier ash, but significant proportions of glass are observed. This is in line with the suggestion that rapid cooling in the lower part of the gasifier prevents crystallisation beyond the formation of anorthite and mullite.

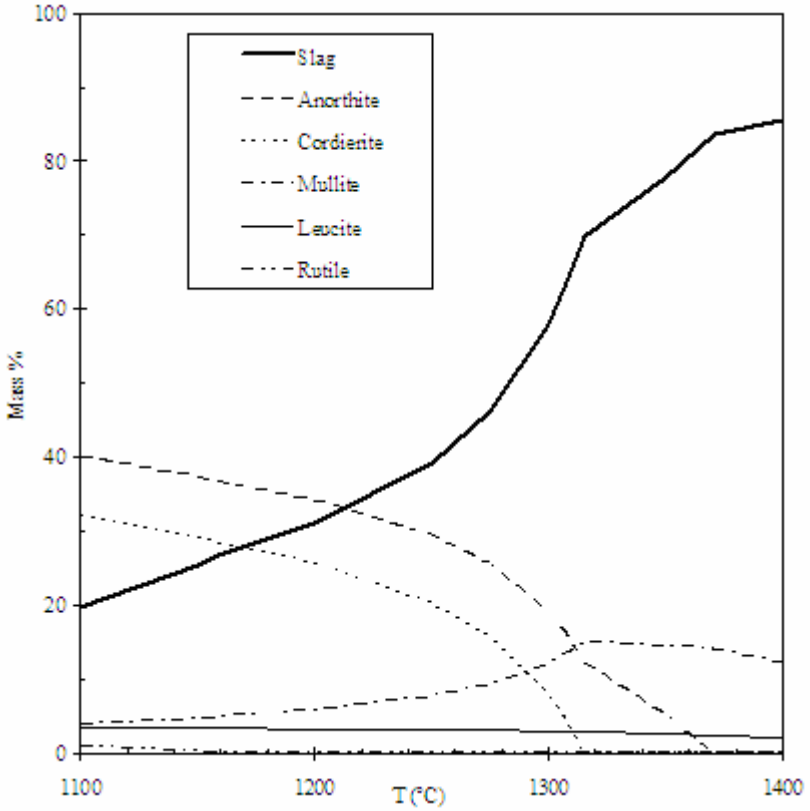


Figure 8.2: Predicted mass percentage in the ash of the float fraction (<1.5g/cm^3).

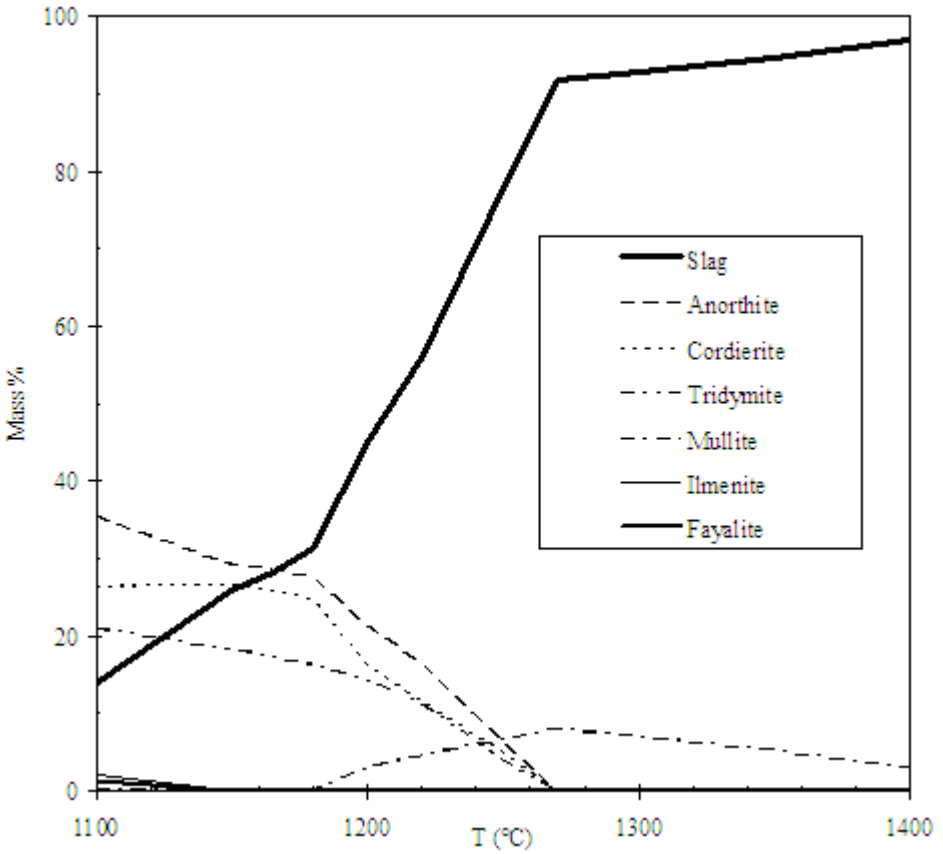


Figure 8.3: Predicted mass percentage in the ash of the sink fraction (>1.8g/cm^3).

8.1.3 Predicted equilibrium phases in the hand-picked dig-out samples

FactSage 5.5 was used to predict the expected equilibrium phases present in the selected fragments from the dig-out samples 6D and 7D. In the present study area analyses (Tables 8.1) of the selected areas of these dig-out samples (determined by SEM-EDS) were used for the input compositions. The predicted equilibrium phases formed at the different temperatures after using the chemical compositions of the selected areas in the heated rock fragments were compared to minerals in the selected areas of the coal ash that were detected by SEM-EDS (Figure 8.4). Note that the major differences in composition are the high CaO content in the coal ash, compared with low CaO (but higher Al_2O_3) in the rock fragment.

Table 8.1: Area analysis of the selected spot fragments of samples taken from the gasifier during the dig-out test (wt %)

Metal oxide	**7.4D**	**6.7D**
Na_2O	0.60	0.40
Al_2O_3	32.83	38.40
SiO_2	42.54	58.70
TiO_2	2.40	0.67
CaO	13.21	0.42
MgO	0.80	0.00
FeO	3.50	0.32
K_2O	1.70	1.09
P_2O_5	1.80	0.00
Total	100.00	100.00

Note: 7.4D = Image of selected region of the dig-out sample 7D shows reacted coal ash (Figure 8.4)
6.7D = Area analysis of rock fragment in Figure 8.4 (bottom right)

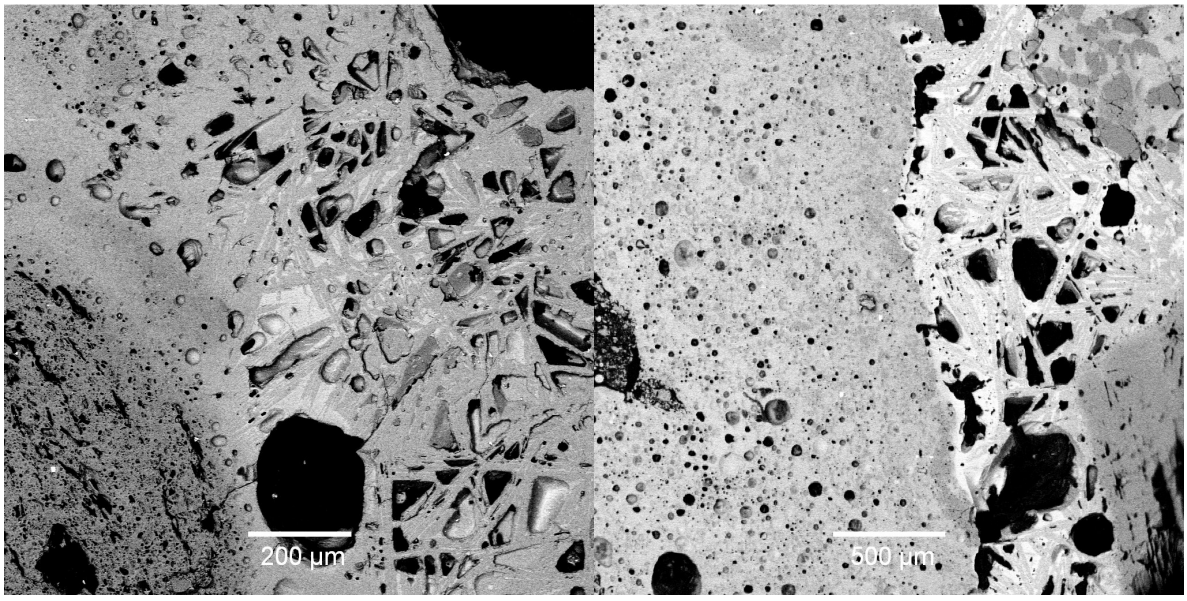


Figure 8.4: Left: BSE image of sample 7.4D showing reacted coal ash, containing anorthite crystals in glass; the region at the bottom left is a heated rock fragment (not included in the area analysis).
Right: Reaction interface in sample 6.7D, showing reacted ash and a rock fragment; the area analysis was taken from the rock fragment at bottom right.

The FactSage results show that mullite is the main solid phase in the heated rock fragment (Figure 8.5), persisting at 1400°C. In contrast, the main high-temperature solid in the coal ash (Figure 8.6) is anorthite. This difference in the identity of the primary solid phase, results from the differences in oxide composition: higher CaO levels favour anorthite formation, while higher Al_2O_3 levels favour mullite formation.

Substantial liquid formation requires high temperatures: for the two examples shown here, approximately 50% liquid is predicted to be presented at 1400°C. The extent of liquid formation depends on the oxide composition. As Figures 8.1 to 8.3 indicated, substantial liquid formation can occur at lower temperatures, for compositions with lower CaO/SiO_2 ratios.

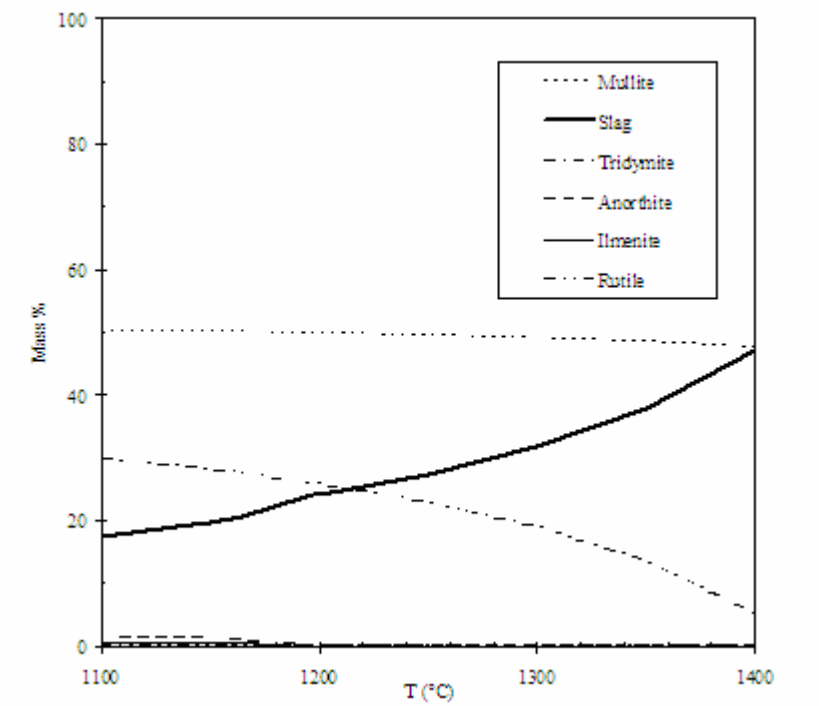


Figure 8.5: Predicted mass percentages of phases in the heated stone 6.7D.

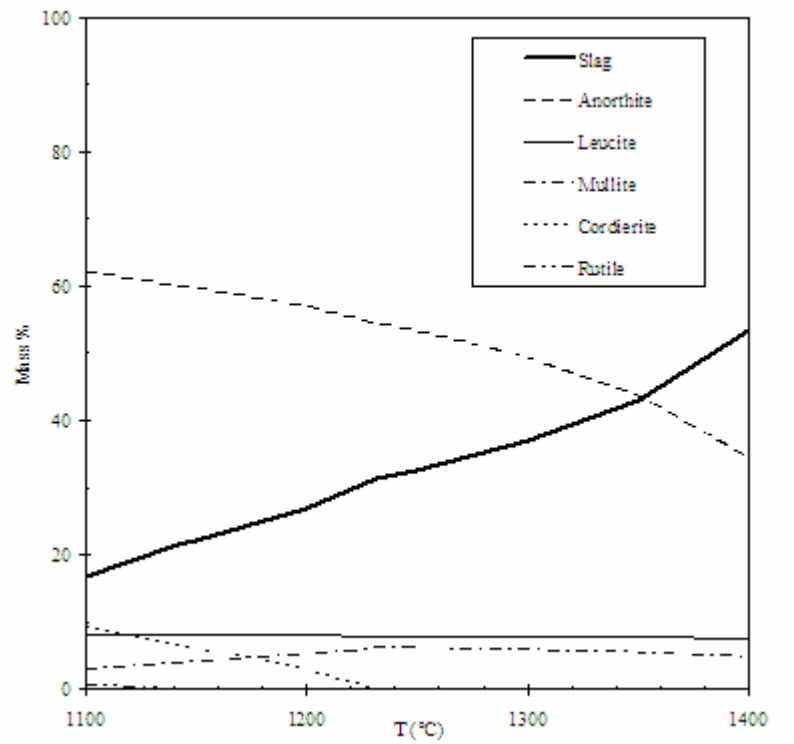


Figure 8.6: Predicted mass percentages of phases in the heated stone 7.4D.

CHAPTER 9

CONCLUSIONS AND RECOMMENDATIONS

The feed coal to gasification consists of coarse coal particles mixed with rock fragments (>6mm coal fraction) derived from the various sources. During coal gasification or combustion, minerals with fluxing elements (Mg, Ca and Fe^{2+}) in the rock fragments and coal macerals interacted with kaolinite at elevated temperatures and pressures to form a melt. On cooling the melt with steam, the anorthite and mullite phases crystallised out from the melt and the heated rock fragments attached to the cooled melt to form clinkers in the gasifier. The clinker formation could significantly affect the permeability for syngas (mixture of carbon monoxide and hydrogen), which is produced by gasification. In some cases, the carbon particles that are supposed to be converted to syngas were encapsulated by the melt and reported to the ash particles during coal gasification.

The principal objective of this study was to test the hypothesis that the included fluxing elements-bearing minerals that are associated with the included kaolinite, lowered the ash fusion temperature of this clay at an elevated temperature of greater than 1000°C, to form a melt. The other objective of this study was to use conventional and advanced analytical techniques to qualify and quantify mineral associations that are responsible for the sintering and slagging of mineral matter in the coal during the gasification process. From this, advances in the management of clinker formation are envisaged, which include decreasing carbon loss in the ash fraction and understanding the influences on the production efficiency of a mixture of carbon monoxide and hydrogen.

This thesis describes the detailed characterisation of coals from mines in the Highveld coalfield, feed coal, gasification ash particles (heated rock fragment and clinker particles), coal fractions from density separation, coal and corresponding ash samples from the selected gasifier, gas liquor and char samples from the pyrolysis experiments and, turn-out and dig-out samples from the different gasifiers, as well as coal and liquid samples from the chemical fractionation method. As stated earlier in this thesis, the different forms of mineral matter are responsible for many of the problems (e.g.

abrasion, stickiness, slagging, sintering, corrosion and pollution) associated with coal handling and use. The conclusions of results for coal and ash samples from the different experiments are discussed in this section.

Chemical analyses of coals from six different Highveld coal mines and feed coal to the coal conversion process

The primary constituents in the ashes of coals from the six different Highveld coal mines including the feed coal were SiO_2, Al_2O_3, CaO, Fe_2O_3, MgO, SO_3 and TiO_2. Minor proportions (<1.0%) of K_2O, Na_2O, P_2O_5, SrO, BaO and Mn_3O_4 were also present in both cases.

Mineralogical analyses of LTA of coals from the different mines and feed coal

Low-temperature oxygen-plasma ashing indicated proportions of mineral matter in the coals ranging from 25 to 45%. These are higher than the proportions of ash indicated by conventional proximate analysis (22-30%) reflecting the breakdown of the different mineral structures at the higher temperatures used in the proximate analysis process. XRD analysis of the low temperature ash indicates that kaolinite ($Al_2Si_2O_5(OH)_4$) and to a lesser extent quartz (SiO_2), dolomite ($CaMg(CO_3)_2$), illite and/or mica are the major minerals present. Minor proportions of fluxing elements-bearing minerals such as calcite ($CaCO_3$), pyrite (FeS_2) and siderite ($FeCO_3$) were also found in some LTA samples.

The XRD technique also detected small amounts of the goyazite group (alumino-phosphate) minerals in the LTA samples, along with small proportions of anatase (TiO_2) and bassanite ($CaSO_4.½H_2O$). More detailed XRD analysis of the clay fraction of the LTA samples, using ethylene glycol and heat treatment further identified the nature of the expandable clay minerals (smectite and interstratified illite/smectite) present in the coal samples.

QEMSCAN analysis of turn-out sample 32T feed coal confirmed high proportions of kaolinite (15.81%), quartz (6.5%), dolomite (2.67%), calcite (2.18%), organic matter (68.76%) and low proportions of pyrite (1.63%), siderite (0.02%), rutile (0.94%), illite (0.42%), apatite (0.07%) and organic sulphur (0.94%)). QEMSCAN and SEM-EDS

show that calcite grains are strongly associated with the carbon-rich fraction and are also associated with dolomite, kaolinite, quartz and apatite. Due to the presence of the fluxing elements-bearing minerals in the coal, this mineral association could contribute significantly to the sintering and slagging of mineral matter at elevated temperatures during coal gasification or combustion.

Petrographic analysis

Petrographic analysis indicates that coals are relatively low in vitrinite (20-25%) and rich in inertinite (70-75%), with minor proportions of liptinite also present. Sample from mine 5 had slightly higher proportions of vitrinite and less inertinite than the other coal samples. Mean maximum vitrinite (telocollinite) reflectance was 0.7 to 0.75%.

Elemental composition of individual coal macerals in the coals from the six different Highveld coal mines by electron microprobe

The vitrinite had significantly higher concentrations of nitrogen and organic sulphur than the inertinite macerals in the same coal samples. Minor proportions of organically-bound inorganic elements, including calcium, aluminium, silicon, magnesium and titanium, were identified in the macerals, especially (for Ti) in the vitrinite components.

The overall proportions of carbon, oxygen and nitrogen for the whole-coal samples, expressed to a dry, ash-free basis (Table 4.2) are intermediate between the carbon, oxygen and nitrogen contents for the vitrinite macerals on the one hand and the inertinite macerals on the other (Table 4.8), as determined by the electron microprobe study. The sulphur in the macerals is also significantly lower than the total sulphur in the coals, as it does not incorporate the additional sulphur present separately as pyrite particles.

Chemical fractionation method

Water washing had no particular effect on the mineral matter in the bituminous feed coal sample. Treatment with ammonium acetate (at 70ºC) removed most of the carbonate minerals from the bituminous coals. The removal of carbonates by the acetate suggests that the common assumption of such solutions providing only an ion-exchange reaction, needs to be re-evaluated. However, hydrochloric acid treatment did remove almost all the Ca and Fe from the coal samples.

Close evaluation of the ash analysis data suggests that some of the Al in the coals was also removed by the selective leaching process. This may reflect a solution of organically-associated Al from the maceral components (cf. Matjie et al., 2007; Li et al., 2007).

The loss of Ca and other fluxing elements from the coals, induced by the different selective leaching processes, is associated with an increase in the different ash fusion temperatures in all cases.

With high pyrite coals, in some cases, the sulfides may oxidise during the extraction process, resulting in a decrease in the pH of the solution, causing the extraction of acid-soluble elements from the minerals. In this leaching step iron, vanadium, titanium and chromium were not dissolved in ammonium acetate solution, indicating that these coals used in the chemical fractionation experiments were not oxidised. These elements are present in Highveld coals in the form of minerals that are insoluble in ammonium acetate.

Characterisation of coal size fractions and density fractions and feed coal by analytical techniques

The -75+53mm size fraction contains high proportions of pyrite, calcite and dolomite and a low proportion of kaolinite, compared with the other coal fractions. Pyrite predominantly occurs as extraneous cleat fragments and to a lesser extent associated with medium to coarse-grained sandstone rock fragments. Calcite in this size fraction also occurs as extraneous cleat fragments and is to a lesser extent included in carbon-rich matrix.

The CCSEM results for the coal size fractions indicated that the proportion of extraneous particles decreases with a decrease in size, while the proportion of carbon-rich particles containing included minerals increase with a decrease in size.

In this context, "extraneous" particles are principally derived from extraneous rock fragments ("stone"), coarse (>1mm) pyrite and/or calcite rich cleats transecting the coal and possibly from mineral-rich layers in the coal.

The mineralogical and petrographic analyses of the density fractions of coal analysed in this study showed the following interesting trends:

- The increase in SiO_2, K_2O and Fe_2O_3 proportions to the >1.8g/cm^3 density fraction is attributed to the increase in the proportion of quartz (Si), microcline (K) and pyrite (Fe), from arkosic sandstone fragments in the 1.8g/cm^3 density fraction.
- The >1.8g/cm^3 density fraction contains a higher proportion of calcite ($CaCO_3$) than dolomite ($CaMg(CO_3)_2$). This is attributed to calcite occurring as coarse extraneous cleat fragments, whereas dolomite tends to mainly occur as inclusions in carbon matrix or cleats transecting the carbon matrix.
- Kaolinite, which is a predominant mineral in the feed coal, concentrates in the 1.5-1.8g/cm^3 density fraction and to a lesser extent in the >1.8 g/cm^3 density fraction. A high proportion of kaolinite occurs as fine inclusions in carbon matrix and to a lesser extent as a component of mudstone and siltstone rock fragments.

Pyrolysis of coal samples from Highveld coal mines

The mineralogical and FactSage results of the coal and char samples show that some of the inorganic elements in the minerals transformed to form new minerals without significant volatilisation, reporting to pyrolysed coal. Further, the XRD analysis of the char samples indicates that some coal minerals are still contained in the char samples produced during the pyrolysis of coal at 600^{o}C and 26bar under reducing conditions.

ICP-MS and IC analyses of all gas liquor samples indicate that Mg, Ca, Fe, Al, Si, Ti, Na, K, NH_4^+, SO_4^{2-}, HCO_3^{2-}, Cl^-, F^- and CO_3^{2-} are present in these liquid samples produced during the pyrolysis experiments. Most of the elements were found to volatilise in relatively high amounts from the mine 5 and mine 6 coals (which had higher inertinite and lower vitrinite contents than the other four coals).

Except for some of the Na, all the metallic elements volatilised from the coals studied during the pyrolysis tests, appear to be associated with the carbon matrix in the coals.

Chemical and mineralogical analyses of gasification ash samples

The mineralogical signature of coarse feed coal and corresponding coarse ash/clinker samples offers an insight into clinker formation.

The first stage of clinker formation is the dehydration of kaolinite and muscovite/illite in the carbon-rich particles and rock fragments and devolatisation of coarse pyrite (yielding SO_2, S_2 or H_2S) and carbonate (yielding CO_2) cleat fragments. Dehydrated rock fragments, Fe-S-oxide and Ca-Mg-oxide particles are formed. As the ash-bed gravitates towards the hotter zone of the gasifier, the fluxing effect of Ca/Mg and Fe (derived from respectively included carbonates/organically bound cations and pyrite) lowers the melting points of included kaolinite and quartz, causing a CaO- and FeO-bearing aluminosilicate melts to form. The reducing conditions (maintaining iron in the divalent form) and higher particle temperatures of carbon-rich particles promote the formation the molten phase. The molten material encapsulates devolatilised rock fragments, coarse Fe-oxide of rich particles, coarse Ca-Mg-oxide particles and char fragments.

Sintering is initiated by the crystallisation of anorthite and mullite from the molten material upon cooling. Mullite crystallisation starts at approximately 1400°C and anorthite at 1360°C, depending on melt composition. As the combustion of the carbon progresses, the residual molten/rock fragment ash load gravitates to the rotating grate and is cooled/quenched by the rising steam and oxygen that are introduced at the base of the gasifier. With a decrease in temperature, crystallisation of anorthite and mullite

is halted and the remnant molten material solidifies to form the CaO/MgO- and FeO-bearing aluminosilicate glass. Predicted quenching temperatures range from 1220°C to as high as 1390°C. This is the final stage of clinker formation.

The bulk gasification ash, heated stone and clinker samples produced by the gasification process contain fragments of heat-altered rock materials, set in an often vesicular, partly crystalline glassy matrix. Quartz and possibly K-feldspar in the feed coal or admixed non-coal rocks may pass unaltered into the bulk gasification ash, along perhaps with titanium or iron-titanium oxides and aluminophosphate minerals. Although products of solid-state reactions may be preserved in some of the heat-altered fragments, anorthite that has crystallised from molten aluminosilicate material is contained within a glassy matrix in a manner analogous to the formation of igneous rocks.

The main objective of this study was to test all hypotheses mentioned in Chapter 2 of this thesis. The CCSEM results indicated that feed coal to gasification consists of three components:

- Carbon-rich coal particles with included mineral matter: The proportion of mineral matter can vary significantly. The major minerals are kaolinite, quartz, dolomite, calcite and pyrite;
- Extraneous rock fragments or “stone”: These rock fragments are derived from footwall, hanging wall and in-seam partings. The major rock fragments are mudstone, siltstone, carbonaceous shale and arkosic sandstone. These fragments have varying proportions of kaolinite, quartz, muscovite/illite and microcline;
- Extraneous calcite-rich and pyrite-rich cleat fragments: These are derived from coarse cleats transecting the coal seam, footwall and hanging wall.

The coarse ash sample is characterised by black porous glass, partially or totally enclosing rock fragments. The included rock fragments are significantly finer than the original rock fragments in the coal feedstock.

A significant proportion of the minerals in the rock fragments transform in-situ. Typically, kaolinite dehydrates and forms a devolatilised aluminosilicate. Mullite was

detected by the scanning electron microscope in the rock fragments. Quartz tends to crack. Muscovite/illite transforms into K-bearing glass with an Al/Si ratio similar to muscovite/illite or microcline.

Based on the CCSEM results for the turn-out samples it is clear that carbonates (dolomite or ankerite, siderite and calcite) associated with kaolinite lower the ash fusion temperature of kaolinite at elevated temperatures, forming a melt. Interestingly, a low proportion of iron-bearing phases derived from the reaction between kaolinite and pyrite was found in the turn-out samples. This implies that pyrite and its composition products contribute minimally to sintering or slagging of mineral matter at elevated temperatures during coal gasification.

FactSage results of coal and ash particles taken from the dig-out test

FactSage results predict that it is not possible for Fe, Na, Al and Si to be removed from the coal during pyrolysis as volatile inorganic compounds. Some of the halogens (chlorine and fluorine) are predicted to be removed from the coal as HCl and HF during pyrolysis.

The area SEM-EDS analysis of the selected spots of clinker and heated rock fragments taken from the dig-out samples were used in the FactSage model to predict equilibrium phases such as anorthite and mullite at temperature between 800°C and 1200°C. In most cases, these phases completely melted at 1400°C. The presence of the equilibrium anorthite and mullite phases are in agreement with the anorthite and mullite crystals produced from the cooled melt, which was formed by the interaction between high temperature transformation products of the included dolomite or ankerite and calcite, associated with the included kaolinite during coal gasification.

RECOMMENDATIONS

This study has highlighted a number of mineralogical features and described a few techniques, which could be used to further understand clinker formation in the rock fragments present in the feed coal to gasification. The following is recommended:

- The types of rock fragments (siltstones, sandstone, mudstone and carbonaceous shale) in the feed coal to gasification, as well as the heated rock fragment particles in the ash, should be examined, e.g. by a scanning electron microscope (such as a QEMSCAN) to determine the proportions of fluxing elements-bearing minerals (minerals containing calcite, dolomite, siderite and pyrite) as well as mineral associations that are responsible for the slagging of mineral matter during heat treatment.
- The impact of rock fragments on the crystallisation of the anorthite and mullite should be determined. The heated rock fragments may initiate the crystallisation of mullite and anorthite, depending on the proportions of calcium, silicon and aluminium in the melt. It is also proposed that some anorthite and mullite particles in the heated rock fragments may form by solid-state reaction. This needs to be confirmed.
- The proportion and mineralogical compositions of the "stone" in the coal feedstock and the "stone" in the corresponding gasifier coarse ash should be measured.
- High temperature XRD should be used to monitor the transformation of individual minerals in the stones under high pressures and oxidising and reducing conditions. It should also be used to analyse molten glass beads formed by heating coal particles under pressure. This data is extremely important for predicting transformation, solidus and liquidus temperatures.
- Combine all the analytical data and methods and develop a clinker prediction model. This model should be used to predict the "clinker" formation propensity of varying coal feedstocks and whether it is possible to manage clinker formation.

A detailed characterisation of South African coals using electron microprobe and QEMSCAN equipment should be done in order to determine the proportions and the chemical structures of the organically-associated inorganic elements present in the individual macerals in these coals. The organically-associated inorganic elements in the coal macerals could contribute significantly to the volatilisation of inorganic species at low temperature under the reducing and oxidising conditions.

The significant volatilisation of inorganic elements derived from the organically-associated inorganic elements is responsible for precipitation of the dissolved metal ions from the gas liquor in the pipe and heat exchangers during the treatment of this liquid.

BIBLIOGRAPHY

Al-Otoom, A.Y., Elliott, L.K., Wall, T.F. and Moghtaderi, B., *Measurement of the sintering kinetics of coal ash,* Cooperative Research Centre for Black Coal Utilisation, Department of Chemical Engineering, The University of Newcastle, Callaghan, NSW 2308, Australia, 2000.

Attalla, M.I., Morgan, S., Riley, K., Bryant, G. and Nelson, P.F., *Trace element deportment in combustion processes,* Research report 50, Cooperative Research Centre for Coal in Sustainable Development (CCSD), CSIRO, University of Newcastle, Macquarie University, Australia, 2004.

Attig, R.C. and Duzy, A.F., "*Coal-ash deposit studies and application to boiler design*", proceedings American Power Conference, 31, pp. 290-300, 1969.

Bailey, C.W., *High temperature transformations of siderite and the performance of a PF fired plant,* PhD Thesis, University of Newcastle, 1999.

Bailey, C.W., Bryant, G.W., Matthews, E.M. and Wall, T.F., *Investigation of the high temperature behavior of excluded siderite grains during pulverised fuel combustion, Energy Fuels* 12(3), pp. 464–469, 1998.

Bale, C.W., Chartrand, P., Degterov, S.A., Eriksson, G., Hack, K., Ben Mahafoud, R., Melancon, J., Pelton, A.D. and Petersen, S., *Fact-Sage thermochemical software and databases*, CALPHAD 26 (2), pp. 189-228, 2002.

Barnhart, D.H. and Williams, P.C., *The sintering test, an index to ash fouling tendency*, Transactions of the American Industry of Mechanical Engineering (AIME), 78, pp. 1229, 1956.

Benson, S.A., *Laboratory studies of ash deposit formation during the combustion of Western U.S. coals*, Ph.D. Thesis, the Pennsylvania State University, 1987.

Benson, S.A. and Holm, P.L., *Composition of inorganic constituents in three low-rank coals*, Ind. Eng. Chem. Prod. Res. Dev., 24, pp. 145-149, 1985.

Bish, D.L. and Post, J.E., *Quantitative mineralogical analysis using the Rietveld full-pattern fitting method,* American Mineralogist 78, pp. 932-940, 1993.

Bogwardt, R.H. and Bruce, K.R., *Effect of specific surface area on the reactivity of CaO with* SO_2*,* AiChe Journal, vol. 32, pp. 239-248, 1986.

Briggs, D.L. and Lindsay, C.G., *High-temperature interactions among minerals occurring in coal, In: Mineral matter and ash in coal* – Symposium of American Chemical Society, Vorres, K., (Ed), pp. 128-137, 1986.

Brown, H.R., Durie, R.A. and Schafer, H.N.S., *The inorganic constituents of Australian coals: I. The direct determination of the total mineral matter content,* Fuel, 38, pp. 295-308, 1959.

Bryers, R.W., *Fireside slagging, fouling and high-temperature corrosion of heat transfer surface due to impurities in steam raising fuels*, Prog. Energy Combust. Sci., 22, pp. 29-120, 1996.

Bryers, R.W., *Influence of segregated mineral matter in coal,* In: Mineral matter and ash in coal, Symposium of American chemical society, Vorres, K., (Ed), pp. 351-374, 1986.

Buhre, B.J.P., Hinkley, J.T., Gupta, R.P., Nelson, P.F. and Wall, T.F., *Fine ash formation during combustion of pulverised coal–coal property impacts,* Cooperative Research Centre for Coal in Sustainable Development, Department of Chemical Engineering, University of Newcastle, Callaghan, NSW 2300, Australia, Graduate School of the Environment, Macquarie University, NSW 2109, Australia, 2005.

Bunt, J.R., *A new dissection methodology and investigation into coal property transformational behaviour impacting on a commercial-scale Sasol-Lurgi MKIV Fixed Bed gasifier,* PhD thesis, University of North-West, Potchefstroom, 2006.

Bustin, R.M., Mastalerz, M. and Wilks, K.R., *Direct determination of carbon, oxygen, and nitrogen content in coal using the electron microprobe*, Fuel, 72, pp. 181-185, 1993.

Bustin, R.M., Mastalerz, M. and Raudsepp, M., *Electron-probe micro analysis of light elements in coal and other kerogen,* International Journal of Coal Geology, 32, pp. 5-30, 1996.

Butcher, A.R., *QEMSCAN Technique Development: Progress, Achievements and the Future, ISG Meeting, 27-28th April 06, Coogee Beach, Sydney, Australia, (2006).*

Carver, R.E., *Procedures in Sedimentary Petrology,* Wiley, 1971.

Chandra, D. and Taylor, G.H., *Thermally altered coal,* In: E.Stach, M–Th. Mackowsky, M. Teichmuller, G.H. Taylor, D. Chandra and R. Teichmuller (Editors), Stach's Textbook of coal petrology, gebruder Borntraeger Berlin Stuttgart, pp. 206-218, 1982.

Chamley, H., *Clay sedimentary,* The University of Lille, The University of Paris, Springer-Verlag, Berlin, Heidelberg, New York, London, Paris, Tokyo, Hongkong, pp. 3-33, 1989.

Chuang Y.Y., Hsieh K.C. and Chang Y.A., *Thermodynamics and phase relationships of transition metal-sulphur systems - Part V: a re-evaluation of the Fe-S system using an*

associated solution model for the liquid phase, Metallurgical Transactions Series B, 16B, pp. 277-285, 1985.

Clarke, L.B. and Sloss, L.L., *Trace elements emissions from coal combustion and gasification,* IEACR/49 London, pp.111, 1992.

Conn, R.E. and Austin, L.G., S*tudies of sintering of coal ash relevant to pulverised coal utility boilers: Part 1. Examination of Raask shrinkage- electrical resistance method,* Fuel, 63, pp. 1664, 1984.

Creelman, R.A. and Ward C.R., *A scanning electron microscope method for automated, quantitative analysis of mineral matter in coal*, International Journal of Coal Geology, 30, pp. 249-269, 1996.

Crelling, J.C. and Dutcher, R.R., *Principles of and applications of coal petrology,* Short course notes, Dept. of Geology and Coal Research Center, Southern Illinois 62901, pp. 2-29, 1980.

Cumming, I.W., Jorce, W.I. and Kyle, J.H., Ad*vanced techniques for the assessment of slagging and fouling propensity in pulverised coal fired boiler plants,* Journal of the institute of energy, pp. 169, December, 1986.

Deer W.A., Howie R.A. and Zussman J., *Rock-forming Minerals*, Volume 4: Framework Silicates. London, Longmans, pp. 435 1963.

Deer, W.A., Howie, R.A. and Zussman J., *An introduction to the rock-foaming minerals,* 2nd.ed, Department of Mineralogy and Petrology, University of Cambridge, Department of Mineralogy, University of London, Department of Geology, University of Manchester, Longman group UK limited, pp. 357-376, 1992.

Diessel, F.K., *Coal-bearing depositional systems,* Department of Geology, The University of New Castle, New Castle, NSW 2308, Australia, Springer-Verlag, Berlin, Heidelberg, New York, London, Paris, Tokyo, HongKong, Barcelona, Budapest, pp. 137-159, 1992.

DME (Department of Minerals & Energy, South Africa)., *Operating and developing coal mines in the Republic of South Africa,* Directory D2/2006; 2006.

Eddings, E.G., Sarofim, A.F., Lee, C.L., Davis, K.A. and Valentine, J.R., *Trends in predicting and controlling ash vaporisation in coal-fired utility boilers,* Fuel Process Technol, 71, pp. 39–51, 2001.

Falcon, R.M.S. and Snyman, C.P., *An introduction to coal petrography: Atlas of petrographic constituents in bituminous coals of Southern Africa,* The Geological Society of South Africa, Review paper number 2, pp. 26, 1986.

Foscolos, A.E., Goodarzi, F., Koukouzas, C.N. and Hatziyannis, G., *Reconnaissance study of mineral matter and trace elements in Greek lignites.* Chem. Geol., 76, pp. 107-130, 1989.

Frazer, F.W. and Belcher, C.B., *Quantitative determination of the mineral matter content of coal by a radio-frequency oxidation technique,* Fuel, 52, pp. 41-46, 1973.

French, D., Dale, L., Matulis, C., Saxby, J., Chatfield, P. and Hurst, H.J., *Characterisation of mineral transformations in pulverised fuel combustion by dynamic high-temperature X-ray diffraction analyser*, Proceedings of 18th Pittsburgh International Coal Conference, Newcastle, Australia, pp. 7, 2001.

Frenkel, J., *Viscous flow of crystalline bodies under the action of surface tension*, Journal of Physics (USSR), 9, pp. 385, 1945.

Gaigher, G.L., *Mineral matter in some South African coals*, MSc, University of Pretoria, South Africa, 1980.

Galbreath, K., Zygarlicke, C., Casuccio, G., Moore, T., Gottieb, P., Agron-Olshina, N., Huffman, G., Shah, A., Yang, N., Vleeskens, J. and Hamburg, G., *Collaborative study of quantitative coal mineral matter analysis using computer-controlled scanning electron microscopy*, Fuel, 75, pp. 424-430, 1996.

Gibb, W.H., *The slagging and fouling characteristics of coal* – II. *A sintering test for determining fouling propensity,* Power Industry Research, 1, pp. 269, 1981.

Given, P.H., *An essay on the organic geochemistry of coal,* In coal science, vol. 3, Gorbaty, M.L., Larsen, J.W. and Wender, I., Eds., pp. 137, 1984.

Given, P.H. and Yarzab, R.F., *Analysis of the organic substance in coals: problems posed by the presence of mineral matter, In*: Karr, C. (Ed.), *Analytical Methods for Coal and Coal Products,* Volume II, Academic, Press, New York, pp. 3-41, 1978.

Glikson, M. and Mastalerz, M., *Organic matter and mineralisation: Thermal alteration, hydrocarbon generation and role in metallogenesis,* University of Queensland, Brisbane, Australia, Indiana University, Roomington, USA, Kluwer Academic Publishers, Dordrecht, Boston, London, pp. 44-45; 319, 2000.

Gluskoter, H.J., *Electronic low-temperature ashing of bituminous coal,* Fuel, 44, pp.285-291, 1965.

Griffin (in R.E. Carver**,** *Procedures in Sedimentary Petrology***,** Wiley, 1971).

Grim, R.E. and Bradley, W.F., *Investigation of the effect of heat on the clay minerals illite and montmorillonite,* J. Am. Ceram. Soc., 23, pp. 242-248, 1940.

Grim, R.E., *Applied clay mineralogy*, University Of Illinois, Urbana, Illinois, Mcgraw-Hill book company Inc., New York, Toronto, London, pp. 97-113, 1962.

Goblirsch, G.M., Benson, S.A., Karner, F.R., Rindt, D.K. and Hajicek, D.R., *AFBC bed material performance with low-rank coals,* Twelfth Biennial Lignite Symposium: Technology and Utilization of Low-Rank Coal Proceedings, W.R. kube, E.A. Sondreal, and C.D. Rao, Eds., DOE/METC/84-13, 2, pp. 557, 1984.

Goldstein, J.I., Newbury, D. E., Echlin, P., Joy, D.C., Romig, Jr., A.D., Lyman, C.E., Fiori, C. and Lifshin, E., *Scanning Electron Microscopy and X-ray Microanalysis*, A text for Biologists, Materials Scientists, and Geologists, Second Edition, Plenum Press, New York and London, pp. 501, 1992.

Govender, A., *Determination and statistical evaluation of the effect of minerals and mineral associations in specific dense medium fractions on ash fusion temperature*, M Sc Dissertation, The University of North-West, Potchefstroom, pp. 36-66, 2005.

Gupta, R.P., *Coal research in Newcastle – past, present and future,* The University of Newcastle, Newcastle, NSW, Australia, Fuel, 84, pp. 1176-1188, 2005.

Gupta, R.P., Yan, L., Kennedy, E.M., Wall, T.F., Masson, M. and Kerison, K., *System accuracy for CCSEM analysis of minerals in coal*, In: Gupta, R.P., Wall, T.F., Baxter, L. (Eds.), *Impact of Mineral Impurities in Solid Fuel Combustion*, Kluwer Academic Publishing/Plenum, New York, pp. 225-235, 1999.

Gurba, L.W., *Coal rank studies in the Gunnedah Basin,* Ph.D. Thesis, University of New South Wales, School of Geology, New South Wales, 1998.

Harvey, R.D. and Ruch, R.R., *Mineral matter in Illinois and other US coals,* In: Vorres, K.S. (Ed.), *Mineral Matter in Coal Ash and Coal,* American Chemical Society Symposium Series 301, pp. 10-40, 1986.

Herod, A.A., Hodges, J., Pritchard, E. and Smith, C.A., *Mass spectrometric study of the release of HCl and other volatiles from coals during mild heat treatment***.** Fuel, 62, pp.1331-1336, 1983.

Hicks, D. and Nagelschmidt, G., *The chemical and X-ray diffraction analysis of the roof and clod from some South Wales seams and of the mineral matter in the coal.* Medical Research Council Special Report 244, 1553-185, 1943.

Huffman, G.P. and Huggins, F.E., *Investigation of partial ash melting by phase analysis of quenched samples,* proceedings of the 1981, Engineering Foundation Conference at Henniker, N.H., *fouling and slagging resulting from impurities in combustion gases,* Bryers, R.W., Ed., Engineering Foundation, N.Y., 1983.

Huggins, F.E. and Huffman, G.P., *How do lithophile elements occur in organic association in bituminous coals,* International Journal of Coal Geology, 58, pp. 193-204, 2004.

Jak, E., Degterov, S., Hayes, P.C. and Pelton, A.D., *Thermodynamic modeling of system $Al2O_3$-SiO_2-CaO-FeO-Fe_2O_3 to predict the flux requirements for coal ash slags*, Fuel, 77, pp. 77-84, 1998.

Jak, E., Degterov, S., Zhao, B., Pelton, A.D. and Hayes, P.C., *Coupled experimental and thermodynamic modeling studies for metallurgical smelting and coal combustion slag system,* Metallurgical and Materials Transformation B, volume 31B, pp. 621-630, 2000.

Jak, E., Kondratiev, A., Christie, S. and Hayes, P.C., *The prediction and representation of phase equilibria and physicochemical properties in complex slag systems,* Metallurgical and Materials Transformation B, volume 34B, pp. 595-600, 2003.

Jung, B. and Schobert, H.H., *Viscous sintering of coal ashes, 1. Relationships of sinter point and sinter strength to particle size and composition,* Energy and Fuel, 5, pp. 555-561, 1991.

Jung, B., *Sintering characteristics of low-rank coal ashes*, Korean Journal of Chemical Engineering, 13(6), pp. 633-639, 1996.

Kalmanovitch, D.P., *Reactions in coal ash melts*, Ph.D.Thesis, University of London, 1983.

Kawamoto, M., Nakajima, K., kanazawa, T. and Nakai, K., *Design principles of mold powder for high speed continuous casting, ISIJ International,* Vol. 34, No. 7, pp. 593-598, 1994.

King, J.G., Maries, M.B. and Crossley, H.E., *Formulas for the calculation of coal analyses to a basis of coal substance free from mineral matter*, Journal of the Society of Chemical Industry, 55, pp. 277-281, 1936.

Kingery, W.D., Bowen, H.K. and Uhlmann, D.R., *Introduction to ceramics*, 2nd Ed., John Wiley and Sons, N.Y., 1976.

Kiss, L.T. and King, T.N., *The expression of results of coal analysis: the case for brown coals*, Fuel, 56, pp. 340-341, 1977.

Kiss, L.T., *Chemistry of Victorian brown coals,* Aust.Coal Geol., 4, pp. 153-168, 1982.

Klug, H.P. and Alexander, L.E., *X-ray diffraction procedures*, 2nd ed., Wiley, New York, pp. 656, 1974.

Koppenaal, D.W. and Manahan, S.E., Hazardous *chemicals from coal conversion processes?* Environmental Science and Technology: 12, pp.1104-1107, 1976.

Lee, C.M., Davis, K.A., Heap, M.P., Eddings, E. and Sarofim, A.F., *Modeling the vaporisation of ash constituents in a coal-fired boiler, 28th symposium (international) on combustion, Edinburgh, Scotland, UK*, pp. 2375–82, 2000.

Lemaitre, J., Bulens, M. and Delmon, B., *Clay minerals*, 11, pp. 313, 1976.

Li, Z., Ward, C.R. and Gurba, L.W., *Occurrence of non-mineral inorganic elements in low-rank coal macerals as shown by electron microprobe element mapping techniques,* International Journal of Coal Geology , 70, pp.137-149, 2006.

Mastalerz, M. and Gurba, L.W., *Determination of nitrogen in coal macerals using electron microprobe technique-experimental procedure*, International Journal of Coal Geology, 47, pp.23-30, 2001.

Matjie, R.H. and Engelbrecht, R. *Selective removal of dissolved silicon and aluminium ions from gas liquor by hydrometallurgical methods,* Hydrometallurgy, 85, pp.172-182, 2007.

Matjie, R.H., van Alphen, C. and Pistorius, P.C., *Mineralogical characterisation of Secunda gasifier feedstock and coarse ash, Minerals Engineering*, 19, pp. 256-261, 2006.

Matjie, R.H., Li, Z. and Ward, C.R, *Determination of mineral matter and elemental composition of individual macerals in coals from Highveld mines,* Proceedings of 24th Pittsburgh International Coal Conference, Johannesburg, South Africa, September 10-14, 2007, Paper 48-5, 14 pp. (CD publication), 2007.

Matjie, R.H., Li, Z., Ward, C.R. and French D., *Chemical composition of glass and crystalline phases in coarse coal gasification ash,* Fuel, 87, pp. 857-869, 2008.

Matjie, R.H., *The selective removal of iron and titanium from an aluminium containing aqueous phase,* Masters'Diploma in Technology, Vaal Triangle Technikon, VanderBijlpark, 1997.

Miller, R.N. and Given, P.H., *A geochemical study of the inorganic constituents in some low-rank coals*, Rep. U.S. Dept. of Energy under Contract EX-76-C-01-2494, Coal Res. Sect., Penn. State Univ., pp. 314, 1978.

Miller, R.N., Yarzab, R.F. and Given, P.H., *Determination of the mineral matter content of coals by low-temperature ashing*, Fuel, 58, pp. 4-10, 1979.

Nawalk, A.J. and Friedel, R.A., *Concentration of minerals in coals by peroxidation of the organic matter,* Proceedings of Symposium on Chemicals and Oil from Coal, Central Fuel Research Institute of India (1969), pp. 526-530, 1972.

Nelson, J.B., *Assessment of mineral species associated with coal,* British Coal Utilisation Research Association Monthly Bulletin, 17 (2), pp. 21-55, 1953.

Nemecz, E., *Clay minerals*, Akademiai, Kiado, Budapest, printed in Hungary, pp. 379-394, 1981.

Neville, M., Quann, R.J., Haynes, B.S. and Sarofim, A.F., *Vaporisation and condensation of mineral matter during pulverised coal combustion,* In eighteenth Symp. (Int) on combustion, The Combustion Instite., pp. 1267-1274, 1981.

Norrish, K. and Chappell BW., X-*ray fluorescence spectrometry*, In: Zussman J (ed), Physical *Methods in Determinative Mineralogy*, London, Academic Press., pp. 201-272, 1977.

Nowok, J.W., Benson, S.A., Jones, M. L. and Kalmanovitch, D.P., *Sintering behavior and strength development in various coal ashes.* Energy & Environmental Research Center, University of North Dakota, Fuel, 1990.

Nowok, J.W., *Densification, shrinkage and strength development in selected coal ashes*, Journal of the Institute of Energy, 69, pp. 9-11, 1996.

O'Connor, B.H. and Raven, M.D., *Applications of the Rietveld refinement procedure in assaying powdered mixtures*, Powder Diffraction 3, pp. 2-6, 1988.

Parr, S.W., *The classification of coal,* University of Illinois Engineering Experimental Station, Bulletin, 180, pp. 62, 1928.

Patterson, J.H., Corcoran, J.K. and Kinealy, K.M., *Chemistry and mineralogy of carbonates in Australian bituminous and sub-bituminous coals*, Fuel, 73, pp. 1735-1745, 1994.

Patterson, J.H., Corcoran, J.K. and Kinealy, K.M., *Carbonate mineralogy of the Hoskissons seam and equivalents in the Sydney and Gunnedah Basins*, In: Boyd, R.L., McKenzie, G.A. (Eds.), Proceedings of the 29th New Castle Symposium, "Advances in the Study of Sydney Basin", Department of Geology, University of New Castle, New Castle, New South Wales, pp. 94-101, 1995.

Pinheiro, H.J., Pretorius, C.C. and Boshoff, H.P., *Analyses of coal product samples of South African Collieries,* Part 2, Bulletin 113, 1998-1999.

Pinetown K.L., Ward C.R. and van der Westhuizen W.A., *Quantitative evaluation of minerals in coal deposits in the Witbank and Highveld Coalfields and the potential impact on acid mine drainage,* International Journal of Coal Geology, in press, 2006.

Quann, R.J. and Sarofim, A.F., *Vaporisation of refractory oxides during pulverised coal combustion, nineteenth symposium (international) on combustion*, pp. 1429–1440, 1982.

Quann, R.J. and Sarofim, A.F., *A scanning electron microscopy study of the transformations of organically bound metals during lignite combustion*, Fuel, 65, pp. 40-446, 1986.

Quann, R.J., Neville, M. and Sarofim, A.F., *A laboratory study of the effect of coal selection on the amount and composition of combustion generated submicron particles,* Combust. Sci, Technol., 74, pp. 245-265, 1990.

Raask, E., *Flame Vitrification and sintering characteristics of silicate ash*, Technical Planning and Research Division, Central Electricity Generating Board, UK, 1986a.

Raask, E., *Flame vitrification and sintering characteristics of silicate ash, in mineral matter and ash in coal,* K.S. Vorres, Ed., ACS Symposium series No. 301, American Chemical Society, Washington, D.C., pp. 138-155, 1986b.

Raask, E., *Mineral impurities in coal combustion*, Hemisphere Publishing Company, New York, 1985.

Raask E., *Creation, capture and coalescence of mineral species in coal falme***,** Journal of the institute of energy 57:231-239:1984.

Radmacher, W. and Mohrhauer, P., *The direct determination of the mineral matter content of coal*, Brennstoff-Chemie, 36, pp. 236, 1955.

Rao, C.P. and Gluskoter, H.J., *Occurrence and distribution of minerals in Illinois coals*, Illinois State, Geol., Surv., Circ. 476, 1973.

Reifenstein, AP, Kahraman H, Coin CDA, Calos NJ, Miller G. and Uwins P., *Behaviour of selected minerals in an improved ash fusion test: quartz, potassium feldspar, sodium feldspar, kaolinite, illite, calcite, dolomite, siderite, pyrite and apatite,* Fuel, 78, pp.1449-1461, 1999.

Reid, W.T., *Coal ash – its effect on combustion systems, in chemistry of coal utilisation,* M.A. Elliot, Ed., John Wiley, N.Y., Chapter 21, pp. 1389-1446, 1981.

Renton, J.J., *Semiquantitative determination of coal minerals by X-ray diffractometry,* In: Vorres, K.S. (Ed.), *Mineral Matter and Ash in Coal,* American Chemical Society Symposium Series 301, pp. 60, 1986.

Rietveld, H.M., *A profile refinement method for nuclear and magnetic structure, Journal of Applied Crystallography* 2**,** pp.65-71, 1969.

Russell, S.J. and Rimmer, S.M., *Analysis of mineral matter in coal, coal gasification ash, and coal liquefaction residues by scanning electron microscopy and X-ray diffraction,* In: Karr, C. (Ed.), *Analytical Methods for Coal Products,* vol. 3. Academic Press, New York, pp. 133-162, 1979.

Snyman, C.P., Van Vuuren, M.C.J. and Barnard, J.M., *Chemical and Physical characteristics of South African coal and a suggested classification system,* National Institute for Coal Research, Coal 8306, pp. 1-63, 1983.

Spackman, W., *The maceral concept and the study of modern environments as a means of understanding the nature of coal,* Trans.,N.Y. Acad. Sci., Ser. II, 20, pp. 411- 423, 1958.

Srinivasachar, S., Helble, J.J. and Boni, A.A., *Mineral behaviour during coal combustion,* 1.- *Pyrite transformations*, prog. Energy Combust. Sci., 16, pp. 281-292, 1990a.

Srinivasachar, S., Helble, J.J., Boni, A.A., Shah, N., Huffman, G.P. and Huggins, F.E., *Mineral behaviour during coal combustion,* 1.-*Illite transformations.* Prog. Energy Combust. Sci., 16, pp. 293-302, 1990b.

Stach, E., Mackowsky, M-Th., Teichmuller, M., Taylor, G.H., Chandra, D. and Teichmuller, R., *Textbook of coal petrology*, 2nd. Rev. Ed. Berlin. Gebruder Borntraeger, pp.314-328; 535, 1982.

Standards A.S.T.M., *Test for total moisture in the analysis sample of coal,* D3174-73, 1979.

Standards Australia, *Higher rank coal-mineral matter and water of constitution,* Australian Standard 1038, Part 22, pp. 20, 2000.

Standards Australia, *Proximate analysis of coal,* Australian Standard 1038, Part 3, 1979.

Standards British, *Proximate analysis of coal*, British Standard 1016, Part 3, 1973.

Straszheim, W.E., Markuszewski, R., *Automated image analysis of minerals and their association with organic components in bituminous coals*, Energy Fuels, 4, 6, pp. 748-754, 1990.

Suzuki, S., Tanaka, M. and Kaneko, T., *Glass-ceramic from sewage sludge ash,* Journal of Materials Science, 32, pp.1775-1779, 1997.

Tangsathitkulchai, M., *Studies of the initiation, growth and sintering in the formation of utility boiler deposits.* Ph.D. Thesis, the Pennsylvania State University, 1986.

Taylor, J.C., *Computer programs for standardless quantitative analysis of minerals using the full powder diffraction profile*, powder Diffraction 6, pp. 2-9, 1991.

Ten Brink, H.M., Smart, J.P., Vleeskens, J.M. and Williamson, J, *Flame transformations and burner slagging in a 2.5 MW furnace firing pulverised coal: 1. Flame transformations*, Fuel, 73, pp. 1706–1711, 1994.

Tomeczek, J. and Palugniok, H., *Kinetics of mineral matter transformation during coal combustion,* Fuel, 81, pp.1251-1258, 2002.

Unsworth, J.F., Barratt, D.J., Park, D., and Titchener, K.J., *Ash formation during pulverised coal combustion.* Shell Research Ltd, Thornton Research Centre, UK. Fuel, 1987.

van Alphen, C., *Factors influencing fly ash formation and slag deposit formation (slagging) on combusting a South African pulverised fuel in a 200 MWe boiler,* Ph.D. Thesis, The Faculty of Engineering and the Built Environment, University of the Witwatersrand, Johannesburg, 2005.

van Alphen C. and Falcon L., *Application of CCSEM to coal processing,* Coal –The Future, 12th International conference on Coal Research, Sandton. The South African Institute of Mining and Metallurgy, Symposium, S26: 197-201, 2000.

Van Dyk, J. C., Baxter, L. L., Van Heerden, J. H. P.and Coetzer, R. L. J., *Chemical fractionation tests on South African coal sources to obtain species-specific information on ash fusion temperatures (AFT)*, Fuel 84, 1768-1777, 2005.

Velde, B., *Clay minerals, a physico-chemical explanation chemical of their occurrences,* Amsterdam, Oxford, New York, Tokyo, pp. 53-125, 1985.

Vuthaluru, H.B. and Zhang, D., *Effect of Ca- and Mg-bearing minerals on particle agglomeration defluidisation during fluidised-bed combustion of a South Australian lignite*, Fuel, 69, pp. 13-17, 2001.

Ward, C.R. (Editor), *Coal Geology and Coal Technology,* School of applied geology, University of New South Wales, Australia, Blackwell Scientific publications, Melbourne, Oxford, London, 40-113, 1984.

Ward, C.R., *Mineral matter in low-rank coals and associated strata of the Mae Moh basin*, Northern Thailand., Int. J. Coal Geol., 17, pp. 69-93, 1991.

Ward, C.R. and French, D., *Analysis and significance of mineral matter in coal, The Society for organic petrology,* Short Course Notes, The University of New South Wales, Sydney, NSW, Australia, pp. 7-68, 2004.

Ward C.R. and French, D., *Determination of glass content and estimation of glass composition in fly ash using quantitative X-ray diffractometr,* Fuel, 85, pp. 2268–2277, 2006.

Ward, C.R., *Isolation of mineral matter from Australian bituminous coals using hydrogen peroxide*, Fuel, 53, 220-221, 1974.

Ward, C.R., Matulis, C.E., Taylor, J.C. and Dale, L.S., *Quantification of mineral matter in Argonne Premium Coals using interactive Rietveld-based X-ray diffraction,* International Journal of Coal Geology, 46, 67-82, 2001a.

Ward, C.R., *Analysis and significance of mineral matter in coal seams,* International Journal of Coal Geology, 50, pp. 135-168, 2002.

Ward, C.R., *Mineral matter in the Harrisburg-Springfield (No.5) Coal Member of the Carbondale Formation, Illinois Basin,* Illinois State Geological Survey, Circular 498, pp. 35, 1977.

Ward, C.R., *Mineral matter in Australia bituminous coals,* Proceedings, Australasian Institute of Mining and Metallurgy 267, pp. 7-25, 1978.

Ward, C.R., *Minerals in bituminous coals of the Sydney Basin (Australia) and Illinois Basin (U.S.A.),* International Journal of Coal Geology 13, pp. 455-479, 1989.

Ward, C.R., Zhongsheng, Li. And Gurba, L.W., *Variations in coal maceral chemistry with rank advance in the German Creek and Moranbah coal measures of the Bowen Basin,*

Australia, using electron microprobe techniques, International Journal of Coal Geology, 63, pp. 117-129, 2005.

Ward C.R., Spears D.A., Booth C.A., Staton I. and Gurba L.W., *Mineral matter and trace elements in coals of the Gunnedah Basin, New South Wales, Australia.* International Journal of Coal Geology, 40, pp.281-308, 1999.

Watt, J.D., *The physical and chemical behaviour of mineral matter in coal under conditions met in combustion plants,* BCURA Industrial laboratories, Leatherhead, Surrey, Part II, 1969.

Wibberly, L.J. and Wall, T.F, *Alkali-ash reactions and deposit formation in pulverised coal-fired boilers: The thermodynamic aspects involving silica, sodium, sulphur, and chlorine,* Fuel, 61, pp. 87, 1982(a).

Wibberly, L.J. and Wall, T.F, *Alkali-ash reactions and deposit formation in pulverised coal-fired boilers: Experimental aspects of sodium silicate formation and the formation deposits,* Fuel, 61, pp 93-99, 1982b.

Yan, L., Gupta, R. and Wall, T.F., *Fragmentation behavior of pyrite and calcite during high-temperature processing and mathematical simulation,* Energy Fuels, 15, pp 389–394, 2001.

Yan, R., Gauthier, D., Flamant, G. and Badie, J.M., *Thermodynamic study of the behaviour of minor coal elements and their affinities to sulphur during coal combustion,* Fuel ,78, pp. 1817-1829, 1999.

Zagar, L. Sci., *Sintering*, Tech. Phys. Leningrad, 7(1), pp. 35-43, 1975.

Zhang, L., Ninomiya, Y. and Yamashita**,** T., *Occurrence of inorganic elements in condensed volatile matter emitted from coal pyrolysis and their contributions to the formation of ultra-fine particulates during coal combustion, Energy & Fuels,* 20, pp.1482-1489, 2006.

Zhang, L. and Ninomiya, Y., *Emission of suspended PM_{10} from laboratory-scale coal combustion and its correlation with coal mineral properties,* Fuel, 85, pp.194-203, 2006.

Zodrow, E.L. and Cleal, C.J., *Anatomically preserved plants in siderite concretions in the shale split of the Foord seam*: mineralogy, geochemistry, genesis (Upper Carboniferous, Canada), International Journal of Coal Geology, 41, pp. 371-393, 1999.

APPENDICES

APPENDIX A

Highveld coal samples before and after chemical fractionation method

Table A1: Ultimate analyses (dry ash-free basis, %) of Highveld coal samples before and after sequential leaching with water, ammonium acetate and hydrochloric acid

Lixiviants	Samples	Carbon	Hydrogen	Nitrogen	Sulphur	Oxygen
	HUC1	56.35	2.93	1.42	1.03	9.78
	HUC2	52.29	2.60	1.34	1.41	8.56
H_2O	HLC1	56.76	2.80	1.42	0.94	9.98
	HLC2	53.59	2.53	1.39	1.17	8.62
NH_4OAc	HLC1	58.52	2.91	1.87	0.96	9.44
	HLC2	54.63	2.64	1.73	1.15	9.25
HCl	HLC1	58.16	2.93	1.69	0.96	11.66
	HLC2	55.28	2.60	1.57	1.02	10.42

Table A2: Inorganic oxide percentages from ICP-OES analysis of LTA samples of Highveld feed coal sample 1 (wt %)

	HUC1	**WL HLC1**	**AAL HLC1**	**HClL HLC1**
	%	**%**	**%**	**%**
SiO_2	51.09	50.88	58.35	57.21
Al_2O_3	22.98	23.16	26.63	28.87
Fe_2O_3	5.23	4.86	5.21	3.60
TiO_2	1.37	1.37	1.57	1.72
P_2O_5	0.24	0.28	0.30	0.22
SrO	0.19	0.20	0.12	0.16
BaO	0.14	0.15	0.16	0.28
CaO	5.24	5.60	0.50	0.30
MgO	1.81	1.99	0.33	0.27
Na_2O	0.38	0.21	0.07	0,09
K_2O	0.51	0.51	0.55	0.27
SO_3	4.20	3.78	0.30	0.21

Table A3: Inorganic oxide percentages from ICP-OES analysis of LTA samples of Highveld coal sample 2 (wt %)

	HUC2 %	**WL HLC2**	**AAL HLC2**	**HClL HLC2**
SiO_2	43.30	43.26	52.77	60.92
Al_2O_3	24.24	23.80	28.81	25.73
Fe_2O_3	3.99	3.92	4.55	4.31
TiO_2	1.28	1.28	1.55	1.66
P_2O_5	0.80	0.77	0.96	0.05
SrO	0.43	0.42	0.36	0.06
BaO	0.28	0.28	0.33	0.09
CaO	9.10	9.10	1.98	0.15
MgO	2.59	2.57	0.82	0.23
Na_2O	0.47	0.34	0.12	0.07
K_2O	0.65	0.66	0.75	0.52
SO_3	5.25	3.56	1.01	0.10

APPENDIX B

Ash samples from gasifier

Table B1: Mass percentages of phases in ash and clinker (determined by CCSEM)

Phase	Description	Ash	Clinker
Interstitial and matrix glass	Ca- and Fe-bearing aluminosilicate glass with trace concentrations of Mg, K, P and Ti	40.6	34.5
K-bearing Al-silicate	K-bearing Al-silicate glass with Al/Si ratio similar to microcline and muscovite	4.3	5.1
Anorthite	Anorthite ($CaAl_2Si_2O_8$)	10.1	19.0
Mullite	$Al_6Si_2O_{13}$	1.5	0.7
Quartz	Unaltered quartz grains	9.2	9.6
Al-silicate	"Honeycomb" Al-silicate with trace K and Fe. (Transformation product of kaolinite)	21.9	19.2
Qtz60Kao40	Fine mixture of quartz and Al-silicate	4.5	4.6
Qtz80Kao20	Fine mixture of quartz and Al-silicate	2.0	2.2
Pyrrhotite/Fe-S-O/ Fe-oxide	Transformation product of extraneous pyrite	2.2	1.4
Carbonate/CaMgOxide	Transformation product of extraneous carbonates and associated with char	2.1	2.6
Char	Uncombusted carbon	1.5	1.0
Other		0.1	0.1
Total		100.0	100.0

APPENDIX C

Homogenised turn-out samples of coal and ash particles taken from the gasifier

Table C1: Proportions of high temperature transformation products of coal minerals formed at elevated temperatures and pressures during coal gasification (wt %) (determined by XRD)

Minerals identified	**Sample 1T**	**Sample 8T**	**Sample 16T**	**Sample 24T**	**Sample 32T**
Anorthite $(Ca,Na)(Si,Al)_2O_6$	18.1	7.7	1.8	0.4	n/d
α-Quartz α-SiO_2	14.4	14.3	11.7	6.2	6.0
Mullite $Al_6Si_2O_{13}$	11.8	5.3	2.4	3.9	n/d
Cristobalite SiO_2	0.5	0.1	<0.1	n/d	n/d
Hematite α-Fe_2O_3	0.3	0.2	<0.1	n/d	n/d
Pyrrhotite Fe_7S_8	n/d	<0.1	0.4	n/d	n/d
Magnetite $FeFe_2O_4$	0.2	0.3	n/d	n/d	n/d
Diopside $Ca(Mg,Al)(Si,Al)_2O_6$	<0.1	0.7	1.0	0.2	n/d
Anhydrite $CaSO_4$	0.2	0.1	0.4	n/d	n/d

Note:
Sample 1T = homogenised gasification ash exiting the gasifier.
Sample 8T = homogenised turn-out sample towards the bottom of the gasifier.
Sample 16T = homogenised sample taken from the centre of the gasifier
Sample 24T = homogenised sample taken from the top of the gasifier.
Sample 32T = Homogenised feed coal

Table C2: Proportions of coal minerals in the turn-out samples and feed coal determined by XRD (wt %)

Minerals identified	**Sample 1T**	**Sample 8T**	**Sample 16T**	**Sample 24T**	**Sample 32T**
α-Quartz α-SiO_2	14.4	14.3	11.7	6.2	6.0
Muscovite $KAl_2(Si_3Al)O_{10}(OH,F)_2$	0.8	0.8	<0.1	1.2	1.1
Kaolinite $Al_2Si_5(OH)_4$	n/d	n/d	1.4	6.7	6.7
Calcite $CaCO_3$	n/d	2.6	3.4	1.5	1.2
Aragonite $CaCO_3$	n/d	n/d	n/d	1.0	1.2
Dolomite $CaMg(CO_3)_2$	n/d	n/d	n/d	2.4	2.0
Pyrite FeS_2	n/d	n/d	<0.1	0.2	0.4
Greigite Fe_3S_4	n/d	n/d	n/d	0.2	0.2
Rutile TiO_2	n/d	0.3	0.1	0.2	0.3
Anatase TiO_2	n/d	n/d	<0.1	n/d	n/d
Gorceixite $BaAl_3(PO_4)PO_3OH)(OH)_6$	n/d	n/d	n/d	0.2	0.2
Non-crystalline content (mainly, glass and/or carbon)	53.3	67.5	76.9	75.7	80.7

Table C3: Mass-% phase proportions determined by CCSEM

Minerals and glasses	Sample 1T	Sample 8T	Sample 16T	Sample 24T	Sample 32T
Interstitial and matrix glass	30.3	25.4	14.9	6.7	4.2
Kaolinite(pyrite)	1.5	0.7	0.6	0.5	0.3
Kaolinite(carbonate, pyrite)	4.9	5.3	2.7	1.4	1.3
Kaolinite(carbonate)	21.8	18.0	10.6	4.3	2.3
Quartz(carbonate, pyrite)	1.1	0.4	0.4	0.1	0.1
Quartz(carbonate)	1.1	1.0	0.7	0.3	0.3
Glass-rock fragments	2.0	1.9	2.1	1.9	1.3
Orthoclase glass	1.2	1.0	0.9	0.9	0.8
Muscovite glass	0.8	0.9	1.2	1.0	0.5
Crystallites	6.1	9.4	5.2	2.6	0.5
Anorthite	5.4	8.3	4.2	1.3	0.3
Mullite	0.7	1.1	1.0	1.2	0.2
Rock fragments	58.6	60.9	72.5	82.0	80.9
Quartz	9.9	9.7	11.4	13.5	12.3
Metakaolinite	39.7	43.4	52.7	60.4	63.4
Qtz60Kao40	6.9	6.2	6.3	6.0	4.0
Qtz80Kao20	2.0	1.6	2.1	2.1	1.2
Extraneous	2.5	2.3	5.1	6.6	12.0
Pyrrhotite/ Fe-S-O/Fe-oxide	1.2	0.8	0.9	1.6	1.4
Carbonate/ CaMgOxide	1.4	1.6	4.2	5.0	10.6
Other	0.4	0.1	0.1	0.2	1.0
Total	100.0	100.0	100.0	100.0	100.0

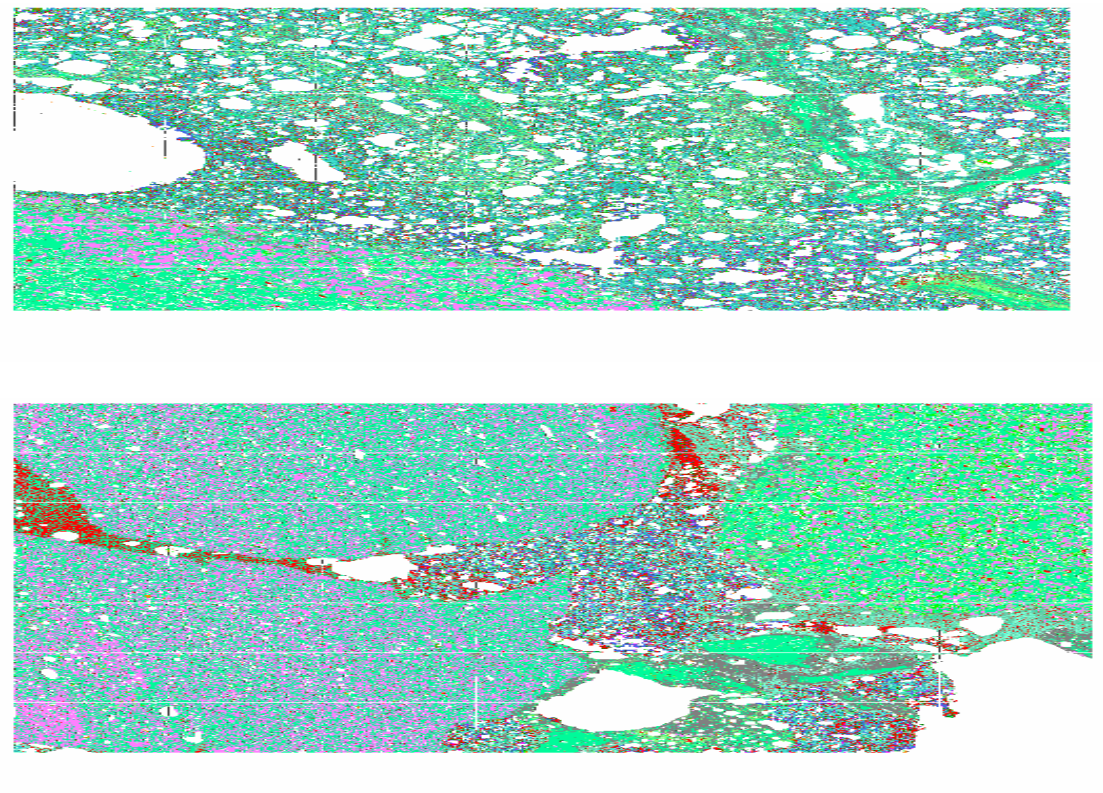
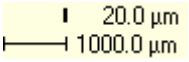


Figure C1: Top image of clinker sample 4, showing siltstone fragment lower left with pink quartz and green clay (kaolinite) in a glassy matrix determined by QEMSCAN
Bottom image of clinker sample 8T.

The scale of the images is 

APPENDIX D

Homogenised dig-out samples of coal and ash taken from the gasifier

Table D1: XRD analysis of the dig-out samples taken from the different zones of the gasifier (%)

Samples (dig-out)	**1D**	**3D**	**5D**	**6D**	**7D**	**9D**	**11D**
Quartz	6.1	6.0	8.7	11.0	11.8	10.8	17.4
Kaolinite	13.7	11.6	1.5	0.5	0.1	0.3	-
Muscovite/ Illite	1.6	1.0	0.3	-	-	-	-
Feldspar	-	-	0.2	-	-	0.3	-
Pyrite	0.6	0.6	0.1	-	-	-	-
Calcite	1.2	1.0	4.4	2.1	1.3	1.5	0.3
Dolomite	1.9	2.0	0.2	0.1	-	-	-
Rutile	0.1	0.1	0.1	0.8	-	0.2	0.3
Cristobalite	-	-	-	2.6	3.8	1.4	2.7
Mullite	-	-	0.1	10.3	16.2	19.9	20.7
Anorthite	-	-	-	2.9	11.3	6.7	7.4
Gehlenite	-	-	-	-	1.2	1.7	0.1
Diopside	-	-	-	1.2	1.1	0.7	0.7
Periclase	-	-	-	-	0.2	0.3	-
Amorphous glass & carbon content	74.8	77.7	84.4	68.5	53.0	56.1	50.4
Total	100	100	100	100	100	100	100

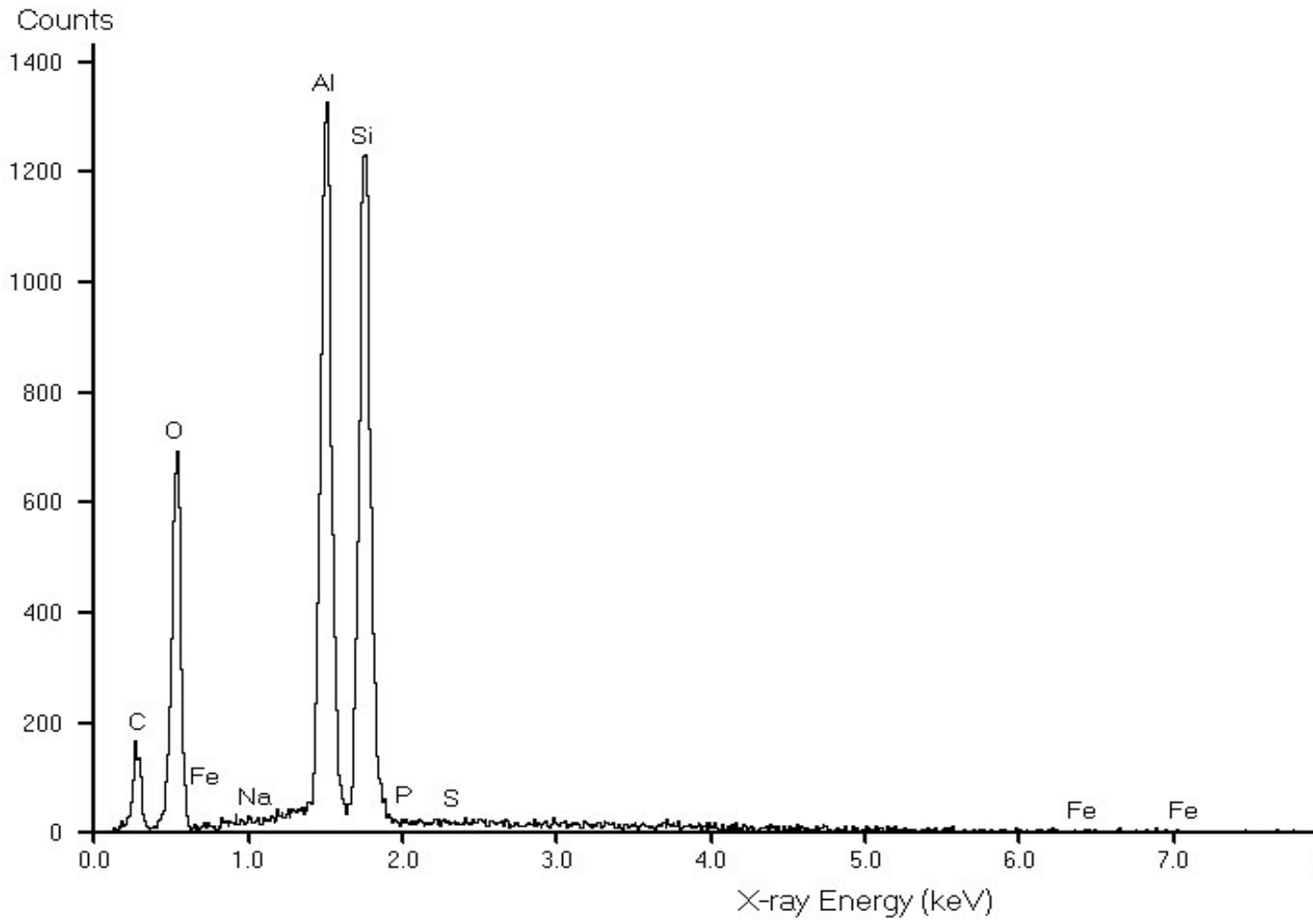


Figure E1: Typical X-ray spectrum of kaolinite in coal sample taken from the dig-out test.

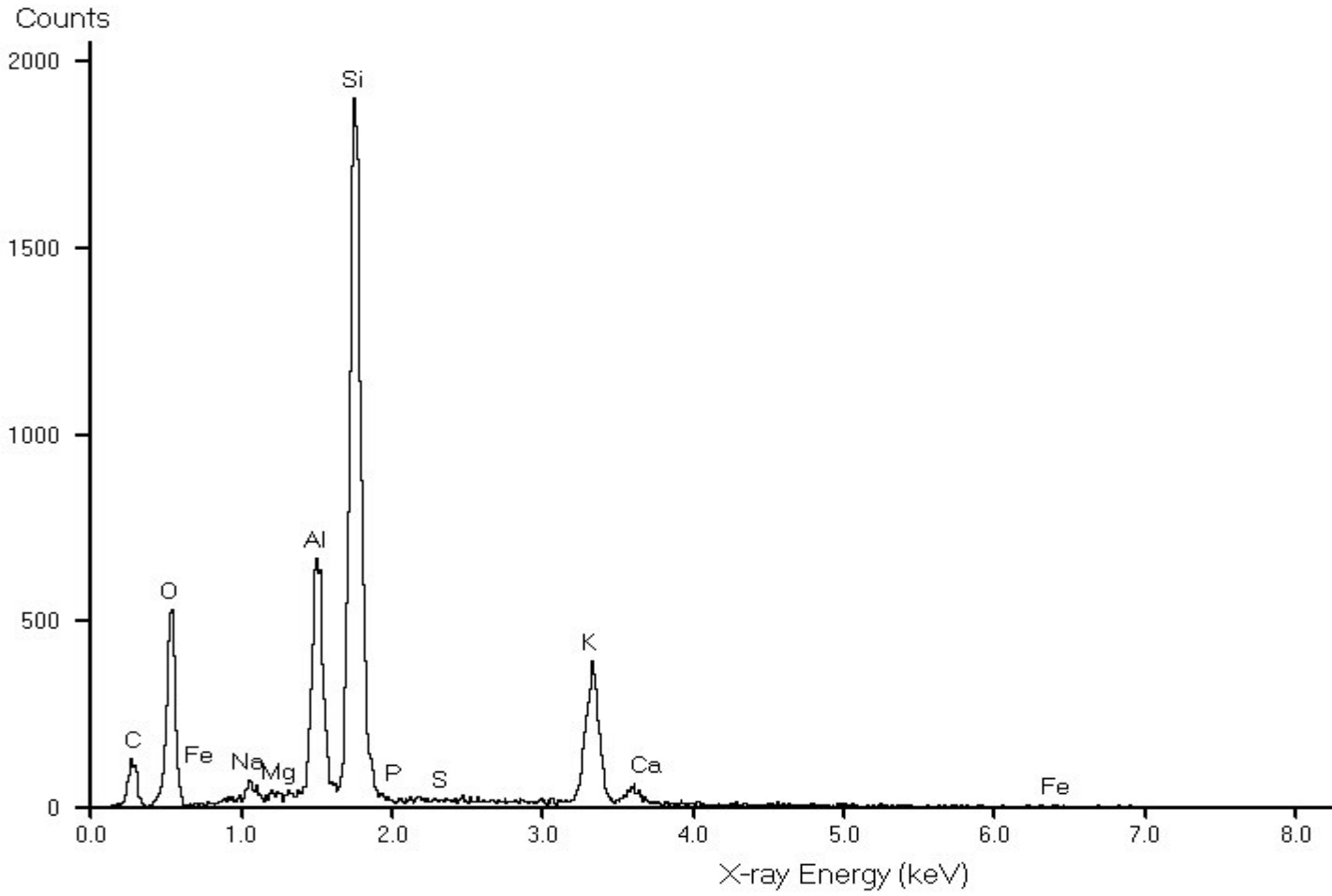


Figure E2: Typical X-ray spectrum of potassium feldspar in rock fragments taken from coal sample 1 during the dig-out test.

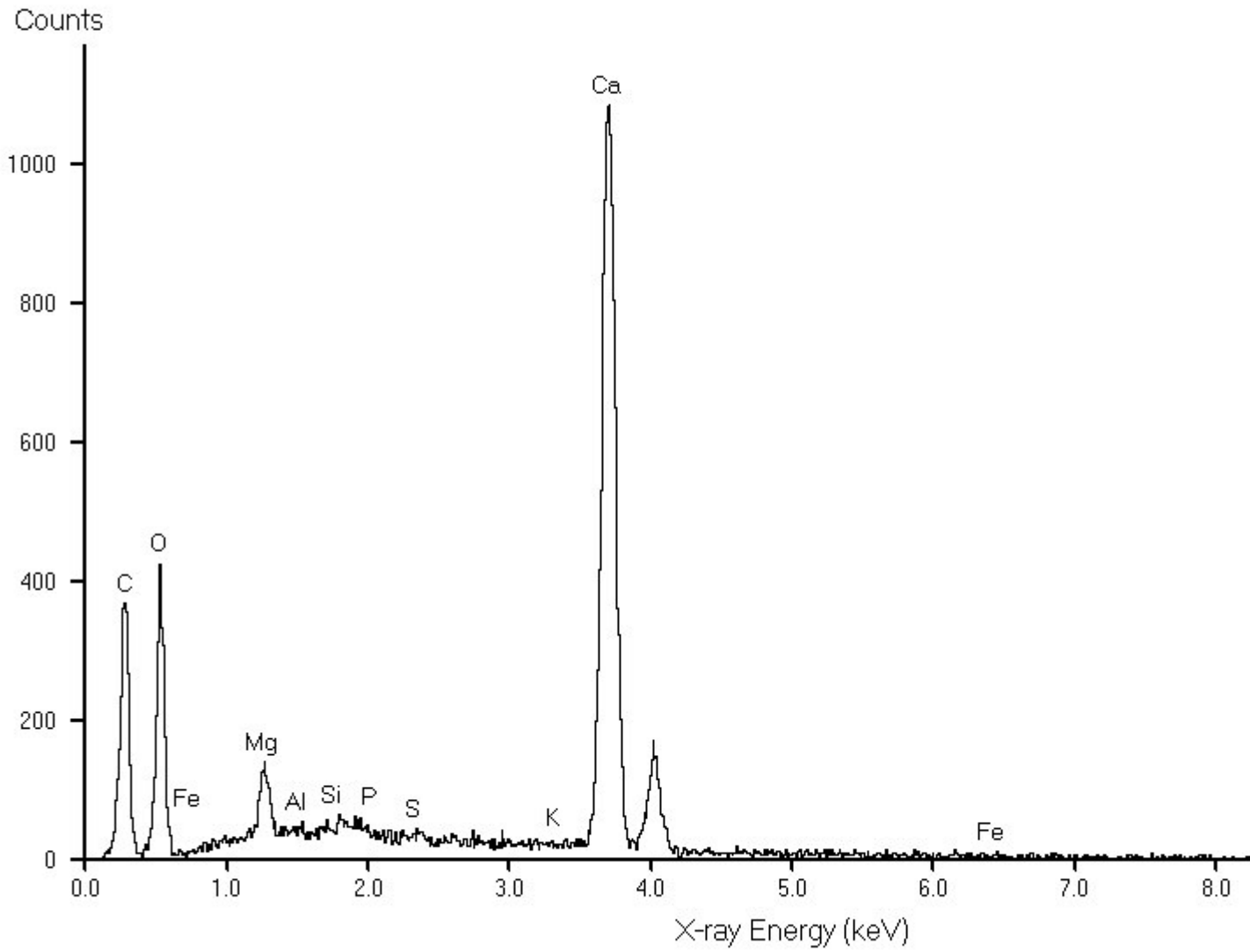


Figure E3: Typical X-ray spectrum of calcite cleats taken from coal sample 1 during the dig-out test.

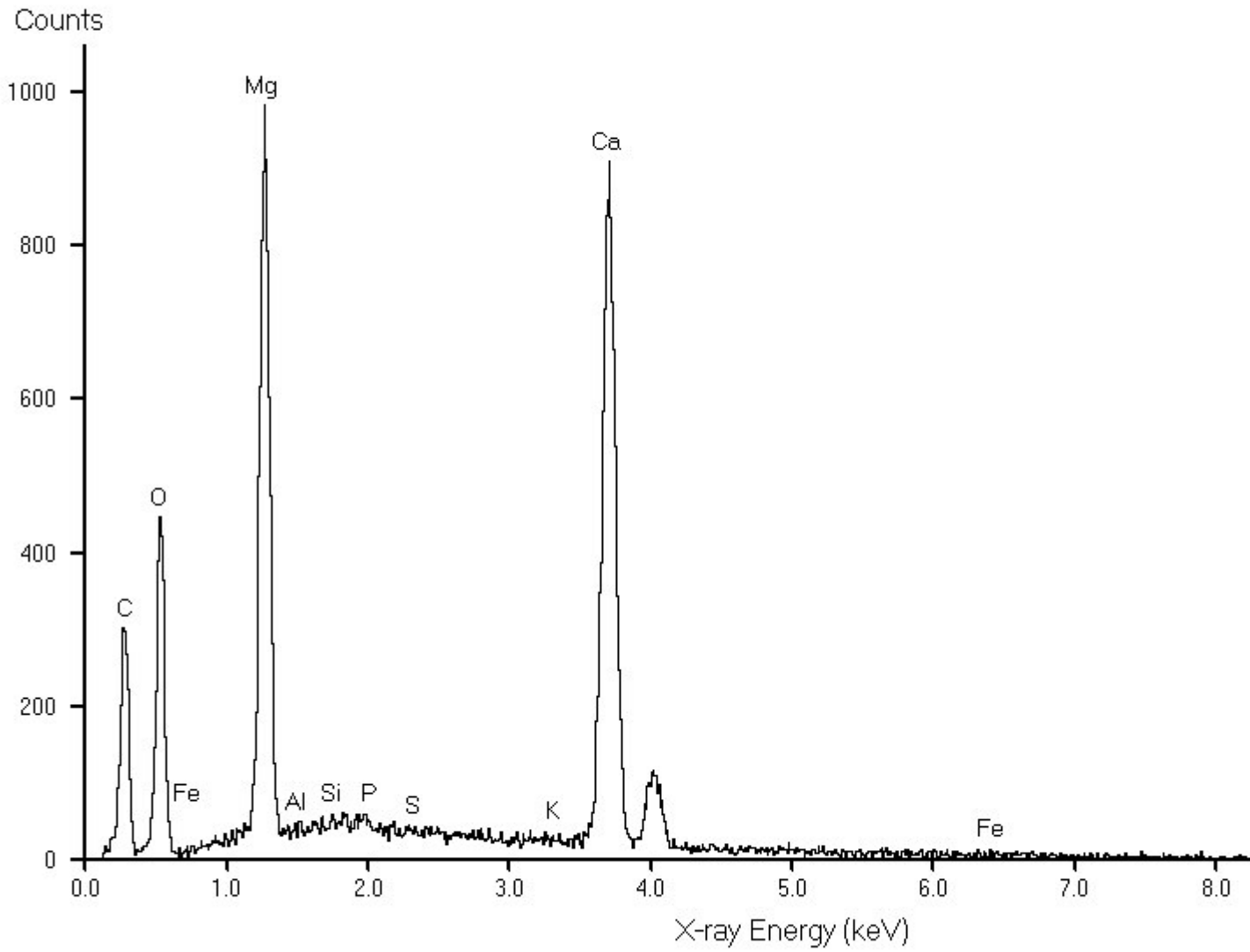


Figure E4: Typical X-ray spectrum of dolomite cleats taken from coal sample 1 during the dig-out …….test.

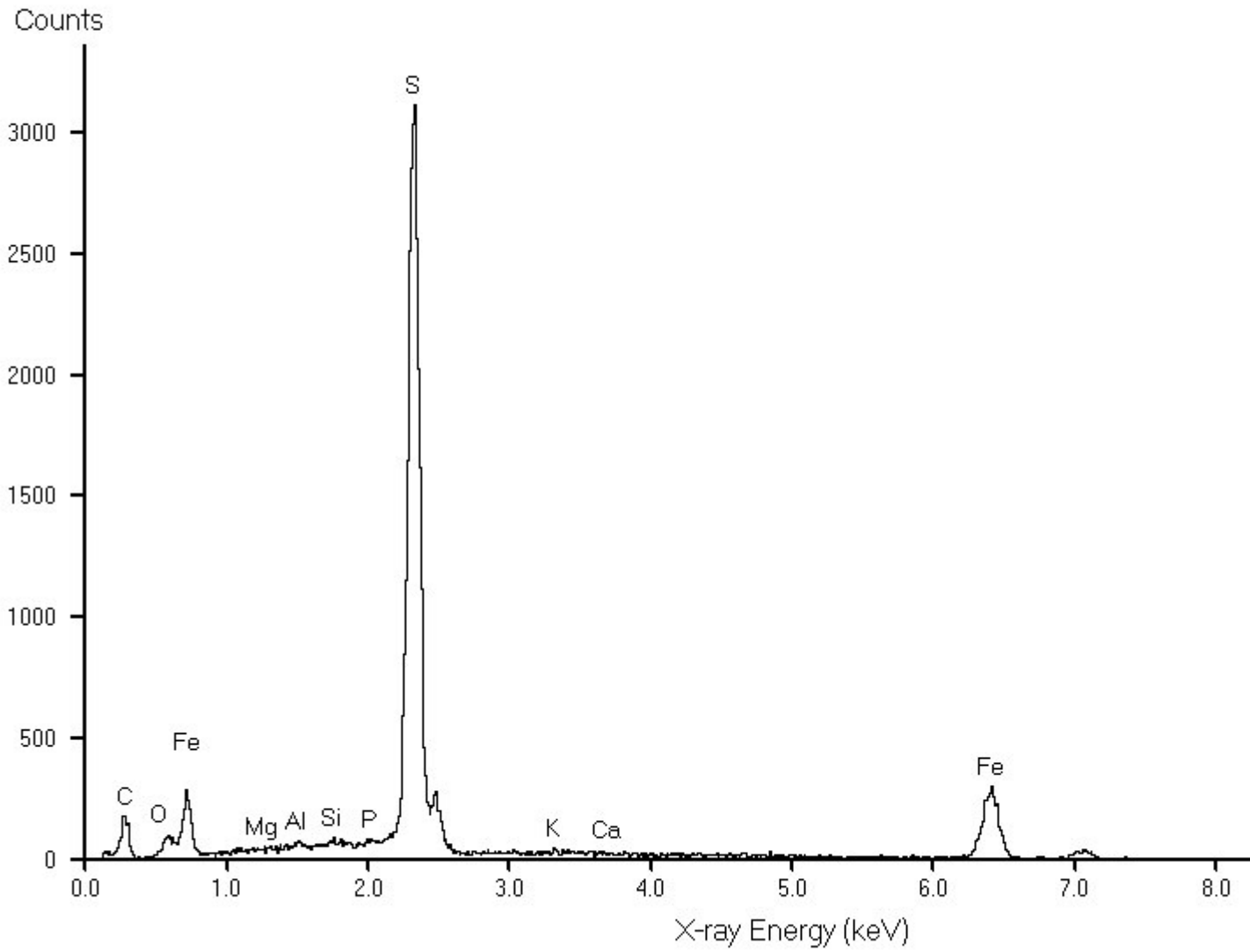


Figure E5: Typical X-ray spectrum of pyrite cleats taken from coal sample 1 during the dig-out test.

APPENDIX F

Sink fraction, float fraction , clinkers and heated rock fragments particles hand-picked from the dig-out samples 6D and 7D

Table F1: Predicted mass of equilibrium phases in sink fraction calculated at 1000 ^{o}C by FactSage model

T	=	1100	^{o}C
P	=	1.00E+00	atm
V	=	0.00E+00	dm^3

STREAM	**CONSTITUENTS**	**AMOUNT/gram**
Na_2O	3.00E-01	
$A_{l2}O_3$	2.14E+01	
SiO_2	5.67E+01	
TiO_2	1.10E+00	
CaO	6.80E+00	
MgO	1.30E+00	
FeO	5.10E+00	
K_2O	9.00E-01	
P_2O_5	0.00E+00	

EQUIL PHASE:	**AMOUNT Slag-liq (gram)**	**MASS FRACTION gram**	**ACTIVITY**
MgO	6.28E-03	4.44E-04	8.26E-04
FeO	4.36E-01	3.08E-02	6.48E-01
Na_2O	3.00E-01	2.12E-02	4.13E-16
SiO_2	1.05E+01	7.40E-01	7.68E-01
TiO_2	7.52E-02	5.32E-03	4.37E-02
Ti_2O_3	1.12E-05	7.93E-07	3.71E-05
CaO	5.33E-01	3.77E-02	2.92E-06
Al_2O_3	1.42E+00	1.01E-01	1.28E-03
K_2O	9.00E-01	6.37E-02	1.98E-18
Fe_2O_3	1.24E-05	8.81E-07	7.18E-05
TOTAL:	1.41E+01	1.00E+00	1.00E+00

PHASE:	**CORDIERITE**	**MASS FRACTION**	**ACTIVITY**
$Al_4Fe_2Si_5O_{18}$	1.69E+01	6.43E-01	3.83E-01
$Al_4Mg_2Si_5O_{18}$	9.39E+00	3.57E-01	1.45E-01
TOTAL:	2.63E+01	1.00E+00	1.00E+00

PHASE:	**MULLITE**	**GRAM FRACTION**	**ACTIVITY**
Al_2O_3	0.00E+00	7.19E-01	1.05E+01
SiO_2	0.00E+00	2.81E-01	1.38E-03
TOTAL:	0.00E+00	1.00E+00	4.66E-01

PHASE	gram	ACTIVITY	
$CaAl_2Si_2O_8$_anorthite(s2)	3.11E+01	1.00E+00	
SiO2_tridymite(h)(s4)	2.02E+01	1.00E+00	
$(FeO)(TiO_2)$_ilmenite(s)	1.95E+00	1.00E+00	
TiO_2_rutile(s)	0.00E+00	1.83E-01	
SiO_2_tridymite(l)(s3)	T	0.00E+00	1.51E-02

Table F2: Predicted mass of equilibrium phases in the float fraction calculated at 1100 °C by FactSage model

T	=	1100	°C
P	=	1.00E+00	atm
V	=	0.00E+00	dm3

STREAM	CONSTITUENTS	AMOUNT/gram
Na_2O	1.00E+00	
Al_2O_3	3.09E+01	
SiO_2	4.42E+01	
TiO_2	2.20E+00	
CaO	8.60E+00	
MgO	3.10E+00	
FeO	2.20E+00	
K_2O	7.00E-01	
P_2O_5	0.00E+00	

EQUIL PHASE:	AMOUNT ?Slag-liq	MASS FRACTION gram	ACTIVITY
MgO	4.14E-02	2.28E-03	2.87E-04
FeO	5.22E-01	2.87E-02	4.26E-02
Na_2O	1.00E+00	5.50E-02	3.57E-15
SiO_2	1.05E+01	5.76E-01	6.60E-01
TiO_2	1.23E+00	6.75E-02	2.39E-01
Ti_2O_3	7.09E-04	3.90E-05	1.99E-05
CaO	1.07E+00	5.87E-02	4.68E-07
Al_2O_3	3.81E+00	2.10E-01	1.08E-02
K_2O	4.20E-02	2.31E-03	6.96E-19
Fe_2O_3	7.88E-04	4.33E-05	1.72E-05
TOTAL:	1.82E+01	1.00E+00	1.00E+00

PHASE:	CORDIERITE	MASS FRACTION	ACTIVITY
$Al_4Fe_2Si_5O_{18}$	7.56E+00	2.54E-01	5.53E-02
$Al_4Mg_2Si_5O_{18}$	2.22E+01	7.46E-01	5.85E-01
TOTAL:	2.98E+01	1.00E+00	1.00E+00

PHASE:	MULLITE	MASS FRACTION	ACTIVITY
Al_2O_3	2.56E+00	7.20E-01	8.87E+01
SiO_2	9.97E-01	2.80E-01	1.19E-03
TOTAL:	3.56E+00	1.00E+00	1.00E+00

PHASE	AMOUNT (gram)	MASS FRACTION	ACTIVITY
$CaAl_2Si_2O_8$_anorthite(s2)	3.74E+01	1.00E+00	
$KAlSi_2O_6$_leucite(rhf(s2)	3.05E+00	1.00E+00	
TiO_2_rutile(s)	9.71E-01	1.00E+00	
$Mg_2Al_4Si_5O_{18}$_cordieri(s)	0.00E+00	5.85E-01	
$KAlSi_2O_6$_leucite(rhf)(s)	T	0.00E+00	1.87E-01

Table F3: Predicted mass of equilibrium phases in the heated rock fragment at 1100°C by FactSage model

T	**=**	**1100**
P	**=**	**1.00E+00**
V	**=**	**0.00E+00**
STREAM	**CONSTITUENTS**	**AMOUNT/gram**
Na_2O	4.00E-01	
Al_2O_3	3.84E+01	
SiO_2	5.87E+01	
TiO_2	6.70E-01	
CaO	4.20E-01	
MgO	0.00E+00	
FeO	3.20E-01	
K_2O	1.09E+00	
P_2O_5	0.00E+00	
EQUIL PHASE:	**AMOUNT ?Slag-liq**	**MASS FRACTION gram**
FeO	2.46E-02	1.40E-03
Na_2O	4.00E-01	2.27E-02
SiO_2	1.41E+01	7.99E-01
TiO_2	2.59E-01	1.47E-02
Ti_2O_3	3.10E-06	1.76E-07
CaO	1.06E-01	6.01E-03
Al_2O_3	1.66E+00	9.43E-02
K_2O	1.09E+00	6.20E-02
Fe_2O_3	3.44E-06	1.96E-07
TOTAL:	1.76E+01	1.00E+00
PHASE:	**Cordierite**	**MASS FRACTION**
$Al_4Fe_2Si_5O_{18}$	0.00E+00	1.00E+00
TOTAL:	0.00E+00	1.00E+00
PHASE:	**MULLITE**	**MASS FRACTION**
Al_2O_3	3.62E+01	7.20E-01
SiO_2	1.41E+01	2.80E-01
TOTAL:	5.03E+01	1.00E+00
PHASE	**AMOUNT**	**MASS FRACTION**
SiO_2_tridymite(h)(s4)	2.99E+01	1.00E+00
$CaAl_2Si_2O_8$_anorthite(s2)	1.56E+00	1.00E+00
(FeO)(TiO_2)_ilmenite(s)	6.24E-01	1.00E+00
TiO_2_rutile(s)	8.30E-02	1.00E+00
SiO_2_tridymite(l)(s3)	T	0.00E+00

APPENDIX G

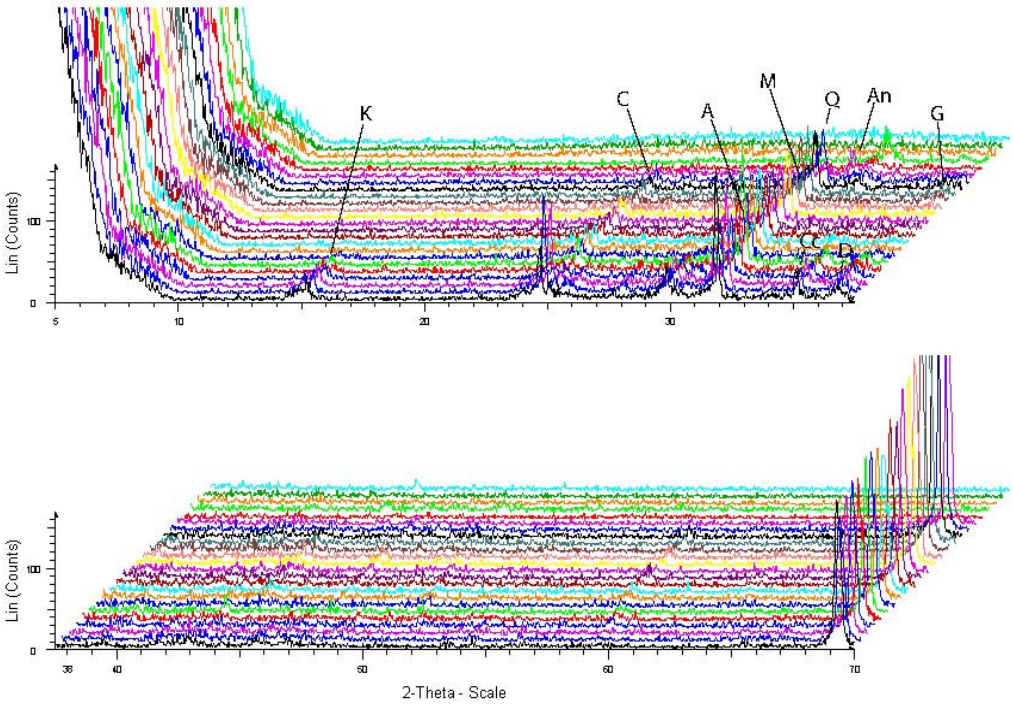


Figure G1: High temperature XRD Scan of minerals in the LTA of feed coal during thermal treatment.

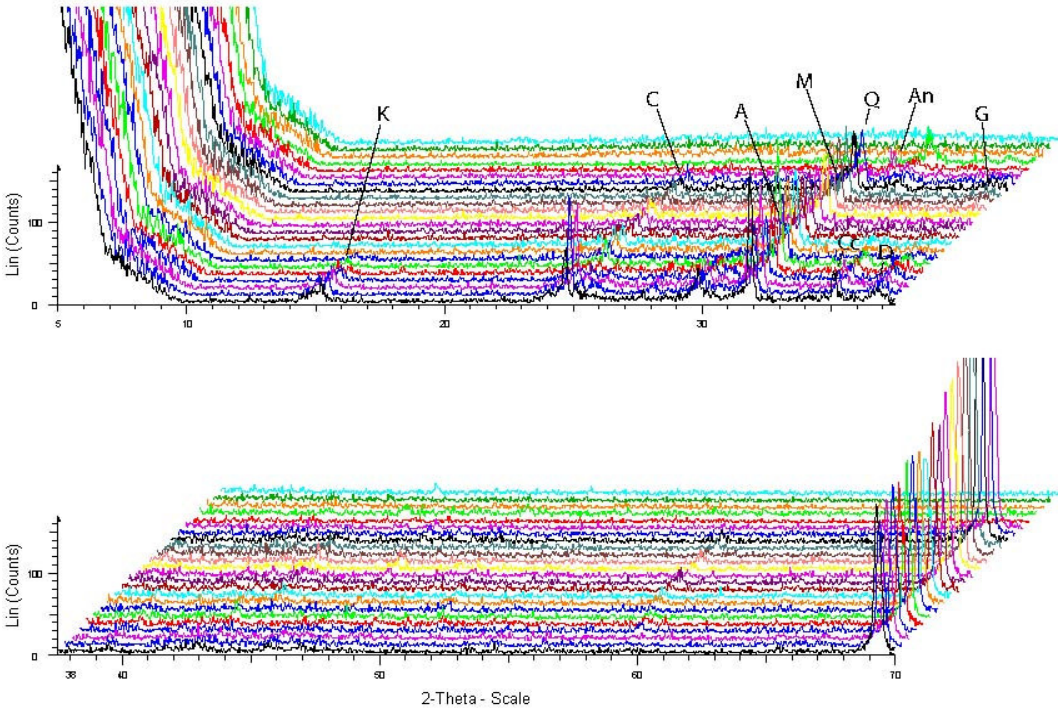


Figure G2: High temperature XRD Scan of minerals in the LTA of fine float coal fraction during thermal treatment.

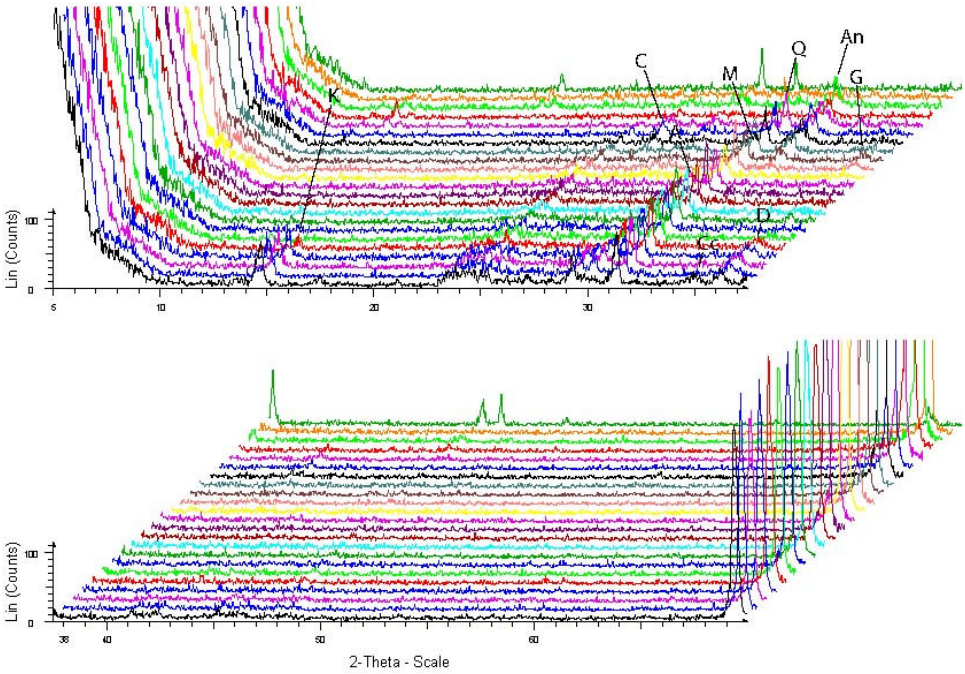


Figure G3: High temperature XRD Scan of minerals in the LTA of fine sink coal fraction during thermal treatment.

Note: K = Kaolinite, C = Cristobalite, CC = Calcite, An = Anorthite, M = Mullite, D = Dolomite G = Gehlenite, A = Bassanite or Anhydrite, Q = Quartz

Table G1: Showing in and out temperatures of the various phases during HT-XRD runs of LTA samples of feed coal, sink and float fractions (^{o}C)

Minerals	**32**		**LTA of Sink**		**LTA Float**	
	In	Out	In	Out	In	Out
Kaolinite		600		700		600
Quartz		1400		1300		1300
Dolomite		600		700		750
Calcite		600		650		400
Mullite	1050	1300	950	1250	1000	1400
Anorthite	1100	1450	1150	1400	950	1450
bassanite	400	750	450	900	400	1000
Gehlenite	950	1300	1000	1350	900	1200
Cristobalite	1250	1400	1150	1250	1100	1250

Note: 32 = In and out temperatures of phases in LTA of sample 32T (feed coal to gasification)
LTA of fine sink = In and out temperatures of phases in LTA of fine sink particles of sample
LTA of Float = In and out temperatures of phases in LTA of fine float particles of sample 32

APPENDIX H

Distribution of inorganic elements in the minerals and macerals in the coals

Table H1: Calculated concentrations of organic and inorganic elements obtained from all macerals in the coal sample from different Highveld collieries when using electron microprobe and optical microscope analyses (wt%)

Elements	Mine 1	Mine 2	Mine 3	Mine 4	Mine 5	Mine 6
C	56.84	54.23	50.39	55.11	55.46	55.76
H	2.63	2.43	1.95	2.58	1.72	3.34
N	0.88	0.59	1.08	0.73	0.94	1.13
O	8.09	6.46	8.71	6.78	7.98	10.90
Na	0.00	0.00	0.00	0.00	0.00	0.00
Mg	0.01	0.03	0.01	0.01	0.02	0.01
Al	0.13	0.09	0.24	0.03	0.14	0.19
Si	0.15	0.08	0.24	0.03	0.12	0.16
P	0.00	0.00	0.00	0.00	0.00	0.00
S	0.26	0.26	0.30	0.17	0.34	0.21
K	0.00	0.00	0.00	0.00	0.00	0.00
Ca	0.08	0.08	0.07	0.07	0.09	0.14
Ti	0.08	0.06	0.06	0.06	0.01	0.02
Fe	0.00	0.00	0.00	0.00	0.00	0.00
Total	69.14	64.31	63.05	65.58	66.82	71.85

Table H2: Calculated concentrations of inorganic elements present in the minerals in coal samples from different Highveld collieries (CCSEM analysis) (wt%)

Elements	Mine 1	Mine 2	Mine 3	Mine 4	Mine 5	Mine 6
C	0.72	0.70	1.20	0.97	0.84	0.83
H	0.22	0.32	0.32	0.28	0.19	0.20
N	0.00	0.00	0.00	0.00	0.00	0.00
O	14.89	18.55	19.31	17.70	16.10	13.92
Na	0.00	0.00	0.00	0.00	0.01	0.00
Mg	0.30	0.30	0.45	0.34	0.30	0.34
Al	2.98	4.57	4.41	3.91	2.88	2.79
Si	6.63	7.84	6.67	7.01	7.43	5.70
P	0.02	0.04	0.02	0.01	0.03	0.02
S	1.73	0.79	0.82	0.89	1.58	1.27
K	0.10	0.24	0.33	0.20	0.32	0.07
Ca	1.43	1.47	2.67	2.15	1.93	1.74
Ti	0.11	0.13	0.12	0.11	0.11	0.07
Fe	1.66	0.69	0.53	0.82	1.40	1.14
Total	30.78	35.64	36.85	34.39	33.11	28.12